**Title**
Bridging the Gap between Native Mass Spectrometry and Biochemistry: Small Droplets for Electrospray Ionization



**Author**
Xia, Zijie

**Publication Date**
2019

Peer reviewed|Thesis/dissertation

# Bridging the Gap between Native Mass Spectrometry and Biochemistry: Small Droplets for Electrospray Ionization

by

Zijie Xia

A dissertation submitted in partial satisfaction

of the requirements for the degree of

Doctor of Philosophy

in

Chemistry

in the

Graduate Division

of the

University of California, Berkeley

Committee in charge:

Professor Evan R. Williams, Chair
Professor Brian D. McCloskey
Professor Kristie A. Boering

Summer 2019

Bridging the Gap between Native Mass Spectrometry and Biochemistry: Small Droplets for Electrospray Ionization



by

Zijie Xia

Abstract

Bridging the Gap between Native Mass Spectrometry and Biochemistry: Small Droplets for Electrospray Ionization

by

Zijie Xia

Doctor of Philosophy in Chemistry

University of California, Berkeley

Professor Evan R. Williams, Chair

Native mass spectrometry is widely used to study the structure, stoichiometry, stability, and interactions of biological macromolecules. In native mass spectrometry, intact biological molecules are directly transferred from solution into the gas phase. However, one disadvantage of native MS is the requirement for volatile buffers, such as ammonium acetate and ammonium bicarbonate, which differ from buffers that are commonly used in other biological methods, such as Tris buffer and phosphate buffered saline. Until very recently, most native mass spectrometry experiments have been done with volatile buffers until very recently. Nonvolatile salts, even at low tens of mM concentrations, can cause the suppression of analyte ions, an increased chemical baseline, and reduced resolution and accuracy of mass measurements. In some cases, no useful mass information is obtained due to the nonvolatile salts in the sample solution. Thus, the mismatched buffer choices between native mass spectrometry and conventional biochemical techniques raise questions about the results obtained with native MS. The development of submicron electrospray emitters enables acquisition of mass spectra with resolved charge state distributions, which can provide useful mass information, for proteins and protein complexes from solutions containing nonvolatile salts at physiologically relevant concentrations ($\geqslant$ 150 mM NaCl). Submicron emitters have additional analytical advantages, including low sample consumption rate, providing results that are independent of instrument interface condition, and elimination of nonspecific dimer formation during electrospray ionization. With submicron emitters, the effects of ammonium acetate and traditional biological buffers on the structures, stabilities, and stoichiometries of proteins and protein complexes can be evaluated. The mass spectral results of the effect of salts on the protein and protein complexes are consistent with the discovery 130 years ago that salts can influence protein stability and solubility, which is known as the Hofmeister effect. This work demonstrates the use and advantages of submicron emitters. It is also the first study to provide mass spectral evidence that nonvolatile salts at a physiologically relevant concentration can influence protein structure, solubility, and stability, which has an important impact on the established native MS community that relies almost exclusively on volatile buffers.

In addition to different emitter sizes that determine whether desalted protein ions can be formed from solutions containing high concentrations of nonvolatile salts during ESI, a different emitter design can provide unique advantages. This work will also discuss theta emitter as an alternative design of ESI emitters. Theta emitters with two separated barrels have the advantage that rapid mixing can be performed during electrospray ionization with controlled reaction time. The lifetime of droplets, which determines the reaction time, can range from 1 μs to several hundred microseconds. Different droplet lifetimes are achieved by varying the flow rate and the distance between the emitter and the instrument. Applications and phenomena related to theta emitters are shown in this work to demonstrate the advantages and limitations of theta emitters of different sizes, especially the submicron theta emitters. This work provides some insights on how to choose a suitable emitter size and design based on the need of the experiments, especially in the area of native MS.

# Table of Contents

# Acknowledgements

I would like to thank my parents for their unconditional love and support. I would like to thank my friendship family, Dan and Starr Kahl, who have been extensively supporting me emotionally and helping me to adjust culturally since my college time. This work would not have been possible without the support from my mentor Dr. Evan Williams and all my friends. Especially, I would like to thank Dr. Hao Zhang, Dr. Anna Susa, Dr. Catherine Going, Dr. Matt DiTucci, Dr. Andrew Elliott, and Dr. Richard Cooper for their mentorship, support, and help during this challenging period of time. I would also like to thank all my college friends, especially Dr. Jiayi Wang, Yuan Ye, Xiaochen Mao, Hao Wen, and Dr. Bifan Chen. Although we no longer live in the same campus, it is great to have friends who pursue the same goal and support each other whenever it is needed. Lastly, I want to thank Hon Yee Li and Karla the German Shepard, my beloved fur baby, who shine the light in my life during the darkest period of time.

# Chapter 1

# Introduction

## 1.1 Overview for Native Mass Spectrometry

Mass spectrometry (MS) is a common analytical technique used to characterize both pure samples and complex mixtures that are in the gas, liquid, or solid phases. Some success in ionizing thermally labile and large biological molecules has been achieved with methods such as $^{252}$Cf plasma desorption,[1,2] field desorption,[3] secondary ion mass spectrometry (SIMS),[4] and fast atom bombardment,[5] as early as the 1970s. These early ionization methods involved many experimental difficulties, including mass limitations for applications with biological molecules. Biological samples, especially large biological complexes, were in general challenging for MS until the development of two soft ionization techniques: matrix-assisted laser desorption ionization (MALDI)[6] and electrospray ionization (ESI)[7] in the 1980s. These two ionization techniques are now routinely used to transfer biological analytes, ranging from short peptides to biological complexes with molecular weights from hundreds of kilodaltons to megadaltons, into the gas phase for MS analysis.[8–10] ESI-MS has a wide range of applications, including proteomics,[11,12] bioinformatics,[13] and native MS,[10,14]. More details about ESI are discussed in sections 1.2 and 1.3.

In particular, ESI can be applied to native mass spectrometry (native MS). In native MS, intact biological molecules and macromolecular complexes are transferred from buffered aqueous solutions, in which the analytes have native or native-like structures, into the gas phase for analysis by mass spectrometry using ESI. The major advantage of native MS is the separation of biological molecules from the solvent while the solution-phase information of biological molecules is generally preserved through kinetic trapping.[15,16] This technique was first demonstrated in the early 1990s by Henion et al. by the detection of noncovalent protein-ligand interactions using ESI.[17] Since then, native MS has been further developed and widely used to study structure, stoichiometry, and intermolecular interactions of biological macromolecules, including proteins, RNA, and DNA.[18–21] Many studies use native MS to obtain stoichiometric information on complicated protein complexes, such as ribosomes[22] and empty virus capsids,[23] from the mass spectra. The connection between subunits within a protein complex beyond the stoichiometric information can be mapped by coupling native MS with collisional activation.[24,25] Native MS is also suitable for kinetics and thermodynamic studies of complex macromolecular assemblies[26] and for probing the intermediate of disease-related protein aggregates, such as αβ-aggregates.[27,28] Not only soluble biological molecules but also membrane proteins and protein complexes can be studied with native MS with the use of soluble detergents in solution combined with gas-phase collisional activation.[29,30]

Ion mobility spectrometry (IMS) combined with native MS provides additional information about the conformations and stabilities of biological molecules.[31–34] IMS can be a stand-alone instrument for separations and analysis, or it can be combined with mass spectrometry. One practical application of IMS as a stand-alone instrument is the detection of explosives at

security checkpoints in airports.[35] The IMS separation relies either on ion-molecular interactions or on the different gas-phase collisional cross sections of the analytes.[35,36] When IMS is coupled with MS, additional structural information for ions that have the same mass-to-charge ratio ($m/z$) can be obtained. The separation of different protein conformers using IMS-MS was first reported by Clemmer et al. with the model protein cytochrome *c*.[37] Also, the stability and thermodynamics of biological ions in the gas phase can be monitored with IMS-MS by studying the gradual structural change with step-wise energy deposition to the analytes.[38,39] Besides all the global information on biological molecules that can be obtained with native MS, native MS can also be combined with top-down proteomics to obtain knowledge about protein sequences, interaction sites, and locations of post-translational modifications.[12,14,40] Native MS is thus becoming one of the important tools for structural biology studies.[14,41]

Native MS had some limitations with respect to the types of biological sample solutions that can be successfully analyzed. One of the major issues was that native MS was predominantly performed from aqueous buffered solutions that contain only volatile salts, such as ammonium acetate and ammonium bicarbonate, which provide the necessary pH and ionic strength for biological molecules to maintain their native states and functions. Native MS from the traditional biochemical buffers that usually contain more than 150 mM nonvolatile salts, such as phosphate buffered saline, was not achieved until very recently. Nonvolatile salts are in general not used for native MS because the salt ions can form adducts with protein ions, resulting in loss of resolution and mass measurement accuracy.[42–46] The formation of salt clusters in the mass spectra also increases chemical noise and causes ion suppression of analytes of interest.[44] The differences in buffer choice result in difficulties in direct comparison between the results from native MS and other biological methods to study the structure and stability of the biological molecules, such as spectroscopy and NMR. The differences also limit the impact of native MS as a tool for structural biology. Methods that can partially or fully address this challenge are discussed in detail in section 1.4. The significance of solving this problem is further explained in section 1.5.

The work described herein focuses on native MS for proteins and protein complexes. In Chapter 2, an application of the rapid mixing during ESI is described using a special ESI emitter, the theta emitter. The theta emitters have two separated barrels where two different solutions can be loaded without mixing until the start of ESI. In Chapter 3, a simple method for native MS to desalt membrane protein ions during ESI from solutions containing a high concentration of nonvolatile salts and detergents is demonstrated. This method is the most efficient to solve the critical limitation of native MS described above. In Chapters 4 and 5, some interesting phenomena of native MS are explored. Lastly, the effect of salt ions in solution on the structure, stoichiometry, stability of proteins and protein complexes are studied with mass spectrometry in Chapter 6 and 7. Together, these represent the first set of studies to demonstrate the importance of expanding the buffer choice of native MS from volatile buffers, such as ammonium acetate, to all buffers, including traditional biological buffers.

## 1.2 Electrospray Ionization for Proteins and Protein Complexes

Electrospray ionization (ESI) is initiated by creating an electric field between an emitter that contains a sample solution and the entrance of a mass spectrometer. The electric field is controlled by the applied potential difference, ranging from 0.5 kV to 5 kV, and the distance between the emitter and the entrance of the instrument. Although metal, borosilicate, and quartz emitters are most commonly used for ESI, studies have shown some relatively cheap and readily

available materials, such as paper,[47,48] microfabricated devices,[49,50] and micropipette tips[51,52] can also be used. This work uses emitters produced from borosilicate capillaries using a heated filament tip puller. The electric field between an emitter tip and the instrument entrance pulls the liquid out from the emitter tip while the surface tension holds the solution together. The competition of the two forces results in the formation of a Taylor cone.[53] Charged droplets are emitted from the Taylor cone when the electric field is stronger than the surface tension at the tip of the cone. As the initial charged droplets travel towards the instrument entrance, the droplets evaporatem resulting in desolvated analyte ions. ESI can be categorized into microESI, with a flow rate of microliters per minute, and nanoESI, with a flow rate of nanoliters per minute.[54] NanoESI is achieved by using smaller emitter tip diameters compared to those used in microESI. NanoESI has several advantages over microESI. NanoESI has a much lower sample consumption rate than microESI, which makes nanoESI essential for cases, in which a limited sample is available.[54–56] Because the electric field at the tip of a small emitter is high, droplets can be produced from solutions with high surface tension, such as water, without the assistance of an organic solvent or sheath gas.[54,57] NanoESI also has a higher tolerance for nonvolatile salts in the sample solution and higher ionization efficiency than microESI.[56,57] This work described herein uses nanoESI exclusively.

The formation of desolvated protein ions is generally believed to follow the charge residue mechanism (CRM). In the CRM, desolvated analyte ions are formed at the very last stage of the droplet evaporation process with the "residual" charges of the droplet partitioned between the departing solvent and solvent clusters and the analyte.[58,59] Experimental evidence for the CRM was shown in several studies. The maximum charge of a globular or globular-like protein in native MS can be estimated by the charge of a similar-sized droplet when the Rayleigh limit is reached,[60] at which

$$Z_R e = 8\pi(\varepsilon_0 \gamma R^3)^{1/2} \qquad \text{(Eq. 1)}$$

in which $Z_R$ is the integer unit of the charge at the Rayleigh limit, $e$ is the elementary charge, $\varepsilon_0$ is the permittivity of the surrounding medium, $\gamma$ is the surface tension of the solution, and $R$ is the radius of the droplet or protein.[61] It has been shown that the number of charges on a globular protein increases proportionally to the square root of the protein mass.[60,62] There are many factors other than the identity and the shape of the protein that can impact protein charge in the mass spectral results, including surface tension of the solution,[63,64] instrument interface condition,[65–67] and gas-phase reactions.[68,69] For example, elevated instrument source temperatures and high electric fields can lead to electrothermal supercharging of a protein that significantly increases the charge of a protein in mass spectra, largely exceeding $Z_R$ from ammonium bicarbonate for which the protein has a folded structure at low solution temperatures.[66,70]

It is essential to understand whether the desolvated ions form before or after the instrument entrance in order to evaluate the mass spectra at a given set of instrument conditions.[66,70–72] The early evidence of the location of desolvated ions formation was shown with optical spectroscopy measurements of ESI plume and mass spectra obtained with specific instrument or solution conditions.[71,73] van Berkel et al. showed that the ESI plume primarily contains dications of octaethylporphyrin, but predominantly monocations of the molecule are observed in the mass spectra.[73] This result indicates that the desolvated ions are formed within the entrance of the MS instrument. A similar conclusion can be drawn from the study on the effect of instrument source temperature on the mass spectra of proteins conducted by Chait et al.[71] In contrast, the optical spectroscopy study on rhodamine 6G shows that some of the desolvated ions are formed in the ESI plume before the droplets enter the MS entrance.[74] Some studies also assumed that the desolvated

ions are formed at the entrance of the mass spectrometer to obtain droplet lifetimes.[75,76] In Chapter 4, where the desolvated ions form using controlled droplet lifetime and instrument source temperature of the mass spectrometer will be investigated. The chapter will demonstrate that the location of the desolvated ion formation correlates to the size of the emitter. Submicron emitters generate initial droplets that produce desolvated ions independent of the instrument conditions, which is an advantage of submicron emitters.

## 1.3 Fast Mixing during ESI: Theta Emitters

MS can also be used as a detector for fast mixing experiments, such as studying the reaction intermediates and protein folding/unfolding intermediates, which happen in a time frame of microseconds or milliseconds during ESI. A mass spectrometer as a detector has the benefits of rapid detection, high chemical specificity, and high sensitivity.[77] There are many conventional mixers compatible with ESI, including laminar flow,[78,79] stopped flow,[80] and continuous flow devices.[81,82] These devices have been used to study the kinetics of protein folding and unfolding or cofactor-binding of a protein. The shortest time scale that is accessible with a conventional mixer using a mass spectrometer as a detector is 200 μs for a laminar flow mixer with a flow rate of 10 μL/s.[79] The more common time scale for a conventional mixer is greater than milliseconds when the mixing results are detected by a mass spectrometer. Many techniques and devices, such as a microfabricated dual spray,[83] multichannel microchip,[84] and microdroplet fusion,[75,85] mix solutions during ESI. Exposing the ESI droplets to an acidic or basic vapor as well as other chemical reagents can also result in mixing during the ESI process.[68,69,86]

Another device that can be used for rapid mixing during ESI is theta emitter, which is name after Greek letter θ because the cross-section of the end of the emitter has the same shape. The middle glass barrier of the emitter divides the emitter into two separate barrels, which allows two different solutions to be loaded into the emitter. Mixing of the two solutions does not occur until ESI is initiated. When desolvated ions are formed, the solution-phase reaction induced by mixing also stops. One key benefit of theta emitters compared to a single barrel emitter is the capability of characterizing and of controlling the lifetimes of the droplets generated from theta emitters.[76,87–90] Many factors influence droplet lifetime, including the diameter of the emitter tip, the applied voltage on the solution, the distance between the emitter tip and the instrument entrance, the backing pressure applied on the solution, and the type of the solvent properties.[76,87–90] Two methods have been used to characterize the droplet lifetime of theta emitters. The first method utilizes the unimolecular interaction of a protein with known folding constant. One barrel is filled with an acidic solution containing denatured protein, and the other barrel is filled with water or an aqueous buffered solution. A jump in pH happens during the mixing of the solution, which induces the folding of the denatured protein. The droplet lifetime is determined with a two-state protein folding model described by equation 2,

$$t = \tau \times ln\frac{A_e - A_0}{A_e - A_t} \qquad \text{(Eq. 2)}$$

in which $t$ is the droplet lifetime, $\tau$ is the folding time constant that depends on the protein and the solvent, and $A_0$, $A_t$, and $A_e$ correspond to the abundances of folded protein at time 0, time t, and at equilibrium. The mass spectra at time zero are obtained by loading the two barrels with the same acidic solution containing protein, and the results at equilibrium are obtained by loading the theta emitters with the same 1:1 mixture of the two solutions that have been allowed to come to

equilibrium.[87–89] This method relies on finding a suitable protein with a known folding time constant at a given pH and ionic strength. Another method to characterize droplet lifetimes from theta emitters uses microparticle imaging velocimetry and two Nd: YAG lasers.[76] The assumption underlying this method is that the desolvated ions form at the atmosphere-instrument interface.[76] Although this method is much more flexible in the choice of reaction materials, velocimetry has a limitation on the spatial resolution. Small initial droplets with diameters of tens of nanometers generated from emitters with submicron diameters cannot be detected by velocimetry using this method.

Because many factors can affect the lifetime of droplets produced from theta emitters, a wide range of mixing times (~1 μs to ~230 μs) is accessible with theta emitters.[76,87–90] It is so far the only device that can achieve rapid mixing around 1 μs and can be combined with MS detection.[89,90] Reaction intermediates,[91] protein folding/unfolding intermediates,[87,89] fast binding interactions,[88,90] and even side-chain hydrogen-deuterium exchange (H/D exchange) can be monitored using theta emitters. In Chapter 2, theta emitters are used to study the sidechain H/D exchange of a peptide that happens in a time scale of microseconds. This method was used to show that a salt bridge of the peptide exists in solution with mass spectrometry, which demonstrates that sidechain H/D exchange can also provide important and maybe additional structural information that is not available with amino acid backbone HDX in a time scale of milliseconds to hours. In Chapter 4 and 5, theta emitters are used to probe some fundamental questions of ESI because the droplets lifetime of theta emitters can be controlled and determined. Together, these work demonstrate the advantages and limitations of theta emitters.

## 1.4 Desalting Methods for Native Mass Spectrometry

High concentrations of nonvolatile salts, such as sodium or potassium chloride, are essential to mimic both *intra*- and *inter*-cellular environments in many studies of biological molecules. In contrast, nonvolatile salts have not been used in native mass spectrometry because nonvolatile salts can adversely affect the mass spectra. Salt ions can form adducts with the protein ions, which can spread the protein ion signal over a broad set of peaks, resulting in lower signal-to-noise ratios (S/N).[22,42,43,46] For large proteins and protein complexes or samples with high concentrations of nonvolatile salts, the number of salt adducts cannot be resolved, causing the loss of mass accuracy.[42,43] In studies of protein-ligand interactions and protein-cofactor interactions, the number of ligands and cofactors cannot be resolved if nonvolatile salt adducts heavily on the analytes.[92] Formation of salt clusters also increases the chemical noise baseline and can suppress protein ion formation.[44] Many methods and practices have been developed to work with samples containing nonvolatile salts. These methods can be divided into two general categories: desalting before ESI and desalting during ESI.

Conventional desalting methods before ESI include ion chromatography,[93,94] dialysis,[95] and ultrafiltration.[96,97] These methods exchange the original buffers containing nonvolatile salts with volatile buffers, such as ammonium acetate and ammonium bicarbonate, that are compatible with native MS. These methods are well developed and relatively easy to implement. However, by replacing some ions with others, the solution environment of proteins is changed, which can affect their structures and stabilities. These methods can also be time consuming. For example, dialysis can take hours to even days to sufficiently remove nonvolatile salts. Loss of sample and significant sample dilution can also occur with these methods.

In contrast, methods that desalt proteins during the ESI process do not change the solution environment of the protein completely. Desalted protein ions in mass spectra can be obtained with additives to the solution. However, the additives need to be carefully chosen so that the protein is not denatured. Buffer loading is one method to desalt protein ions during ESI through additives to the sample solution.[46] Adding up to 7 M ammonium acetate to protein-containing solutions with nonvolatile salts results in protein ions that have a remarkably lower number of sodium adducts. The S/N of ubiquitin from a solution containing 20 mM NaCl is increased by a factor of ~10 with this method.[46] However, the ionic strength of 7 M is significantly higher than the standard ionic strength used for mass spectrometry experiments and physiological conditions (~200 mM). Too high an ionic strength can change protein structures and activities.[98–100] Not all additives need to be added at a remarkably high concentration. Relatively clean mass spectra can also be effectively obtained with other additives at low concentration. Other ammonium salts (bromide and iodide salts),[101] $NaSbF_6$,[101] serine,[102] the supercharging reagent *m*-nitrobenzyl alcohol,[103] and ion chelators[104] at millimolar concentrations can significantly decrease the abundance of salt adducted protein ions from solutions containing nonvolatile salts. For example, by adding 25 mM ammonium bromide in a protein solution containing 1 mM NaCl, the ion abundance for the fully protonated protein increased by 72% compared to the ion abundance from a solution without ammonium bromide.[101] Gas-phase additives can also help to desalt protein ions after the ESI process. Adding chelator[105] or organic vapor[106,107] in the gas phase can remove metal ion adducts on the protein and protein complex ions. Although a small number of additives in the solution or the gas phase do not significantly change protein structures in the solution, the best of all these methods work only for up to 20 mM nonvolatile salts, which falls short of traditional biological buffers containing on average hundreds of millimolar concentrations of nonvolatile salts.

In the last few years, two additional desalting methods during ESI have been developed without additives in the protein solution, and both methods can work with complex solutions containing hundreds of millimolar of nonvolatile salts. One of the methods separates the nonvolatile salt ions from the proteins ions through electrophoretic movement generated by applying a usual ESI voltage continuously and an additional separate voltage intermittently. The separate voltage is not in contact with the solution.[108] This method separates the salt and protein ions based on their electrophoretic velocity. Cooks et al. reported desalted peptides and proteins even from phosphate buffered saline using this method.[108] However, because of the high mobility of protons with the separate voltage applied, there is accumulation of protons in the region around protein ions in solution, resulting in the acidification of the solution locally, which leads to denaturation of the protein and observation of unusually high charge states out of aqueous buffered solutions. The second method is so far the only method that can desalt protein and protein complexes from traditional biochemical buffers without denaturation. The method uses nanoESI emitters that have very small tip diameters.[42,43,55,109] Standard nanoESI emitters have an inner tip diameter of 1.5 μm to 10 μm. The nanoESI emitters that can efficiently desalt protein ions have an inner tip diameter of ~500 nm or lower. This method is efficient for obtaining clean mass spectra of *intra*- and *extra*-cellular soluble proteins from a wide range of traditional biological buffers containing ≥150 mM nonvolatile salts.[42,43,92,109]

The proposed mechanism attributes the formation of desalting protein ions from submicron emitters to the initial droplet sizes. The sizes of initial droplets formed from ESI emitters depend on many factors, including ion current,[110–112] flow rate,[113,114] emitter size,[55] and solution composition.[115–117] Initial droplets have been reported to have diameters between 1/14 and 1/20 of the emitter tip diameter.[42] Bush et al. reported emitters with 1 to 3 μm in diameter generate initial

droplets with a diameter of 60 nm, which is approximately 1/17 or less of the emitter tip diameter.[110] Given this information, an emitter with a 1.6 μm diameter produces initial droplets with a diameter of ~100 nm. This size emitter is on the low end of standard nanoESI emitter sizes. A 100 nm initial droplet can contain on average more than one protein and thousands of salt ions. In contrast, an emitter with a 500 nm diameter will produce droplets that have an initial diameter of ~29 nm. The volume of a 29 nm droplet is ~40 times lower than that of a 100 nm droplet. If a solution has 10 μM protein and 150 mM nonvolatile salts, and the initial 29 nm droplets have the same solution composition as the bulk solution, then on average, only one out of 13 droplets will contain a protein molecule. For droplets that contain just one protein molecule, fewer salt ions surround the protein in the droplet because of the small initial droplet size. Therefore, by simply using submicron emitters for the ESI, a separation between the protein and salt ions is achieved. Desalted protein ions do not form until several minutes after the ion current from ESI becomes stabile. There is also a decrease in total ion abundance when the desalted protein ions are formed than without the formation of desalted protein ions.[42] These phenomena indicate that there may be a spray mode change that different sized initial droplets are formed during ESI when the protein ions are desalted during ESI.

In Chapter 3, submicron emitter is used to obtain useful mass spectra of membrane proteins from solutions containing nonionic and ionic detergents in addition to nonvolatile salts. Membrane proteins were a challenge for native mass spectrometry due to its solubility in water solution. The common practice is to add a small amount of detergent, which is carefully screened to find the optimal conditions, in solution. Chapter 3 demonstrates that using submicron emitters can generate useful mass spectra of membrane proteins from solutions containing high concentrations of nonvolatile salts in addition to the necessary concentrations of the detergents. It may also provide a possibility to reduce detergent screening for membrane proteins in native MS analysis.

In Chapter 5, more analytical advantages of the submicron emitters other than producing desalted protein ions from solutions containing high concentrations of nonvolatile salts are discussed. The chapter demonstrates that submicron emitters are beneficial in many aspects and should be considered for future native MS experiments.

## 1.5 Importance of Salts in Native Mass Spectrometry

The solution environment plays an important role in the function, activity, and structures of biological molecules. The ionic strength, pH, and temperature of a solution are three commonly investigated factors in many protein studies. Many biological molecules become destabilized, disassemble, unfold, or aggregate at extreme pH and temperature.[118–120] Some proteins require specific salts in solution in addition to certain pH and ionic strength ranges in order to form appropriate structures and activity. Understanding specific salt and protein interactions can be essential for studies of disease mechanisms and for drug development. For example, one of the crucial cancer-related proteins, p53, requires zinc to stabilize the binding domain between the protein and DNA. A misfolded p53 protein that has limited DNA binding capability can increase its sensitivity to cancer drugs with the facilitation of zinc.[121,122] In another example, manganese binding will change prion protein structures that usually bind copper. The manganese-bound prion protein functions as a catalyst for the aggregation of the metal-free prion protein that can be transmitted from an infected organism to a different organism.[123,124]

More generally, non-specific salts can influence protein stability and solubility in solution. Franz Hofmeister discovered 130 years ago that the solubility of a protein depends on the identity

of salt ions present in solution.[125] This early work led to the Hofmeister series which orders cations or anions based on their capability of stablizing a protein in solution. A general Hofmeister series of ions is:

$$\text{Cations: } N(CH_3)_4^+ > NH_4^+ > Cs^+ > K^+ > Na^+ > Li^+ > Mg^{2+} > Ca^{2+} > \text{Guanidine}^+$$
$$\text{Anions: citrate}^{3-} > SO_4^{2-} > HPO_4^{2-} > C_2H_3O_2^- > HCO_3^- > CHO_2^- > Cl^- > Br^- > I^- > ClO_4^- > SCN^-$$

Ions on the left end of the series decrease the protein solubility ("salt out"). In contrast, ions on the right end of the series increase protein solubility and tend to stabilize denatured protein in solution ("salt in"). Anions tend to have a greater effect than cations. Many of these ions are used because of their "salting in" and "salting out" capabilities. For example, sulfate ion is commonly used in protein crystallography to "salt out" the native form of the proteins from solution.[126] Guanidine, on the other hand, is a commonly used chemical denaturant in studies of the stability and thermodynamics of proteins.[127,128] It disrupts protein native structure and increases protein solubility in solution. The order of ions in the Hofmeister series varies depending on other conditions, such as ionic strength, solution pH, temperature, and protein pI.[129–131] For example, at low salt concentrations, a reversed Hofmeister series may be observed.[131] However, the Hofmeister's experiment of salts on the solubility of the protein is the first evidence that different salt ions can significantly influence the structures of proteins in solution. The mechanism underlying the Hofmeister series is still debated. There are mainly two theories. In one theory, the Hofmeister series is a result of direct ion-protein interactions in solution.[128,132] In the other theory, the Hofmeister series is attributed to salt ions affecting the water hydrogen bond network surrounding the proteins resulting in different protein solubility and stability.[133,134] Experimental evidence supporting both theories has been reported. For example, studies have shown that some salt ions can affect the hydrogen-bonding network of water molecules at long range from the ion, beyond four water shells.[134] There are also many studies showing non-specific direct interaction between protein and salt ions in solution, such as the weak interaction between sulfate ions with protein backbone to stabilize the protein.[132]

Non-specific ion effects on protein structure and stability also have important implications in mass spectrometry studies of biological molecules. One example is that the efficiency of different anions in electrothermal supercharging can be explained with the Hofmeister series.[66,70,135] During electrothermal supercharging, electrospray droplets are formed with higher than usual electrospray voltages (usually > 1.1 kV) and transferred into an instrument interface that is heated to higher than typical conditions (> 150 °C). The rapid heating of the droplets due to the high electric field and heated instrument interface leads to protein unfolding in the electrospray droplet, which results in higher charge protein ions than the ones obtained at lower spray voltage and cooler instrument interface where ion unfolding does not occur.[136,137] The effectiveness of different ammonium salts for electrothermal supercharging follows a reversed Hofmeister series, indicating that Hofmeister anion effect on protein stability has a significant contribution in the mechanism of electrothermal supercharging.[135] Salt adducts are also observed in the gas phase,[138–143] where they can affect the conformations of the intermediate charge states by transitioning from a less compact structure to a more compact structure. For example, the 6+ charge state of ubiquitin, an intermediate charge state, has three conformations that are elongated to different extents in the gas phase when the protein ion has no salt adducts. It takes seven $Ca^{2+}$ ions adducted to the protein to shift the elongated conformations to a conformation that is more compact than the ones without any adducts. However, 13 $Na^+$ adducts on the same protein ion are needed to achieve the same

effect in the gas phase.[142] The multiply-charged salt ion adducts are in general more efficient than a singly charged salt ion adduct in compacting the structure of protein ions in the gas phase.[141–143]

Studying the effect of salts on protein structure at higher salt concentrations in solution using mass spectrometry was not possible until the discovery of submicron electrospray emitters. In Chapter 6 and 7, the effects of salt at the physiologically relevant concentration on proteins and protein complexes are demonstrated using submicron emitters. These are the first set of studies to bridge the differences in buffers used in mass spectrometry with those used in traditional biological techniques. They demonstrate the importance of the buffer choice for mass spectrometry in order to obtain accurate structural and stability data for a biological molecule.

## 1.6 References


(1) Torgerson, D. F.; Skowronski, R. P.; Macfarlane, R. D. New Approach to the Mass Spectroscopy of Non-Volatile Compounds. *Biochem. Biophys. Res. Commun.* **1974**, *60* (2), 616–621.

(2) Sundqvist, B.; Kamensky, I.; Håkansson, P.; Kjellberg, J.; Salehpour, M.; Widdiyasekera, S.; Fohlman, J.; Peterson, P. A.; Roepstorff, P. Californium-252 Plasma Desorption Time of Flight Mass Spectroscopy of Proteins. *Biol. Mass Spectrom.* **1984**, *11* (5), 242–257.

(3) Winkler, H. U.; Beckey, H. D. Field Desorption Mass Spectrometry of Peptides. *Biochem. Biophys. Res. Commun.* **1972**, *46* (2), 391–398.

(4) Benninghoven, A.; Sichtermann, W. K. Detection, Identification and Structural Investigation of Biologically Important Compounds by Secondary Ion Mass Spectrometry. *Anal. Chem.* **1978**, *50* (8), 1180–1184.

(5) Barber, M.; Bordoli, R. S.; Sedgwick, R. D.; Tyler, A. N. Fast Atom Bombardment of Solids (F.A.B.): A New Ion Source for Mass Spectrometry. *J. Chem. Soc. Chem. Commun.* **1981**, No. 7, 325.

(6) Karas, M.; Bachmann, D.; Hillenkamp, F. Influence of the Wavelength in High-Irradiance Ultraviolet Laser Desorption Mass Spectrometry of Organic Molecules. *Anal. Chem.* **1985**, *57* (14), 2935–2939.

(7) Yamashita, M.; Fenn, J. B. Electrospray Ion Source. Another Variation on the Free-Jet Theme. *J. Phys. Chem.* **1984**, *88* (20), 4451–4459.

(8) Lu, I.-C.; Lee, C.; Lee, Y.-T.; Ni, C.-K. Ionization Mechanism of Matrix-Assisted Laser Desorption/Ionization. *Annu. Rev. Anal. Chem.* **2015**, *8* (1), 21–39.

(9) Winston, R. L.; Fitzgerald, M. C. Mass Spectrometry as a Readout of Protein Structure and Function. *Mass Spectrom Rev* **1997**, *16* (4), 165–179.

(10) Leney, A. C.; Heck, A. J. R. Native Mass Spectrometry: What Is in the Name? *J. Am. Soc. Mass Spectrom.* **2017**, *28* (1), 5–13.

(11) Chandramouli, K.; Qian, P.-Y. Proteomics: Challenges, Techniques and Possibilities to Overcome Biological Sample Complexity. *Hum. Genomics Proteomics* **2009**, *2009*.

(12) Catherman, A. D.; Skinner, O. S.; Kelleher, N. L. Top Down Proteomics: Facts and Perspectives. *Biochemical and Biophysical Research Communications*. Elsevier Inc. 2014, pp 683–693.

(13) Chong, Y.-K.; Ho, C.-C.; Leung, S.-Y.; Lau, S. K. P.; Woo, P. C. Y. Clinical Mass Spectrometry in the Bioinformatics Era: A Hitchhiker's Guide. *Comput. Struct. Biotechnol. J.* **2018**, *16*, 316–334.

(14) Li, H.; Nguyen, H. H.; Ogorzalek Loo, R. R.; Campuzano, I. D. G.; Loo, J. A. An Integrated Native Mass Spectrometry and Top-down Proteomics Method That Connects Sequence to Structure and Function of Macromolecular Complexes. *Nat. Chem.* **2018**, *10* (2), 139–148.
(15) Fort, K. L.; Silveira, J. A.; Pierson, N. A.; Servage, K. A.; Clemmer, D. E.; Russell, D. H. From Solution to the Gas Phase: Factors That Influence Kinetic Trapping of Substance P in the Gas Phase. *J. Phys. Chem. B* **2014**, *118* (49), 14336–14344.
(16) Gross, D. S.; Zhao, Y.; Williams, E. R. Dissociation of Heme-Globin Complexes by Blackbody Infrared Radiative Dissociation: Molecular Specificity in the Gas Phase? *J. Am. Soc. Mass Spectrom.* **1997**, *8* (5), 519–524.
(17) Ganem, B.; Li, Y. T.; Henion, J. D. Detection of Noncovalent Receptor-Ligand Complexes by Mass Spectrometry. *J. Am. Chem. Soc.* **1991**, *113* (16), 6294–6296.
(18) Shah, S.; Friedman, S. H. An ESI-MS Method for Characterization of Native and Modified Oligonucleotides Used for RNA Interference and Other Biological Applications. *Nat. Protoc.* **2008**, *3* (3), 351–356.
(19) Satiaputra, J.; Sternicki, L. M.; Hayes, A. J.; Pukala, T. L.; Booker, G. W.; Shearwin, K. E.; Polyak, S. W. Native Mass Spectrometry Identifies an Alternative DNA-Binding Pathway for BirA from Staphylococcus Aureus. *Sci. Rep.* **2019**, *9* (1), 1–13.
(20) Marchand, A.; Gabelica, V. Native Electrospray Mass Spectrometry of DNA G-Quadruplexes in Potassium Solution. *J. Am. Soc. Mass Spectrom.* **2014**, *25* (7), 1146–1154.
(21) Van Den Heuvel, R. H. H.; Heck, A. J. R. Native Protein Mass Spectrometry: From Intact Oligomers to Functional Machineries. *Curr. Opin. Chem. Biol.* **2004**, *8* (5), 519–526.
(22) Videler, H.; Ilag, L. L.; McKay, A. R. C.; Hanson, C. L.; Robinson, C. V. Mass Spectrometry of Intact Ribosomes. *FEBS Lett.* **2005**, *579* (4), 943–947.
(23) Shoemaker, G. K.; van Duijn, E.; Crawford, S. E.; Uetrecht, C.; Baclayon, M.; Roos, W. H.; Wuite, G. J. L.; Estes, M. K.; Prasad, B. V. V.; Heck, A. J. R. Norwalk Virus Assembly and Stability Monitored by Mass Spectrometry. *Mol. Cell. Proteomics* **2010**, *9* (8), 1742–1751.
(24) Benesch, J. L. P.; Aquilina, J. A.; Ruotolo, B. T.; Sobott, F.; Robinson, C. V. Tandem Mass Spectrometry Reveals the Quaternary Organization of Macromolecular Assemblies. *Chem. Biol.* **2006**, *13* (6), 597–605.
(25) Sharon, M. How Far Can We Go with Structural Mass Spectrometry of Protein Complexes? *J. Am. Soc. Mass Spectrom.* **2010**, *21* (4), 487–500.
(26) Gülbakan, B.; Barylyuk, K.; Zenobi, R. Determination of Thermodynamic and Kinetic Properties of Biomolecules by Mass Spectrometry. *Curr. Opin. Biotechnol.* **2015**, *31*, 65–72.
(27) Muneeruddin, K.; Thomas, J. J.; Salinas, P. A.; Kaltashov, I. A. Characterization of Small Protein Aggregates and Oligomers Using Size Exclusion Chromatography with Online Detection by Native Electrospray Ionization Mass Spectrometry. *Anal. Chem.* **2014**, *86* (21), 10692–10699.
(28) Esparza, T. J.; Wildburger, N. C.; Jiang, H.; Gangolli, M.; Cairns, N. J.; Bateman, R. J.; Brody, D. L. Soluble Amyloid-Beta Aggregates from Human Alzheimer's Disease Brains. *Sci. Rep.* **2016**, *6* (1), 38187.
(29) Laganowsky, A.; Reading, E.; Hopper, J. T. S.; Robinson, C. V. Mass Spectrometry of Intact Membrane Protein Complexes. *Nat. Protoc.* **2014**, *8* (4), 639–651.

(30) Bechara, C.; Robinson, C. V. Different Modes of Lipid Binding to Membrane Proteins Probed by Mass Spectrometry. *J. Am. Chem. Soc.* **2015**, *137* (16), 5240–5247.
(31) Bohrer, B. C.; Merenbloom, S. I.; Koeniger, S. L.; Hilderbrand, A. E.; Clemmer, D. E. Biomolecule Analysis by Ion Mobility Spectrometry. *Annu. Rev. Anal. Chem.* **2008**, *1*, 293–327.
(32) Wyttenbach, T.; Pierson, N. a; Clemmer, D. E.; Bowers, M. T. Ion Mobility Analysis of Molecular Dynamics. *Annu. Rev. Phys. Chem.* **2014**, *65*, 175–196.
(33) Bleiholder, C.; Contreras, S.; Do, T. D.; Bowers, M. T. A Novel Projection Approximation Algorithm for the Fast and Accurate Computation of Molecular Collision Cross Sections (II). Model Parameterization and Definition of Empirical Shape Factors for Proteins. *International Journal of Mass Spectrometry*. 2013, pp 89–96.
(34) Kanu, A. B.; Dwivedi, P.; Tam, M.; Matz, L.; Hill, H. H. Ion Mobility-Mass Spectrometry. *J. Mass Spectrom.* **2008**, *43* (1), 1–22.
(35) Ewing, R. G.; Atkinson, D. A.; Eiceman, G. A.; Ewing, G. J. A Critical Review of Ion Mobility Spectrometry for the Detection of Explosives and Explosive Related Compounds. **2001**, *54*, 515–529.
(36) Hill, H. H.; William, F.; Louis, R. H. S.; Mcminn, D. G. Ion Mobility Spectrometry. *Anal. Chem.* **1990**, *62* (23), 1201–1209.
(37) Clemmer, D. E.; Jarrold, M. F. Ion Mobility Measurements and Their Applications to Clusters and Biomolecules. *J. Mass Spectrom.* **1997**, *32* (April).
(38) Hyung, S.; Robinson, C. V; Ruotolo, B. T. Gas-Phase Unfolding and Disassembly Reveals Stability Differences in Ligand-Bound Multiprotein Complexes. *Cell Chem. Biol.* **2009**, *16* (4), 382–390.
(39) Pagel, K.; Hyung, S.; Ruotolo, B. T.; Robinson, C. V. Alternate Dissociation Pathways Identified in Charge-Reduced Protein Complex Ions. *Anal. Chem.* **2010**, *82* (12), 5363–5372.
(40) Siuti, N.; Kelleher, N. L. Decoding Protein Modifications Using Top-down Mass Spectrometry. **2007**, *4* (10), 817–821.
(41) Lössl, P.; Waterbeemd, M. Van De; Heck, A. J. R. The Diverse and Expanding Role of Mass Spectrometry in Structural and Molecular Biology. *EMBO J.* **2016**, *35* (24), 2634–2657.
(42) Susa, A. C.; Xia, Z.; Williams, E. R. Small Emitter Tips for Native Mass Spectrometry of Proteins and Protein Complexes from Nonvolatile Buffers That Mimic the Intracellular Environment. *Anal. Chem.* **2017**, *89* (5), 3116–3122.
(43) Susa, A. C.; Xia, Z.; Williams, E. R. Native Mass Spectrometry from Common Buffers with Salts That Mimic the Extracellular Environment. *Angew. Chemie Int. Ed.* **2017**, 1–5.
(44) Pan, P.; McLuckey, S. A. The Effect of Small Cations on the Positive Electrospray Responses of Proteins at Low PH. *Anal. Chem.* **2003**, *75* (20), 5468–5474.
(45) Wang, G.; Cole, R. B. Effect of Solution Ionic Strength on Analyte Charge State Distributions in Positive and Negative Ion Electrospray Mass Spectrometry. *Anal. Chem.* **1994**, *66* (21), 3702–3708.
(46) Iavarone, A. T.; Udekwu, O. A.; Wiliams, E. R. Buffer Loading for Counteracting Metal Salt-Induced Signal Suppression in Electrospray Ionization. *Anal. Chem.* **2004**, *76* (14), 3944–3950.

(47) Liu, W.; Mao, S.; Wu, J.; Lin, J. M. Development and Applications of Paper-Based Electrospray Ionization-Mass Spectrometry for Monitoring of Sequentially Generated Droplets. *Analyst* **2013**, *138* (7), 2163–2170.
(48) Yang, Q.; Wang, H.; Maas, J. D.; Chappell, W. J.; Manicke, N. E.; Cooks, R. G.; Ouyang, Z. Paper Spray Ionization Devices for Direct, Biomedical Analysis Using Mass Spectrometry. *Int. J. Mass Spectrom.* **2012**, *312* (2), 201–207.
(49) Prudent, M.; Rossier, J. S.; Lion, N.; Girault, H. H. Microfabricated Dual Sprayer for On-Line Mass Tagging of Phosphopeptides. *Anal. Chem.* **2008**, *80* (7), 2531–2538.
(50) Cho, S.; Shim, T. S.; Yang, S. M. High-Throughput Optofluidic Platforms for Mosaicked Microfibers toward Multiplex Analysis of Biomolecules. *Lab Chip* **2012**, *12* (19), 3676–3679.
(51) Rahman, M. M.; Hiraoka, K.; Chen, L. C. Realizing Nano Electrospray Ionization Using Disposable Pipette Tips under Super Atmospheric Pressure. *Analyst* **2014**, *139* (3), 610–617.
(52) Rahman, M.; Wu, D.; Chingin, K. Direct Analysis of Aqueous Solutions and Untreated Biological Samples Using Nanoelectrospray Ionization Mass Spectrometry with Pipette Tip in Series with High-Ohmic Resistor as Ion Source. *J. Am. Soc. Mass Spectrom.* **2019**, *30* (5), 814–823.
(53) Rosell-Llompart, J.; Grifoll, J.; Loscertales, I. G. Electrosprays in the Cone-Jet Mode: From Taylor Cone Formation to Spray Development. *J. Aerosol Sci.* **2018**, *125*, 2–31.
(54) Juraschek, R.; Dülcks, T.; Karas, M. Nanoelectrospray - More than Just a Minimized-Flow Electrospray Ionization Source. *J. Am. Soc. Mass Spectrom.* **1999**, *10* (4), 300–308.
(55) Schmidt, A.; Karas, M.; Dülcks, T. Effect of Different Solution Flow Rates on Analyte Ion Signals in Nano-ESI MS, or: When Does ESI Turn into Nano-ESI? *J. Am. Soc. Mass Spectrom.* **2003**, *14* (5), 492–500.
(56) Karas, M.; Bahr, U.; Dülcks, T. Nano-Electrospray Ionization Mass Spectrometry: Addressing Analytical Problems beyond Routine. *Fresenius. J. Anal. Chem.* **2000**, *366* (6–7), 669–676.
(57) Wilm, M.; Mann, M. Analytical Properties of the Nanoelectrospray Ion Source. *Anal. Chem.* **1996**, *68* (1), 1–8.
(58) Dole, M.; Mack, L. L.; Hines, R. L.; Chemistry, D. O.; Mobley, R. C.; Ferguson, L. D.; Alice, M. B. Molecular Beams of Macroions. *J. Chem. Phys.* **1968**, *49* (5), 2240–2249.
(59) Winger, B. E.; Light-Wahl, K. J.; Ogorzalek Loo, R. R.; Udseth, H. R.; Smith, R. D. Observation and Implications of High Mass-to-Charge Ratio Ions from Electrospray Ionization Mass Spectrometry. *J. Am. Soc. Mass Spectrom.* **1993**, *4* (7), 536–545.
(60) Fernandez de la Mora, J. Electrospray Ionization of Large Multiply Charged Species Proceeds via Dole's Charged Residue Mechanism. *Anal. Chim. Acta* **2000**, *406* (1), 93–104.
(61) Rayleigh, Lord. XX. On the Equilibrium of Liquid Conducting Masses Charged with Electricity. *London, Edinburgh, Dublin Philos. Mag. J. Sci.* **1882**, *14* (87), 184–186.
(62) Heck, A. J. R.; Van Den Heuvel, R. H. H. Investigation of Intact Protein Complexes by Mass Spectrometry. *Mass Spectrom. Rev.* **2004**, *23* (5), 368–389.
(63) Iavarone, A. T.; Williams, E. R. Mechanism of Charging and Supercharging Molecules in Electrospray Ionization. *J. Am. Chem. Soc.* **2003**, *125* (8), 2319–2327.

(64) Iavarone, A. T.; Jurchen, J. C.; Williams, E. R. Effects of Solvent on the Maximum Charge State and Charge State Distribution of Protein Ions Produced by Electrospray Ionization. *J. Am. Soc. Mass Spectrom.* **2000**, *11* (11), 976–985.
(65) Chowdhury, S. K.; Katta, V.; Chait, B. T. Probing Conformational Changes in Proteins by Mass Spectrometry. *J. Am. Chem. Soc.* **1990**, *112* (24), 9012–9013.
(66) Sterling, H. J.; Cassou, C. A.; Susa, A. C.; Williams, E. R. Electrothermal Supercharging of Proteins in Native Electrospray Ionization. *Anal. Chem.* **2012**, *84* (8), 3795–3801.
(67) Thomson, B. A. Declustering and Fragmentation of Protein Ions from an Electrospray Ion Source. *J. Am. Soc. Mass Spectrom.* **1997**, *8* (10), 1053–1058.
(68) Kharlamova, A.; Prentice, B. M.; Huang, T.; Mcluckey, S. A. Electrospray Droplet Exposure to Gaseous Acids for the Manipulation of Protein Charge State Distributions. *Society* **2010**, *82* (17), 7422–7429.
(69) Kharlamova, A.; McLuckey, S. A. Negative Electrospray Droplet Exposure to Gaseous Bases for the Manipulation of Protein Charge State Distributions. *Anal. Chem.* **2011**, *83* (1), 431–437.
(70) Cassou, C. A.; Sterling, H. J.; Susa, A. C.; Williams, E. R. Electrothermal Supercharging in Mass Spectrometry and Tandem Mass Spectrometry of Native Proteins. *Anal. Chem.* **2013**, *85* (1), 138–146.
(71) Mirza, U. A.; Cohen, S. L.; Chait, B. T. Heat-Induced Conformational Changes in Proteins Studied by Electrospray Ionization Mass Spectrometry. *Anal. Chem.* **1993**, *65* (1), 1–6.
(72) Mirza, U. A.; Chait, B. T. Do Proteins Denature during Droplet Evolution in Electrospray Ionization. *Int. J. Mass. Spectrom. Ion Proc.* **1997**, *162* (96), 173–181.
(73) Zhou, S.; Edwards, A. G.; Cook, K. D.; Van Berkel, G. J. Investigation of the Electrospray Plume by Laser-Induced Fluorescence Spectroscopy. *Anal. Chem.* **1999**, *71* (4), 769–776.
(74) Wortmann, A.; Kistler-Momotova, A.; Zenobi, R.; Heine, M. C.; Wilhelm, O.; Pratsinis, S. E. Shrinking Droplets in Electrospray Ionization and Their Influence on Chemical Equilibria. *J. Am. Soc. Mass Spectrom.* **2007**, *18* (3), 385–393.
(75) Lee, J. K.; Kim, S.; Nam, H. G.; Zare, R. N. Microdroplet Fusion Mass Spectrometry for Fast Reaction Kinetics. *Proc. Natl. Acad. Sci.* **2015**, *112* (13), 201503689.
(76) Jansson, E. T.; Lai, Y.-H.; Santiago, J. G.; Zare, R. N. Rapid Hydrogen-Deuterium Exchange in Liquid Droplets. *J. Am. Chem. Soc.* **2017**, *139* (20), 6851–6854.
(77) Lee, E. D.; Muck, W.; Henion, J. D.; Covey, T. R. Real-Time Reaction Monitoring by Continuous-Introduction Ion-Spray Tandem Mass Spectrometry. *J. Am. Chem. Soc.* **1989**, *111* (13), 4600–4604.
(78) Wu, L.; Lapidus, L. J. Combining Ultrarapid Mixing with Photochemical Oxidation to Probe Protein Folding. *Anal. Chem.* **2013**, *85* (10), 4920–4924.
(79) Vahidi, S.; Stocks, B. B.; Liaghati-Mobarhan, Y.; Konermann, L. Submillisecond Protein Folding Events Monitored by Rapid Mixing and Mass Spectrometry-Based Oxidative Labeling. *Anal. Chem.* **2013**, *85* (18), 8618–8625.
(80) Kolakowski, B. M.; Konermann, L. From Small-Molecule Reactions to Protein Folding: Studying Biochemical Kinetics by Stopped-Flow Electrospray Mass Spectrometry. *Anal. Biochem.* **2001**, *292* (1), 107–114.
(81) Zinck, N.; Stark, A.; Wilson, D. J.; Sharon, M. An Improved Rapid Mixing Device for Time-Resolved Electrospray Mass Spectrometry Measurements. *ChemistryOpen* **2014**, *3* (3), 109–114.

(82) Simmons, D. A.; Konermann, L. Characterization of Transient Protein Folding Intermediates during Myoglobin Reconstitution by Time-Resolved Electrospray Mass Spectrometry with on-Line Isotopic Pulse Labeling. *Biochemistry* **2002**, *41* (6), 1906–1914.
(83) Miladinovic, S. M.; Fornelli, L.; Lu, Y.; Piech, K. M.; Girault, H. H.; Tsybin, Y. O. In-Spray Supercharging of Peptides and Proteins in Electrospray Ionization Mass Spectrometry. *Anal. Chem.* **2012**, *84* (11), 4647–4651.
(84) Yu, C.; Tang, F.; Qian, X.; Chen, Y.; Yu, Q.; Ni, K.; Wang, X. Multi-Channel Microfluidic Chip Coupling with Mass Spectrometry for Simultaneous Electro-Sprays and Extraction. *Sci. Rep.* **2017**, *7* (1), 17389.
(85) Shieh, I. F.; Lee, C. Y.; Shiea, J. Eliminating the Interferences from TRIS Buffer and SDS in Protein Analysis by Fused-Droplet Electrospray Ionization Mass Spectrometry. *J. Proteome Res.* **2005**, *4* (2), 606–612.
(86) Yang, S. H.; Wijeratne, A. B.; Li, L.; Edwards, B. L.; Schug, K. A. Manipulation of Protein Charge States through Continuous Flow-Extractive Desorption Electrospray Ionization: A New Ambient Ionization Technique. *Anal. Chem.* **2011**, *83* (3), 643–647.
(87) Mortensen, D. N.; Williams, E. R. Investigating Protein Folding and Unfolding in Electrospray Nanodrops Upon Rapid Mixing Using Theta-Glass Emitters. *Anal. Chem.* **2015**, *87* (2), 1281–1287.
(88) Mortensen, D. N.; Williams, E. R. Theta-Glass Capillaries in Electrospray Ionization: Rapid Mixing and Short Droplet Lifetimes. *Anal. Chem.* **2014**, *86* (18), 9315–9321.
(89) Mortensen, D. N.; Williams, E. R. Ultrafast (1 Ms) Mixing and Fast Protein Folding in Nanodrops Monitored by Mass Spectrometry. *J. Am. Chem. Soc.* **2016**, *138* (10), 3453–3460.
(90) Mortensen, D. N.; Williams, E. R. Microsecond and Nanosecond Polyproline II Helix Formation in Aqueous Nanodrops Measured by Mass Spectrometry. *Chem. Commun.* **2016**, *52*, 12218–12221.
(91) Mark, L. P.; Gill, M. C.; Mahut, M.; Derrick, P. J. Dual Nano-Electrospray for Probing Solution Interactions and Fast Reactions of Complex Biomolecules. *Eur. J. Mass Spectrom.* **2012**, *18* (5), 439–446.
(92) Nguyen, G. T. H.; Tran, T. N.; Podgorski, M. N.; Bell, S. G.; Supuran, C. T.; Donald, W. A. Nanoscale Ion Emitters in Native Mass Spectrometry for Measuring Ligand-Protein Binding Affinities. *ACS Cent. Sci.* **2019**, *5* (2), 308–318.
(93) Jiang, Y.; Hofstadler, S. A. A Highly Efficient and Automated Method of Purifying and Desalting PCR Products for Analysis by Electrospray Ionization Mass Spectrometry. *Anal. Biochem.* **2003**, *316* (1), 50–57.
(94) Hernández, H.; Robinson, C. V. Determining the Stoichiometry and Interactions of Macromolecular Assemblies from Mass Spectrometry. *Nat. Protoc.* **2007**, *2* (3), 715–726.
(95) Xiang, F.; Lin, Y.; Wen, J.; Matson, D. W.; Smith, R. D. An Integrated Microfabricated Device for Dual Microdialysis and On-Line ESI-Ion Trap Mass Spectrometry for Analysis of Complex Biological Samples. *Anal. Chem.* **1999**, *71* (8), 1485–1490.
(96) DeMarco, M. L.; Burnham, C. A. D. Diafiltration MALDI-TOF Mass Spectrometry Method for Culture-Independent Detection and Identification of Pathogens Directly from Urine Specimens. *Am. J. Clin. Pathol.* **2014**, *141* (2), 204–212.
(97) Prodanov, M.; Garrido, I.; Vacas, V.; Lebrón-Aguilar, R.; Dueñas, M.; Gómez-Cordovés, C.; Bartolomé, B. Ultrafiltration as Alternative Purification Procedure for the

Characterization of Low and High Molecular-Mass Phenolics from Almond Skins. *Anal. Chim. Acta* **2008**, *609* (2), 241–251.
(98) Kříž, Z.; Klusák, J.; Krištofíková, Z.; Koča, J. How Ionic Strength Affects the Conformational Behavior of Human and Rat Beta Amyloids - A Computational Study. *PLoS One* **2013**, *8* (5).
(99) Yang, A. S.; Honig, B. Structural Origins of PH and Ionic Strength Effects on Protein Stability: Acid Denaturation of Sperm Whale Apomyoglobin. *Journal of Molecular Biology*. 1994, pp 602–614.
(100) Sterling, H. J.; Batchelor, J. D.; Wemmer, D. E.; Williams, E. R. Effects of Buffer Loading for Electrospray Ionization Mass Spectrometry of a Noncovalent Protein Complex That Requires High Concentrations of Essential Salts. *J. Am. Soc. Mass Spectrom.* **2010**, *21* (6), 1045–1049.
(101) Flick, T. G.; Cassou, C. a.; Chang, T. M.; Williams, E. R. Solution Additives That Desalt Protein Ions in Native Mass Spectrometry. *Anal. Chem.* **2012**, *84* (17), 7511–7517.
(102) Clarke, D. J.; Campopiano, D. J. Desalting Large Protein Complexes during Native Electrospray Mass Spectrometry by Addition of Amino Acids to the Working Solution. *Analyst* **2015**, *140* (8), 2679–2686.
(103) Cassou, C. A.; Williams, E. R. Desalting Protein Ions in Native Mass Spectrometry Using Supercharging Reagents. *Analyst* **2014**, *139* (19), 4810–4819.
(104) Pan, J.; Xu, K.; Yang, X.; Choy, W. Y.; Konermann, L. Solution-Phase Chelators for Suppressing Nonspecific Protein-Metal Interactions in Electrospray Mass Spectrometry. *Anal. Chem.* **2009**, *81* (12), 5008–5015.
(105) Turner, K. B.; Monti, S. A.; Fabris, D. Like Polarity Ion/Ion Reactions Enable the Investigation of Specific Metal Interactions in Nucleic Acids and Their Noncovalent Assemblies. *J. Am. Chem. Soc.* **2008**, *130* (40), 13353–13363.
(106) Pope, R. M.; Shen, N.; Hofstadler, S. A.; Dearden, D. V. Gas Phase Stripping of Alkali Cations from Biomolecules via Reaction with Crown Ethers. *Int. J. Mass Spectrom. Ion Process.* **1998**, *175* (1–2), 179–186.
(107) Demuth, J. C.; McLuckey, S. A. Electrospray Droplet Exposure to Organic Vapors: Metal Ion Removal from Proteins and Protein Complexes. *Anal. Chem.* **2015**, *87* (2), 1210–1218.
(108) Zhang, Z.; Pulliam, C. J.; Flick, T.; Cooks, R. G. Electrophoretic Desalting to Improve Performance in Electrospray Ionization Mass Spectrometry. *Anal. Chem.* **2018**, *90* (6), 3856–3862.
(109) Hu, J.; Guan, Q.-Y.; Wang, J.; Jiang, X.-X.; Wu, Z.-Q.; Xia, X.-H.; Xu, J.-J.; Chen, H.-Y. Effect of Nanoemitters on Suppressing the Formation of Metal Adduct Ions in Electrospray Ionization Mass Spectrometry. *Anal. Chem.* **2017**, *89* (3), 1838–1845.
(110) Davidson, K. L.; Oberreit, D. R.; Hogan, C. J.; Bush, M. F. Nonspecific Aggregation in Native Electrokinetic Nanoelectrospray Ionization. *Int. J. Mass Spectrom.* **2017**, *420*, 35–42.
(111) Srikanth, A.; Karnawat, J.; Kushari, A. The Effect of Charge Density on Electro-Sprayed Droplets. *Open Appl. Phys. J.* **2009**, *2*, 53–57.
(112) Gañán-Calvo, A. M.; Dávila, J.; Barrero, A. Current and Droplet Size in the Electrospraying of Liquids. Scaling Laws. *J. Aerosol Sci.* **1997**, *28* (2), 249–275.
(113) Chen, D.; Pui, D. Y. H.; Kaufmar, S. L. ES for Monodisperse Aerosol Generation.Pdf. *J. Aerosol Sci.* **1995**, *26* (6), 963–977.

(114) Gomez, A.; Tang, K. Charge and Fission of Droplets in Electrostatic Sprays. *Phys. Fluids* **1994**, *6* (1), 404–414.
(115) Taflin, D. C.; Ward, T. L.; Davis, E. J. Electrified Droplet Fission and the Rayleigh Limit. *Langmuir* **1989**, *5* (2), 376–384.
(116) Smith, J. N.; Flagan, R. C.; Beauchamp, J. L. Droplet Evaporation and Discharge Dynamics in Electrospray Ionization. *J. Phys. Chem. A* **2002**, *106* (42), 9957–9967.
(117) Grimm, R. L.; Beauchamp, J. L. Evaporation and Discharge Dynamics of Highly Charged Multicomponent Droplets Generated by Electrospray Ionization. *J. Phys. Chem. A* **2010**, *114* (3), 1411–1419.
(118) Liu, Q.; Geng, R.; Zhao, J.; Chen, Q.; Kong, B. Structural and Gel Textural Properties of Soy Protein Isolate When Subjected to Extreme Acid PH-Shifting and Mild Heating Processes. *J. Agric. Food Chem.* **2015**, *63* (19), 4853–4861.
(119) Tehei, M.; Madern, D.; Franzetti, B.; Zaccai, G. Neutron Scattering Reveals the Dynamic Basis of Protein Adaptation to Extreme Temperature. *J. Biol. Chem.* **2005**, *280* (49), 40974–40979.
(120) Palmer, B.; Angus, K.; Taylor, L.; Warwicker, J.; Derrick, J. P. Design of Stability at Extreme Alkaline PH in Streptococcal Protein G. *J. Biotechnol.* **2008**, *134* (3–4), 222–230.
(121) Loh, S. N. The Missing Zinc: P53 Misfolding and Cancer. *Metallomics* **2010**, *2* (7), 442–449.
(122) Blanden, A. R.; Yu, X.; Loh, S. N.; Levine, A. J.; Carpizo, D. R. Reactivating Mutant P53 Using Small Molecules as Zinc Metallochaperones: Awakening a Sleeping Giant in Cancer. *Drug Discov. Today* **2015**, *20* (11), 1391–1397.
(123) Brazier, M. W.; Davies, P.; Player, E.; Marken, F.; Viles, J. H.; Brown, D. R. Manganese Binding to the Prion Protein. *J. Biol. Chem.* **2008**, *283* (19), 12831–12839.
(124) Choi, C. J.; Anantharam, V.; Martin, D. P.; Nicholson, E. M.; Richt, J. A.; Kanthasamy, A.; Kanthasamy, A. G. Manganese Upregulates Cellular Prion Protein and Contributes to Altered Stabilization and Proteolysis: Relevance to Role of Metals in Pathogenesis of Prion Disease. *Toxicol. Sci.* **2010**, *115* (2), 535–546.
(125) Hofmeister, F. Zur Lehre von Der Wirkung Der Salze - Zweite Mittheilung. *Arch. Exp. Pathol. und Pharmakologie* **1888**, *24* (4–5), 247–260.
(126) Wingfield, P. Protein Precipitation Using Ammonium Sulfate. In *Current Protocols in Protein Science*; John Wiley & Sons, Inc.: Hoboken, NJ, USA, 1998; Vol. Appendix 3, p A.3F.1-A.3F.8.
(127) Nall, B. T.; Landers, T. a. Guanidine Hydrochloride Induced Unfolding of Yeast Iso-2 Cytochrome C. *Biochemistry* **1981**, *20* (19), 5403–5411.
(128) Monera, O. D.; Kay, C. M.; Hodges, R. S. Protein Denaturation with Guanidine Hydrochloride or Urea Provides a Different Estimate of Stability Depending on the Contributions of Electrostatic Interactions. *Protein Sci.* **1994**, *3* (11), 1984–1991.
(129) Salis, A.; Cugia, F.; Parsons, D. F.; Ninham, B. W.; Monduzzi, M. Hofmeister Series Reversal for Lysozyme by Change in PH and Salt Concentration: Insights from Electrophoretic Mobility Measurements. *Phys. Chem. Chem. Phys.* **2012**, *14* (13), 4343–4346.
(130) Boström, M.; Tavares, F. W.; Finet, S.; Skouri-Panet, F.; Tardieu, A.; Ninham, B. W. Why Forces between Proteins Follow Different Hofmeister Series for PH above and below PI. *Biophys. Chem.* **2005**, *117* (3), 217–224.

(131) Boström, M.; Parsons, D. F.; Salis, A.; Ninham, B. W.; Monduzzi, M. Possible Origin of the Inverse and Direct Hofmeister Series for Lysozyme at Low and High Salt Concentrations. *Langmuir* **2011**, *27* (15), 9504–9511.
(132) Tadeo, X.; López-Méndez, B.; Castaño, D.; Trigueros, T.; Millet, O. Protein Stabilization and the Hofmeister Effect: The Role of Hydrophobic Solvation. *Biophys. J.* **2009**, *97* (9), 2595–2603.
(133) Hribar, B.; Southall, N. T.; Vlachy, V.; Dill, K. A. How Ions Affect the Structure of Water. *J. Am. Chem. Soc.* **2002**, *124* (41), 12302–12311.
(134) DiTucci, M. J.; Williams, E. R. Nanometer Patterning of Water by Tetraanionic Ferrocyanide Stabilized in Aqueous Nanodrops. *Chem. Sci.* **2017**, *8* (2), 1391–1399.
(135) Cassou, C. A.; Williams, E. R. Anions in Electrothermal Supercharging of Proteins with Electrospray Ionization Follow a Reverse Hofmeister Series. *Anal. Chem.* **2014**, *86* (3), 1640–1647.
(136) Sterling, H. J.; Cassou, C. A.; Trnka, M. J.; Burlingame, A. L.; Krantz, B. A.; Williams, E. R. The Role of Conformational Flexibility on Protein Supercharging in Native Electrospray Ionization. *Phys. Chem. Chem. Phys.* **2011**, *13* (41), 18288–18296.
(137) Sterling, H. J.; Kintzer, A. F.; Feld, G. K.; Cassou, C. A.; Krantz, B. A.; Williams, E. R. Supercharging Protein Complexes from Aqueous Solution Disrupts Their Native Conformations. *J. Am. Soc. Mass Spectrom.* **2012**, *23* (2), 191–200.
(138) Han, L.; Hyung, S. J.; Mayers, J. J. S.; Ruotolo, B. T. Bound Anions Differentially Stabilize Multiprotein Complexes in the Absence of Bulk Solvent. *J. Am. Chem. Soc.* **2011**, *133* (29), 11358–11367.
(139) Han, L.; Hyung, S. J.; Ruotolo, B. T. Dramatically Stabilizing Multiprotein Complex Structure in the Absence of Bulk Water Using Tuned Hofmeister Salts. *Faraday Discuss.* **2013**, *160*, 371–388.
(140) Merenbloom, S. I.; Flick, T. G.; Daly, M. P.; Williams, E. R. Effects of Select Anions from the Hofmeister Series on the Gas-Phase Conformations of Protein Ions Measured with Traveling-Wave Ion Mobility Spectrometry/Mass Spectrometry. *J. Am. Soc. Mass Spectrom.* **2011**, *22* (11), 1978–1990.
(141) Han, L.; Ruotolo, B. T. Hofmeister Salts Recover a Misfolded Multiprotein Complex for Subsequent Structural Measurements in the Gas Phase. *Angew. Chemie Int. Ed.* **2013**, *52* (32), 8329–8332.
(142) Han, L.; Hyung, S.-J.; Ruotolo, B. T. Bound Cations Significantly Stabilize the Structure of Multiprotein Complexes in the Gas Phase. *Angew. Chemie Int. Ed.* **2012**, *51* (23), 5692–5695.
(143) Flick, T. G.; Merenbloom, S. I.; Williams, E. R. Effects of Metal Ion Adduction on the Gas-Phase Conformations of Protein Ions. *J. Am. Soc. Mass Spectrom.* **2013**, *24* (11), 1654–1662.

# Chapter 2

# Hydrogen-Deuterium Exchange of Bradykinin Using Fast Mixing with Theta Emitters and Mass Spectrometry: Structural Information from Fast Exchanging (Non-amide) Sites

## 2.1 Abstract

Hydrogen-deuterium exchange (H/D exchange) is a common technique to study protein structure, interaction, and dynamics in solution. Typical H/D exchange experiments focus on protein backbone amide hydrogens that take minutes to hours to exchange. Hydrogens located at the polar amino acid side chain and C- and N- terminals have fast exchange rate in the timeframe of seconds and sub-seconds. Studying fast H/D exchange can provide extra structural information about proteins. In this study, fast H/D exchange of bradykinin and bradykinin methyl ester is investigated using theta emitters that produce droplets with a lifetime of ~40 μs and ~100 μs coupled with mass spectrometry. Fewer than one hydrogen per peptide goes through the exchange within the mixing time because of the gas-phase back exchange and short droplet lifetimes. At pH = 2.8, both bradykinin and bradykinin methyl ester have on average ~0.2 hydrogens per peptide exchanged during the ~100 μs droplet lifetime. However, increasing the solution pH to 7.6, bradykinin methyl ester has double amount of hydrogen exchanged than bradykinin in the same solution, although bradykinin methyl ester has one fewer exchangeable hydrogen. This result indicates the existence of salt bridge between deprotonated C- terminal and the protonated amine group of bradykinin in solution. Although theta emitters are not efficient enough to observe a large extent of fast H/D exchange, this study shows an application of fast H/D exchange coupled with mass spectrometry and the first experimental evidence of bradykinin salt bridge in solution.

## 2.2 Introduction

Hydrogen-deuterium exchange (H/D exchange) is a powerful technique to study the structure, dynamic information, and intermolecular interaction interface of biological molecules ranging from small peptides to large macromolecule complexes.[1–6] For example, H/D exchange can be used to map protein secondary and tertiary structures with a known sequence.[7–9] It can also be used to monitor the conformational changes of protein or protein complexes with changing conditions or time.[10–12] The common H/D exchange technique for peptides and proteins monitors the H/D exchange rate of backbone amide hydrogens.[13–15] The intrinsic exchange timeframe measured using NMR for backbone amid hydrogens in dipeptides is ranging from ~10 milliseconds to ~1000 milliseconds, depending on the sequences and solution conditions.[16] These hydrogens in peptides and proteins that have a defined structure can require much longer to go through exchange, ranging from seconds to hours. The H/D exchange rates of backbone amide

hydrogens depend on many factors, including solution pH, ionic strength, the accessibility to the solvent, and interactions between amino acids.[6,16–19] In contrast, some hydrogens, such as the hydrogens on α-carbons and in the carbohydrate groups, have too slow of an exchange rate in the range of days, which is not useful in practice.[20] Hydrogens located in the hydroxy and amine groups have too fast exchange rates in the timeframe of seconds and sub-seconds, which is also difficult to be captured using standard techniques due to the rapid exchange rates.[17,18,21] Previous NMR study showed that single amino acid (His, Cys, Thr, Ser, Arg, Lys, and Tyr) with N- and C-terminals capped with acetyl and methyl groups has an H/D exchange rate approximately 700 $s^{-1}$ to 5000 $s^{-1}$, corresponding to mixing times of 200 μs to 1.4 ms, depending on the identity of amino acid at pH 7 and 36 °C.[18] For example, the two-dimensional nuclear Overhauser effect spectroscopy (NOESY) experiment determines 20 mM acetyl-lysine-$NH_2$ has an intrinsic exchange rate 4000 $s^{-1}$ in 80 mM sodium phosphate at pH 7.0 and 36 °C. These rates also depend on pH and temperature.[18]

Measuring amino acid side-chain H/D exchange rate may provide complementary structural information in solution, such as hydrogen bonds and interaction with bound water. The amino acid side-chain H/D exchange studies were pioneered with 2D NMR.[16,22,23] For example, in 1998, Klevit et al. reported side-chain H/D exchange rate for Gln and Asn in the millisecond timeframe in a small *E. coli.* protein (9 kDa), which was the first report of side chain H/D exchange rate in a protein. The study confirmed a hydrogen bond interaction involving Gln51 of the protein that was observed in X-ray structure.[23] Mass spectrometry can also be used as a detector to study fast H/D exchange rate. Mass spectrometry has the advantages that it requires lower sample concentration and sample consumption than NMR due to the high sensitivity and rapid detection of mass spectrometry.[3,11,24,25] Fast H/D exchange coupled with mass spectrometry was initially observed through a reaction with $ND_3$ in the gas phase in a timeframe of sub-milliseconds to milliseconds.[26–28] However, the fast H/D exchange of small molecules and peptides in solution coupled with mass spectrometry has not been reported until the use of the theta emitters[29,30] and microdroplet fusion.[31]

Theta emitters are named after Greek letter θ because of the shape of the emitter's opening. A glass wall divides a theta emitter to two separate barrels that allow two different solutions to be loaded. Solution mixing occurs after voltage is applied to both solution and electrospray ionization is initiated. One of the major advantages of theta emitters is that the lifetimes of droplets produced with these emitters can be controlled and readily characterized. Solution flow rates affect the droplet lifetimes produced by the theta emitters and can be varied by changing emitter diameter, backing pressure, electrospray ionization voltage, and solution composition. The distance between the emitter and the instrument entrance can also affect droplet lifetimes.[29,32–36] The lifetimes of nanodrops produced by theta emitters have been measured using two different methods. In one method, unimolecular reaction of protein folding is measured for proteins that have well-characterized folding time constants. The droplet lifetime is determined based on the extent of protein folding that occurs prior to desolvation and ion formation. The extent of folding is monitored from the resulting charge-state distributions and ion mobility spectrometry.[32–36] In the other method, the velocity of droplets are measured optically using a CCD camera.[29] Droplet desolvation and ion formation is assumed to occur at the entrance of the mass spectrometer.[29] Despite the different methodology and assumptions in these methods, similar droplet lifetimes have been reported from experiments done under similar conditions. Theta emitters with diameters from ~250 nm to ~4.5 μm have been characterized with various backing pressures and electric fields between emitters and instrument entrance.[36] Droplet lifetimes ranging from ~1 μs to hundreds of microseconds have been reported.[29,32–36] In comparison, the fastest timeframe for a

conventional mixer coupled with mass spectrometry is 200 μs achieved with a laminar flow mixer with a flow rate of 10 μL/s.[37] Mixing with theta emitters is much faster, and ~1 μs mixing time is the fastest so far that can be achieved in any mixing apparatus and has the advantage that a mass spectrometer is used as a detector.

In this study, a fast H/D exchange in solution of bradykinin (BK) and its methyl ester (BKME) form is studied using theta emitters coupled with mass spectrometry. Measurable exchange occurs for nanodrops with 100 μs lifetimes, which makes possible deduction of structural information of the peptide bradykinin. These results obtained at different pH values reveals a salt bridge structure of bradykinin has been reported in the gas phase, but this is the first report that indicates a salt bridge structure in solution at neutral pH. These results demonstrate the advantages of probing structures of biomolecules from non-amide HDX.

## 2.3 Experimental Method

Mass spectra were obtained using a Berkeley-Bruker 9.4 T Fourier Transform ion cyclotron resonance (FT-ICR) mass spectrometer as well as a commercial 7.0 T LTQ-FT-ICR hybrid mass spectrometer (Thermo Fischer Scientific, Waltham, MA, USA). Theta glass emitters with inner diameters of 1.7 ± 0.1 μm and 4.5 ± 0.2 μm were pulled from borosilicate theta glass capillary (1.50 mm o.d./1.17 mm i.d., Sutter Instruments, Novato, CA, USA) using a model P-87 flaming/brown tip puller (Sutter Instruments, Novato, CA, USA) and the tip diameters were measured using a TM-1000 scanning electron microscope (Hitachi High-Technologies Co, Tokyo, Japan). Two platinum wires were inserted into the two barrels of the theta tip emitter and are in contact with the solution. The emitter tip is positioned approximately 1 to 2 mm away from instrument entrance. Electrospray ionization was initiated by applying ~ 700 V to 1 kV to the wire relative to the instrument potential. 99.9% $D_2O$ was micro sprayed for two hours at 3 μL/min on the Thermal LTQ instrument, then sheath gas was applied on LTQ-FT-ICR to reduce gas-phase back exchange when spraying from $D_2O$. A nitrogen backing pressures at 40 psi and 10 psi were applied to theta emitter with a diameter of 1.7 μm and 4.5 μm, respectively.

Leucine enkephalin or methionine enkephalin were added to the two separate solutions in order to monitor the relative flow rates of solution from the two separate channels during theta tip mixing experiments. The isotopic distribution of the peptide ions was deconvoluted to eliminate carbon, nitrogen, and oxygen isotopic effect by subtracting experimental isotopic distribution from mass spectra of the peptide in water. The centroid C of the deconvoluted isotope distribution was calculated using equation 1:

$$C = \frac{\sum_i (m/z)_i I_i}{\sum_i I_i} \qquad \text{(Eq.1)}$$

where $I_i$ is the relative abundance of $(m/z)_i$. The average difference between deuteration levels of a peptide was defined as the difference between the centroid *C*. The reported uncertainty corresponds to one standard deviation of triplicate measurements.

Bradykinin, leucine enkephalin, methionine enkephalin, cytochrome *c*, ammonium bicarbonate, $D_2O$ (99.9 atom %D), acetic acid, methanol, sulfuric acid was purchased from Sigma (St. Louis, MO, USA) and used without further purification. 1 M bradykinin methyl ester stock solution was made by dissolving a suitable amount of BKN in methanol with 0.5% sulfuric acid and allowing the reaction to happen at room temperature for 24 hours as described before.[38]

## 2.4 Results and Discussion

### 2.4.1 Droplet Lifetimes

The lifetimes of nanodrops produced by electrospray ionization depend on several factors, including the initial droplet size which can be varied by changing emitter tip size or flow rates using a backing pressure. The lifetimes of nanodrops produced by theta emitters can range from ~1 μs to ~100 μs for emitters that have inner diameters between 244 nm and ~4.5 μm using backing pressures between 5 psi and 40 psi.[32–34,36] Larger nanodrops produced by emitters with large diameter tips can enter the interface of the mass spectrometer where they can be thermally heated so lifetimes can depend on instrumental conditions.[36] The lifetimes of the largest nanodrops produced in this study were invested under conditions of the H/D experiments. The droplet lifetimes are determined by measuring the extent of folding that occurs in nanodrops for proteins with well characterized folding time constants. In these experiments, an acid denatured protein solution in one barrel of the theta glass emitter is mixed with either pure water or a buffered solution in the other barrel during the electrospray ionization process to induce folding as a result of a pH jump upon solution mixing.[32–34,36] To determine whether the interface conditions affect droplet lifetimes in these experiments, the droplet lifetimes of theta emitters with an inner diameter of ~4.5 μm measured previously on a different instrument were measured here.

Cytochrome *c* does not have a well-defined structure in water at pH ≤ 2 but has a folded structure between pH 3 and 7.[39,40] The charge-state distribution of cytochrome *c* produced from an aqueous solution with 1% acetic acid (pH = 2.8) is trimodal with distributions centered around 9+, 12+, and 17+, indicating the protein adopts conformations with various extents of unfolded structure at this pH (Figure 2.1a). The abundance of folded structures is estimated from the sum of ion abundances of the 6+ to 9+ charge states and corresponds to 36% ± 2% of the population. The population of folded form of the protein increases to 92% ±1% (Figure 2.1b) when this solution is mixed 50/50 with pure water (0.5% acetic acid; pH = 3.0) and is allowed to come to equilibrium. Results from fast mixing experiments of the initial 1% acetic acid solution with water using 1.7 μm theta emitters with a backing pressure of 40 psi and 4.5 μm theta emitters with a backing pressure of 10 psi are shown in Figures 2.2c and 2.2d, respectively. In these mixing experiments, the fraction of folded protein is 68% ± 2% and 80% ± 8%, respectively. These values are lower than the equilibrium value of 92% ±1%, indicating that equilibrium is not established during the nanodrop lifetime in these mixing experiments. The droplet lifetimes are determined using equation 2:

$$t = \tau \times \ln \frac{A_e - A_0}{A_e - A_t} \qquad \text{(Eq.2)}$$

where t is the droplet lifetime, τ is the folding time constant of the protein. $A_e$, $A_0$, and $A_t$ are the abundances of the folded protein at equilibrium, time zero and time *t,* respectively. The folding time constant, τ, of cytochrome *c* in 50 mM sodium acetate and 50 mM sodium phosphate is 57 μs.[40] Using this time constant, nanodrop lifetimes of 38 ± 2 μs and 101 ± 36 μs are obtained from the 1.7 μm and 4.5 μm theta emitters under these conditions. Protein folding time constants depend on many factors, including solution composition and ionic strength. The evaporation of the droplets can lead to a pH change, which further increase the uncertainty of the nanodrop lifetimes determined from these experiments.[41] Previous studies done in 100 mM ammonium acetate vs. water indicate that the folding time constant in water is effectively half of that in ammonium

acetate.[32–34,36] The 38 ± 2 μs lifetime for nanodrops produced by the 1.7 μm theta emitters is approximately doubled the droplet lifetime of 22 ± 4 μs obtained from ammonium acetate solutions,[33,34] consistent with the effect of ionic strength on the folding time constant. For the 4.5 μm theta emitters, the estimated droplet lifetime is 101 ± 36 μs, consistent with the droplet lifetime obtained on another instrument, indicating that the droplet lifetimes can be consistent between instruments when low activation conditions are used.[36]

### 2.4.2 Hydrogen-Deuterium Exchange with Theta Emitters

In order to explore the application of theta emitters in fast hydrogen-deuterium exchange, a short peptide, bradykinin (BK: RPPGFSPFR), was chosen because the structure of this small peptide has been extensively studied both in solution as well as the gas phase. $(BK + 2H)^{2+}$ has 19 exchangeable hydrogen atoms. There are five amide hydrogen atoms and ten exchangeable hydrogen atoms associated with protonated arginine side changes. These types of hydrogen atoms undergo slow exchange at neutral pH at room temperature on the time scale ranging from100 ms to hours in solution. The remaining four hydrogen atoms at the N- and C-terminus as well as the serine side chain can exchange more quickly and may be possible to monitor in these experiments.

Partial mass spectra around the molecular ion region of BK obtained from solution consisting of $H_2O$ and 1:1 mixture of $H_2O$ and 99.9% $D_2O$, are shown in Figure 2.3a and 2.3b, respectively. A low abundance (< 5%) of a sodium adducted molecular ion is also observed. The average mass of $(BK + 2H/D)^{2+}$ is 7.7 ± 0.1 Da higher when these ions are produced from the equal mixture of deuterated and undeuterated water. This extent of exchange is lower than 19/2 = 9.5 corresponding to half of the exchangeable sites, a result consistent with some back exchange occurring in the source. The mass spectrum of BK in 99.9% $D_2O$ is centered at a mass corresponding to 16 exchanges (Figure 2.4b). There are no ions corresponding to fully deuterated BK identified in the mass spectrum (Figure 2.4b), consistent with some gas-phase back exchange that occurs prior to ion detection.

The extent of H/D exchange is very low when these solutions are mixed using 1.7 μm emitters (Figure 2.3c). The extent of exchange corresponds to less than 0.1 hydrogen atoms indicating that a 40 μs nanodrop lifetime is too short to allow for meaningful H/D exchange. In contrast, the extent of exchange increases to 0.26 ±0.12 with 4.5 μm emitters, which produces nanodrops with 100 μs lifetime (Figure 2.3d). This corresponds to less than 4% of the equilibrium H/D exchange value. There is more sodium adduction on the peptide with the 4.5 μm emitters than that with a 1.7 μm emitters, consistent with previous observations of lower sodium adduction with smaller emitter size.

Fast H/D exchange measurements of BK have also been reported from microdroplet fusion experiments where a 0.5 Da mass shift was reported for a reaction time of 15 μs. This exchange rate is much faster than what we report here.[31] This discrepancy may be due to differences in estimated droplet lifetimes in these two experiments. An initial droplet diameter around 13 μm was reported in the microdroplet fusion experiments. The initial droplet size generated from theta emitters is estimated to be 1/14 to 1/20 of the diameter of emitters based on prior experiments on extents of sodium adduction with emitter tip size and ion mobility results from polymer containing solutions.[42,43] Thus, the microdroplets are approximately two order of magnitude larger than the ones produced from theta emitter. The microdroplet fusion experiment measures the droplet lifetime assuming that the desolvated ions are formed at the entrance of the instrument.[31] Given the size of the initial droplets, this assumption may not be correct. In a different

study of fast H/D exchange done with 4 μm theta emitters of angiotensin I (2+ charge state), which has a similar size of BK, the extent of fast H/D exchange observed with a droplet lifetime of 133 μs is comparable with the results observed in this study.[29]

### 2.4.3 Effects of Instrument source designs on the Extent of Gas-Phase Back Exchange

In order to evaluate the extent to which different instrument source affect the extent of gas-phase back exchange, a mass spectrum from fully exchanged BK was measured using a Thermo LTQ instrument. The mass spectra of bradykinin from undeuterated water are nearly identical with the two instruments (Figure 2.4a and c). The extent of exchanged sites observed for the fully deuterated sample differs between the two instruments. With the Thermo LTQ instrument, the isotopic distribution is centered around 18 exchanges with ~16% of population corresponding to all 19 sites are exchanged (Figure 2.4d). In comparison, the isotopic distribution is centered around 16 exchanges with no fully deuterated species with the 9.4 T FT-ICR instrument (Figure 2.4c). The results obtained on the Thermo LTQ instrument show much less gas-phase back exchange than the 9.4 T FT-ICR instrument. Thus, less back exchange is observed with the Thermal LTQ instrument. This is likely because of the chamber in this instrument that was exchanged by spraying $D_2O$ solution at a flow rate of 3 μL/min for two hours prior to these experiments. In contrast, 9.4 T FT-ICR instrument has an open instrument source.

### 2.4.4 Effects of pH on Side Chain H/D Exchange

Effects of pH on the exchange rates of amide backbone hydrogen atoms in peptides and proteins have been extensively investigated. In contrast, less is known about how pH affects exchange rates of amino acid side chains with fast exchanging hydrogen atoms. The exchange rates for bradykinin and its methyl ester were investigated at two different pH values of 2.8 (acidified with trace sulfuric acid) and 7.6 (10 mM ammonium bicarbonate) using 4.5 μm theta tip emitters that produces nanodrops with100 μs lifetimes. Partial mass spectra of BK and bradykinin methyl ester (BKME) from aqueous solutions at these two pHs are shown in Figure 2.5a and 2.5b. A 1:1 premixed solution with 99.9% $D_2O$ results in both a broadening in the distribution and shift in the distribution to higher mass. The median of the distribution is shifts by 7.6 ± 0.1 Da and 8.0 ± 0.1 Da at pH = 2.8 (Figure 2.5b) and by 7.4 ±0.2 Da and 7.8 ±0.2 Da at pH = 7.6 (Figure 2.5e) for BK and BKME, respectively. When the BK and BKME in water are mixed with deuterated water with 4.5 μm theta emitters, only a small extent of H/D exchange occurs. At pH = 2.8, 0.22 ±0.11 and 0.24 ± 0.05 hydrogen atoms are exchanged (Figure 2.5c) wheras 0.38 ±0.1 and 0.78 ±0.12 hydrogen atoms are exchanged at pH = 7.6 (Figure 2.5f) for BK and BKME, respectively.

The rate of backbone amide hydrogen exchange is several orders of magnitude faster at pH = 7.6 than it is at pH = 2.8.[16] In contrast, these rates differ by less than a factor of three in these rapid mixing experiments. The hydrogen atoms of the arginine side chain have the lowest H/D exchange rate around pH 4 (less than 0.1 $s^{-1}$ at 25 °C) and values of ~1 $s^{-1}$ and 10 $s^{-1}$ at pH = 3 and 7, respectively at 25 °C.[18] These rates are all to small to produce measurable exchange on the time scale of these mixing experiments. Serine has an H/D exchange rate around 900 $s^{-1}$ at 36 °C at pH 7, and lowering solution pH will increase this rate. Because the exchange rates depend both on pH and on temperature and because it is difficult to know for sure the exact temperature of these ESI droplets, it is difficult to predict the exchange rates for BK and BKME on this time scale.

### 2.4.5 Structure of BK in solution

It is interesting that the total exchange in BK and BKME at the equilibrium studies is nearly the same at both pH values even though BKME has one less exchangeable hydrogen atom at the C-terminus. In the mixing experiments, the extents of exchange are also the same at pH = 2.8 (Figure 2.5c with 0.22 ± 0.11 and 0.24 ± 0.05 exchanges for BK and BKME, respectively). In contrast, the exchange rates for these two molecules differ at pH = 7.6 (Figure 2.5f with 0.38 ± 0.11 and 0.78 ± 0.12 exchanges for BK and BKME, respectively). Thus, the exchange rate of BKME is about twice that of BK at the higher pH. This difference in the exchange rate must be due to the acidic hydrogen atom at the C-terminus of BK but not in BKME. The pI value for the C-terminus of individual amino acids ranges from 1.6 to 2.4, but this value for peptides and proteins depends on the sequence and structure.[44,45] Pace et al. showed that the pI value of the C-terminus for 22 proteins ranges from 2.4 to 5.9, with an average of 3.3.[46] The pI value of the C-terminus in BK was estimated using PROPKA simulations[47–49] to be 3.3 and 3.4 for a fully extended and more compact conformation containing a beta-turn that is known to exist in solution,[50] respectively. At pH = 2.8, the C-terminus in BK should be predominantly protonated, whereas at pH = 7.6, it should be deprotonated where it could form a salt-bridge with the positively charged N-terminus or the protonated side chains of arginine.

In the gas phase, singly and doubly protonated bradykinin has a structure in which there is a salt bridge between the deprotonated C-terminus and protonated arginine residues.[26,38,51,52] Molecular dynamic simulation suggests that a salt bridge structure may also exist in the solution.[53] Experimental evidence from NMR and rotating frame nuclear Overhauser spectroscopy showed the interaction between the protonated guanidine group of Arg and the deprotonated C-terminus of the C-terminal peptide (SPFR) of bradykinin in solution and the interaction is strongly dependent on pH.[5] However, the existence of a salt bridge in the intact bradykinin has not been shown experimentally before at our best knowledge.

## 2.5 Conclusion

Theta glass electrospray emitters were used to rapidly mix aqueous solutions containing peptides with $D_2O$ in order to measure the extent of exchange that occurs during droplet lifetime of ~40 μs and ~100 μs. Little measurable exchange occurs for bradykinin or bradykinin methyl ester on the shorter time frame, but pH dependent differences in exchange are observed for these two peptides at ~100 μs. At pH = 2.8, the total extent of H/D exchange is essentially the same for these two peptides, but the H/D exchange rate of BKME is double that of BK at pH = 7.6. These results suggest that there is a salt bridge between the deprotonated C-terminal of BK and protonated N-terminal or guanidine group of arginine. To the best of our knowledge, this is the first experimental evidence of a salt bridge structure of bradykinin in water. This illustrates the advantage of using non amine H/D exchange for determining information about peptide and potentially protein structure. The rates of exchange for the peptides investigated are slow even on the 100 μs time scale. This suggests that more conventional mixing apparatus, such as laminar flow mixers that can access 100s of microseconds and longer time frames may be better suited to monitoring side-chain exchange in larger proteins.

## 2.6 Acknowledgments

This material is based upon work supported by the National Science Foundation Division of Chemistry under grant number CHE-1609866. The authors also thank Dr. Daniel Mortensen, Dr. Anna Susa, and Dr. Anthony Iavarone for helpful discussion.

## 2.7 References

(1) Englander, S. W.; Kallenbach, N. R. Hydrogen Exchange and Structural Dynamics of Proteins and Nucleic Acids. *Q. Rev. Biophys.* **1983**, *16* (4), 521–655.
(2) Czerski, L.; Vinogradova, O.; Sanders, C. R. NMR-Based Amide Hydrogen-Deuterium Exchange Measurements for Complex Membrane Proteins: Development and Critical Evaluation. *J. Magn. Reson.* **2000**, *142* (1), 111–119.
(3) Wales, T. E.; Engen, J. R. Hydrogen Exchange Mass Spectrometry for the Analysis of Protein Dynamics. *Mass Spectrom. Rev.* **2006**, *25* (1), 158–170.
(4) Konermann, L.; Tong, X.; Pan, Y. Protein Structure and Dynamics Studied by Mass Spectrometry: H/D Exchange, Hydroxyl Radical Labeling, and Related Approaches. *J. Mass Spectrom.* **2008**, *43* (8), 1021–1036.
(5) Otter, A.; Scott, P. G.; Cann, J. R.; Vavrek, R. J.; Stewart, J. M.; Kotovych, G. High-Field NMR and Circular Dichroism Solvent-Dependent Conformational Studies of the Bradykinin C-Terminal Tetrapeptide Ser-Pro-Phe-Arg. *J. Biomol. Struct. Dyn.* **1988**, *6* (3), 609–625.
(6) Engen, J. R.; Smith, D. L. Investigating Protein Structure and Dynamics by Hydrogen Exchange MS. *Anal. Chem.* **2001**, *73* (9), 256A-265A.
(7) Pan, J.; Han, J.; Borchers, C. H.; Konermann, L. Electron Capture Dissociation of Electrosprayed Protein Ions for Spatially Resolved Hydrogen Exchange Measurements. *J. Am. Chem. Soc.* **2008**, *130* (35), 11574–11575.
(8) Raschke, T. M.; Marqusee, S. Hydrogen Exchange Studies of Protein Structure. *Curr. Opin. Biotechnol.* **1998**, *9* (1), 80–86.
(9) Rand, K. D. Pinpointing Changes in Higher-Order Protein Structure by Hydrogen/Deuterium Exchange Coupled to Electron Transfer Dissociation Mass Spectrometry. *Int. J. Mass Spectrom.* **2013**, *338*, 2–10.
(10) Uzawa, T.; Nishimura, C.; Akiyama, S.; Ishimori, K.; Takahashi, S.; Dyson, H. J.; Wright, P. E. Hierarchical Folding Mechanism of Apomyoglobin Revealed by Ultra-Fast H/D Exchange Coupled with 2D NMR. *Proc. Natl. Acad. Sci.* **2008**, *105* (37), 13859–13864.
(11) Demmers, J. A.; Haverkamp, J.; Heck, A. J.; Koeppe, R. E.; Killian, J. A. Electrospray Ionization Mass Spectrometry as a Tool to Analyze Hydrogen/Deuterium Exchange Kinetics of Transmembrane Peptides in Lipid Bilayers. *Proc.Natl.Acad.Sci.U.S.A* **2000**, *97* (7), 3189–3194.
(12) Going, C. C.; Xia, Z.; Williams, E. R. Real-Time HD Exchange Kinetics of Proteins from Buffered Aqueous Solution with Electrothermal Supercharging and Top-Down Tandem Mass Spectrometry. *J. Am. Soc. Mass Spectrom.* **2016**, *27* (6), 1019–1027.
(13) Hvidt, A.; Nielsen, S. O. Hydrogen Exchange in Protein. *Adv. Protein Chem.* **1966**, *21*, 287–386.

(14) Engen, J. R. Analysis of Protein Conformation and Dynamics by Hydrogen/Deuterium Exchange MS. *Anal. Chem.* **2009**, *81* (19), 7870–7875.
(15) Konermann, L.; Pan, J.; Liu, Y.-H. Hydrogen Exchange Mass Spectrometry for Studying Protein Structure and Dynamics. *Chem. Soc. Rev.* **2011**, *40* (3), 1224–1234.
(16) Bai, Y.; Milne, J. S.; Mayne, L.; Englander, S. W. Primary Structure Effects on Peptide Group Hydrogen Exchange. *Proteins Struct. Funct. Genet.* **1993**, *17* (1), 75–86.
(17) Englander, S. W. Hydrogen Exchange and Mass Spectrometry: A Historical Perspective. *J. Am. Soc. Mass Spectrom.* **2006**, *17* (11), 1481–1489.
(18) Liepinsh, E.; Otting, G. Proton Exchange Rates from Amino Acid Side Chains--Implications for Image Contrast. *Magn. Reson. Med.* **1996**, *35* (1), 30–42.
(19) Englander, S. W.; Sosnick, T. R.; Englander, J. J.; Mayne, L. Mechanisms and Uses of Hydrogen Exchange. *Curr. Opin. Struct. Biol.* **1996**, *6* (1), 18–23.
(20) Kostyukevich, Y.; Acter, T.; Zherebker, A.; Ahmed, A.; Kim, S.; Nikolaev, E. Hydrogen/Deuterium Exchange in Mass Spectrometry. *Mass Spectrom. Rev.* **2018**, *37* (6), 811–853.
(21) Zhou, B.; Zhang, Z.-Y. Application of Hydrogen/Deuterium Exchange Mass Spectrometry to Study Protein Tyrosine Phosphatase Dynamics, Ligand Binding, and Substrate Specificity. *Methods* **2007**, *42* (3), 227–233.
(22) Krishna, N. R.; Sarathy, K. P.; Huang, D. H.; Stephens, R. L.; Glickson, J. D.; Smith, C. W.; Walter, R. Primary Amide Hydrogen Exchange in Model Amino Acids: Asparagine, Glutamine, and Glycine Amides. *J. Am. Chem. Soc.* **1982**, *104* (19), 5051–5053.
(23) Rajagopal, P.; Jones, B. E.; Klevit, R. E. Solvent Exchange Rates of Side-Chain Amide Protons in Proteins. *J. Biomol. NMR* **1998**, *11* (2), 205–212.
(24) Chalmers, M. J.; Busby, S. A.; Pascal, B. D.; He, Y.; Hendrickson, C. L.; Marshall, A. G.; Griffin, P. R. Probing Protein Ligand Interactions by Automated Hydrogen/Deuterium Exchange Mass Spectrometry. *Anal. Chem.* **2006**, *78* (4), 1005–1014.
(25) Balasubramaniam, D.; Komives, E. A. Hydrogen-Exchange Mass Spectrometry for the Study of Intrinsic Disorder in Proteins. *Biochim. Biophys. Acta - Proteins Proteomics* **2013**, *1834* (6), 1202–1209.
(26) Lifshitz, C. A Review of Gas-Phase H/D Exchange Experiments: The Protonated Arginine Dimer and Bradykinin Nonapeptide Systems. *Int. J. Mass Spectrom.* **2004**, *234* (1–3), 63–70.
(27) Rožman, M. The Gas-Phase H/D Exchange Mechanism of Protonated Amino Acids. *J. Am. Soc. Mass Spectrom.* **2005**, *16* (11), 1846–1852.
(28) Mistarz, U. H.; Brown, J. M.; Haselmann, K. F.; Rand, K. D. Probing the Binding Interfaces of Protein Complexes Using Gas-Phase H/D Exchange Mass Spectrometry. *Structure* **2016**, *24* (2), 310–318.
(29) Jansson, E. T.; Lai, Y.-H.; Santiago, J. G.; Zare, R. N. Rapid Hydrogen-Deuterium Exchange in Liquid Droplets. *J. Am. Chem. Soc.* **2017**, *139* (20), 6851–6854.
(30) Mark, L. P.; Gill, M. C.; Mahut, M.; Derrick, P. J. Dual Nano-Electrospray for Probing Solution Interactions and Fast Reactions of Complex Biomolecules. *Eur. J. Mass Spectrom.* **2012**, *18* (5), 439–446.
(31) Lee, J. K.; Kim, S.; Nam, H. G.; Zare, R. N. Microdroplet Fusion Mass Spectrometry for Fast Reaction Kinetics. *Proc. Natl. Acad. Sci.* **2015**, *112* (13), 201503689.
(32) Mortensen, D. N.; Williams, E. R. Theta-Glass Capillaries in Electrospray Ionization: Rapid Mixing and Short Droplet Lifetimes. *Anal. Chem.* **2014**, *86* (18), 9315–9321.

(33) Mortensen, D. N.; Williams, E. R. Ultrafast (1 Ms) Mixing and Fast Protein Folding in Nanodrops Monitored by Mass Spectrometry. *J. Am. Chem. Soc.* **2016**, *138* (10), 3453–3460.
(34) Mortensen, D. N.; Williams, E. R. Investigating Protein Folding and Unfolding in Electrospray Nanodrops Upon Rapid Mixing Using Theta-Glass Emitters. *Anal. Chem.* **2015**, *87* (2), 1281–1287.
(35) Mortensen, D. N.; Williams, E. R. Microsecond and Nanosecond Polyproline II Helix Formation in Aqueous Nanodrops Measured by Mass Spectrometry. *Chem. Commun.* **2016**, *52*, 12218–12221.
(36) Xia, Z.; Williams, E. R. Effect of Droplet Lifetime on Where Ions Are Formed in Electrospray Ionization. *Analyst* **2019**, *144* (1), 237–248.
(37) Vahidi, S.; Stocks, B. B.; Liaghati-Mobarhan, Y.; Konermann, L. Submillisecond Protein Folding Events Monitored by Rapid Mixing and Mass Spectrometry-Based Oxidative Labeling. *Anal. Chem.* **2013**, *85* (18), 8618–8625.
(38) Schnier, P. D.; Price, W. D.; Jockusch, R. A.; Williams, E. R. Blackbody Infrared Radiative Dissociation of Bradykinin and Its Analogues: Energetics, Dynamics, and Evidence for Salt-Bridge Structures in the Gas Phase. *J. Am. Chem. Soc.* **1996**, *118* (30), 7178–7189.
(39) Konno, T. Conformational Diversity of Acid-Denatured Cytochrome c Studied by a Matrix Analysis of Far-UV CD Spectra. *Protein Sci.* **1998**, *7* (4), 975–982.
(40) Shastry, M. C. C.; Luck, S. D.; Roder, H. A Continuous-Flow Capillary Mixing Method to Monitor Reactions on the Microsecond Time Scale. *Biophys. J.* **1998**, *74* (5), 2714–2721.
(41) Zhou, S.; Prebyl, B. S.; Cook, K. D. Profiling PH Changes in the Electrospray Plume. *Anal. Chem.* **2002**, *74* (19), 4885–4888.
(42) Susa, A. C.; Xia, Z.; Williams, E. R. Small Emitter Tips for Native Mass Spectrometry of Proteins and Protein Complexes from Nonvolatile Buffers That Mimic the Intracellular Environment. *Anal. Chem.* **2017**, *89* (5), 3116–3122.
(43) Davidson, K. L.; Oberreit, D. R.; Hogan, C. J.; Bush, M. F. Nonspecific Aggregation in Native Electrokinetic Nanoelectrospray Ionization. *Int. J. Mass Spectrom.* **2017**, *420*, 35–42.
(44) Forsyth, W. R.; Antosiewicz, J. M.; Robertson, A. D. Empirical Relationships between Protein Structure and Carboxyl PKa Values in Proteins. *Proteins Struct. Funct. Genet.* **2002**, *48* (2), 388–403.
(45) Quijada, J.; López, G.; Versace, R.; Ramírez, L.; Tasayco, M. L. On the NMR Analysis of PKa Values in the Unfolded State of Proteins by Extrapolation to Zero Denaturant. *Biophys. Chem.* **2007**, *129* (2–3), 242–250.
(46) Grimsley, G. R.; Scholtz, J. M.; Pace, C. N. A Summary of the Measured PK Values of the Ionizable Groups in Folded Proteins. *Protein Sci.* **2009**, *18* (1), 247–251.
(47) Søndergaard, C. R.; Olsson, M. H. M.; Rostkowski, M.; Jensen, J. H. Improved Treatment of Ligands and Coupling Effects in Empirical Calculation and Rationalization of p K a Values. *J. Chem. Theory Comput.* **2011**, *7* (7), 2284–2295.
(48) Olsson, M. H. M.; Søndergaard, C. R.; Rostkowski, M.; Jensen, J. H. PROPKA3: Consistent Treatment of Internal and Surface Residues in Empirical PKa Predictions BT - Journal of Chemical Theory and Computation. *J. Chem. Theory Comput.* **2011**, *7* (2), 525–537.

(49) Dolinsky, T. J.; Nielsen, J. E.; McCammon, J. A.; Baker, N. A. PDB2PQR: An Automated Pipeline for the Setup of Poisson-Boltzmann Electrostatics Calculations. *Nucleic Acids Res.* **2004**, *32* (WEB SERVER ISS.), 665–667.
(50) Cann, J. R.; London, R. E.; Unkefer, C. J. CD-NMR Study of the Solution Conformation of Bradykinin Analogs Containing a-Aminoisobutyric Acid. *Int. J. Pept. Protein Res.* **1987**, *29* (1), 486–496.
(51) Wyttenbach, T.; Bowers, M. T. Gas Phase Conformations of Biological Molecules: The Hydrogen/Deuterium Exchange Mechanism. *J. Am. Soc. Mass Spectrom.* **1999**, *10* (1), 9–14.
(52) Rodriquez, C. F.; Orlova, G.; Guo, Y.; Li, X.; Siu, C. K.; Hopkinson, A. C.; Siu, K. W. M. Gaseous Bradykinin and Its Singly, Doubly, and Triply Protonated Forms: A First-Principles Study. *J. Phys. Chem. B* **2006**, *110* (14), 7528–7537.
(53) Pierson, N. A.; Chen, L.; Valentine, S. J.; Russell, D. H.; Clemmer, D. E. Number of Solution States of Bradykinin from Ion Mobility and Mass Spectrometry Measurements. *J. Am. Chem. Soc.* **2011**, *133* (35), 13810–13813.

## 2.8 Figures

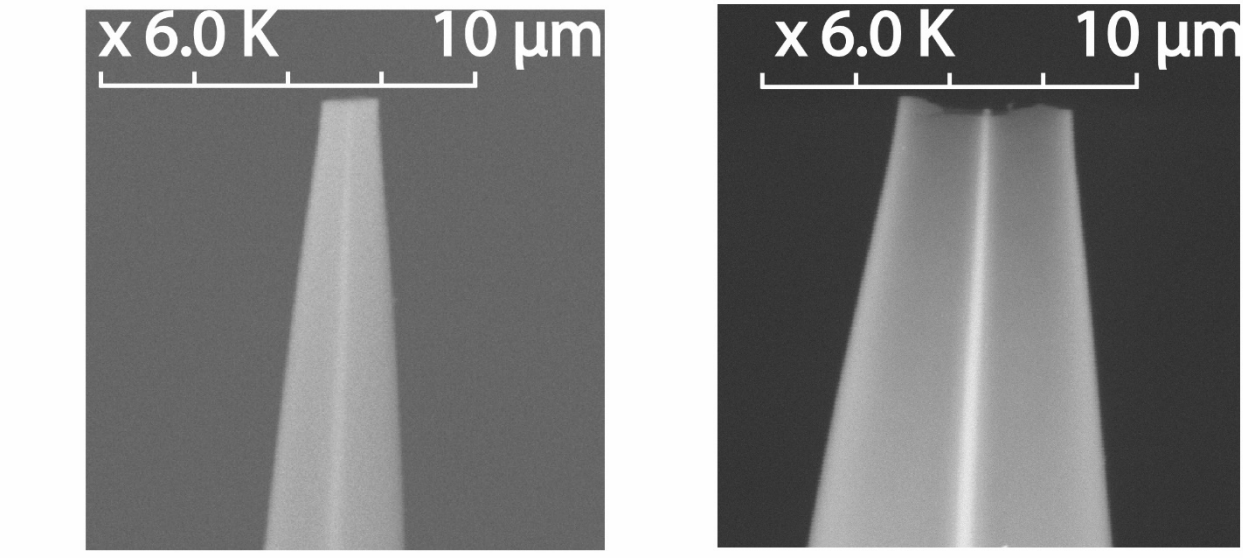


**Figure 2.1.** SEM images of theta tip emitters with inner diameter in the long dimension of 1.7 µm (left) and 4.5 µm (right).

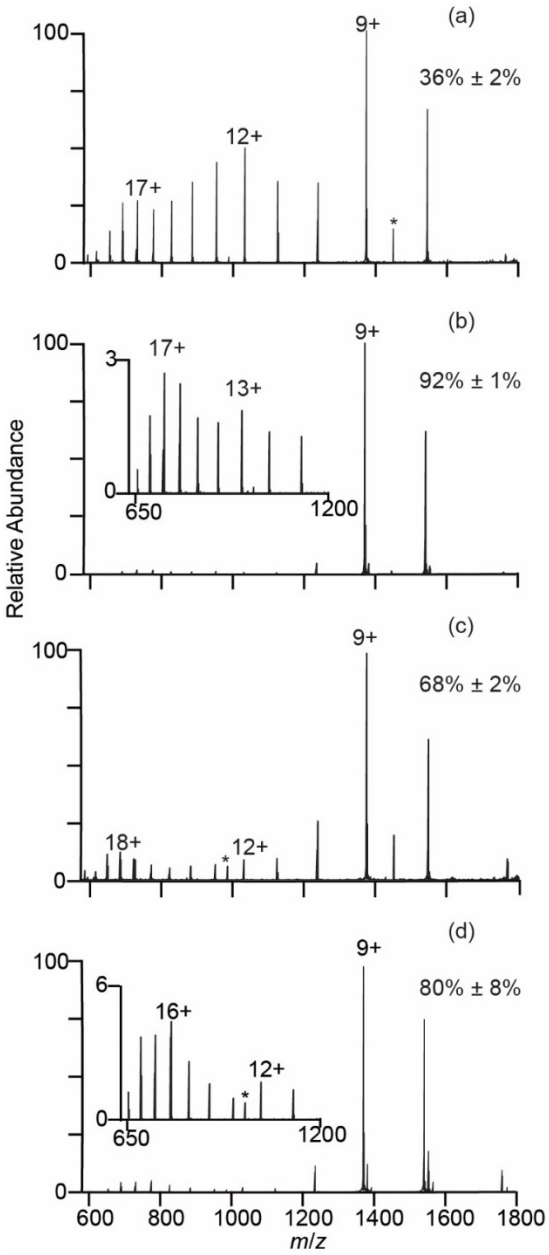


**Figure 2.2.** ESI mass spectra obtained on a 9.4 T FT-ICR mass spectrometer from 10 μM cytochrome *c* in (a) water with 1% acetic acid (pH 2.8), and (b) water with 0.5% acetic acid (pH 3.0). (c) upon mixing cytochrome *c* in 1% acetic acid with water using 1.7 μm theta tip emitter with 40 psi backing pressure, and (d) mixing with 4.5 μm theta tip emitter with 10 psi backing pressure. The asterisk indicates a frequency. Percentages of folded cytochrome *c* obtained from the abundances of peaks in the corresponding charge-state distributions are labeled.

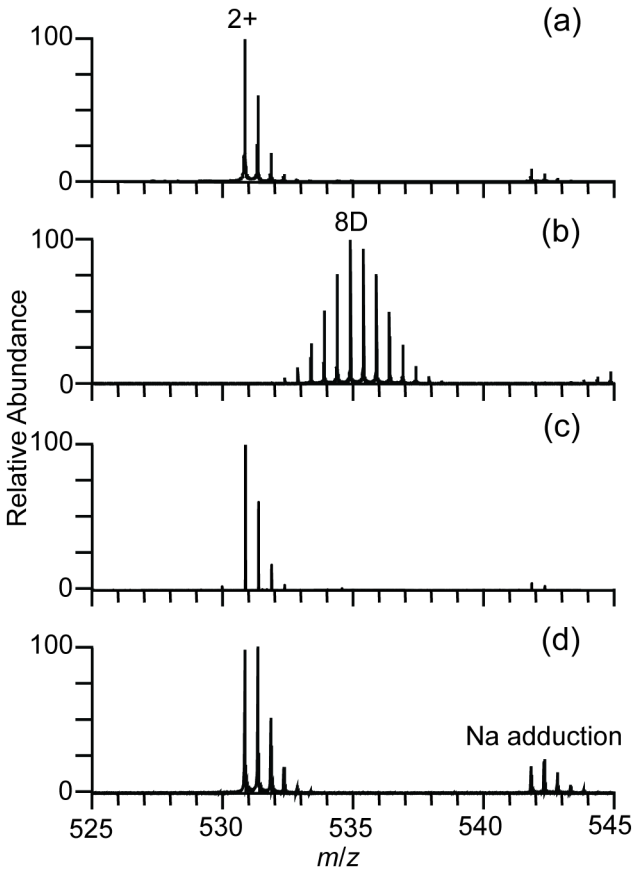


**Figure 2.3.** Partial ESI mass spectra around the 2+ charge state of bradykinin from (a) water and (b) 1 : 1 premixed water and 99.9% $D_2O$ (c) rapid mixing of bradykinin in water and 99.9% $D_2O$ using theta emitters with droplet lifetime of (c) ~ 40 μs (1.7 μm emitter), and (d) ~ 100 μs (4.5 μm emitter).

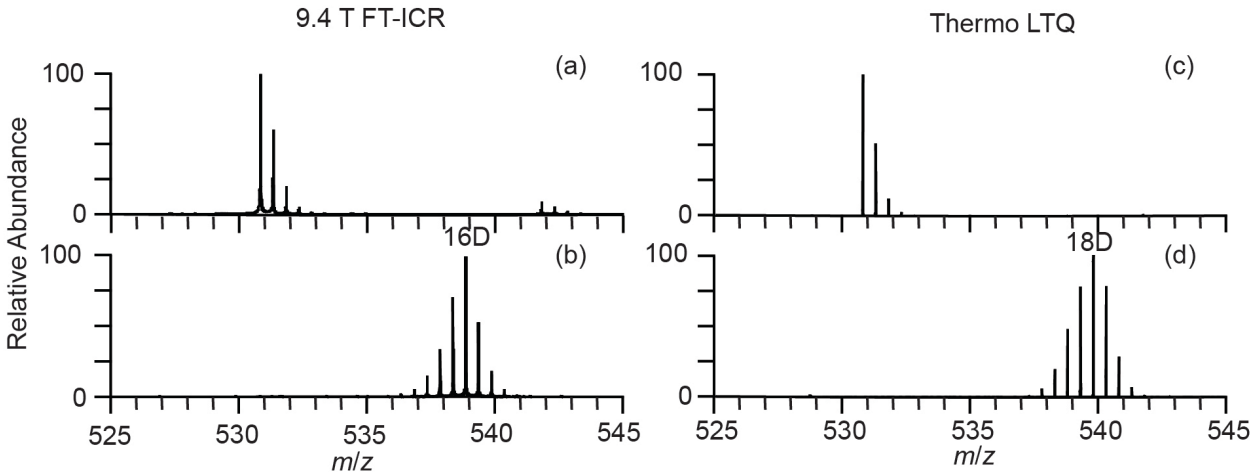


**Figure 2.4.** Partial ESI mass spectra around the 2+ charge state of bradykinin formed from (a) water and (b) 99.9 $D_2O$ obtained on the 9.4 T FT-ICR instrument and from these same solutions (c – d, respectively) obtained with a on the Thermal LTQ instrument.

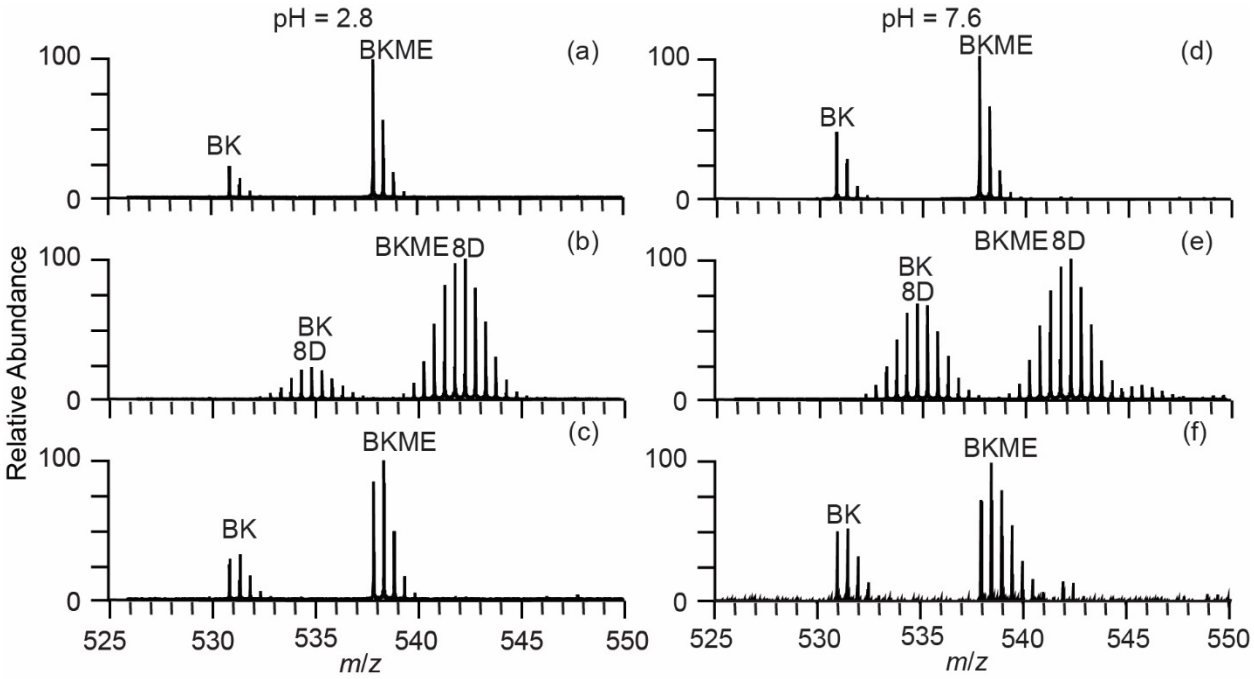


**Figure 2.5.** Partial ESI mass spectra around the 2+ charge state of bradykinin (BK) and bradykinin methyl ester (BKME) measured at (a – c) pH = 2.8 and (d – f) 7.6 in (a, d) water, (b, e) 1 : 1 premixed water and $D_2O$, and (c, f) 99.9% $D_2O$ mixed into water using theta tip emitter to produce nanodrops with lifetime ~100 μs (4.5 μm emitter).

# Chapter 3

# Submicrometer Emitter ESI Tips for Native Mass Spectrometry of Membrane Proteins in Ionic and Non-ionic Detergents

This chapter is reproduced with permission from:

Anna C. Susa, Jennifer L. Lippens, Zijie Xia, Joseph A. Loo, Iain D.G. Campuzano, Evan R. Williams

"Submicrometer Emitter ESI Tips for Native Mass Spectrometry of Membrane Proteins in Ionic and Non-ionic Detergents"

*Journal of the American Society for Mass Spectrometry*, **2018**, *29*(1): 203–206



## 3.1 Abstract

Native mass spectrometry (native-MS) of membrane proteins typically requires a detergent screening protocol, protein solubilization in the preferred detergent, followed by protein liberation from the micelle by collisional activation. Here, submicrometer nano-ESI emitter tips are used for native-MS of membrane proteins solubilized in both non-ionic and ionic detergent solutions. With the submicrometer nano-ESI emitter tips, resolved charge-state distributions of membrane protein ions are obtained from a 150 mM NaCl, 25 mM Tris-HCl with 1.1% octyl glucoside solution. The relative abundances of NaCl and detergent cluster ions at high m/z are significantly reduced with the submicrometer emitters compared to larger nano-ESI emitters that are commonly used. This technique is beneficial for significantly decreasing the abundances (by two to three orders of magnitude compared to the larger tip size: 1.6 μm) of detergent cluster ions formed from aqueous ammonium acetate solutions containing detergents that can overlap with the membrane protein ion signal. Resolved charge-state distributions of membrane protein ions from aqueous ammonium acetate solutions containing ionic detergents were obtained with the submicrometer nano-ESI emitters, which is the first report of native-MS of membrane proteins solubilized by ionic detergents.

## 3.2 Introduction

Membrane proteins currently make up approximately 50% of therapeutic targets[1,2] making their structural characterization a high priority. Native mass spectrometry (native-MS) has emerged as a powerful tool to characterize these difficult to analyze proteins.[3–8] As a result of their hydrophobicity, they are typically solubilized by encapsulation in either non-ionic or zwitterionic detergent micelles for analysis by native MS.[4,9] However, these detergents can broaden the mass spectral peaks and can reduce the signal-to-noise ratios (S/N) of the membrane protein ions.[4] Upon collisional activation of protein-micelle complexes, which subsequently liberates the membrane proteins from the micelles, detergent related ions are frequently present in high abundance that can greatly suppress protein signal and increase spectral complexity.[10] During native-MS, it is essential to strike a balance between membrane protein ejection and dissociation of any membrane protein complexes, such as protein-protein or protein-ligand complexes, because preservation of these interactions while simultaneously disrupting the protein interactions with the detergent micelle can be difficult. Therefore, complete removal of detergent micelle signal from the spectrum may not be achieved.

Another challenge of native-MS is salt adduction. Nonvolatile salts can adduct to protein and protein complexes, broadening mass spectral peaks and decreasing mass measuring accuracy. To circumvent the adverse effects of nonvolatile salts in ESI solutions, protein solutions are typically exchanged into volatile ammonium salt solutions such as ammonium acetate or ammonium bicarbonate.[11] Specific salts in solution are often necessary to maintain the structures and functions of proteins, and buffer solutions containing ~150 mM KCl or NaCl are often used to mimic the cellular environment. Several methods for desalting protein ions, including adding reagents to ESI solutions[11–15] or reacting the protein ions with organic vapors[16] can be used but are only effective for solutions containing up to about 25 mM NaCl. Nano-ESI tip diameters are typically >1 μm, but emitter tips less than 1 μm in diameter can decrease salt adduction to protein and protein complex ions.[17–20] Recently, ESI mass spectra with resolved charge-state distributions of proteins and protein complexes were obtained from solutions containing ≥150 mM NaCl or KCl and a variety of commonly used buffers, such as Tris-HCl and HEPES.[19,20] This effect was attributed to the formation of small nanodrops that limit the number of nonvolatile ions that can interact with the protein or protein complex and limit the size of clusters that can be formed.[19,20]

Here, the effectiveness of submicrometer nano-ESI emitter tips for desalting membrane protein ions from aqueous solutions containing detergents was investigated. Membrane protein ions, bacteriorhodopsin T47A (bR) and Aquaporin Z (AqpZ), were formed from aqueous ammonium acetate and a commonly used buffer that mimics the cellular environment (150 mM NaCl, 25 mM Tris-HCl) containing two times the critical micelle concentration (CMC) of non-ionic and ionic detergents with both conventionally sized and submicrometer nano-ESI tips.

## 3.3 Experimental Method

Mass spectral data were acquired using a Synapt G2Si mass spectrometer (Waters, Milford, MA) in the QB3/Chemistry Mass Spectrometry Facility at the University of California, Berkeley. Borosilicate capillary emitters (1.0 mm o.d./ 0.78 mm i.d., Sutter Instruments, Novato, CA) were pulled with a Flaming/Brown micropipette puller (Model P-87, Sutter Instruments, Novato, CA).

Emitter tip diameters were measured with a scanning electron microscope (Hitachi TM-1000 SEM, Schaumburg, IL) at the Robert D. Ogg Electron Microscope Laboratory (University of California, Berkeley). Tip inner diameters were either 1.6 ± 0.1 μm or 0.57 ± 0.04 μm and replicate measurements were made with at least three different tips of each size (Supplemental Figure 3.1).[20]

Nano-electrospray was initiated by applying a potential of about +0.6 to 1.2 kV to a 0.127 mm diameter platinum wire inserted into the emitter and in contact with the solution. The sampling cone and source offset voltages were both 50 V, and the source temperature was 80 °C. A flow rate of argon collision gas of 6.0 mL/min was used in the trap. Ion activation at a collision voltage of 100-150 V in the trap to facilitate release the ions from the micelles.

The concentrations of bR and AqpZ were ~2 μM and ~30 μM, respectively. The bR stock solution containing octyl glucoside (OG) was diluted 100-fold with the buffer and detergent of interest. The AqpZ stock solution (150 mM NaCl 20 mM Tris-HCl 5% glycerol 1.1% OG) was diluted 5-fold. Two times the CMC of OG, sodium dodecyl sulfate (SDS), cetrimonium bromide (CTAB) or sarkosyl is 1.1, 0.55, 0.073, 0.85 % (w/v), respectively.

## 3.4 Results and Discussion

To determine the effects of nano-ESI emitter tip size on salt and detergent adduction to membrane protein ions, bR and AqpZ ions were formed from aqueous 200 mM ammonium acetate with 1.1% OG with two sizes of nano-ESI emitter tips (1.6 μm and 0.5 μm inner diameters, Figure 3.1a-d). Well-resolved charge-state distributions of bR and AqpZ ions are obtained from aqueous ammonium acetate and OG solutions with both size emitters (Figure 3.1). The charge-state distribution of bR ions formed with the submicrometer tips is slightly higher than from the larger tips consistent with previous results.[21] The charge state-distributions of AqpZ monomer and tetramer ions are similar with both tip sizes. Salt cluster ions are formed with both tip sizes, but the abundances of these clusters are lower by up to four orders of magnitude with the 0.5 μm emitter tips compared to the protein ion signal (Supplemental Figure 3.2a-c). For example, the abundance of the most intense cluster, $(2OG + Na)^+$ (*m/z* 607), is one to three orders of magnitude lower with the submicrometer emitter tips than with the larger tips (Supplemental Figure 3.2a). Large cluster ions from *m/z* ~1500 to >4000 that overlap the charge-state distributions of bR and AqpZ ions are nearly eliminated with the 0.5 μm tips resulting in higher signal-to-noise ratios (S/N) for the protein ions with the small tips. For example, the S/N of the 10+ charge state of AqpZ monomer ions is seven times higher with the small tips. This demonstrates that submicrometer emitter tips are useful for decreasing the abundances of detergent cluster ions that can interfere with membrane protein ion signal. Several different peaks for each charge state of the AqpZ tetramer that are not resolved with the larger tips are resolved with the small tips. These differ in mass by ~760-1800 Da and may be due to adduction of sodiated OG dimers or due to the presence of phospholipids.

To determine if the submicrometer emitter tips are effective at forming ions of membrane proteins from a commonly used buffer that mimics the cellular environment, bR and AqpZ ions were formed from 150 mM NaCl, 25 mM Tris-HCl and 1.1% OG with both emitter tip sizes (Figure 3.1c, d, g and h). The bR ions formed from this solution with the 1.6 μm tips are not resolved, but rather a broad distribution of NaCl and OG clusters ions from *m/z* ~2000 to 7000 is produced. A few broad peaks at *m/z* 3060 and 3410 may correspond to the 9+ and 8+ charge states of bR, which would result in a molecular weight (MW) of 27.5 kDa which is 3% greater than the

un-adducted molecular weight of bR (MW = 26.75 kDa, calculated from elemental composition). AqpZ monomer and tetramer ions formed with the 1.6 μm tips from this solution are resolved (likely because the concentration of AqpZ is six times greater than that of bR) but high *m*/*z* cluster ions interfere with the protein ion signal. In contrast, AqpZ and bR ions formed with the submicrometer emitter tips from the same solution are clearly resolved with little background chemical noise. As previously demonstrated, high *m/z* cluster ions are nearly eliminated.[19,20] The masses of bR and AqpZ ions formed from 150 mM NaCl, 25 mM Tris-HCl and 1.1 % OG with the submicrometer tips are 588 and 880 Da higher in mass than the calculated values, respectively, indicating that substantial adduction of salts and possibly detergent still occurs (Supplemental Table 3.1). This adduction results in broad peaks that spread the tetramer signal in *m*/*z* and this contributes to the apparent high abundance of the monomer, which is significantly less adducted. Notably, there is no significant difference in the ratio of tetramer to monomer with the two tip sizes indicating that the small tips do not affect the stability of the tetramer. These results show that submicrometer emitter tips can be beneficial for native-MS of membrane protein complexes from solutions containing high ionic strengths of nonvolatile salts in addition to non-ionic detergents, which would be advantageous for membrane proteins that are only stable in specific buffers containing nonvolatile salts.

Ionic detergents are often added to membrane protein solutions because they are typically more effective at solubilizing membrane proteins than non-ionic detergents.[22] To determine if submicrometer nano-ESI tips are effective for native-MS from aqueous solutions containing ionic detergents, bR and AqpZ ions were formed with both size emitter tips from 200 mM ammonium acetate containing two times the CMC of SDS, a common ionic detergent (Figure 3.2). With the 1.6 μm emitter tips, no bR ions are observed (Figure 3.2a). AqpZ monomer ions are resolved from solution with the 1.6 μm tips, but there is a very broad peak of cluster ions from *m*/*z* ~2000-5000 (Figure 3.2c.) In contrast, charge-state distributions of the monomers of both proteins are clearly resolved with the 0.5 μm tips (Figure 3.2b,d). The charge states of the tetramer are not resolved, but the maxima in the distribution likely correspond to the 15+ and 14+ charge states. With the maximum possible collision energy, narrower peaks corresponding to the 16 to 18+ appear, consistent with removal of negatively charged SDS adducted to the protein ions. The high *m*/*z* cluster ions are nearly eliminated with the small tips (Supplemental Figure 3.2b). Resolved charge-state distributions of bR ions formed from 200 mM ammonium acetate containing two times the CMC of two other ionic detergents, sarkosyl and CTAB were obtained with submicrometer emitter tips (Supplemental Figure 3.3). Resolved charge-state distributions of AqpZ ions formed from 150 mM NaCl 25 mM Tris-HCl and 0.55% SDS were obtained with the submicrometer emitters, but not for bR ions (Supplemental Figure 3.4). This is the first report of native-MS of membrane protein from aqueous solutions containing ionic detergents. The use of submicrometer nano-ESI tips for native-MS of membrane proteins could be useful for membrane proteins that require ionic detergents for solubilization.

## 3.5 Conclusions

Submicrometer nano-ESI emitter tips are useful for decreasing the abundances of cluster ions of both ionic and non-ionic detergents for membrane protein ions formed from aqueous solutions containing two times the CMC of the detergent. The submicrometer emitter tips also are

useful for obtaining resolved charge-state distributions of membrane protein ions from solutions containing high ionic strengths of nonvolatile salts (150 mM) with these detergents. This technique reduces the chemical noise over conventional nanoESI and makes possible native-MS of membrane proteins from solutions that are more conventionally used by biochemists to investigate the structures, dynamics and functions of these types of proteins. Importantly, this method may afford for the reduction in performing multiple detergent screens, which are currently used to find optimal conditions for native-MS analysis.[4]

## 3.6 Acknowledgment

The authors are grateful for financial support from the National Institutes of Health (R01GM097357 to E.R.W. and R01GM103479 to J.A.L.) and for funds to acquire the Synapt G2Si (S10OD020062) used in these experiments. The authors thank Drs. Ryan Leib and Anthony Iavarone for helpful discussions, Drs. Nicholas Woodall and James U. Bowie (UCLA) for the generous gift of the bacteriorhodopsin T47A mutant and Dr. Pascal Egea (UCLA) for preparation and gift of Aquaporin Z.

## 3.7 References

(1) Hopkins, A. L.; Groom, C. R. The Druggable Genome. *Nat. Rev. Drug Discov.* **2002**, *1* (9), 727–730.

(2) Arinaminpathy, Y.; Khurana, E.; Engelman, D. M.; Gerstein, M. B. Computational Analysis of Membrane Proteins: The Largest Class of Drug Targets. *Drug Discov. Today* **2009**, *14* (23–24), 1130–1135.

(3) Hopper, J. T. S.; Yu, Y. T.-C.; Li, D.; Raymond, A.; Bostock, M.; Liko, I.; Mikhailov, V.; Laganowsky, A.; Benesch, J. L. P.; Caffrey, M.; et al. Detergent-Free Mass Spectrometry of Membrane Protein Complexes. *Nat. Methods* **2013**, *10* (12), 1206–1208.

(4) Laganowsky, A.; Reading, E.; Hopper, J. T. S.; Robinson, C. V. Mass Spectrometry of Intact Membrane Protein Complexes. *Nat. Protoc.* **2014**, *8* (4), 639–651.

(5) Harvey, S. R.; Liu, Y.; Liu, W.; Wysocki, V. H.; Laganowsky, A. Surface Induced Dissociation as a Tool to Study Membrane Protein Complexes. *Chem. Commun. (Camb).* **2017**, *53* (21), 3106–3109.

(6) Cong, X.; Liu, Y.; Liu, W.; Liang, X.; Russell, D. H.; Laganowsky, A. Determining Membrane Protein–Lipid Binding Thermodynamics Using Native Mass Spectrometry. *J. Am. Chem. Soc.* **2016**, *138* (13), 4346–4349.

(7) Campuzano, I. D. G.; Li, H.; Bagal, D.; Lippens, J. L.; Svitel, J.; Kurzeja, R. J. M.; Xu, H.; Schnier, P. D.; Loo, J. A. Native MS Analysis of Bacteriorhodopsin and an Empty Nanodisc by Orthogonal Acceleration Time-of-Flight, Orbitrap and Ion Cyclotron Resonance. *Anal. Chem.* **2016**, *88* (24), 12427–12436.

(8) Kintzer, A. F.; Sterling, H. J.; Tang, I. I.; Abdul-Gader, A.; Miles, A. J.; Wallace, B. A.; Williams, E. R.; Krantz, B. a. Role of the Protective Antigen Octamer in the Molecular Mechanism of Anthrax Lethal Toxin Stabilization in Plasma. *J. Mol. Biol.* **2010**, *399* (5), 741–758.

(9) Reading, E.; Liko, I.; Allison, T. M.; Benesch, J. L. P.; Laganowsky, A.; Robinson, C. V. The Role of the Detergent Micelle in Preserving the Structure of Membrane Proteins in the Gas Phase. *Angew. Chemie - Int. Ed.* **2015**, *54* (15), 4577–4581.
(10) Barrera, N. P.; Robinson, C. V. Advances in the Mass Spectrometry of Membrane Proteins: From Individual Proteins to Intact Complexes. *Annu. Rev. Biochem.* **2011**, *80* (1), 247–271.
(11) Hernández, H.; Robinson, C. V. Determining the Stoichiometry and Interactions of Macromolecular Assemblies from Mass Spectrometry. *Nat. Protoc.* **2007**, *2* (3), 715–726.
(12) Iavarone, A. T.; Udekwu, O. A.; Wiliams, E. R. Buffer Loading for Counteracting Metal Salt-Induced Signal Suppression in Electrospray Ionization. *Anal. Chem.* **2004**, *76* (14), 3944–3950.
(13) Clarke, D. J.; Campopiano, D. J. Desalting Large Protein Complexes during Native Electrospray Mass Spectrometry by Addition of Amino Acids to the Working Solution. *Analyst* **2015**, *140* (8), 2679–2686.
(14) Cassou, C. A.; Williams, E. R. Desalting Protein Ions in Native Mass Spectrometry Using Supercharging Reagents. *Analyst* **2014**, *139* (19), 4810–4819.
(15) Flick, T. G.; Cassou, C. a.; Chang, T. M.; Williams, E. R. Solution Additives That Desalt Protein Ions in Native Mass Spectrometry. *Anal. Chem.* **2012**, *84* (17), 7511–7517.
(16) Demuth, J. C.; McLuckey, S. A. Electrospray Droplet Exposure to Organic Vapors: Metal Ion Removal from Proteins and Protein Complexes. *Anal. Chem.* **2015**, *87* (2), 1210–1218.
(17) Hu, J.; Guan, Q.-Y.; Wang, J.; Jiang, X.-X.; Wu, Z.-Q.; Xia, X.-H.; Xu, J.-J.; Chen, H.-Y. Effect of Nanoemitters on Suppressing the Formation of Metal Adduct Ions in Electrospray Ionization Mass Spectrometry. *Anal. Chem.* **2017**, *89* (3), 1838–1845.
(18) Schmidt, A.; Karas, M.; Dülcks, T. Effect of Different Solution Flow Rates on Analyte Ion Signals in Nano-ESI MS, or: When Does ESI Turn into Nano-ESI? *J. Am. Soc. Mass Spectrom.* **2003**, *14* (5), 492–500.
(19) Susa, A. C.; Xia, Z.; Williams, E. R. Native Mass Spectrometry from Common Buffers with Salts That Mimic the Extracellular Environment. *Angew. Chemie Int. Ed.* **2017**, 1–5.
(20) Susa, A. C.; Xia, Z.; Williams, E. R. Small Emitter Tips for Native Mass Spectrometry of Proteins and Protein Complexes from Nonvolatile Buffers That Mimic the Intracellular Environment. *Anal. Chem.* **2017**, *89* (5), 3116–3122.
(21) Mortensen, D. N.; Williams, E. R. Electrothermal Supercharging of Proteins in Native MS: Effects of Protein Isoelectric Point, Buffer, and NanoESI-Emitter Tip Size. *Analyst* **2016**, *141* (19), 5598–5606.
(22) Seddon, A. M.; Curnow, P.; Booth, P. J. Membrane Proteins, Lipids and Detergents: Not Just a Soap Opera. *Biochim. Biophys. Acta* **2004**, *1666* (1–2), 105–117.

## 3.8 Figures

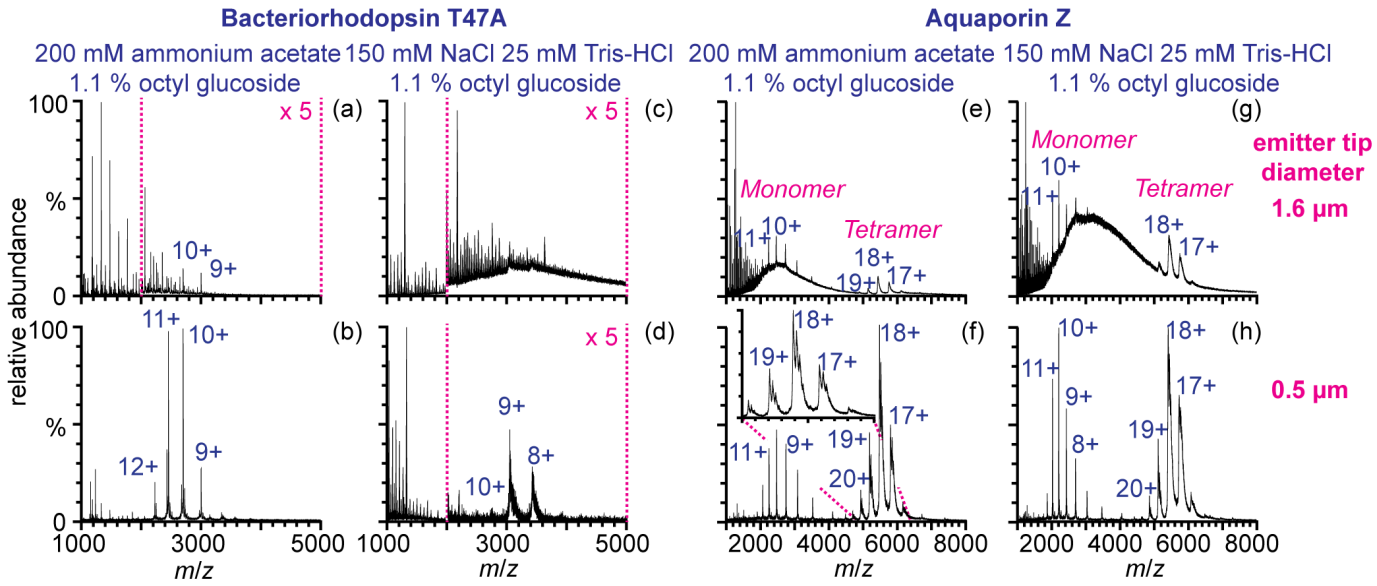


**Figure 3.1.** (a-d) bR and AqpZ ions (e-h) formed from aqueous (a-b, e-f) 200 mM ammonium acetate with 1.1 % (w/v) OG or (c-d, g-h) 150 mM NaCl 25 mM Tris-HCl 1.1 % (w/v) OG with (a, c, e, g) 1.6 µm and (b, d, f, h) 0.5 µm emitter tips. The collision voltage was 100 V

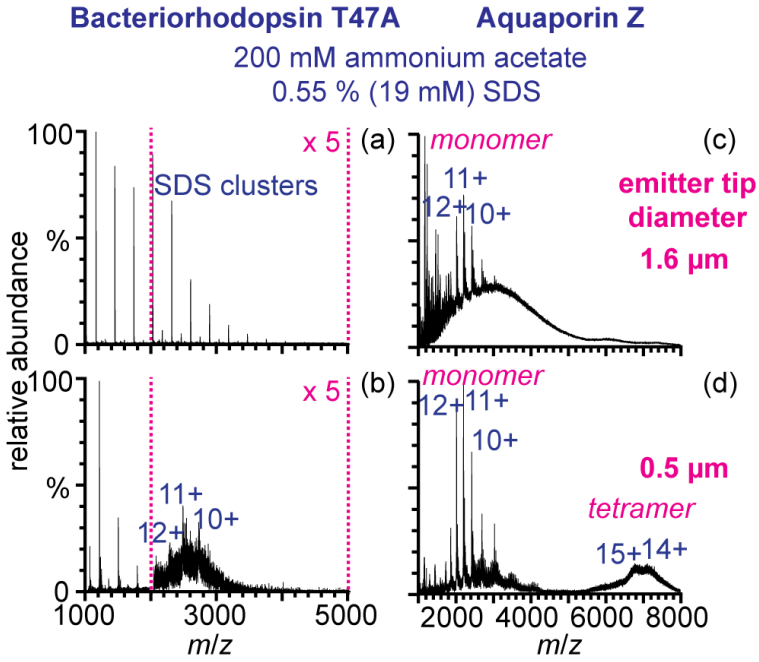


**Figure 3.2.** (a-b) bR and (c-d) AqpZ ions formed from aqueous 200 mM ammonium acetate containing 0.55 % (w/v) SDS with (a,c) 1.6 µm and (b, d) 0.5 µm emitter tips. The collision voltage was 150 V.

## 3.9 Supplemental Information

**Supplemental Table 3.1.** Mass increase from adduction for bR and AqpZ ions formed from 200 mM ammonium acetate or 150 mM NaCl 25 mM Tris-HCl and detergents with 0.5 µm and 1.6 µm emitter tips. The adduction to AqpZ tetramer was calculated with reference to the measured monomer mass of AqpZ (times four). The adduction to bR was calculated with reference to the elemental composition of bR.

| | **Mass increase from adduction (Da)** | |
|---|---|---|
| | **0.5 µm tip** | **1.6 µm tip** |
| ***bR***<br>*200 mM ammonium acetate* | | |
| + 1.1 % OG | 151 ± 5 | 148 ± 20 |
| + 0.55 % SDS | 102 ± 49 | - |
| + 0.073 % CTAB | 123 ± 4 | - |
| + 0.85 % sarkosyl | 315 ± 107 | - |
| *150 mM NaCl 25 mM Tris-HCl* 1.1 % OG | 588 ± 25 | - |
| ***AqpZ tetramer***<br>*200 mM ammonium acetate* | | |
| + 1.1 % OG | 769 ± 100 | 798 ± 370 |
| + 0.55 % SDS | ~1400 | - |
| *150 mM NaCl 25 mM Tris-HCl* 1.1 % OG | 880 ± 72 | 1835 ± 1200 |

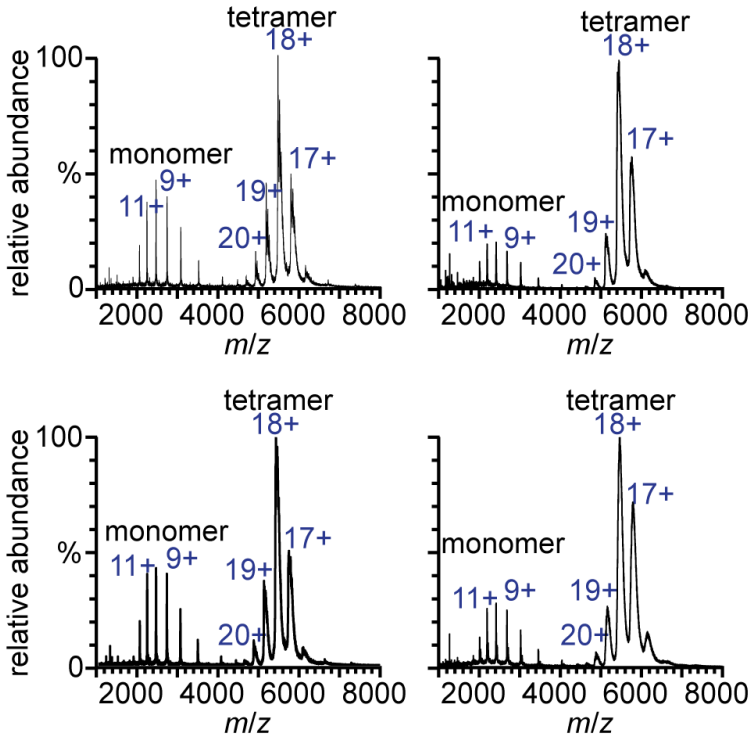


**Supplemental Figure 3.1.** Four replicate mass spectra for AqpZ ions formed from 200 mM ammonium acetate with 1.1 % octyl glucoside using four different 0.5 µm emitter tips. These data show the reproducibility of mass spectra obtained with different nano-ESI emitters that are approximately the same size.

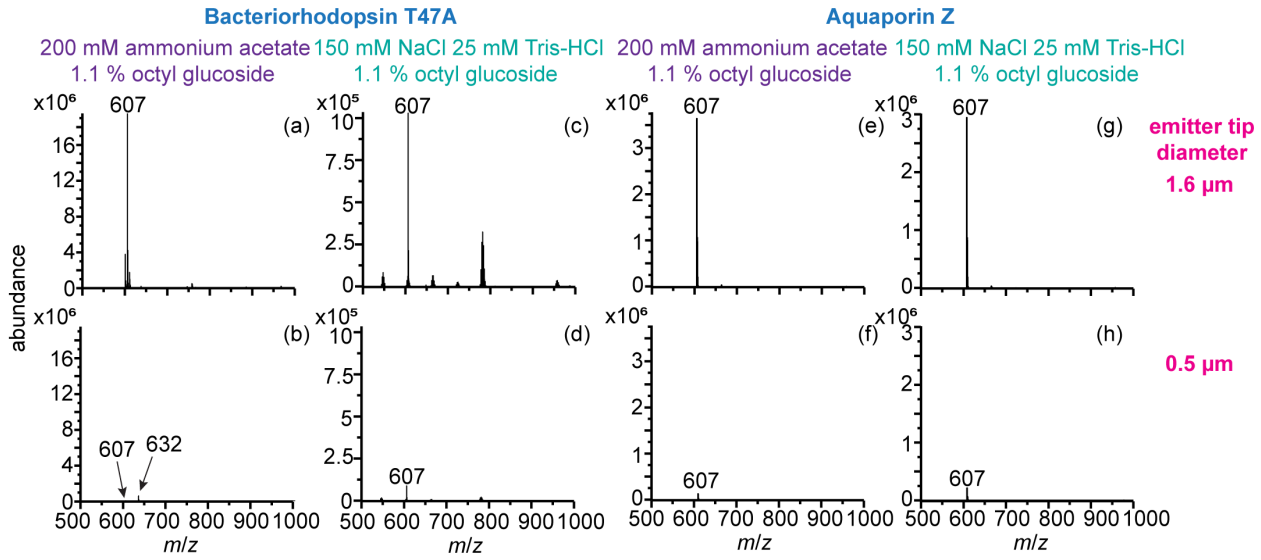


**Supplemental Figure 3.2a.** Mass spectra shown in Figure 1 in the *m/z* range from 500 to 1000 for (a-d) bR and AqpZ (e-h) from aqueous (a-b, e-f) 200 mM ammonium acetate with 1.1 % (w/v) OG or (c-d, g-h) 150 mM NaCl 25 mM Tris-HCl 1.1 % (w/v) OG with (a, c, e, g) 1.6 µm and (b, d, f, h) 0.5 µm emitter tips. The collision voltage was 100 V. These data show that the absolute abundance of *m/z* 607 corresponding to sodiated dimer of OG is lower by between >10 to ~1000 with the small tips compared to the larger tips.

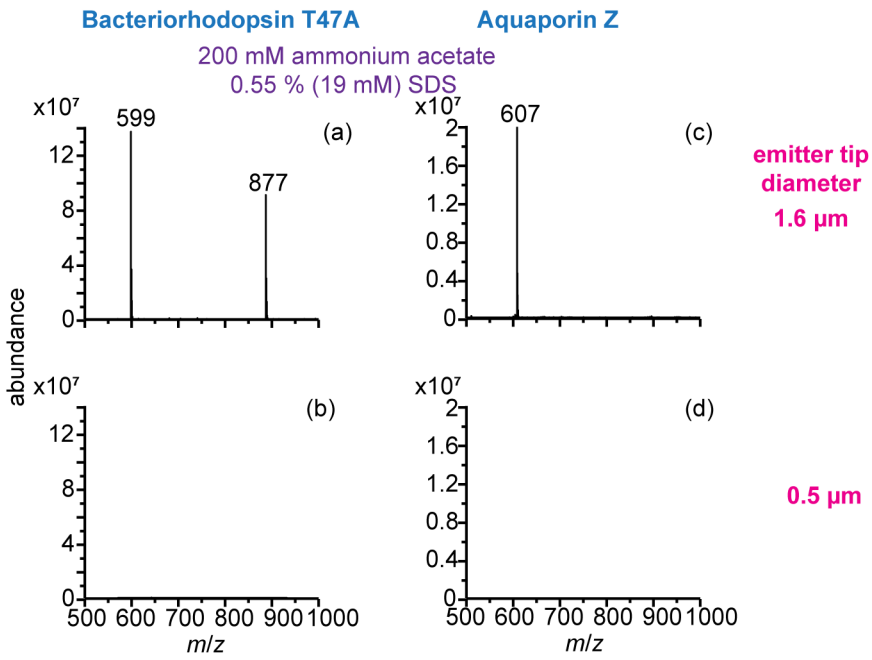


**Supplemental Figure 2b.** Mass spectra shown in Figure 2 with *m/z* from 500 to 1000 for (a-b) bR and (c-d) AqpZ ions from aqueous 200 mM ammonium acetate containing 0.55 % (w/v) SDS with (a,c) 1.6 µm and (b, d) 0.5 µm emitter tips. These data show that the absolute abundance of *m/z* 599 corresponding to sodiated dimer of SDS is lower by ~1000 and *m/z* 607 corresponding to sodiated dimer of OG is lower by ~10,000 with the small tips compared to the larger tips.

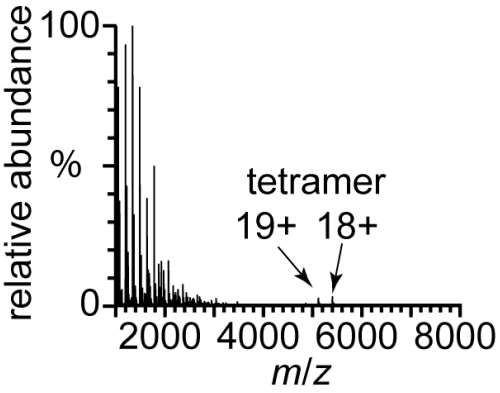


**Supplemental Figure 2c.** AqpZ ions formed from 200 mM ammonium acetate with 1.1% octyl glucoside. The spectrum was acquired using >1 micron tips with a Synapt G2 mass spectrometer at Amgen. Nano-electrospray ionization was initiated by applying a potential of 0.6 kV. Sample cone was set at 40 V. Ion activation at 60 V and a backing pressure of 5 mbar were applied to facilitate release the ions from the micelles. These data show that a higher backing pressure can result in a lower abundance of clusters at higher *m*/*z*.

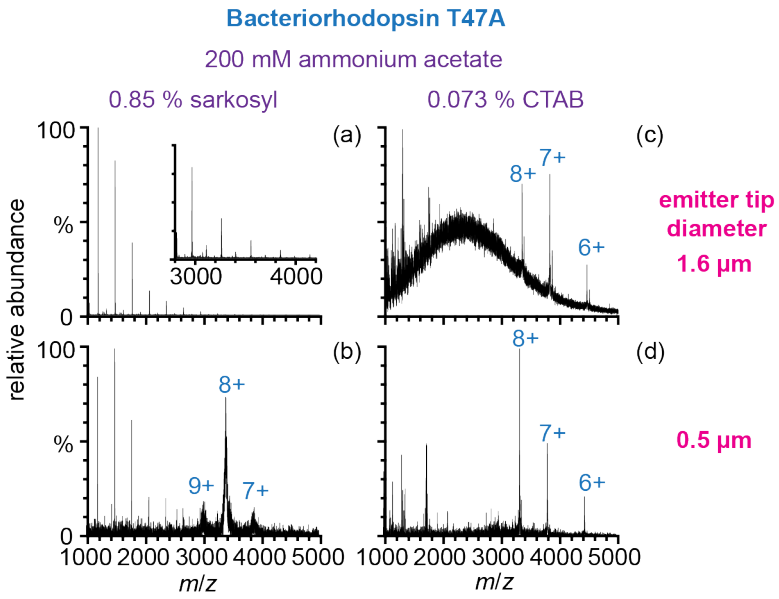


**Supplemental Figure 3.** bR formed from aqueous ammonium acetate with (a-b) 0.85 % sarkosyl or (c-d) 0.073 % CTAB with 0.5 µm and 1.6 µm emitter tips.

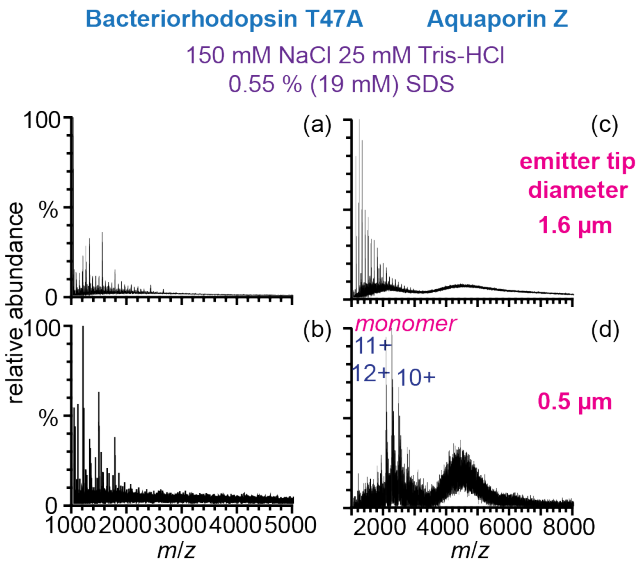


**Supplemental Figure 4.** (a-b) bR and (c-d) AqpZ ions formed from 150 mM NaCl 25 mM with 0.5 µm and 1.6 µm emitter tips.

# Chapter 4

# Protein-Glass Surface Interactions and Ion Desalting in Electrospray Ionization with Submicron Emitters

This chapter is reproduced with permission from:

Zijie Xia, Evan R. Williams

"Protein-Glass Surface Interactions and Ion Desalting in Electrospray Ionization with Submicron Emitters"

*Journal of the American Society for Mass Spectrometry*, **2018**, *29*(1): 194–202



## 4.1 Abstract

Theta glass electrospray emitters can rapidly mix solutions to investigate fast reactions that occur as quickly as one microsecond, but emitters with submicron tips have the unusual properties of desalting protein ions and affecting the observed abundances of some proteins as a result of protein-surface interactions. The role of protein physical properties on ion signal was investigated using 1.7 ± 0.1 μm and 269 ± 7 nm emitters and 100 mM aqueous ammonium acetate or ammonium bicarbonate solutions. Protein ion desalting occurs for both positive and negative ions. The signal of a mixture of proteins with the 269 nm tips is time dependent and the order in which ions of each protein is observed is related to the expected strenghts of the protein-surface interactions. These results indicate that it is not just the high surface-to-volume ratio that plays a role in protein adsorption and reduction or absence of initial ion signal, but the small diffusion distance and extremely low flow rates of the smaller emitters can lead to complete adsorption of some proteins and loss of signal until the adsorption sites are filled and the zeta potential is significantly reduced. After about 30 minutes, signal for a protein mixture from the two different size capillaries are similar. These results show the advantages of submicron emitters but also indicate that surface effects must be taken into account in experiments using such small tips or that coating the emitter surface to prevent adsorption should be considered.

## 4.2 Introduction

Nanoelectrospray ionization (nanoESI) enables low sample flow rates resulting in little sample consumption and is widely used in applications where low sample consumption is essential [1,2]. The electric field strength at the tip of small emitters is high and droplets can be efficiently produced from solutions with high surface tension, such as water, even without other methods to

facilitate droplet formation, such as sheath gas flow or addition of low surface tension solvents [3,4]. The ability to form droplets directly from aqueous solutions containing high concentrations of buffer makes nanoESI especially important in native mass spectrometry [5,6]. NanoESI can be implemented in a number of different ways, including borosilicate or fused silica emitters with or without metal coatings and microfabricated devices. Microfabricated devices can incorporate buffer exchange and nanoLC for proteomics applications [7,8]. Theta glass borosilicate nanoESI emitters have two separate barrels and can be used to rapidly mix two solutions during the electrospray ionization process [9–14]. The reaction time can be controlled by changing droplet size, which depends on flow rate [10,12,13] or by changing the distance of the emitter tip to the ESI interface [14]. Flow rates can be controlled by varying the backing pressure on the emitter and/or by changing the emitter tip size. Reaction times of 100s of microseconds have been achieved with emitter tip sizes ~4 μm [14] and reaction times as low as 1 μs has been achieved with ~300 nm tips [12,14]. These small tips have made possible the fastest mixing times of two different solutions to date.

In addition to enabling fast mixing, the submicron tips have some unusual properties with nanoESI, one of which appear to be highly advantageous. Fewer salt adducts are formed with smaller tips and this effect has been reported from both water/methanol/acetic acid solutions in which proteins are denatured [15,16] as well as from buffered aqueous solutions in which proteins have native conformations and activities [17,18]. The phenomenon of ion desalting in small tips was investigated using traditional single barrel borosilicate emitters from buffered aquous solutions containing high levels of nonvolatile salts and buffers. Charge-state distributions of proteins and protein complexes could be readily observed in nanoESI spectra of solutions containing 150 mM KCl and 25 mM Tris-HCl buffer at pH 7 using 0.5 μm tips but not with 1.7 μm tips [17]. Similar results were obtained with aqueous solutions with six commonly used nonvolatile buffers containing ≥150 mM of $Na^+$ [18]. These results suggest a mechanism for salt adduct reduction in which initial ESI droplets are sufficiently small that they contain on average fewer than one protein molecule per droplet. The majority of droplets contain salt but no protein, and the droplets that do contain a protein molecule have a much lower salt to protein ratio than that in the initial solution. The lowering of the salt to protein ratio in smaller droplets may result in less extensive adduction of nonvolatile salts to protein ions. Nonvolatile salts are often removed from solution prior to ESI owing to their adverse effects on mass spectrometry performance, but submicron tips can be used to form protein and protein complex ions directly from solutions containing high levels of nonvolatile salts and buffers that are used to mimic either the intracellular or the extracellular environment [17,18].

The relative abundances of protein ions can depend on tip size. For example, a mixture of myoglobin and cytochrome *c* in 100 mM aqueous ammonium bicarbonate resulted in formation of ions of both proteins with 1.5 μm theta emitter tips but formation of only myoglobin ions with 310 nm emitter tips [19]. It was proposed that the absence of cytochrome *c* signal in the smaller tips was due to the high surface to volume ratio, which enhances interactions between the positively charged proteins in solution and the negatively charged glass surface near neutral pH [19].

Here, we investigate the unusual observation of selective protein ion signal observed when using submicron theta glass emitter tips and show that the ion desalting is also effective for negative ions. Emitters with smaller tips have lower volume-to-surface ratios at or near the emitter tip. Because of the central divider, theta-glass emitters have even greater surface areas than single barrel emitters of the same size. In this study, we compare two theta emitter sizes, 269 nm and 1.7 μm in diameter (Supplemental Figure 4.1a-b) to explore the protein-glass surface interactions of proteins that have different conformations and physical properties. We also show that the effects

of these surface-interactions and the resulting protein ion signal is time dependent. These effects should be taken into consideration or eliminated by surface modifications in future studies that use submicron emitters for fast mixing or for ion desalting of biological samples.

## 4.3 Experimental Method

Nanoelectrospray ionization emitters are made from boroslicate theta capillaries (1.2 mm o.d./0.9 mm i.d., 0.15 mm septum thickness, Sutter Instruments, Novato, CA, USA) by pulling the tips to outer diameters of 269 ± 7 nm or 1.7 ± 0.1 μm in the long dimension (the short dimension is 82% and 78% of the long dimension, respectively) with a Flaming/Brown micropipette puller (Model P-87, Sutter Instruments, Novato, CA, USA). Tip diameters are measured with a scanning electron microscope (Hitachi TM-1000 SEM, Schaumburg, IL, USA). Both channels are filled with the same aqueous ammonium acetate or ammonium bicarbonate solution containing proteins. Two 0.127 mm diameter platinum wires are inserted into the two barrels of a theta emitter and are in contact with the sample solution. Ion formation is initiated by placing the emitter tips 1 to 2 mm distant from the instrument orifice and applying the lowest possible (± 0.6 – 1 kV) voltage to the platinum wires in order to produce stable ion formation. A nitrogen gas backing pressure of 10 psi is applied to the end of the theta emitters. Mass spectra are acquired with an LTQ mass spectrometer (Thermo Fisher Scientific, Waltham, MA, USA) with a capillary temperature of 265 °C.

Reduced/alkylated RNase A solution is prepared by dissolving lyophilized RNase A powder in a 100 mM ABC (pH 8.7) solution containing 6 M guanidine hydrochloride, 15 mM dithiothreitol and 100 mM iodoacetamide. The sample is reacted in the dark for approximately two hours and buffer exchanged once into 100 mM ABC using a biospin column (Bio-Rad, Hercules, CA, USA). The final concentration of the stock solution of reduced/alkylated RNase A is 200 μM. Reduced/alkylated lysozyme is prepared by first reducing the lysozyme in 6 M guanidine hydrochloride, 15 mM dithiothreitol and 100 mM ABC solution (pH 8.8) for half an hour at 37 °C, then reacted in the dark with 150 mM iodoacetic acid at room temperature for about two hours. The 200 μM stock solution of reduced/alkylated lysozyme is buffer exchanged once into 100 mM ABC using a biospin column (Bio-Rad, Hercules, CA, USA). The change in the isolectric point for the reduced protiens compared to the intact protein is computed using ExPASy (SIB Swiss Institute of BioInformatics) [20] by replacing cysteine residues with acidic or basic residues in the protein sequence and computing the shift in isolectric point for the two forms of the protein.

Lyophilized protein powders of equine cytochrome *c*, bovine pancreatic ribonuclease A (RNase A), egg white lysozyme, bovine ubiquitin, ammonium acetate, ammonium bicarbonate, guanidine hydrochloride, dithiothreitol, iodoacetamide and iodoacetic acid are from Sigma (St. Louis, MO). Protein solutions were prepared at different concentrations either in 100 mM ABC or 100 mM AA.

## 4.4 Results and Discussion

### 4.4.1 Protein Conformation and Signal with Small Tips

Many factors affect protein signal in ESI, including solvents, sequence, conformation, instrument parameters, etc [21–24]. Recent results indicate that interactions between positively charged proteins and the negatively charged emitter surface at small tip size can also be a contributing factor[19]. The role of emitter tip size was investigated with theta glass capillaries with tip sizes of 1.7 ± 0.1 μm and 269 ± 7 nm. The effects of protein conformation on nanoESI signal with these two different size theta emitters was investigated by reducing internal disulfide bonds of bovine pancreatic bovine pancreatic ribonuclease A (RNase A) and capping the S-H groups by alkylation to prevent reformation of these bonds. RNase A is a 13.7 kDa protein with a high isoelectric point (pI 9.6) [25,26] and it has a net positive charge in ammonium acetate and ammonium bicarbonate solutions. Results from circular dichroism [27,28], hydrogen-deuterium exchange [29,30] and X-ray scattering [31] show that reduced RNase A is significantly unfolded whereas intact RNase A has a compact, folded structure. Ubiquitin (pI 6.8) [32] has a net negative charge in ABC and has no net charge in AA. It is used as an internal standard because it should not interact significantly with the negatively charged surfaces of the borosilicate emitters. Mass spectra of the mixture of 10 μM RNase A and 1 μM ubiquitin from 100 mM ABC using 1.7 μm and 269 nm theta emitters are shown in Figure 4.1a and d, respectively. The relative abundances of these two proteins differ slightly with the two different tips. The charge-state distributions of both proteins are shifted to slightly lower charge with the 269 nm emitters. Higher charging with small tips has been reported previously and this has been attributed to electrothermal supercharging or higher electric field with small tips [16,19,33]. Here, this effect may be due to the different droplet sizes and thus lifetimes of these droplets. The 269 nm theta emitters form smaller droplets that have lifetimes of around 1 μs whereas droplets from the 1.7 μm emitters are larger and have lifetimes of about 26 μs [12]. The emitter tips are approximately 1 to 2 mm away from the instrument orifice. In order for the small droplets formed from 269 nm theta emitters to enter the instrument orifice, they must have a velocity that is at least 1000 m/s. Thus, ions formed from these small droplets are likely desolvated or nearly de-solvated before entering the heated capiliary of the instrument. In contrast, the larger droplets formed from the 1.7 μm emitters have sufficient lifetimes that they likely enter the heated ion transfer tube. Heating of the droplet inside the heated transfer tube can destabilize the folded form of proteins,which leads to higher protein charge states in the mass spectra using the 1.7 μm theta emitters. There is no effect of tip size on protein charge state in AA, which is consistent with electrothermal supercharging results that suggest that thermal protein unfolding occurs less readily in AA [34,35].

Mass spectra of a mixture of 10 μM reduced carbamidomethylated RNase A ("amide form") and 5 μM ubiquitin in 100 mM ABC are shown in Figure 4.1b and e for the two different tip sizes. The charge-state distribution of reduced RNase A is bimodal with the higher charge states (10+ to 18+) most abundant, indicating that reduced RNase A is predominantly unfolded in solution. Both ubiquitin and reduced RNase A ions are formed with the 1.7 μm theta emitters. In contrast, the abundance of reduced RNase A ions is dramatically lower with the 269 nm theta emitters. The abundance of reduced RNase A ions relative to the total protein ion abundance (reduced RNaseA and ubiquitin) is 82% ± 1% and 5.1% ± 0.3% with the 1.7 μm and 269 nm theta emitters, respectively. The significantly lower abundance of reduced RNase A compared to folded

RNase A with the 269 nm theta emitters indicates that the unfolded conformation of the protein is likely the origin of the very low signals with the 269 nm emitters.

Effects of conformation on protein ion signal and tip size was further investigated by measuring ESI mass spectra of 10 μM egg white lysozyme, 5 μM reduced carboxymethylated lysozyme ("acid form") and 2.5 μM ubiquitin mixture in 100 mM ABC (Figure 4.1c and f). Lysozyme is a 14.7 kDa basic protein (pI 11.4) with four disulfide bonds and has a net positive charge in these solutions [36,37]. The conformation of reduced lysozyme is similar to that of lysozyme denatured in 4 M guanidine hydrochloride [38]. Charge-state distributions for all three proteins are produced with the 1.7 μm theta emitters. In contrast, there is no signal for reduced lysozyme with the 269 nm theta tips. The absense of signal for reduced lysozyme but not intact lysozyme in the 269 nm tips is consistent with the results for reduced/intact RNase A, providing additional evidence that the ion signal for largely denatured proteins with isoelectric points higher than 7 is significantly reduced with submicron emitters.

To determine the effect of protein charge, mass spectra of reduced α-lactalbumin (four disulfide bonds) with carboxymethylated S-H groups ("acid form") were obtained with both 1.7 μm and 269 nm tips from ABC. The ion signal for carboxymethylated α-lactalbumin is comparable to but slightly lower with the 269 nm tips (Supplemental Figure 4.2). The pI of carboxymethylated α-lactalbumin is lower than 4.2 so this unfolded protein has a net negative charge in these solutions [39]. The observation that significantly lower signal is observed for unfolded proteins with net positive charge in solution but only slightly lower signal is observed for unfolded proteins with a net negative charge in solution is consistent with positively charged proteins interacting strongly with the negatively charged surface of the smaller emitters where the surface-to-volume ratio is greatest. Unfolded proteins have potentially more sites of interaction with surfaces and may be expected to interact more strongly when the number of positive charges exceed the number of negative charges on the protein.

Another feature of the 269 nm theta emitters is that the protein ions have fewer salt adducts (Figure 4.1d – f) compared to those formed by the 1.7 μm theta emitters (Figure 4.1a – c). This effect of small tips on desalting protein ions has been reported with both buffered aqueous solutions with ≥ 150 mM $Na^+$ or $K^+$ [17,18] and water/methanol/acetic acid solutions [15,16]. These results are consistent with the hypothesis that the smaller initial droplets formed with the 269 nm emitters have fewer than one protein per droplet so that the initial droplets have a much lower salt-to-protein ratio compared to that in the original solution or to the larger droplets formed from 1.7 μm tips which have on average more than one protein molecule. The lower salt-to-protein ratio in the initial droplet leads to fewer salt adducts on the desolvated protein ions [17].

### 4.4.2 Time evolution of protein signals

To further investigate the origin of the extraordinarily low signal for unfolded proteins in the 269 nm emitter tips, experiments focusing on time as a variable were conducted. NanoESI mass spectra of a mixture of 2.5 μM ubiquitin, 10 μM lysozyme, 5 μM reduced lysozyme and 5 μM cytochrome *c* in 100 mM ABC and 100 mM AA were continuously acquired for 30 minutes with both 1.7 μm and 269 nm emitters. A time sequence of mass spectra obtained from 100 mM ABC, each signal average for six minutes over the course of 30 minutes, is shown in Figure 4.2. With the 1.7 μm theta emitters, there are ions for all four proteins in the first six-minute signal averaged mass spectrum (Figure 4.2a). The charge-state distributions are similar to reported values for ubiquitin (5+ to 7+), lysozyme (6+ to 8+), reduced lysozyme (bimodal distribution 8+ to 17+)

and cytochrome *c* (7+ to 8+) from ABC [34,40,41]. With the 269 nm theta emitters, charge-state distributions of only ubiquitin and lysozyme are observed for the first 12 minutes (Figure 4.2b - c), consistent with the results shown in Figure 4.1f. The peaks for both proteins are narrower due to fewer salt adducts. After 12 minutes, ions of reduced lysozyme appear (Figure 4.2d-e), and cytochrome *c* ions appear after 24 minutes (Figure 4.2f). After 24 minutes, the mass spectrum with a 269 nm theta emitter (Figure 4.2f) is comparable to the mass spectrum initially obtained with the 1.7 μm theta emitters, albeit with fewer salt adducts to the protein ions (Figure 4.2a). The same results are obtained for these proteins when 100 mM AA is used instead indicating that this effect is not unique to ABC (Supplemental Figure 4.3). The protein signal of reduced lysozyme and cytochrome *c* takes many minutes to appear in mass spectra obtained with the 269 nm theta emitters, but there is signal for all four proteins with the 1.7 μm emitters at the start (Supplemental Figure 4.3). Mortensen et al. found that cytochrome *c* signal was not obtained from 100 mM ABC but was from 100 mM AA with a ~300 nm theta emitter [19]. Time was not a parameter considered in the previous studies, which may account for this earlier observation.

Acidification of solutions can occur when nanoESI occurs for a long time [42,43]. In these experiments, voltage is applied to the two platinum wires that are in contact with the protein solution. The platinum wire is 3 - 5 mm away from the emitter tip where droplet formation occurs. Thus, it takes time for excess protons to diffuse to the end of the emitter tip. The effect of acidification on protein signal and charge state was investigated by spraying the same mixture of the four protein in the ABC solution from 1.7 μm theta emitters for thirty minutes. No significant change of charge-state distribution occurs after thirty minutes (Supplemental Figure 4.4). Similarly, the protein charge states that are formed with the 269 nm tips at the end of 30 minutes (Figure 4.2f) are similar as those formed with the larger tips at the start and in the end (Figure 4.2a and Supplemental Figure 4.4). These results indicate that acidification does not play an important role in the time evolution of protein signal observed with the 269 nm tips.

The time evolution of the protein ion signal in one-minute intervals for lysozyme, reduced lysozyme, cytochrome *c* and ubiquitin is shown in Figure 4.3. Both the signal of each protein relative to that of ubiquitin and the fraction of signal of each protein relative to the total ion abundance are shown are shown in Figure 4.3a and 4.3b, respectively. The relative ion abundance of each protein relative to the absolute ion abundance of ubiquitin shown on the *y*-axis is defined as

$$Relative\ Abundance = \frac{\sum I_i}{\sum I_j} \qquad \text{(Eq. 1)}$$

where $I_i$ is the total abundance of a protein ions of interest and $I_j$ is the total abundance of ubiquitin ions. These data show that there is significant variability of signal with these small tips but there are clear trends in the ion abundances with time. Data for two additional emitters and three emitters for AA show the same trends of ion abundance with time (Supplemental Figure 4.5a,b). Initially, only ubiquitin ions are formed in both ABC and AA solutions. Lysozyme ions appear 1 to 5 minutes after nanoESI is initiated and ubiquitin ions are observed (Supplemental Figure 4.4). The time required for reduced lysozyme signal to appear depends on the individual theta emitter, and ranges from several minutes to 15 minutes. The signal for both forms of lysozyme increases with time. Cytochrome *c* signal appears after 25 minutes to 30 minutes with either AA or ABC solutions. The order of appearance of the four proteins ions is consistently ubiquitin, lysozyme, reduced lysozyme, and cytochrome *c* for both ABC and AA buffer using the 269 nm theta emitters.

These results show that reduced lysozyme and cytochrome *c* ions can be formed from the 269 nm theta emitters with both ABC and AA solutions, but it takes significantly longer for these ions to appear than when these ions are formed with the 1.7 μm theta emitters. The significant delay of ion formation for reduced lysozyme and cytochrome *c* indicates that these two proteins do not enter the droplets when nanoESI is initiated with a 269 nm theta emitter. We hypothesize that these proteins present in the solution near the emitter tip interact with the inner surface of the glass emitter thereby making them unavailable to enter the initial droplets that are formed when nanoESI is initiated. The hydroxyl groups at the glass surface are deprotonated when the solution pH is greater than 3 [44,45]. The pH of the ammonium bicarbonate and ammonium acetate solutions are 7.8 and 6.8, respectively. Thus, the inner surface of the emitter is deprotonated and has a net negative charge with these solutions. Ubiquitin has an isoelectric point of 6.8, so it has no net charge in the AA solution and has a net negative charge in ABC solution. Cytochrome *c* has a slightly lower isoelectric point (pI 10.04) [46] than lysozyme (pI 11.4) but does not have disulfide bonds. Both proteins are positively charged in AA or ABC solution. Calculations indicate that the additional acidic groups on the eight cysteine residues of lysozyme lower the isoelectric point from 11.4 to 8.64. Thus, reduced carboxymethylated lysozyme has lower pI than cytochrome *c,* but a net positive charge in the aqueous buffer solutions. The favorable electrostatic interactions between positively charged proteins and the negatively charged emitter inner surface can lead to a decrease in concentration of free protein in solution and a loss of signal for these proteins in the initial electrospray droplets.

It is interesting to compare lysozyme and cytochrome because both proteins are positively charged in solution, are similar in size and have similar radii of gyration (Rg) (13.1 Å for folded cytochrome *c* [47] and 13.3 Å for folded lysozyme [48,49]) . However, lysozyme ions appear a short time after nanoESI is initiated, but cytochrome *c* appears after ~25 minutes with the 269 nm emitter tips. There are more basic residues on one side of cytochrome *c* and more acidic residues on the other side resulting in a high dipole moment for this protein [50]. In contrast, lysozyme has more uniformly dispersed basic and acidic residues resulting in a lower dipole moment (Figure 4.4) [50]. The lower dipole moment and lower density of basic residues on one side of lysozyme may lead to a weaker interaction with the negatively charged borosilicate glass surface than cytochrome *c*.

The order of appearance of the protein ion signal with the 269 nm emitter tips is different from that in cation exchange chromatography, where lysozyme binds more strongly to a stationary phase consisting of agarose or cellulose beads coated with anionic polymers [51]. In contrast, Morez et al. showed that at the pH of the ABC and AA buffers, more than twice as much cytochrome *c* absorbs onto SBA-15 silica particles than lysozyme [52]. The latter result is consistent with our observations for a nearly identical material although differences in surface roughness may also affect these results.

The binding affinities between the emitter surface and the different proteins depends not only on protein net charge and size, but it also depends on the accessibility of the charged amino acid residues. The conformation of reduced lysozyme is considerably more flexible than that of intact lysozyme, which has limited structural flexibility owing to the four internal disulfide bonds. More conformational flexibility should lead to a greater number of possible interactions between protonated basic residues and the negatively charge surface and hence a greater electrostatic interaction for reduced lysozyme and the glass surface (Figure 4.4). Reduced lysozyme appears sooner in mass spectra than cytochrome *c* possibly because reduced lysozyme has lower pI than cytochrome *c*. This may also be due to higher repulsive interactions between the negatively charged amino acid groups in reduced lysozyme, which must also be stronger owing to their closer

proximity to the glass surface (Figure 4.4). Thus, the order in which these proteins are observed in time appears to be related to their relative binding strengths of these proteins to the anionic surface of the emitters.

In order to estimate the surface coverage corresponding to adsorption of all protein onto the emitter surface, the surface area and volume of solution in each channel up to 1.0 mm from the tip was estimated. For a 600 nm tip, the open area of each channel is about 150 nm in the long dimension (Supplemental Figure 4.1c). Thus, the open area of the 269 nm theta emitter cross section was estimated as a split circle with 135 nm diameter. The surface area was estimated by using a volume element of a half cylinder with a radius of 68 nm and length of 1.0 mm. With 20 μM total concentration of proteins with a net positive charge, only about 0.3% of the surface of the capillary would be covered with protein if every protein in solution in this volume adhered to the surface (modeled with cytochrome *c* with a diameter of 3.4 nm). Thus, there is more than sufficient capillary surface area in these 269 nm emitters to completely remove protein from the initial solutions at the capillary tips. Even with the 1.7 μm theta emitters, less than 2% of the surface would be covered if all of the protein in solution adhered to the capillary surface. The low surface coverage for both the 269 nm and the 1.7 μm theta emitters indicates that diffusion plays an important role. The diffusion distance is six times longer in the 1.7 μm theta emitters than it is in the 269 nm emitters. Moreover, the solution flow rate in the 1.7 μm theta emitters (~1000 pL/s) is one order of magnitude higher than the 269 nm theta emitters (~100 pL/s) [12]. As a result, a much smaller fraction of protein molecules can interact with capillary surface inside the 1.7 μm theta emitters owing to both the longer diffusion length and significantly faster flow rate. Thus, the surface effects observed with the smaller capillaries are significant not just because of the higher surface-to-volume ratio, but also because of the smaller diffusion length and significantly lower flow rates that enable a greater fraction of the proteins to interact with the surface. As solution flows through the emitter tip, more protein in solution can bind to the surface until the surface is sufficiently coated with positively charged protein ions. This will significantly lower the zeta potential and result in significantly lower protein-surface interactions. Competitive binding of proteins should result in displacement of weaker binding proteins consistent with the order of appearance of protein ions in these experiments with time.

### 4.4.3 Competing protein-surface interaction

In order to investigate potential competitive binding of proteins to the emitter surfaces, solutions of just cytochrome *c* (10 μM) and ubiquitin (2.5 μM) without other proteins present were prepared in AA and ABC. Results with both positive and negative ions were obtained and are consistent (Figure 4.5a-f and Supplemental Figure 4.6a-f). Results for negative ions are shown to illustrate that the ion desalting effect with the small tips also occurs for protein anions. Both ubiquitin and cytochrome *c* anions are initially formed with the 1.7 μm theta emitters (Figure 4.5a-b). With the 269 nm emitters, only ubiquitin ions are formed initially. No cytochrome *c* ions are observed for the first eight minutes but ions for both proteins are observed from 9 – 13 min (Figure 4.5e and 4.5f). The slightly lower charge states formed from ABC may reflect differences in protein conformation or stabilities in these different buffers. Cytochrome *c* signal is delayed with the 269 nm theta emitters for both buffers when either positive or negative ions are formed, consistent with our proposed mechanism that proteins that are positively charged in solution can interact with the negatively charged glass surface prior to the droplet formations.

Cytochrome *c* ions appears at shorter time in this solution (10 μM) than the one that contains 5 μM reduced lysozyme and 5 μM cytochrome *c* and appear at a time comparable to where reduced lysozyme is first observed in the latter solution. These results are consistent with cytochrome *c* displacing reduced lysozyme on the surface when both these proteins are present at lower concentration.

## 4.5 Conclusions

The effects of protein structure and charge on ion signal was investigated using 1.7 μm and 269 nm theta glass emitters. Significantly lower salt adduction to both positive and negative ions occurs with the submicron emitters. This affect is attributed to a lower salt-to-protein ratio in nanoESI droplets that are sufficiently small that most droplets contain salt but no protein which lowers the salt-to-protein ratio in small nanodrops that do contain a protein molecule. The signal for a mixture of proteins does not depend on time over the course of 30 minutes with the 1.7 μm emitters but a significant time dependence is observed with the 269 nm tips. The signal for unfolded forms of a protein are initially signficantly reduced or absent compared to the folded forms of the same protein with the 269 nm tips, but signals for these proteins appear after times as long as 25 minutes. The same effect is not observed for an unfolded form of a protein that is negatively charged in solution, indicating that the charge of the protein in solution plays a key role. These results are all consistent with positively charged proteins in solution interacting with and adhearing to the negatively glass surface of the emitters thereby reducing the concentration of these proteins in the initial electrospray droplets. A key finding of this work is that it is not just the high surface to volume ratio of the small emitters that is important because both the small and large emitters have sufficient surface areas to adsorb all the protein in the first 1.0 mm distance from the tip. However, the diffusion length of the smaller emitters is significantly shorter and the flow rate is significantly slower. These factors enable the protein in the small emitters to interact with and adhere to the emitter surface more efficiently. The use of small emitters appears to be highly advantageous for desalting protein ions and for mixing two solutions at a fast rate that is not achievable with conventional mixing apparatus. However, analyte-surface interactions can occur with these small emitters and these effects should be considered in experiments using such small tips. These interactions could potentially be significantly reduced or even eliminated by derivatizing the emitter surface to produce little or no net surface charge. The charge of the glass surface depends on pH and is deprotonated above pH 3. Thus, the surface effects observed with the submicron emitters are significant when using buffered aqueous solutions near neutral pH that are commonly used in native mass spectrometry. These effects should be considerably less significant for solutions consisting of water/methanol/acetic acid solutions when the pH is below 3 and the hydroxyl groups at the glass surface are predominately protonated with no net charge.

## 4.6 Acknowledgements

The authors thank the National Institutes of Health (Grant no. R01GM097357) for financial support. The authors also thank Dr. Anna Susa and Dr. Daniel Mortensen for helpful discussions.

## 4.7 Reference


(1) Valaskovic, G. a; Kelleher, N. L.; Little, D. P.; Aaserud, D. J.; McLafferty, F. W. Attomole-Sensitivity Electrospray Source for Large-Molecule Mass Spectrometry. *Anal. Chem.* **1995**, *67* (20), 3802–3805.

(2) Gong, X.; Zhao, Y.; Cai, S.; Fu, S.; Yang, C.; Zhang, S.; Zhang, X. Single Cell Analysis with Probe ESI-Mass Spectrometry: Detection of Metabolites at Cellular and Subcellular Levels. *Anal. Chem.* **2014**, *86* (8), 3809–3816.

(3) Juraschek, R.; Dülcks, T.; Karas, M. Nanoelectrospray - More than Just a Minimized-Flow Electrospray Ionization Source. *J. Am. Soc. Mass Spectrom.* **1999**, *10* (4), 300–308.

(4) Wilm, M.; Mann, M. Analytical Properties of the Nanoelectrospray Ion Source. *Anal. Chem.* **1996**, *68* (1), 1–8.

(5) Hernández, H.; Robinson, C. V. Determining the Stoichiometry and Interactions of Macromolecular Assemblies from Mass Spectrometry. *Nat. Protoc.* **2007**, *2* (3), 715–726.

(6) Heck, A. J. R. Native Mass Spectrometry: A Bridge between Interactomics and Structural Biology. *Nat. Methods* **2008**, *5* (11), 927–933.

(7) Zhang, S.; Van Pelt, C. K. Chip-Based Nanoelectrospray Mass Spectrometry for Protein Characterization. *Expert Rev. Proteomics* **2004**, *1* (4), 449–468.

(8) Nissila, T.; Sainiemi, L.; Franssila, S.; Ketola, R. A. Fully Polymeric Integrated Microreactor/Electrospray Ionization Chip for on-Chip Digestion and Mass Spectrometric Analysis. *Sensors Actuators B Chem.* **2009**, *143* (1), 414–420.

(9) Mark, L. P.; Gill, M. C.; Mahut, M.; Derrick, P. J. Dual Nano-Electrospray for Probing Solution Interactions and Fast Reactions of Complex Biomolecules. *Eur. J. Mass Spectrom.* **2012**, *18* (5), 439–446.

(10) Mortensen, D. N.; Williams, E. R. Theta-Glass Capillaries in Electrospray Ionization: Rapid Mixing and Short Droplet Lifetimes. *Anal. Chem.* **2014**, *86* (18), 9315–9321.

(11) Fisher, C. M.; Hilger, R. T.; Zhao, F.; Mcluckey, S. A. Electroosmotically Driven Solution Mixing in Borosilicate Theta Glass NESI Emitters. *J. Mass Spectrom.* **2015**, *50* (9), 1063–1070.

(12) Mortensen, D. N.; Williams, E. R. Ultrafast (1 Ms) Mixing and Fast Protein Folding in Nanodrops Monitored by Mass Spectrometry. *J. Am. Chem. Soc.* **2016**, *138* (10), 3453–3460.

(13) Mortensen, D. N.; Williams, E. R. Microsecond and Nanosecond Polyproline II Helix Formation in Aqueous Nanodrops Measured by Mass Spectrometry. *Chem. Commun.* **2016**, *52*, 12218–12221.

(14) Jansson, E. T.; Lai, Y.-H.; Santiago, J. G.; Zare, R. N. Rapid Hydrogen-Deuterium Exchange in Liquid Droplets. *J. Am. Chem. Soc.* **2017**, *139* (20), 6851–6854.

(15) Schmidt, A.; Karas, M.; Dülcks, T. Effect of Different Solution Flow Rates on Analyte Ion Signals in Nano-ESI MS, or: When Does ESI Turn into Nano-ESI? *J. Am. Soc. Mass Spectrom.* **2003**, *14* (5), 492–500.

(16) Hu, J.; Guan, Q.-Y.; Wang, J.; Jiang, X.-X.; Wu, Z.-Q.; Xia, X.-H.; Xu, J.-J.; Chen, H.-Y. Effect of Nanoemitters on Suppressing the Formation of Metal Adduct Ions in Electrospray Ionization Mass Spectrometry. *Anal. Chem.* **2017**, *89* (3), 1838–1845.

(17) Susa, A. C.; Xia, Z.; Williams, E. R. Small Emitter Tips for Native Mass Spectrometry of Proteins and Protein Complexes from Nonvolatile Buffers That Mimic the Intracellular Environment. *Anal. Chem.* **2017**, *89* (5), 3116–3122.
(18) Susa, A. C.; Xia, Z.; Williams, E. R. Native Mass Spectrometry from Common Buffers with Salts That Mimic the Extracellular Environment. *Angew. Chemie Int. Ed.* **2017**, 1–5.
(19) Mortensen, D. N.; Williams, E. R. Electrothermal Supercharging of Proteins in Native MS: Effects of Protein Isoelectric Point, Buffer, and NanoESI-Emitter Tip Size. *Analyst* **2016**, *141* (19), 5598–5606.
(20) Gasteiger, E.; Hoogland, C.; Gattiker, A.; Duvaud, S.; Wilkins, M. R.; Appel, R. D.; Bairoch, A. Protein Identification and Analysis Tools on the ExPASy Server. In *The Proteomics Protocols Handbook*; Walker, J. M., Ed.; Humana Press, 2005; pp 571–607.
(21) Liang, Z.; Yang, Q.; Zhang, W.; Zhang, L.; Zhang, Y. Effects of Experimental Parameters on the Signal Intensity of Capillary Electrophoresis Electrospray Ionization Mass Spectrometry in Protein Analysis. *Chromatographia* **2003**, *57* (9–10), 617–621.
(22) Cech, N. B.; Enke, C. G. Practical Implications of Some Recent Studies in Electrospray Ionization Fundamentals. *Mass Spectrom. Rev.* **2001**, *20* (6), 362–387.
(23) Iavarone, A. T.; Jurchen, J. C.; Williams, E. R. Effects of Solvent on the Maximum Charge State and Charge State Distribution of Protein Ions Produced by Electrospray Ionization. *J. Am. Soc. Mass Spectrom.* **2000**, *11* (11), 976–985.
(24) Kuprowski, M. C.; Konermann, L. Signal Response of Coexisting Protein Conformers in Electrospray Mass Spectrometry. *Anal. Chem.* **2007**, *79* (6), 2499–2506.
(25) Smyth, D. G.; Stein, W. H.; Moore, S. The Sequence of Amino Acid Residues in Bovine Pancreatic Ribonuclease: Revisions and Confirmations. *J. Biol. Chem.* **1963**, *238* (1), 227–234.
(26) Tanford, C.; Hauenstein, J. D. Hydrogen Ion Equilibria of Ribonuclease. *J. Am. Chem. Soc.* **1956**, *78* (20), 5287–5291.
(27) Takahashi, S.; Kontani, T.; Yoneda, M.; Ooi, T. A Circular Dichroic Spectral Study on Disulfide-Reduced Pancreatic Ribonuclease A and Its Renaturation to the Active Enzyme. *J. Biochem.* **1977**, *82* (4), 1127–1133.
(28) Qi, P. X.; Sosnick, T. R.; Englander, S. W. The Burst Phase in Ribonuclease A Folding and Solvent Dependence of the Unfolded State. *Nat. Struct. Biol.* **1998**, *5* (10), 882–884.
(29) Woodward, C. K.; Rosenberg, A. Oxidized RNase as a Protein Model Having No Contribution to the Hydrogen Exchange Rate from Conformational Restrictions. *Proc. Natl. Acad. Sci. U. S. A.* **1970**, *66* (4), 1067–1074.
(30) Bai, Y.; Milne, J. S.; Mayne, L.; Englander, S. W. Primary Structure Effects on Peptide Group Hydrogen Exchange. *Proteins Struct. Funct. Genet.* **1993**, *17* (1), 75–86.
(31) Jacob, J.; Dothager, R. S.; Thiyagarajan, P.; Sosnick, T. R. Fully Reduced Ribonuclease A Does Not Expand at High Denaturant Concentration or Temperature. *J. Mol. Biol.* **2007**, *367* (3), 609–615.
(32) Rechesteiner, M. C. *Ubiquitin*; Plenum Press: New York, 1988.
(33) Yuill, E. M.; Sa, N.; Ray, S. J.; Hieftje, G. M.; Baker, L. A. Electrospray Ionization from Nanopipette Emitters with Tip Diameters of Less than 100 Nm. *Anal. Chem.* **2013**, *85* (18), 8498–8502.
(34) Sterling, H. J.; Cassou, C. A.; Susa, A. C.; Williams, E. R. Electrothermal Supercharging of Proteins in Native Electrospray Ionization. *Anal. Chem.* **2012**, *84* (8), 3795–3801.

(35) Cassou, C. A.; Williams, E. R. Anions in Electrothermal Supercharging of Proteins with Electrospray Ionization Follow a Reverse Hofmeister Series. *Anal. Chem.* **2014**, *86* (3), 1640–1647.
(36) Canfield, R. E. The Amino Acid Secpence of Egg White Lysozyme. *J. Bioloqical Chem.* **1963**, *228* (8).
(37) Wetter, L. R.; Deutsch, H. F. Immunological Studies on Egg White Proteins. IV. Immunochemical and Physical Studies of Lysozyme. *J. Biol. Chem.* **1951**, *192* (1), 237–242.
(38) Millett, I. S.; Doniach, S.; Plaxco, K. W. Toward a Taxonomy of the Denatured State: Small Angle Scattering Studies of Unfolded Proteins. *Adv. Protein Chem.* **2002**, *62*, 241–262.
(39) Bramaud, C.; Aimar, P.; Daufin, G. Whey Protein Fractionation: Isoelectric Precipitation of α-Lactalbumin under Gentle Heat Treatment. *Biotechnol. Bioeng.* **1997**, *56* (4), 391–397.
(40) Going, C. C.; Xia, Z.; Williams, E. R. New Supercharging Reagents Produce Highly Charged Protein Ions in Native Mass Spectrometry. *Analyst* **2015**, *140* (21), 7184–7194.
(41) Robinson, E. W.; Sellon, R. E.; Williams, E. R. Peak Deconvolution in High-Field Asymmetric Waveform Ion Mobility Spectrometry (FAIMS) to Characterize Macromolecular Conformations. *Int. J. Mass Spectrom.* **2007**, *259* (1–3), 87–95.
(42) Gatlin, C. L.; Turecek, F. Acidity Determination in Droplets Formed by Electrospraying Methanol-Water Solutions. *Anal. Chem.* **1994**, *66* (5), 712–718.
(43) Van Berkel, G. J.; Zhou, F.; Aronson, J. T. Changes in Bulk Solution PH Caused by the Inherent Controlled-Current Electrolytic Process of an Electrospray Ion Source. *Int. J. Mass Spectrom. Ion Process.* **1997**, *162* (1–3), 55–67.
(44) Brinker, C. J. Hydrolysis and Condensation of Silicates: Effects on Structure. *J. Non. Cryst. Solids* **1988**, *100* (1–3), 31–50.
(45) Behrens, S. H.; Grier, D. G. The Charge of Glass and Silica Surfaces. *J. Chem. Phys.* **2001**, *115* (14), 6716–6721.
(46) Barlow, G. H.; Margoliash, E. Electrophoretic Behavior of Mammalian-Type Cytochromes C. *J. Biol. Chem.* **1966**, *241* (7), 1473–1477.
(47) Shiu, Y.-J.; Jeng, U.-S.; Huang, Y.-S.; Lai, Y.-H.; Lu, H.-F.; Liang, C.-T.; Hsu, I.-J.; Su, C.-H.; Su, C.; Chao, I.; et al. Global and Local Structural Changes of Cytochrome c and Lysozyme Characterized by a Multigroup Unfolding Process. *Biophys. J.* **2008**, *94* (12), 4828–4836.
(48) Hamill, A. C.; Wang, S. C.; Lee, C. T. Probing Lysozyme Conformation with Light Reveals a New Folding Intermediate. *Biochemistry* **2005**, *44* (46), 15139–15149.
(49) Ghosh, A.; Brinda, K. V.; Vishveshwara, S. Dynamics of Lysozyme Structure Network: Probing the Process of Unfolding. *Biophys. J.* **2007**, *92* (7), 2523–2535.
(50) Bharti, B.; Findenegg, G. H. Protein-Specific Effects of Binding to Silica Nanoparticles. *Chem. Lett.* **2012**, *41* (10), 1122–1124.
(51) DePhillips, P.; Lenhoff, A. M. Determinants of Protein Retention Characteristics on Cation-Exchange Adsorbents. *J. Chromatogr. A* **2001**, *933* (1–2), 57–72.
(52) Moerz, S. T.; Huber, P. PH-Dependent Selective Protein Adsorption into Mesoporous Silica. *J. Phys. Chem. C* **2015**, *119* (48), 27072–27079.

## 4.8 Figures

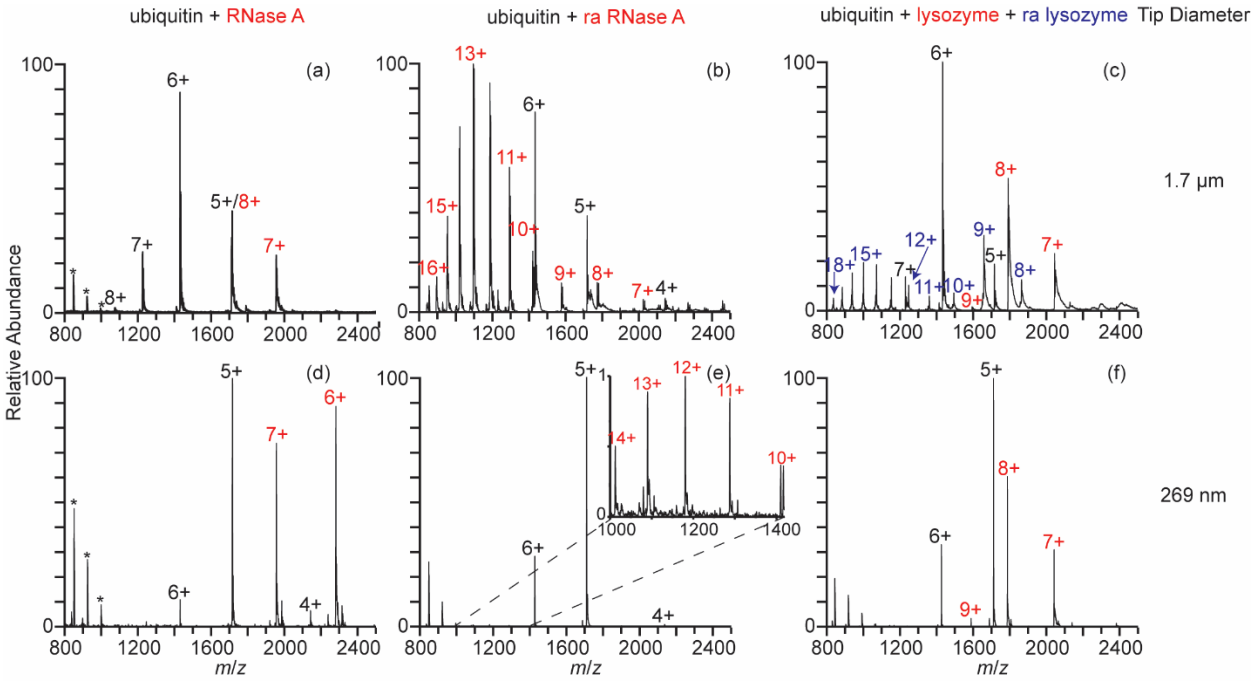


**Figure 4.1.** Electrospray ionization mass spectra of ubiquitin with RNase A (a,d), reduced RNase A (b,e), and both lysozyme and reduced lysozyme (c,f) in 100 mM ABC with 1.7 µm theta emitters (a-c) and 269 nm theta emitters (d-f). The charge states of each protein are color coded and labeled. * indicates polydimethylsiloxane clusters that are present as an impurity.

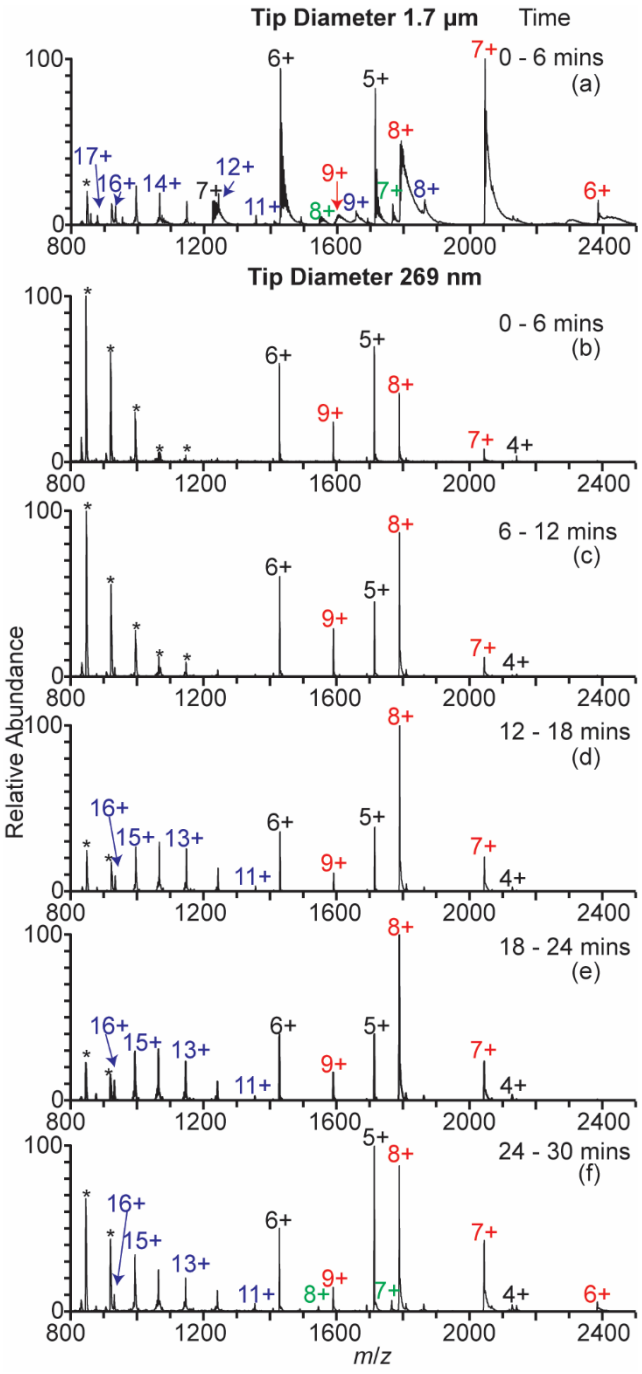


**Figure 4.2.** NanoESI mass spectra of ubiquitin (black), lysozyme (red), reduced lysozyme (blue) and cytochrome *c* (green) in 100 mM ABC solution obtained 1.7 µm theta emitters (a) and 269 nm theta emitters (b-f). Each mass spectrum is signal averaged for six minutes. * indicates polydimethylsiloxane clusters that are present as an impurity.

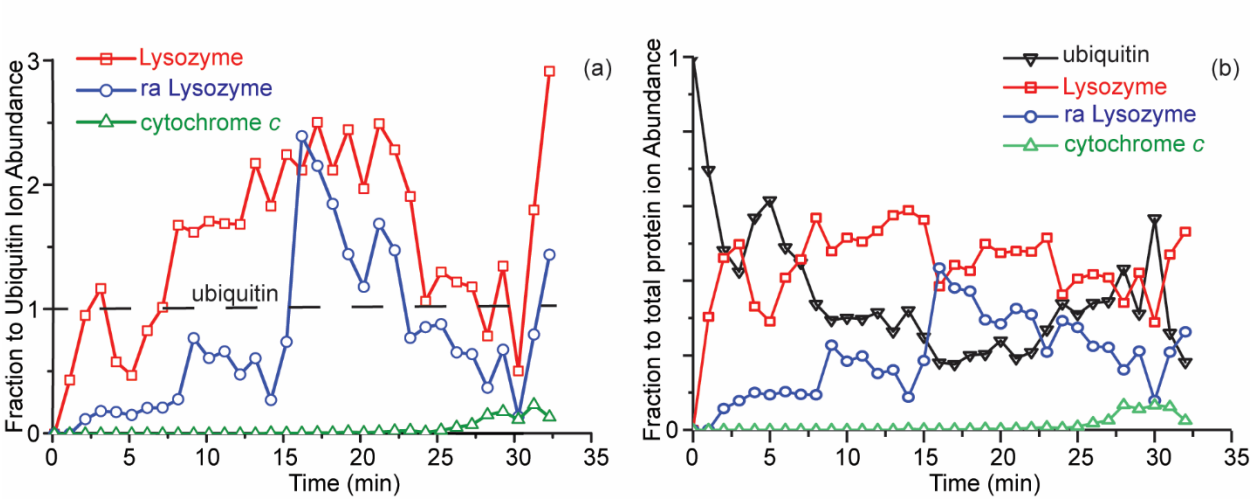


**Figure 4.3.** Ion abundances of lysozyme, reduced lysozyme and cytochrome *c* relative to the normalized total ion abundance of ubiquitin (a) and the individual protein ion abundances to total protein ion abundance (b) over 30 minutes with one minute increments. Data were obtained using a 269 nm theta emitter.

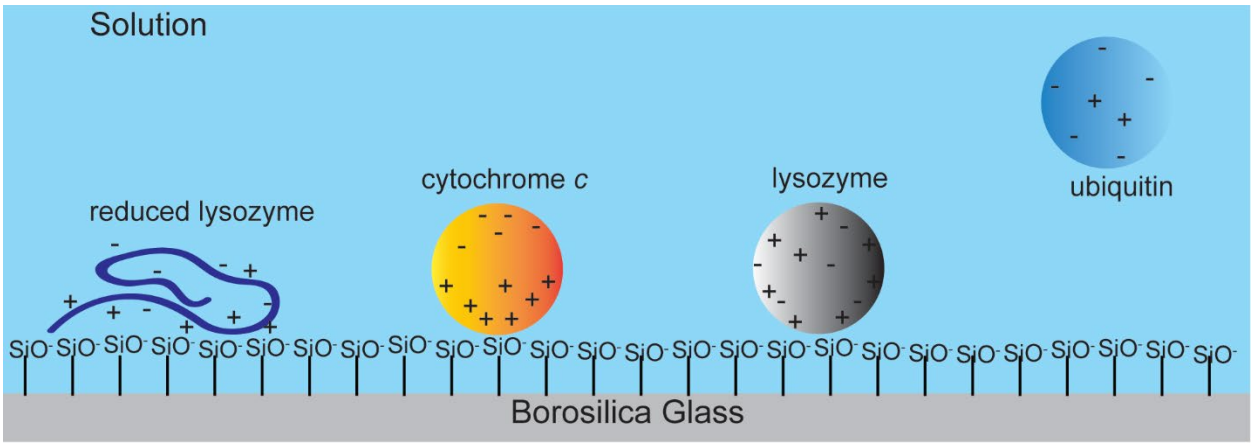


**Figure 4.4.** A schematic illustration of protein conformation and the distribution of charges of reduced lysozyme, lysozyme, cytochrome *c*, and ubiquitin. Ubiquitin has a net negative charge in 100 mM ABC and is neutral in 100 mM AA, thus it should have minimal interactions with the surface. Cytochrome *c* has net positive charge, and has more positive charges on one side of the molecule. Lysozyme also has a net positive charge but the positive charges are more uniformly distributed over the molecule. Reduced lysozyme has a net positive charge and has a flexible conformation that allows more interactions with the glass surface.

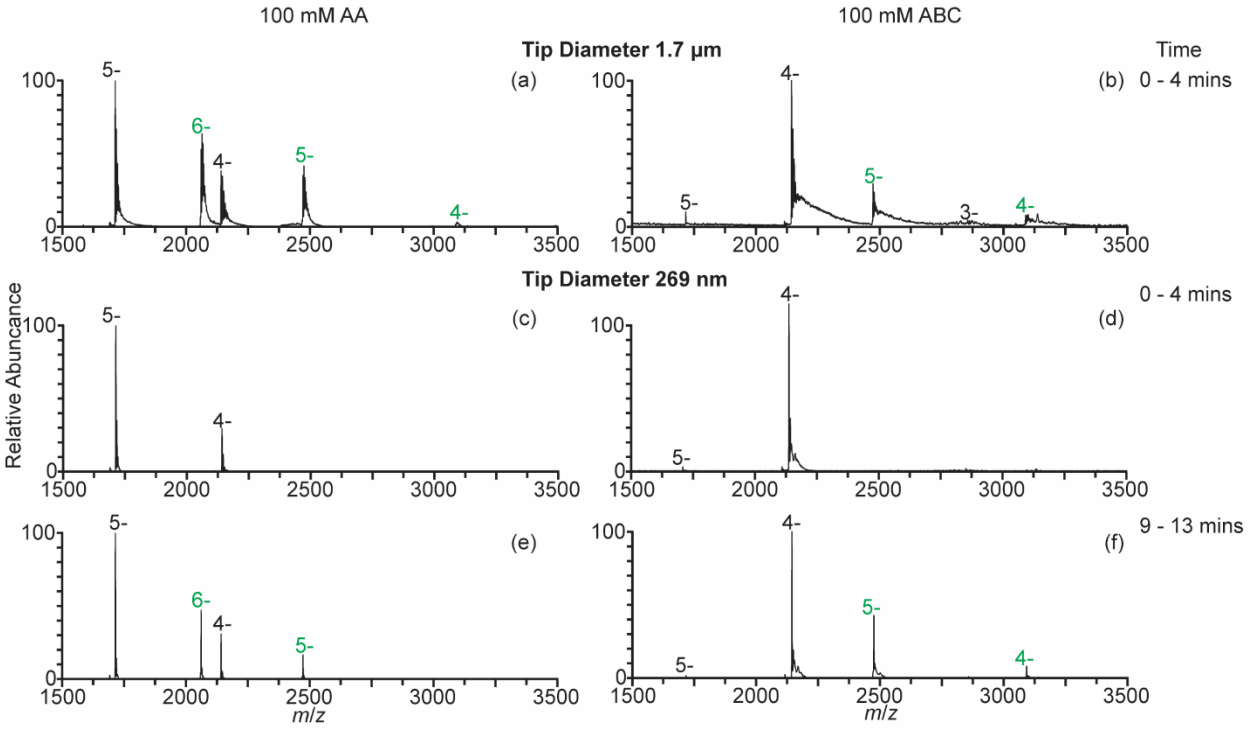


**Figure 4.5.** Negative ion nanoESI mass spectra of a mixture of ubiquitin (black) and cytochrome *c* (green) in 100 mM AA (a,c,e) or 100 mM ABC (b,d,f) acquired with 1.7 µm theta emitters (a-b) and 269 nm theta emitters (c-f) . Each mass spectrum is signal averaged for four minutes.

## 4.9 Supplemental Information

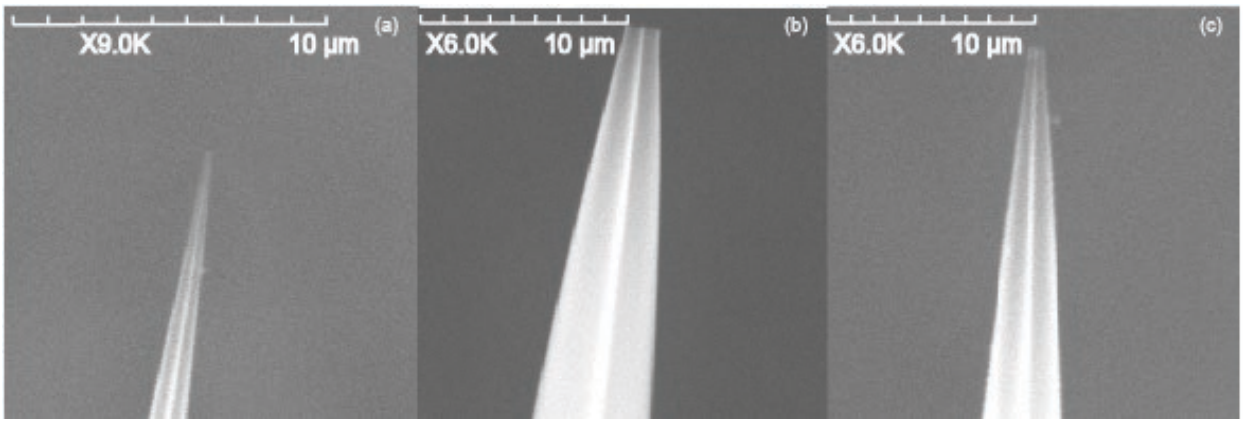


**Supplemental Figure 4.1.** Scanning electron microscope images of 269 nm (a), 1.7 µm (b), and 540 nm (c) theta emitters in long dimension. The short dimension is 211 nm, 1.4 µm, and 470 nm, respectively.

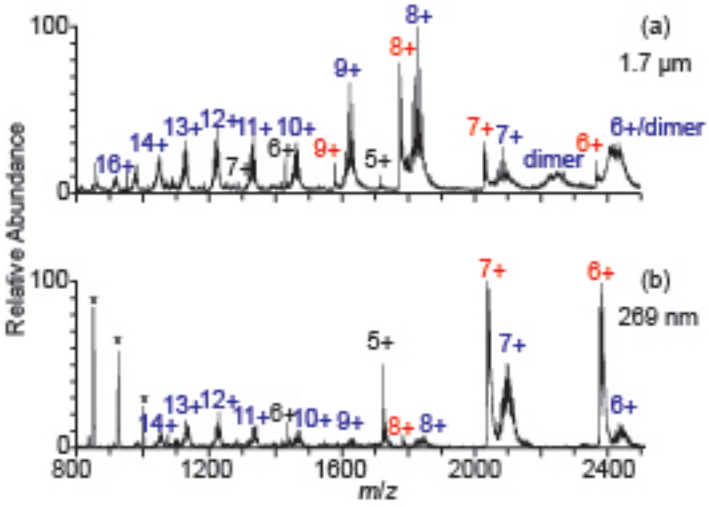


**Supplemental Figure 4.2.** NanoESI mass spectra of a mixture of ubiquitin (black), α-lactalbumin (red), reduced α-lactalbumin (blue) in 100 mM ABC solution with 1.7 µm theta emitters (a) and 269 nm theta emitters (b). * indicates polydimethylsiloxane clusters that are present as an impurity.

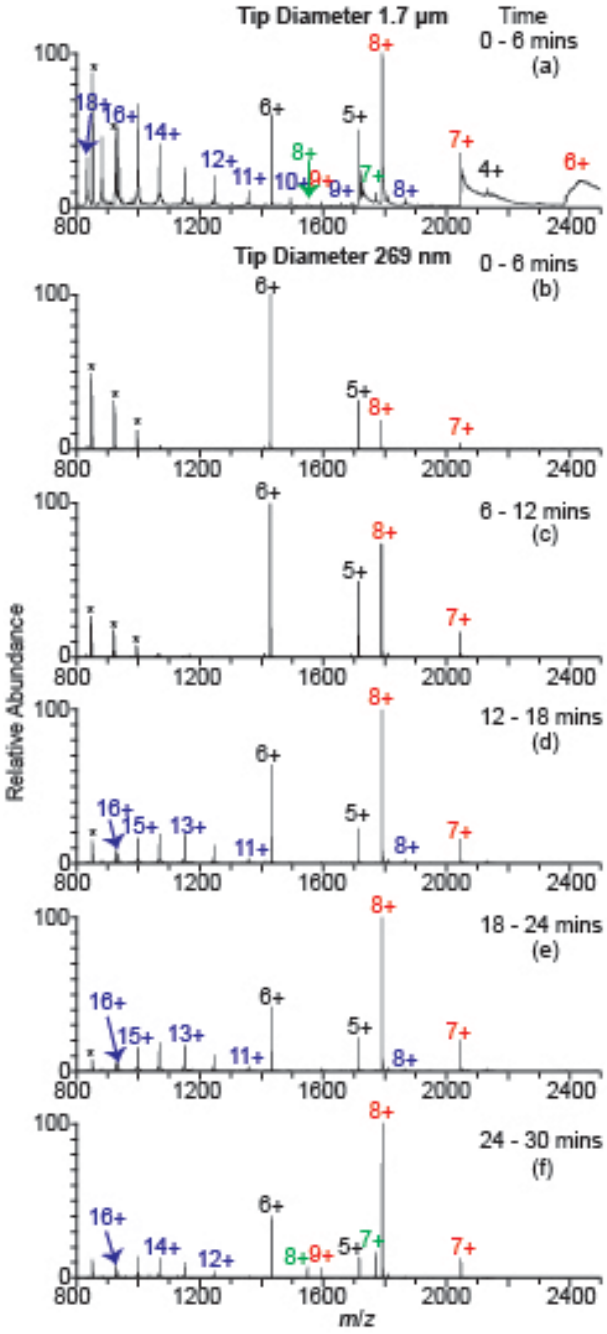


**Supplemental Figure 4.3.** NanoESI mass spectra of a mixture of ubiquitin (black), lysozyme (red), reduced lysozyme (blue) and cytochrome *c* (green) in 100 mM AA solution. Each mass spectrum is signal averaged for six minutes. The 1.7 µm theta emitters (a) and the 269 nm theta emitters (b-f) are used to spray the same protein mixture. * indicates polydimethylsiloxane clusters that are present as an impurity.

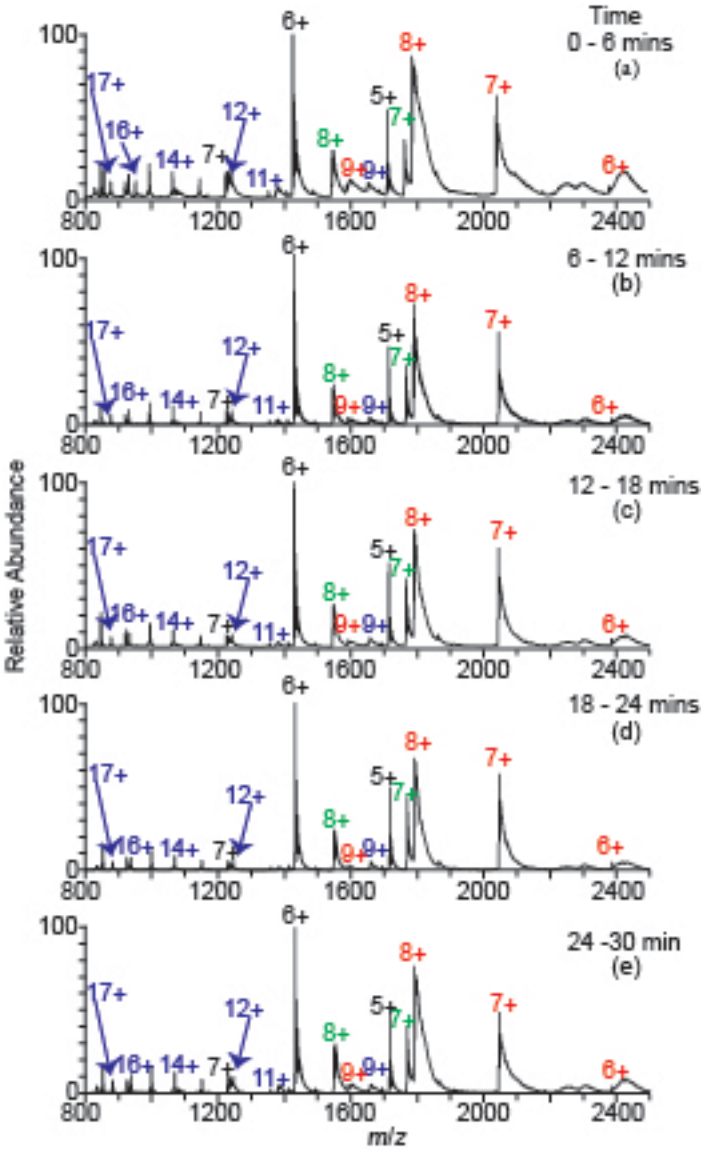


**Supplemental Figure 4.4.** NanoESI mass spectra of a mixture of ubiquitin (black), lysozyme (red), reduced lysozyme (blue) and cytochrome *c* (green) in 100 mM ABC solution using 1.7 µm theta emitters for 30 minutes. Each mass spectrum is signal averaged for six minutes.

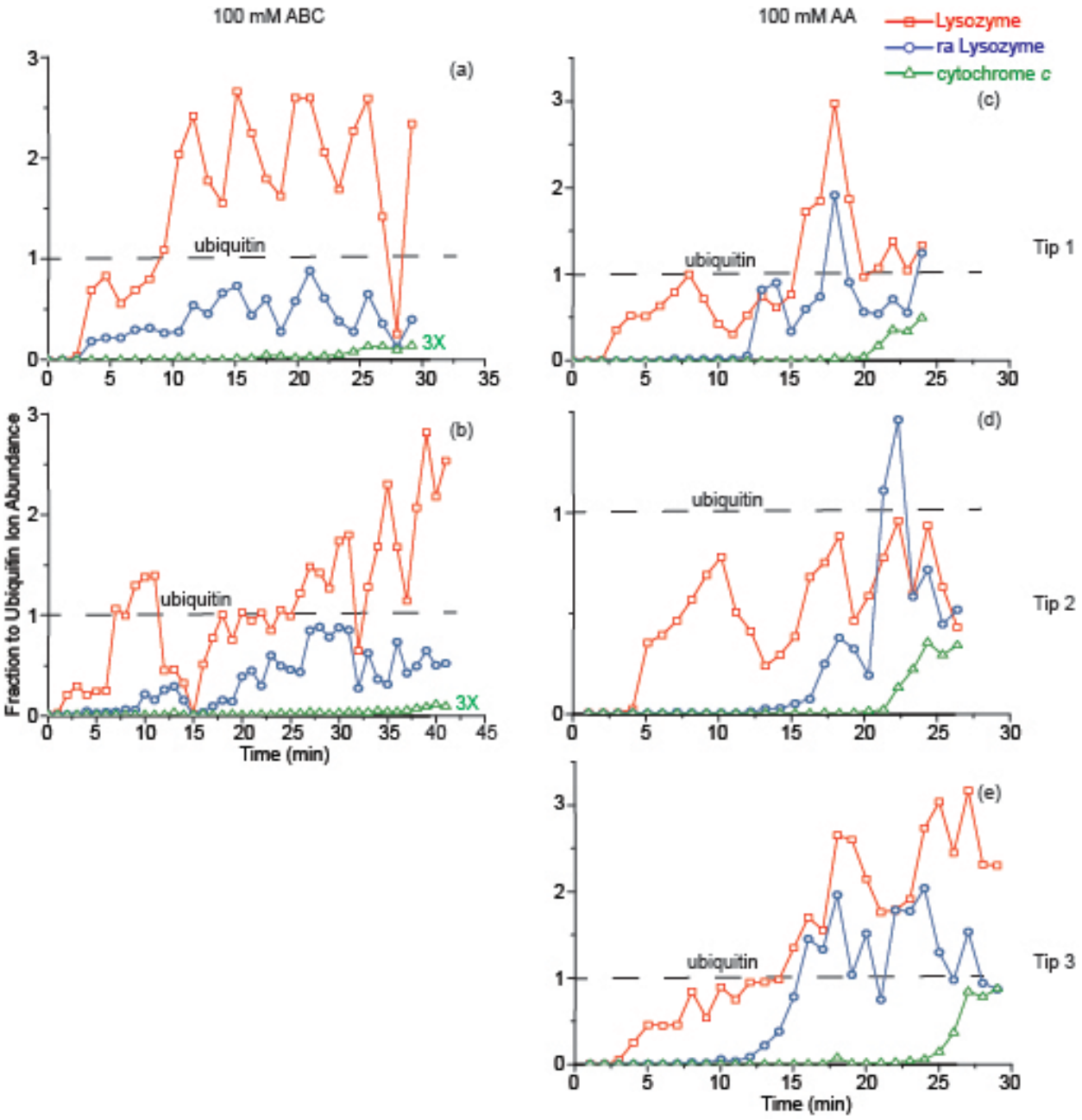


**Supplemental Figure 4.5.** Ion abundances of lysozyme, reduced lysozyme and cytochrome *c* compared to the ion abundance of ubiquitin from 100 mM ABC (a, b) and in 100 mM AA (d – e) over 25 minutes to 40 minutes. Each point is one-minute signal average. Data were obtained using 269 nm theta emitters.

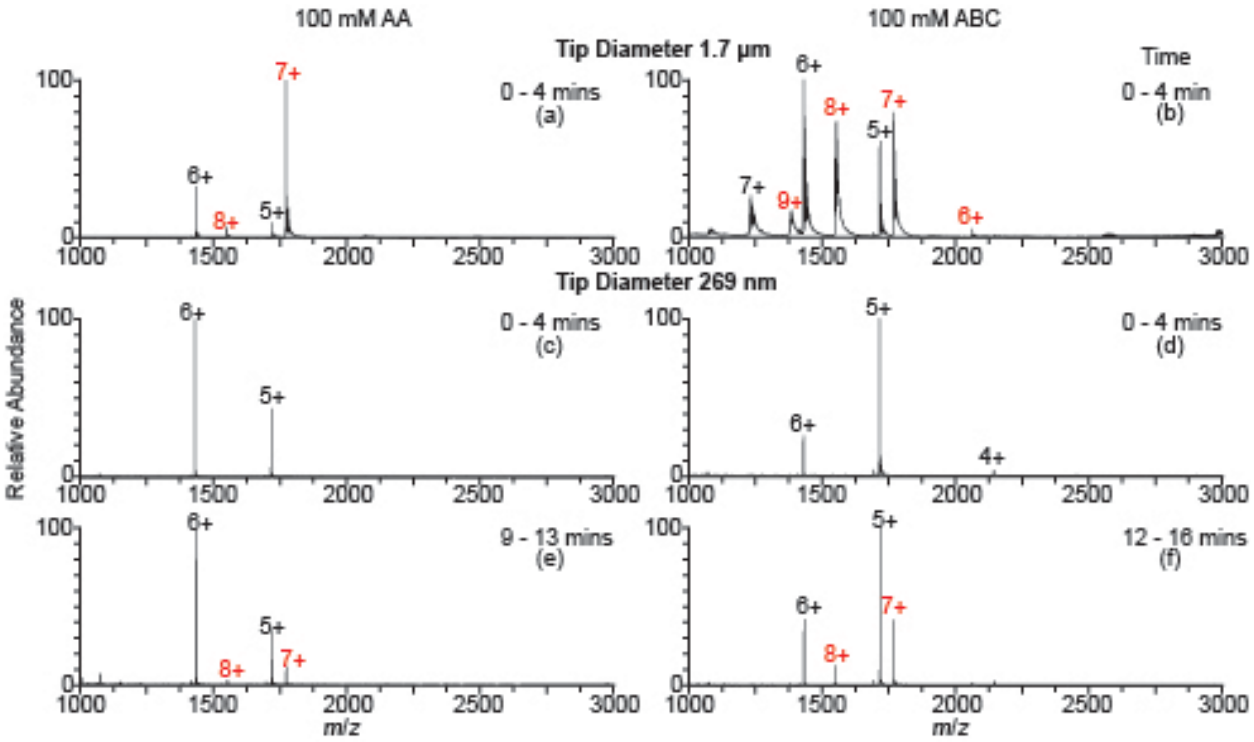


**Supplemental Figure 4.6.** NanoESI positive ion mass spectra of a mixture of ubiquitin (black) and cytochrome *c* (green) in 100 mM AA (a,c,e) or 100 mM ABC (b,d,f) acquired with 1.7 µm theta emitters (a-b) and 269 nm theta emitters (c-f). Each mass spectrum is signal averaged for four minutes.

# Chapter 5

# Effect of Droplet Lifetime on Where Ions are Formed in Electrospray Ionization

This chapter is reproduced with permission from:

Zijie Xia, Evan R. Williams

"Effect of Droplet Lifetime on Where Ions are Formed in Electrospray Ionization"

*Analyst*, **2019**, *144*(1): 237–248



## 5.1 Abstract

The location of gaseous ion formation in electrospray ionization under native mass spectrometry conditions was investigated using theta emitters with tip diameters between 317 nm and 4.4 μm to produce droplets with lifetimes between 1 and 50 μs. Mass spectra of β-lactoglobulin do not depend on instrument source temperatures between 160 and 300 °C with the smallest tips. A high charge-state distribution is observed for larger tips that produce droplets with lifetimes ≥ 10 μs and this distribution increases at higher source temperatures. These and other results show that gaseous protein ions originating from the smallest droplets are formed outside of the mass spectrometer whereas the majority of protein ions formed from the larger droplets are formed inside of the mass spectrometer where thermal heating of the droplet and concomitant protein unfolding occurs. These results show that small emitter tips are advantageous in native mass spectrometry by eliminating effects of thermal destabilization of proteins in droplets inside of the mass spectrometer, eliminating the effects of non-specific protein dimerization and aggregation that can occur in larger droplets that contain more than one protein molecule, andsignificantly reducing salt adduction.

## 5.2 Introduction

Despite the widespread use of electrospray ionization (ESI) to produce gaseous ions from a diverse range of samples for analysis by mass spectrometry (MS), the mechanism by which these ions are produced is still debated.[1–3] In the ion evaporation mechanism, ions are ejected from small droplets owing to the high electric field at the droplet surface, and gaseous ions can be continuously produced throughout the droplet evaporation process.[4,5] In the charge residue mechanism, gaseous ions are formed upon solvent evaporation in the late stages of the droplet lifetime.[6,7] Other mechanisms based upon these principles have been proposed, such as the chain ejection model[8]

and the charge residue-field emission model.[9] Extensive information about these mechanisms and evidence supporting various mechanisms has been reported elsewhere.[5,7–9]

Knowledge about *where* ions are formed is important for understanding the effects of instrument conditions on the appearance of mass spectra and for obtaining reliable reaction rates from reactions that occur in droplet mixing experiments. Information about the conformation of proteins or other biomolecules in solution is often inferred from the resulting charge-state distributions observed in ESI mass spectra, where higher charge states indicate more unfolded conformations than lower charge states, which are indicative of more folded structures.[10–12] However, some instrument conditions can affect charge-state distributions.[13,14] For example, high electrospray potentials used in otherwise native mass spectrometry conditions can lead to high charge states in a mass spectrum. These high charge states are indicative of protein denaturation in the electrospray droplets as a result of droplet heating outside of the mass spectrometer by the high electric field. This effect is the basis of the method called electrothermal supercharging and can be enhanced at elevated electrospray source temperatures illustrating that understanding the effects of these two essential instrument parameters is critical for preserving information about molecular conformation that exists in the original solution.[14,15]

Many studies indicate that desolvated ions are formed at or inside of the atmospheric-interface of the mass spectrometer. Optical spectroscopic measurements by van Berkel and coworkers showed that primarily dications of octaethylporphyrin exist in the ESI plume whereas monocations were observed in the mass spectra indicating that the gaseous ions are produced inside of the atmospheric interface.[16] In contrast, fluorescence measurements by Zenobi and coworkers indicated that some gaseous rhodamine 6G ions are formed in the plume.[17] Chait and coworkers found that higher metal capillary interface temperatures lead to the formation of higher charge states of proteins in water/methanol solutions that contain ammonium acetate but only for some proteins without ammonium acetate.[13] They hypothesized that ammonium acetate affected the droplet lifetime and attributed the change in the charge-state distribution with temperature to the droplets entering the interface prior to gaseous ion formation.[13] A similar conclusion was reported from organic reactions that occur in electrospray droplets.[18] Correlations between the time evolution of different intermediates and the distance between the ESI emitter and instrument inlet suggest that there is a sudden discontinuity in the droplet desolvation process that occurs in the MS inlet. Heating the transfer tube between electrospray emitter and instrument inlet or increasing instrument inlet temperature can also result in different reaction products and intermediates at the same distance, which is consistent with the influence of instrument conditions on the MS results. In recent droplet fusion experiments aimed at obtaining information about reaction rates, ion formation is assumed to occur at the entrance of the mass spectrometer and this assumption is used to establish a reaction time.[19]

A key advance to understanding where ion formation occurs is the ability to form droplets of different size and to measure their corresponding lifetimes. This can be done using theta-emitters in which two different solutions are mixed during the electrospray ionization process.[20–24] To obtain the droplet lifetimes, a unimolecular reaction with a known rate constant in solution is induced by mixing two solutions and the progress of the reaction is monitored using MS.[22,23] A unimolecular process is used because droplet evaporation rapidly increases reagent concentrations with time leading to a large increase in apparent bimolecular reaction rates in droplets although other factors may also play a role.[18,25] The folding of proteins initiated by mixing induced by the electrospray process has been used to establish droplet lifetimes.[22,23] An acidified solution containing a protein that is significantly denatured or unfolded is mixed with either pure water or

an aqueous buffer solution to induce a pH jump upon mixing. The extent of folding that occurs inside of the electrospray droplet is inferred from the resulting charge-state distributions. The droplet lifetime depends on the solution flow rate, which can be changed by varying the emitter tip diameter or backing pressure applied to the solution. This method has been used to produce droplet lifetimes between 1 and ~20 μs using theta emitters with tip diameters ranging from 246 nm to ~1.7 μm and a backing pressure between 5 and 40 psi.[22–24] A mixing time of 1 μs is significantly shorter than that possible in conventional mixing apparatus and this mixing time can be achieved with a 1000 fold lower flow rate. This method has enabled investigations of fast peptide folding that occurs much too rapidly to be observed using other mixing methods.[23,24] The lifetime of droplets can be varied by changing the distance between the emitter tip and the mass spectrometer and by changing spray potentials.[18,26] Velocities of droplets have been measured optically to obtain information about how long the droplets spend outside of the mass spectrometer. In experiments in which mixing is induced upon droplet collisions, gaseous ion formation is assumed to occur at the entrance of the mass spectrometer in order to establish a droplet lifetime from these velocity measurements.[19,26] Droplets formed from emitters with ~4 μm tip diameters with lifetimes ranging from 20 to 230 μs were reported.[26]

In this study, theta emitters with tip diameters ranging from 317 nm to 4.4 μm are used to produce droplets with lifetimes between 1 and 50 μs. The effects of instrument source temperature on β-lactoglobulin ions produced from buffered aqueous solutions using these varying droplet sizes were investigated. Results from these experiments clearly show that gaseous ions that originate from the smallest droplets are formed outside of the mass spectrometer whereas ions originating from the larger droplets are formed inside of the heated electrospray interface of the mass spectrometer. Moreover, these results demonstrate three significant advantages for using sub-micron tips in native mass spectrometry: significant reduction of non-volatile salt adducts, the elimination of effects of source temperature on the resulting mass spectra and the elimination of non-specific dimerization or aggregation that can occur when multiple protein molecules are present in the initial droplet formed from larger emitters.

## 5.3 Experimental Method

### 5.3.1 Mass Spectrometry

Mass spectra are acquired using an LTQ mass spectrometer (Thermo Fisher Scientific, Waltham, MA, USA) with nanoelectrospray ionization (nano-ESI). Borosilicate theta capillaries (1.2 mm o.d./0.9 mm i.d., 0.15 mm septum thickness, Sutter Instruments, Novato, CA, USA) were pulled into emitters with tip outer diameters of 317 ±14 nm (shorter dimension 228 nm), 1.7 ± 0.1 μm (shorter dimension 1.1 μm), and 4.4 μm ± 0.1 μm (shorter dimension 2.1 μm) (Supplemental Figure 5.1). Borosilicate capillaries (1.0 mm o.d./0.78 mm i.d., Sutter Instruments, Novato, CA, USA) are pulled into single barrel emitters with tip diameter of 1.7 μm. Nano-ESI is initiated by applying a spray potential (+ 600 V – 1 kV) on 0.127 mm diameter platinum wires that are inserted into the two barrels of the theta emitters or the single barrel emitters and are in contact with the solutions containing proteins. The emitter tips are placed approximately 1.5 to 2 mm away from the instrument entrance, and the spray voltage is kept as low as possible while maintaining spray stability. A spray potential of 1.3 kV is used to induce electrothermal supercharging.[14] A 10 psi backing pressure of nitrogen gas is applied on all the theta emitters but not on the single barrel

emitters. The instrument source temperature is adjusted from 160 °C to 300 °C, keeping the other instrument parameters constant. The fraction of unfolded protein in the ESI droplets immediately prior to ion formation is determined from the ion abundances in the charge-state distributions using Equation 1,

$$F = \frac{\sum_{unfolded} I_i}{\sum_{total} I_i} \quad \text{(Eq. 1)}$$

where $I_i$ is the protein ion abundance for individual charge states corresponding to the highly charged unfolded protein and the entire charge-state distribution. Ammonium acetate (AA), ammonium bicarbonate (ABC), and lyophilized powder of β-lactoglobulin are from Sigma Aldrich (St. Louis, MO) and were used without further purification.

### 5.3.2 Tryptophan Fluorescence

Emission spectra resulting from tryptophan fluorescence of β-lactoglobulin in 100 mM AA, 10 mM AA and 100 mM ABC are obtained with a FluoroMax-3 spectrometer (Horiba Scientific, Kyoto, Japan). The sample is excited at 280 nm and the resulting emission is measured from 200 nm to 390 nm. Both the entrance and exit slit widths are 2 nm. The inner chamber temperature is raised from 25 °C to 87.5 °C (±0.2 °C tolerance) in 2.5 °C increments. The solution is equilibrated for five minutes at each temperature prior to measurements. Three emission scans are acquired, background subtracted, and averaged for each temperature. A gaussian fit is used to obtain the maximum of the emission peak of β-lactoglobulin tryptophan for the emission peak using OriginPro (Northampton, MA). Temperature melt curves are generated by plotting the maximum of the tryptophan emission peak as a function of temperature.

## 5.4 Results and Discussion

### 5.4.1 Droplet Lifetimes

The lifetimes of droplets produced by nano-ESI using theta emitters depend on several factors, including the solution flow rate, which can be controlled by changing the diameter of the emitter tip or by varying the backing pressure, the spray voltage, and the distance between the emitter tip and the entrance of the mass spectrometer.[22,23,26] Droplets with lifetimes ranging from ~1 μs to 10 μs can be produced with tip sizes between 244 nm and ~1.5 μm using a backing pressure between 5 and 40 psi at a fixed distance of about 1 to 2 mm.[22–24] In order to extend the droplet lifetimes for this study, theta emitters with tip diameters of 4.4 μm ± 0.1 μm (shorter dimension 2.1 μm) where prepared and the droplet lifetime was determined as done previously using pH-induced folding of cytochrome *c* using a 10 psi backing pressure.[23] The lifetime of droplets produced by these larger emitters was measured by mixing an acidified solution containing cytochrome *c* with pure water to induce a pH jump upon droplet formation in the ESI process. Aqueous solutions of 5 μM cytochrome *c* at two different pH values corresponding to the initial solution (1% acetic acid; pH = 2.8) and the final mixed solution (this solution mixed 50/50 with pure water resulting in 0.5% acetic acid after mixing; pH = 3.0) were prepared and nano-ESI mass spectra were obtained (Figure 5.1a and 5.1b, respectively). The charge-state distributions of

cytochrome *c* ions in both spectra are bimodal, with the summed intensity of lower charge states (7+ to 10+) corresponding to 2% ± 1% and 26% ± 1% of the total protein ion abundances in these respective solutions. Fast mixing of this initial cytochrome *c* solution with pure water using the 4.4 μm theta emitters induces protein folding in the nano-ESI droplets and results in 22% ± 1% of total protein ion abundance in the 7+ to 10+ charge states (Figure 5.1c). This value is lower than the 26% ± 1% value measured under equilibrium conditions indicating that the folding process is largely, but not entirely complete.

The integrated rate equation for a two-state reaction (Eq. 2) is used to model cytochrome *c* folding as a two-state process;

$$t = \tau \times ln\frac{A_e - A_0}{A_e - A_t} \quad \text{(Eq.2)}$$

where *t* is the reaction time, $\tau$ is the folding time constant that depends on the protein and solution composition, $A_e$, $A_0$, and $A_t$ are the abundances of the folded protein at equilibrium, time 0 and time *t*, respectively. The folding time constant depends on many factors including the ionic strength and composition of the solution which results in some uncertainty in the droplet lifetime obtained from these measurements. Cytochrome *c* has a folding time constant of 57 μs in 50 mM sodium acetate and 50 mM sodium phosphate.[27] Results obtained from ammonium acetate solution at the same ionic strength and in pure water indicates that the folding time constant $\tau$ in pure water is about half that in ammonium acetate (Supplemental Table 5.1). Thus, the droplet lifetime for the 4.4 μm theta emitters with a 10 psi backing pressure in these experiments obtained from the Figure 5.1 is ~50 ± 7 μs.

Droplet lifetimes in ESI have also been estimated from micro-particle image velocimetry measurements, which showed that 4 μm theta emitters produced droplets with lifetimes between 20 μs and 320 μs depending on the spray voltage and the distance between emitter tip and the instrument entrance (between 0.5 mm and 3 mm).[26] In the experiments here, the theta emitters are about 1.5 mm to 2 mm away from the instrument entrance and the droplets are formed with ~1 kV applied to the solution. Jansson et al. reported 73 μs to 133 μs for the similar spray voltage and tip position.[26] Despite the significant differences in experimental methodologies, the droplet lifetime measured with both techniques are remarkably similar.

### 5.4.2 Effects of Droplet Lifetime and Source Temperature on Protein Unfolding in Droplets

In order to answer the question about where desolvated gaseous protein ions are formed during electrospray ionization, theta emitters with diameters of 317 nm, 1.7 μm and 4.4 μm were used to produce droplets with lifetimes ranging from 1 μs to 50 μs.[23] The instrument source temperature was varied between 160 °C and 300 °C to investigate effects, if any, of thermal activation of droplets that may enter the mass spectrometer inlet system. The spray voltage was kept as low as possible while still maintaining a stable spray to avoid electrothermal supercharging.[14,15] Experiments were performed with β-lactoglobulin, which is a major whey protein in cow and goat milk because the thermal stability of this protein has been widely studied under different pH and salt conditions.[28–31] The melting temperature of β-lactoglobulin is reported in various studies to be between 70 and 80 °C at neutral pH.[29,31] β-lactoglobulin has pI at 5.1 and is negatively charged in the aqueous buffered solutions used in these experiments.[28] Thus, these protein ions in solution should not interact significantly with the glass surface of the theta emitters, which can also induce protein destabilization and partial unfolding in solution before electrospray droplet formation.[32,33]

Results for β-lactoglobulin (10 μM in 100 mM ABC) obtained with 317 nm theta emitters at source temperatures between 160 °C and 300 °C are shown in Figure 5.2a-c. Charge states between 7+ and 9+ are observed, and the relative abundances of these charge states do not change significantly with instrument source temperature. In striking contrast, nano-ESI spectra obtained from this same solution using 4.4 μm theta emitters show a charge-state distribution that is shifted to slightly higher charge at 160 °C (Figure 5.2d) and the appearance of a second higher charge-state distribution (11+ to 17+) centered at 14+ that increases in relative abundance with increasing source temperature (Figure 5.2e and 5.2f). The higher charge-state distribution is indicative of a small population of unfolding proteins *in solution* that increases with source temperature.
The fraction of β-lactoglobulin that is unfolded in solution was estimated from the abundances of the 11+ to 17+ ions divided by the total protein ion signal (Eq. 1). These values obtained from the 4.4 μm emitters are 1.7% ±1.1%, 7.6% ±3.4%, and 18.1% ±1.3% at source temperatures of 160 °C, 230 °C and 300 °C, respectively. It should also be noted that the charge-state distribution of the folded form of the protein is shifted from 8+ with the 317 nm emitters to 9+ with the 4.4 μm suggesting that the native structure of the protein may be partially destabilized with the larger emitter at all source temperatures, although other factors may also contribute. Heating the instrument source increases the surrounding air temperature, and some heating of the solution in the emitter tip and the droplets may also occur before the droplets enter the mass spectrometer. The air temperature measured near the instrument source increases slightly from 38 °C to 48 °C when the instrument source temperature increases from 160 °C to 300 °C. This does not appear to impact the structure of the protein in the emitter tip because no change in the charge-state distribution is observed with the smallest theta emitters and this range of temperatures is below the melting transition of this protein. A similar trend in increasing unfolded population with increasing source temperature occurs with 1.7 μm theta emitters (Supplemental Figure 5.2a-c) but to a lesser extent than with the 4.4 μm theta emitters. In striking contrast, the fraction of ions corresponding to an unfolded protein formed from 317 nm theta emitters is less than 1%, and there is no trend with increasing source temperature. The trend of increasing unfolded protein population with increasing instrument source temperature indicates that the droplets generated from 1.7 μm and 4.4 μm theta emitters experience the high temperature inside the heated ion transfer tube of the instrument. As the larger droplets are heated inside the ion transfer tube of the instrument source, some protein melting or unfolding occurs inside the droplets. Protein ion peaks are also broader from 1.7 μm and 4.4 μm emitters than the ones formed from 317 nm emitters due to sodium adducts, which is consistent with previously reported desalting effects of submicron single and theta emitters during electrospray ionization.[32,34–36]

The temperature inside of the ion transfer tube is likely significantly lower than the elevated set temperature owing to the heat transfer between room temperature air and the heated ion transfer tube. The droplet temperature can be further reduced as a result of evaporative cooling. Thus, the temperatures of the larger droplets inside the transfer tube is unknown. To confirm that the low charge state ions produced from the larger droplets at higher temperature are formed inside the source and not before entering the mass spectrometer, the native form of β-lactoglobulin was destabilized by adding 3% (v/v) ammonium hydroxide in 100 mM ABC (pH 10). A nano-ESI spectrum obtained with the 317 nm theta emitters at a source temperature of 160 °C shows that approximately 5% of the protein is unfolded in this solution (Supplemental Figure 5.3), consistent with the native form of the protein somewhat destabilized so that both folded and unfolded forms are in equilibrium. Even with a 300 °C source temperature, there is no significant increase of unfolded protein with the small emitters (Supplemental Figure 5.3a-b), consistent with the

hypothesis that the droplets generated from the submicron theta emitters do not experience the high temperature inside the source. In striking contrast, 66% of the ion population formed using the 4.4 μm theta emitters corresponds to proteins that are unfolded in solution at a source temperature of 300 °C (Supplemental Figure 5.3c-d). This indicates that the majority of the droplets formed by the larger emitters enter the source and that heat from the source results in melting of the protein in solution inside of the mass spectrometer prior to protein ion formation. It appears from these results that the droplets are insufficiently heated even at this source temperature to completely unfold the protein in solution under these conditions, consistent with results from a prior study.[13]

### 5.4.3 Droplet Velocities and Location of Ion Formation

In order to more thoroughly understand why the charge-state distribution of ions formed from the smallest theta emitters are not affected by the temperature of the source whereas the droplets formed from the larger emitters are affected, the initial droplet velocities and air flow velocity through the heated ion transfer tube were determined. The initial droplet velocity with the 317 nm theta emitters is about 2 m/s. The initial velocity of droplets formed from larger emitters is even less (estimated to be about 0.25 m/s with the 4.4 μm theta emitters based on a flow rate of 3461±509 pL/s). The theta emitters are approximately 1.5 mm to 2 mm away from the instrument entrance, so this initial velocity is insufficient for the smallest nanodrops that have a 1 μs lifetime to reach the mass spectrometer. However, the droplets are accelerated by the applied electric field, and this force is resisted by collisions with the ambient background gas. There is also gas flow into the mass spectrometer induced by the pressure difference between where the ions are formed (~760 Torr) and the first vacuum stage (~0.6 Torr). The air flow into the instrument was estimated using a simplified Hagen-Poiseuille equation for viscous airflow (Eq 3).

$$C = \frac{\pi d^4}{128 \mu l} * \frac{(P_1 + P_2)}{2} \qquad \text{(Eq. 3)}$$

Where $d$ is the diameter of instrument entrance (0.58 mm), $l$ is the length of the ion transfer tube (58.42 mm), μ is the viscosity of air in Poise, $P_1$ and $P_2$ are the pressures before and after the ion transfer tube. The viscosity of air changes from $1.82\text{x}10^{-4}$ Poise to $2.98\text{x}10^{-4}$ Poise with increasing temperature from 20 °C to 300 °C. This is a relatively small change, and the temperature of the air is significantly lower than the set temperature of 300 °C of the ion transfer tube. Thus, the viscosity of air at room temperature was used to obtain an estimate of the air flow conductance into the instrument. The calculated air flow conductance is 0.102 L/s, and the air flow velocity inside of the transfer tube is 386 m/s. The airflow velocity between the emitter and the source should be less, but the electrostatic force should result in a higher velocity of the droplet than that of the air itself. If the droplet velocity outside the mass spectrometer is roughly the same as the air flow velocity through the ion transfer tube, then the droplets formed from theta emitters would have to last at least 5 μs in order to enter the instrument entrance as intact droplets. The 1 μs lifetime of droplets formed by the 317 nm theta emitters is much too short indicating that the desolvated gaseous ions must be formed outside of the mass spectrometer. This result is consistent with the observation that the charge-state distribution obtained with these small emitters do not depend on the source temperature. In contrast, the 1.7 μm and 4.4 μm theta emitters generate droplets that survive for about 10 μs and 50 μs, respectively. These lifetimes are sufficient that the majority of the droplets enter the ESI interface of the mass spectrometer before gaseous ion

formation occurs, consistent with the protein melting observed inside the droplets at the higher source temperatures.

Significantly lower droplet velocities between 8 and 23 m/s were reported by Jansson et al. with 4 μm diameter emitters over a range of distance and spray voltages.[26] The flow of air through the ion transfer tube should be similar in those experiments. If the droplet velocities in our experiments are at the highest velocity of 23 m/s reported by Jansson et al., then it would require ~65 μs for these droplets to reach the source. However, our results indicate that the droplets formed from 1.7 μm emitters which have a lifetime of 10 μs do in fact experience the higher temperature inside the ion transfer tube. Thus, we conclude that the droplets on our experiments must be moving at a higher velocity. This discrepancy between the droplet velocities reported by Jansson et al. and the results of our experiments may be related to assumptions made in the earlier experiments. Jansson et al. reported that the droplets formed from 4 μm theta emitters are around 4.3 μm in diameter.[26] However, results from other studies using similar emitters indicate that the initial size of the majority of droplets that result in charged analyte ions is about 1/10 to 1/17 of the electrospray emitter diameter.[37,38] For example, Bush and coworkers reported that the initial droplets formed from single barrel emitters with diameters of ~1 to 3 μm using common native electrospray conditions are approximately 60 nm in diameter.[38] Jansson et al. measured the droplet sizes optically using a setup where a single pixel in their CCD camera corresponds to ~0.8 μm.[26] Thus, this optical detection method is not capable of measuring the < 0.4 μm droplets that result in protein ions observed in the mass spectrometer. Although larger droplets may be formed as well, these droplets may not produce the majority of the protein ions that are observed. It should also be emphasized that reaction kinetics that have been reported previously based on optically measured velocities have included the explicit assumption that bare protein ion formation occurs at the entrance of the mass spectrometer.[26] Our results reported here clearly show that this is not the case. The similar droplet lifetimes for the 4 μm emitters deduced from these two experiments may be a result of an underestimation of both the droplet velocity and the distance traveled prior to ion formation in the optical-based studies.

### 5.4.4 Buffer Effect on Protein Unfolding in Droplets

It is well known that different buffers can stabilize or destabilize the native forms of proteins. Ammonium acetate is a more commonly used buffer in native mass spectrometry experiments than ammonium bicarbonate despite the fact that ammonium acetate is a poor buffer at neutral pH.[39] The effect of ammonium acetate on the extent of thermal induced protein unfolding in longer-lived droplets was investigated by measuring nano-ESI mass spectra of β-lactoglobulin (10 μM) in 100 mM AA using 317 nm, 1.7 μm, and 4.4 μm theta emitters at instrument source temperatures between 160 °C and 300 °C (Figure 5.3 and Supplemental Figure 5.2d-f). With 317 nm emitters, the spectra are similar to those formed under the same conditions but with 100 mM ABC and there is no dependence on source temperature. Results with the 4.4 μm theta emitters show there is a source temperature dependence, as was the case with 100 mM ABC, but the fraction of unfolded protein is much less at higher temperatures. At 230 °C, the fraction of unfolded β-lactoglobulin is 3.4% ± 1.5%, which is approximately half that from 100 mM ABC. At 300 °C, the fraction of the unfolded protein is 7.2% ± 1.5%, again, less than half that from 100 mM ABC (Figure 5.3). A similar trend of the formation of unfolded protein from 100 mM AA is observed using 1.7 μm theta emitters (Supplemental Figure 5.2d-f). The increasing trend of the unfolded protein with increasing source temperature from 100 mM AA using larger theta emitters is consistent with the

hypothesis that protein ions formed from larger theta emitters are formed inside the heated ion transfer tube, which causes thermal denaturation of the protein. However, it appears that less unfolding occurs with 100 mM AA than with 100 mM ABC. This is also consistent with the 8+ being the most abundant ion with AA, but the 9+ is most abundant with ABC at this same emitter size. It is also interesting to note that dimer abundance is significantly higher in the spectra obtained from the AA solution.

Ionic strength can affect protein conformation and stability.[40] These experiments were repeated in 10 mM AA (Supplemental Figure 5.4). There is no significant change in the charge-state distribution with source temperature using 317 nm theta emitters, but there is an increase in the abundance of unfolded protein with 4.4 μm emitters with increasing temperature. The fraction of unfolded protein formed from the 10 mM AA solution is slightly higher than that formed from the 100 mM AA solution at high source temperature with both the 1.7 μm and 4.4 μm emitters (Figure 5.4). This result is consistent with lower ionic strength causing a small reduction in the stability of the folded form of the protein.

The effects of these buffers on the stability of the native form of β-lactoglobulin were studied with fluorescence. Upon thermal denaturation, exposure of tryptophan to solvent typically increases the fluorescent emission intensity. However, for β-lactoglobulin, tryptophan fluorescence emission intensity decreases with increasing temperature (Supplemental Figure 5.5). This phenomenon has been attributed to the thermal deactivation of the tryptophan fluorophores or the change in tertiary structure resulting in increasing proximity between primary amines of lysine residues and tryptophan fluorophores, which leads to fluorescent quenching.[29,41] A measure of β-lactoglobulin unfolding can also be obtained from the wavelength of the maximum of the tryptophan emission peak, which provides a measure of the polarity of the environment around tryptophan. As β-lactoglobulin unfolds, tryptophan that is buried inside the fully folded protein in a less polar environment transitions to exposure to polar solvent in the unfolded state.[29]
Temperature melting curves for β-lactoglobulin in the three different buffers were obtained by plotting the wavelength of the tryptophan emission peak maximum as a function of temperature (Figure 5.5). The melting curves obtained from 10 mM AA and 100 mM AA are similar, but between 50 °C and 70 °C, the wavelength maximum is consistently higher from 10 mM AA compared to that from 100 mM AA, indicating more exposure of tryptophan to the polar solvent at lower AA concentration within this temperature range. In contrast, the melting curve obtained from 100 mM ABC shows that considerably more unfolding occurs at a lower temperature compared to either AA solution. These results show that β-lactoglobulin is thermally less stable in ABC than AA even at the same ionic strength. The fluorescence results from the three different buffers support the observation that more thermal unfolding occurs in droplets that are heated by the source for ABC than it does for AA. It is interesting that the air near the instrument source can reach 50 °C, a temperature at which some unfolding should occur in ABC, yet no significant unfolding is observed with the 317 nm theta emitters. Either the nanodrops have lifetimes that are too short to experience these elevated temperatures as droplets or evaporative cooling of the droplet may compete with resistive and ambient heating resulting in a somewhat lower temperature in the droplet compared to the ambient air.

### 5.4.5 Droplet Size Effect on Protein Dimerization

It is interesting to note that there is substantial dimer signal in the mass spectra obtained with the 1.7 μm and 4.4 μm theta emitters but not with the 317 nm emitters with the 100 mM AA

solution (Figure 5.3). β-lactoglobulin is predominantly a dimer at physiological conditions (> 50 μM protein concentration), and the dimer-monomer equilibrium depends on pH, buffer, and ionic strength.[42] Because the protein concentration in these studies is low, there should be a relatively low concentration of protein dimers in solution. With the 317 nm theta emitters, less than 9% of the total protein ion signal corresponds to the β-lactoglobulin dimer. However, the dimer abundance is up to 35% with the 1.7 μm and 4.4 μm emitters (Figure 5.3 and Supplemental Figure 5.2d-f). We hypothesize that the dimer abundance is related to the presence of multiple protein molecules in large droplets produced by the larger emitters. If the initial droplet diameter is ~ 1/17 the diameter of the theta emitter,[38] the initial droplet size for the 317 nm theta emitters is about 18 nm (approximating the theta emitter as a single barrel emitter). At this initial droplet size, only 1 out of ~60 nanodrops that are formed contains a protein molecule. Unless the protein molecule enters the droplet in the dimeric form, it is an extremely low probability event for a droplet to contain two individual protein molecules. Thus, the protein dimer ions from 317 nm theta emitters likely exist as molecular dimers in the bulk solution.

The initial droplet diameters of a 1.7 μm and 4.4 μm theta emitter are 100 nm and 261 nm, respectively. A 100 nm nanodrop contains on average slightly fewer than three protein molecules per droplet whereas a 261 nm droplet initially contains about 50 protein molecules. Because the initial droplets may contain more than two protein molecules, the formation of β-lactoglobulin dimer can occur within the droplets as solvent evaporation occurs and the concentration of protein in the shrinking droplets increases. Thus, the extent of dimer ions observed in the nano-ESI mass spectra obtained with 317 nm emitters more accurately reflects the dimer concentrations in the original solution compared to the results from larger emitter sizes when dimers are formed as droplets evaporate during the ESI process.

The abundance of the protein dimers decreases with increase in instrument source temperature. For mass spectra obtained using 4.4 μm theta emitters, the fraction of protein dimer out of total protein ion signals is 30% ± 1%, 24% ±3%, and 19% ± 1% at source temperatures of 160 °C, 230 °C, and 300 °C, respectively. The decrease in protein dimer abundance with increasing temperature indicates that the protein dimer thermally dissociates into monomers in the droplets. Although dimeric protein ions are also observed in mass spectra obtained for β-lactoglobulin in 10 mM AA and 100 mM ABC using 1.7 μm and 4.4 μm theta emitters, the abundance of protein dimer is much lower than in 100 mM AA (Figure 5.2, Supplemental Figure 5.2a-c, Supplemental Figure 5.4d-i). Higher ionic strength favors dimer formation.[42] The absence of dimer ions with ABC may indicate that the native structures are sufficiently destabilized that the equilibrium disfavors the formation of the dimer in this buffer.

### 5.4.6 Electrothermal Supercharging Mechanism

Results from these temperature melt studies provide additional insights into the mechanism of electrothermal supercharging.[14,15] Prior results indicate that proteins which have native forms in bulk solution can be rapidly denatured prior to their entrance into the mass spectrometer within the droplets due to a rise in droplet temperature as a result of resistive heating of the droplet induced by higher electrospray voltages.[14] The fluorescence results (Figure 5.5) provide insights into why the effectiveness of this method depends on buffer identity.

To determine how emitter size, source temperature, and buffer identity affects electrothermal supercharging, mass spectra of β-lactoglobulin (10 μM) from 100 mM ABC and 100 mM AA solutions were obtained using 1.7 μm single barrel emitters at three instrument source

temperatures at 1.3 kV and 800 V, respectively (Figure 5.6 and Supplemental Figure 5.6). Single barrel emitters were used in order to more directly compare with previous protein electrothermal supercharging results. As reported previously, very little supercharging occurs in AA regardless of source temperatures (Figure 5.6a-c).[15] There is a slight increase in the average charge state with increasing source temperature as was observed at lower spray voltages. It is interesting to note that the extent of thermal denaturation of the protein at high source temperature even at 1.3 kV with single barrel emitters is lower than it is with low spray voltage using similar size theta emitters. The difference is likely due to the absence of backing pressure for single barrel emitter, which should result in a shorter droplet lifetime for similar size emitters. Mortensen et al. previously showed that decreasing backing pressure from 10 psi to 5 psi decreases the droplet lifetime by half.[23]

Electrothermal supercharging does occur for β-lactoglobulin in ABC at 1.3 kV, and the fraction of unfolded protein increases with increasing source temperature (Figure 5.6d-f). These results from the two buffers are consistent with those of previous studies.[14,15] The abundances of the 10+ and 11+ charge states formed at 1.3 kV increase with increasing temperature and appear to correspond to unfolding intermediates. Similar results are obtained with theta emitters at 300 °C and at 1.3 kV spray voltage (Supplemental Figure 5.7) indicating that this is not unique to single barrel emitters. The difference observed between purely source temperature induced heating and electrothermal supercharging indicates that the mechanism for electrothermal supercharging may be more complex and involve the kinetics of folding and unfolding. The higher electric field in electrothermal supercharging heats up the droplets *outside* of the mass spectrometer. Upon entering the ion transfer tube, they may evaporatively cool to a steady state temperature that they would have had in the absence of electrothermal supercharging. This rapid heating and subsequent cooling may trap unfolding intermediates that may not otherwise be observed in conventional heating experiments. Recent ion mobility results exploring unfolding of ubiquitin upon laser heating different size droplets has provided evidence for short-lived unfolding intermediates.[43]

## 5.5 Conclusions

The lifetime of droplets formed by nano-ESI can be varied between 1 and 50 μs by changing the diameter of theta emitter tips from 317 nm to 4.4 μm. The location of where ions are formed during nano-ESI from buffered aqueous solutions, whether inside or outside of the mass spectrometer, can be determined from the extent to which high charge-state distributions are induced by increasing the electrospray interface temperature. With 317 nm tips, which produce droplets that last about 1 μs, only low charge state ions of β-lactoglobulin are observed at all instrument source temperatures for solutions consisting of ammonium acetate or ammonium bicarbonate. Very few high charge states are observed under basic conditions in which the native form of the protein is destabilized. In contrast, a higher charge-state distribution, indicative of unfolded protein molecules in solution, is observed with 1.7 and 4.4 μm theta emitters and this population increases with temperature. These results indicate that droplets with lifetimes of ~1 μs do not survive long enough to enter the source inlet capillary and that ions are formed outside of the mass spectrometer. In contrast, droplets formed from micron size emitters with lifetimes ≥ 10 μs enter the mass spectrometer and are heated inside of the transfer tube prior to ion formation. This can lead to a population of unfolded proteins in solution prior to the formation of gaseous ions. Results from basic solutions in which the native form of the protein is destabilized indicate

that the majority of protein ions originating from the larger droplets are formed inside of the mass spectrometer. These results are consistent with the charge residue mechanism for ion formation in native mass spectrometry. Our results also indicate that the assumption that ions are formed at the entrance of the mass spectrometer in kinetic experiments aimed at measuring rates of chemical reactions will lead to errors.

A larger temperature effect is observed from larger droplets formed from ammonium bicarbonate compared to ammonium acetate solutions. Results from temperature melt studies show that the native form of β-lactoglobulin is thermally less stable in ammonium bicarbonate buffer. Electrothermal supercharging is also more effective in ammonium bicarbonate than ammonium acetate, consistent with the proposed mechanism of the voltage induced droplet heating that occurs before droplets enter the mass spectrometer.

These studies demonstrate the advantages of preparing droplets with known lifetimes. The use of small tips to produce droplets with short lifetimes has the advantage that the mass spectra obtained under native conditions do not depend on the desolvation temperature used in the mass spectrometer because ions originating from these droplets are formed outside of the mass spectrometer. These small tips have the additional advantage that effects of protein dimerization or aggregation that can occur in larger droplets are eliminated when the droplets contain on average much fewer than one protein molecule per droplet. Thus, in addition to the protein desalting effects reported earlier for submicron emitter tips,[32,34–36] these small tips should be advantageous for native mass spectrometry by eliminating artifacts of protein aggregation that can occur in droplets and any adverse effects of thermal activation in the ion source.

### 5.6 Acknowledgments

This material is based upon work supported by the National Science Foundation Division of Chemistry under grant number CHE-1609866. The authors also thank Dr. Moitrayee Bhattacharyya for helpful discussions on the fluorescence results.

## 5.7 Reference

(1) Konermann, L.; Ahadi, E.; Rodriguez, A. D.; Vahidi, S. Unraveling the Mechanism of Electrospray Ionization. *Anal. Chem.* **2013**, *85* (1), 2–9.

(2) Kebarle, P.; Verkerk, U. H. A Brief Overview of the Mechanisms Involved in Electrospray Mass Spectrometry. In *Reactive Intermediates:MS Investigations in Solution*; Wiley-VCH Verlag GmbH & Co. KGaA: Weinheim, Germany, 2010; pp 1–35.

(3) Wilm, M. Principles of Electrospray Ionization. *Mol. Cell. Proteomics* **2011**, *10* (7), M111.009407.

(4) Iribarne, J. V.; Thomson, B. A. On the Evaporation of Small Ions from Charged Droplets. *J. Chem. Phys.* **1976**, *64* (6), 2287–2294.

(5) Loscertales, I. G.; Fernández De La Mora, J. Experiments on the Kinetics of Field Evaporation of Small Ions from Droplets. *J. Chem. Phys.* **1995**, *103* (12), 5041–5060.

(6) Dole, M.; Mack, L. L.; Hines, R. L.; Chemistry, D. O.; Mobley, R. C.; Ferguson, L. D.; Alice, M. B. Molecular Beams of Macroions. *J. Chem. Phys.* **1968**, *49* (5), 2240–2249.

(7) Winger, B. E.; Light-Wahl, K. J.; Ogorzalek Loo, R. R.; Udseth, H. R.; Smith, R. D. Observation and Implications of High Mass-to-Charge Ratio Ions from Electrospray Ionization Mass Spectrometry. *J. Am. Soc. Mass Spectrom.* **1993**, *4* (7), 536–545.
(8) Metwally, H.; Duez, Q.; Konermann, L. Chain Ejection Model for Electrospray Ionization of Unfolded Proteins: Evidence from Atomistic Simulations and Ion Mobility Spectrometry. *Anal. Chem.* **2018**, *90*, 10069–10077.
(9) Hogan, C. J.; Carroll, J. A.; Rohrs, H. W.; Biswas, P.; Gross, M. L. Combined Charged Residue-Field Emission Model of Macromolecular Electrospray Ionization. *Anal. Chem.* **2009**, *81* (1), 369–377.
(10) Chowdhury, S. K.; Katta, V.; Chait, B. T. Probing Conformational Changes in Proteins by Mass Spectrometry. *J. Am. Chem. Soc.* **1990**, *112* (24), 9012–9013.
(11) Winston, R. L.; Fitzgerald, M. C. Mass Spectrometry as a Readout of Protein Structure and Function. *Mass Spectrom Rev* **1997**, *16* (4), 165–179.
(12) Kaltashov, I. A.; Eyles, S. J. Studies of Biomolecular Conformations and Conformational Dynamics by Mass Spectrometry. *Mass Spectrom. Rev.* **2002**, *21* (1), 37–71.
(13) Mirza, U. A.; Chait, B. T. Do Proteins Denature during Droplet Evolution in Electrospray Ionization. *Int. J. Mass. Spectrom. Ion Proc.* **1997**, *162* (96), 173–181.
(14) Sterling, H. J.; Cassou, C. A.; Susa, A. C.; Williams, E. R. Electrothermal Supercharging of Proteins in Native Electrospray Ionization. *Anal. Chem.* **2012**, *84* (8), 3795–3801.
(15) Cassou, C. A.; Sterling, H. J.; Susa, A. C.; Williams, E. R. Electrothermal Supercharging in Mass Spectrometry and Tandem Mass Spectrometry of Native Proteins. *Anal. Chem.* **2013**, *85* (1), 138–146.
(16) Chillier, X. D.; Monnier, A.; Bill, H.; Gülacar, F. O.; Buchs, A.; McLuckey, S. A.; Van Berkel, G. J. A Mass Spectrometry and Optical Spectroscopy Investigation of Gas-Phase Ion Formation in Electrospray. *Rapid Commun. Mass Spectrom.* **1996**, *10* (3), 299–304.
(17) Chingin, K.; Frankevich, V.; Balabin, R. M.; Barylyuk, K.; Chen, H.; Wang, R.; Zenobi, R. Direct Access to Isolated Biomolecules under Ambient Conditions. *Angew. Chemie - Int. Ed.* **2010**, *49* (13), 2358–2361.
(18) Bain, R. M.; Pulliam, C. J.; Cooks, R. G. Accelerated Hantzsch Electrospray Synthesis with Temporal Control of Reaction Intermediates. *Chem. Sci.* **2015**, *6* (1), 397–401.
(19) Lee, J. K.; Kim, S.; Nam, H. G.; Zare, R. N. Microdroplet Fusion Mass Spectrometry for Fast Reaction Kinetics. *Proc. Natl. Acad. Sci.* **2015**, *112* (13), 201503689.
(20) Mark, L. P.; Gill, M. C.; Mahut, M.; Derrick, P. J. Dual Nano-Electrospray for Probing Solution Interactions and Fast Reactions of Complex Biomolecules. *Eur. J. Mass Spectrom.* **2012**, *18* (5), 439–446.
(21) Fisher, C. M.; Kharlamova, A.; McLuckey, S. A. Affecting Protein Charge State Distributions in Nano-Electrospray Ionization via in-Spray Solution Mixing Using Theta Capillaries. *Analytical Chemistry*. 2014, pp 4581–4588.
(22) Mortensen, D. N.; Williams, E. R. Investigating Protein Folding and Unfolding in Electrospray Nanodrops Upon Rapid Mixing Using Theta-Glass Emitters. *Anal. Chem.* **2015**, *87* (2), 1281–1287.
(23) Mortensen, D. N.; Williams, E. R. Ultrafast (1 Ms) Mixing and Fast Protein Folding in Nanodrops Monitored by Mass Spectrometry. *J. Am. Chem. Soc.* **2016**, *138* (10), 3453–3460.

(24) Mortensen, D. N.; Williams, E. R. Microsecond and Nanosecond Polyproline II Helix Formation in Aqueous Nanodrops Measured by Mass Spectrometry. *Chem. Commun.* **2016**, *52*, 12218–12221.
(25) Girod, M.; Moyano, E.; Campbell, D. I.; Cooks, R. G. Accelerated Bimolecular Reactions in Microdroplets Studied by Desorption Electrospray Ionization Mass Spectrometry. *Chem. Sci.* **2011**, *2* (3), 501.
(26) Jansson, E. T.; Lai, Y.-H.; Santiago, J. G.; Zare, R. N. Rapid Hydrogen-Deuterium Exchange in Liquid Droplets. *J. Am. Chem. Soc.* **2017**, *139* (20), 6851–6854.
(27) Shastry, M. C. C.; Luck, S. D.; Roder, H. A Continuous-Flow Capillary Mixing Method to Monitor Reactions on the Microsecond Time Scale. *Biophys. J.* **1998**, *74* (5), 2714–2721.
(28) Ding, X.; Yang, Y.; Zhao, S.; Li, Y.; Wang, Z. Analysis of α-Lactalbumin, β-Lactoglobulin A and B in Whey Protein Powder, Colostrum, Raw Milk, and Infant Formula by CE and LC. *Dairy Sci. Technol.* **2011**, *91* (2), 213–225.
(29) Bhattacharjee, C.; Das, K. P. Thermal Unfolding and Refolding of β-Lactoglobulin. *Eur. J. Biochem.* **2000**, *267* (13), 3957–3964.
(30) Anema, S. G.; McKenna, A. B. Reaction Kinetics of Thermal Denaturation of Whey Proteins in Heated Reconstituted Whole Milk. *J. Agric. Food Chem.* **1996**, *44* (2), 422–428.
(31) Kella, N. K.; Kinsella, J. E. Enhanced Thermodynamic Stability of Beta-Lactoglobulin at Low PH. A Possible Mechanism. *Biochem. J.* **1988**, *255* (1), 113–118.
(32) Xia, Z.; Williams, E. R. Protein-Glass Surface Interactions and Ion Desalting in Electrospray Ionization with Submicron Emitters. *J. Am. Soc. Mass Spectrom.* **2018**, *29* (1), 194–202.
(33) Mortensen, D. N.; Williams, E. R. Surface-Induced Protein Unfolding in Submicron Electrospray Emitters. *Anal. Chem.* **2016**, *88* (19), 9662–9668.
(34) Susa, A. C.; Xia, Z.; Williams, E. R. Small Emitter Tips for Native Mass Spectrometry of Proteins and Protein Complexes from Nonvolatile Buffers That Mimic the Intracellular Environment. *Anal. Chem.* **2017**, *89* (5), 3116–3122.
(35) Susa, A. C.; Xia, Z.; Williams, E. R. Native Mass Spectrometry from Common Buffers with Salts That Mimic the Extracellular Environment. *Angew. Chemie Int. Ed.* **2017**, 1–5.
(36) Susa, A. C.; Lippens, J. L.; Xia, Z.; Loo, J. A.; Campuzano, I. D. G.; Williams, E. R. Submicrometer Emitter ESI Tips for Native Mass Spectrometry of Membrane Proteins in Ionic and Nonionic Detergents. *J. Am. Soc. Mass Spectrom.* **2018**, *29* (1), 203–206.
(37) Schmidt, A.; Karas, M.; Dülcks, T. Effect of Different Solution Flow Rates on Analyte Ion Signals in Nano-ESI MS, or: When Does ESI Turn into Nano-ESI? *J. Am. Soc. Mass Spectrom.* **2003**, *14* (5), 492–500.
(38) Davidson, K. L.; Oberreit, D. R.; Hogan, C. J.; Bush, M. F. Nonspecific Aggregation in Native Electrokinetic Nanoelectrospray Ionization. *Int. J. Mass Spectrom.* **2017**, *420*, 35–42.
(39) Konermann, L. Addressing a Common Misconception: Ammonium Acetate as Neutral PH "Buffer" for Native Electrospray Mass Spectrometry. *J. Am. Soc. Mass Spectrom.* **2017**, *28* (9), 1827–1835.
(40) Cohn, E. J.; Edsall, J. T. *Proteins, Amino Acids and Peptides as Ions and Dipolar Ions*; Reinhold Publishing: New York, 1943.
(41) Gally, J. A.; Edelman, G. M. The Effect of Temperature on the Fluorescence of Some Aromatic Amino Acids and Proteins. *Biochim. Biophys. Acta* **1962**, *60* (3), 499–509.

(42) Gottschalk, M.; Nilsson, H.; Roos, H.; Halle, B. Protein Self-Association in Solution: The Bovine β -Lactoglobulin Dimer and Octamer. *Protein Sci.* **2009**, *12* (11), 2404–2411.
(43) El-Baba, T. J.; Woodall, D. W.; Raab, S. A.; Fuller, D. R.; Laganowsky, A.; Russell, D. H.; Clemmer, D. E. Melting Proteins: Evidence for Multiple Stable Structures upon Thermal Denaturation of Native Ubiquitin from Ion Mobility Spectrometry-Mass Spectrometry Measurements. *J. Am. Chem. Soc.* **2017**, *139* (18), 6306–6309.
(44) Leonil, J.; Molle, D.; Fauquant, J.; Maubois, J. L.; Pearce, R. J.; Bouhallab, S. Characterization by Ionization Mass Spectrometry of Lactosyl β-Lactoglobulin Conjugates Formed During Heat Treatment of Milk and Whey and Identification of One Lactose-Binding Site. *J. Dairy Sci.* **1997**, *80* (10), 2270–2281.

## 5.8 Figures

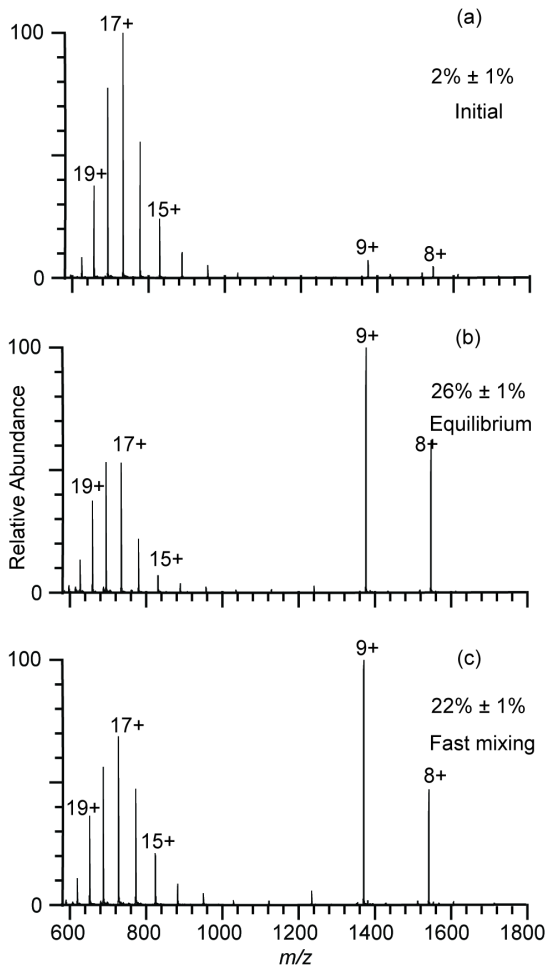


**Figure 5.1.** Electrospray ionization mass spectra for cytochrome *c* refolding experiments with a 4.4 μm theta emitter with 10 psi backing pressure used to deduce droplet lifetime: spectra obtained for solutions consisting of (a) water with 1% acetic acid (pH = 2.8), (b) 1:1 mixture of water with 1% acetic acid and pure water at equilibrium (pH = 3.0), and (c) rapid mixing of the acidified aqueous solution used in (a) and water using a theta emitter. Percentages of folded cytochrome *c* are labeled in the spectra.

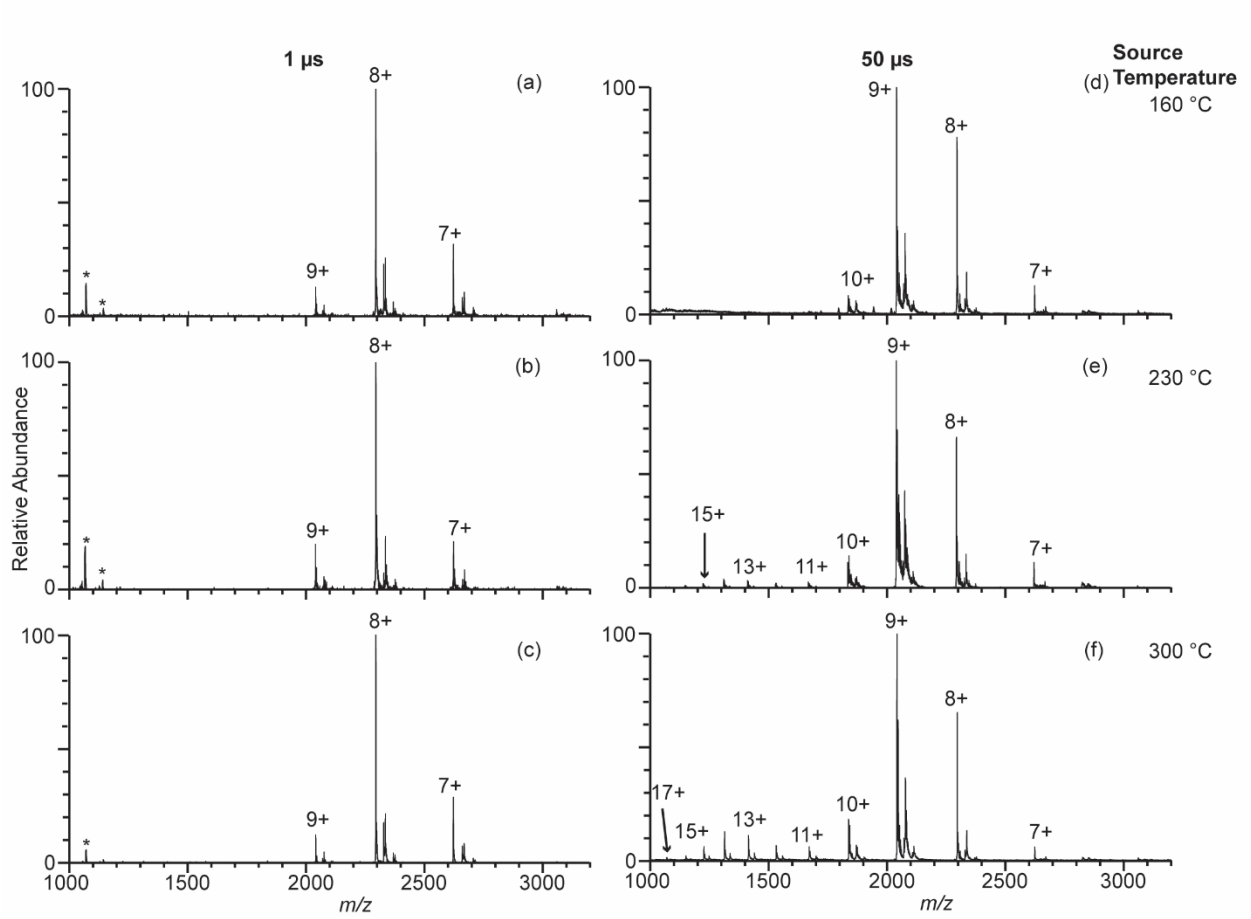


**Figure 5.2.** Electrospray ionization mass spectra obtained from solutions consisting of 10 µM β-lactoglobulin in 100 mM ABC using 317 nm (a-c) and 4.4 µm (d-f) theta emitters at source temperatures of 160 °C (a, d), 230 °C (b, e), and 300 °C (c, f). Peaks at slightly higher *m*/*z* corresponds to lactosyl covalently bound to β-lactoglobulin.[44] * indicates polydimethylsiloxane clusters that are present as an impurity.

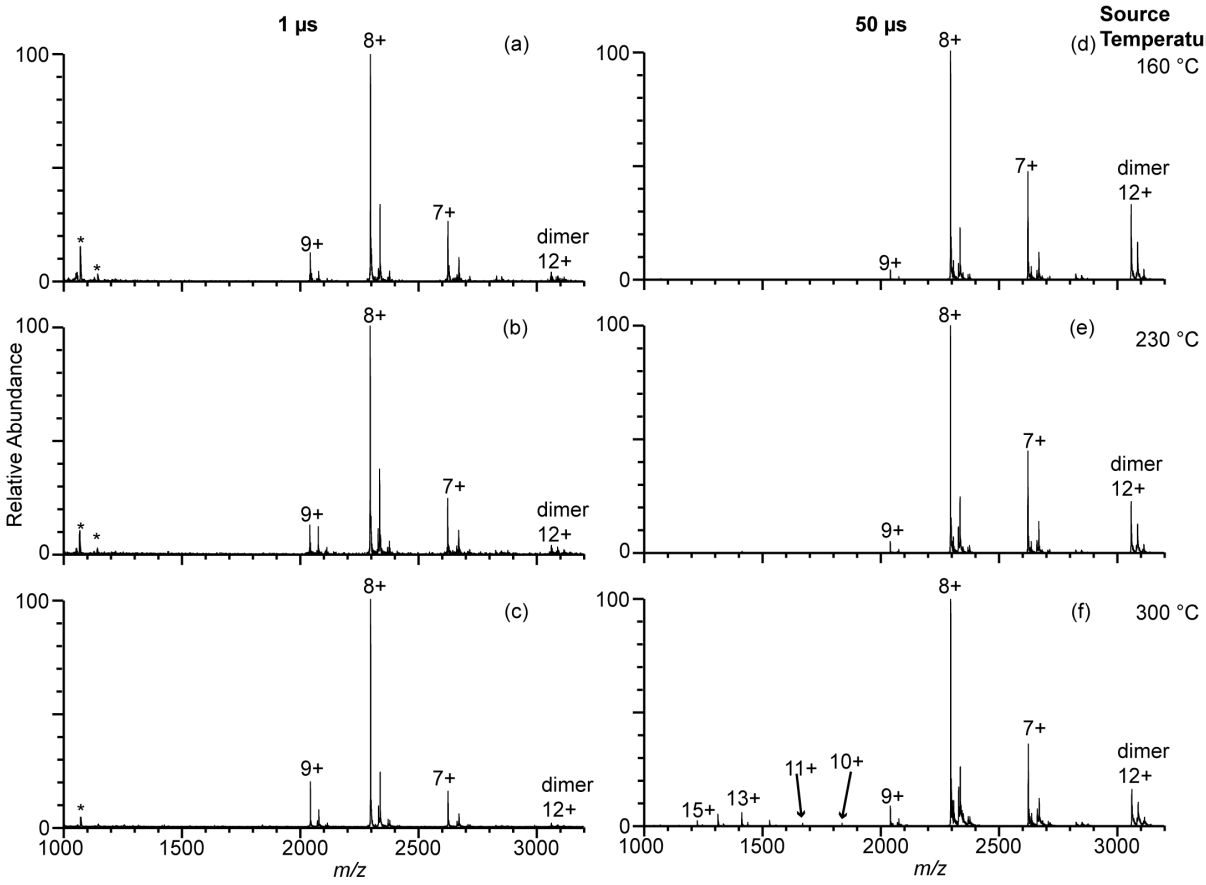


**Figure 5.3.** Electrospray ionization mass spectra obtained from solutions consisting of 10 µM β-lactoglobulin in 100 mM AA using 317 nm (a-c) and 4.4 µm (d-f) theta emitters at source temperature 160 °C (a, d), 230 °C (b, e), and 300 °C (c, f). Peaks at slightly higher *m*/*z* corresponds to lactosyl covalently bound to β-lactoglobulin.[44] * indicates polydimethylsiloxane clusters that are present as an impurity.

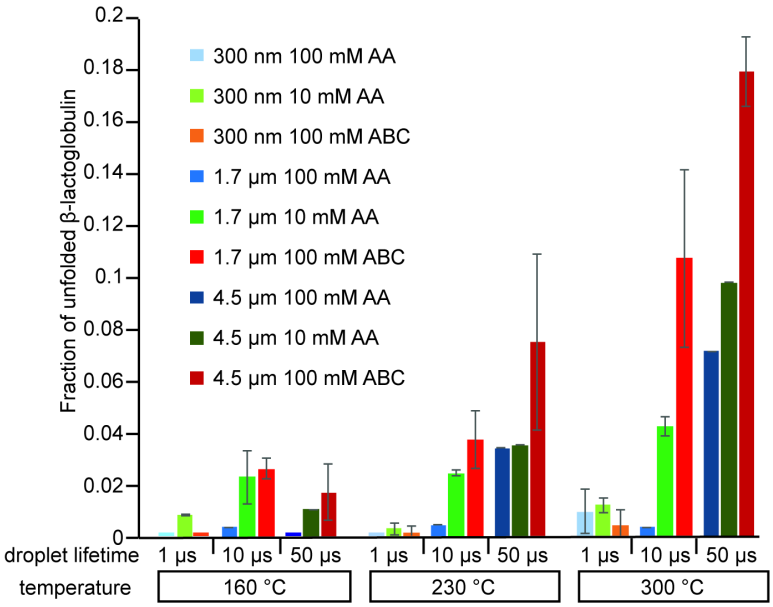


**Figure 5.4.** The fraction of unfolded β-lactoglobulin ions obtained from electrospray ionization using 317 nm (light shades), 1.7 µm (medium shades), and 4.4 µm (dark shades) theta emitters from solutions consisting of 10 mM AA (green), 100 mM AA (blue), and 100 mM ABC (red) at three different instrument source temperatures.

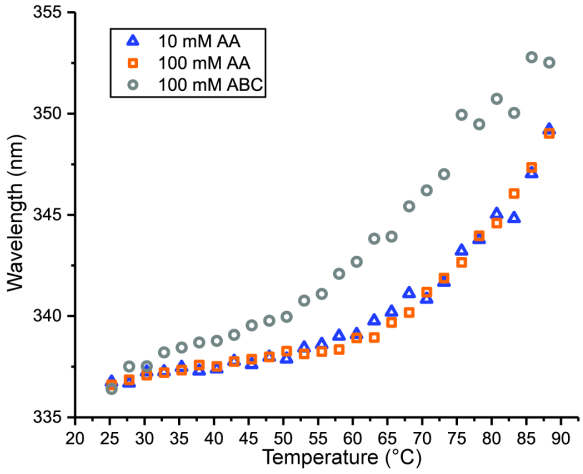


**Figure 5.5.** Temperature melt of β-lactoglobulin obtained by measuring the shift in the wavelength of the maximum fluorescence emission intensity of tryptophan in solutions consisting of 10 mM AA, 100 mM AA and 100 mM ABC at temperatures between 25 °C and 87.5 °C measured in 2.5 °C increments.

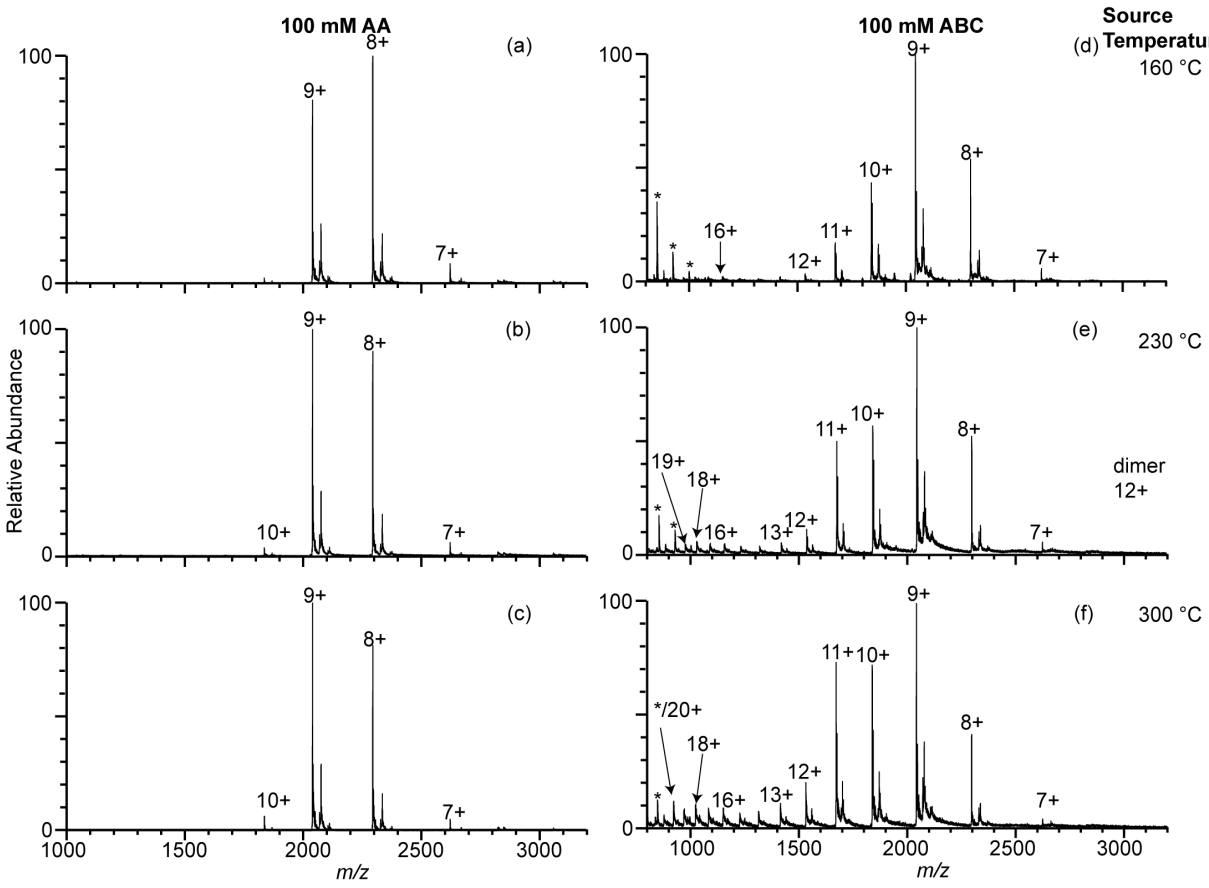


**Figure 5.6.** Electrospray ionization mass spectra obtained with electrothermal supercharging of 10 μM β-lactoglobulin in 100 mM ABC and 100 mM AA at a spray voltage of 1.3 kV using 1.7 μm single barrel emitters at source temperature 160 °C (a, d), 230 °C (b, e), and 300 °C (c, f). Peaks at slightly higher *m*/*z* corresponds to lactosyl covalently bound to β-lactoglobulin.[44] * indicates polydimethylsiloxane clusters that are present as an impurity.

## 5.9 Supplemental Information

**Supplemental Table 5.1.** Summary of droplet lifetimes obtained from acidified water containing cytochrome *c* and aqueous buffered solutions with theta emitters that have tip diameters ranging in size from 0.24 µm to 4.4 µm using cytochrome *c* folding constant.[1,2] Nitrogen gas backing pressure used to change the solution flow rate and resulting droplet lifetime is either 10 psi or 40 psi.

| tip size (µm) | Backing pressure (psi) | Droplet lifetime (µs) | Solution |
|---|---|---|---|
| 0.24 | 10 | 1 ± 0 | 100 mM AA |
| 0.3 | 10 | 2.8 +/- 0.6 | 100 mM AA |
| 1.5 | 10 | 9 +/- 2 | 100 mM AA |
| 1.5 | 40 | 20 +/-3 | 100 mM AA |
| 1.4 | 10 | 25 +/- 7 | water |
| 1.4 | 10 | 7 +/- 2 | 500 mM AA |
| 1.7 | 40 | 38 +/- 2 | water |
| 4.4 | 10 | 99 +/-14 | water |

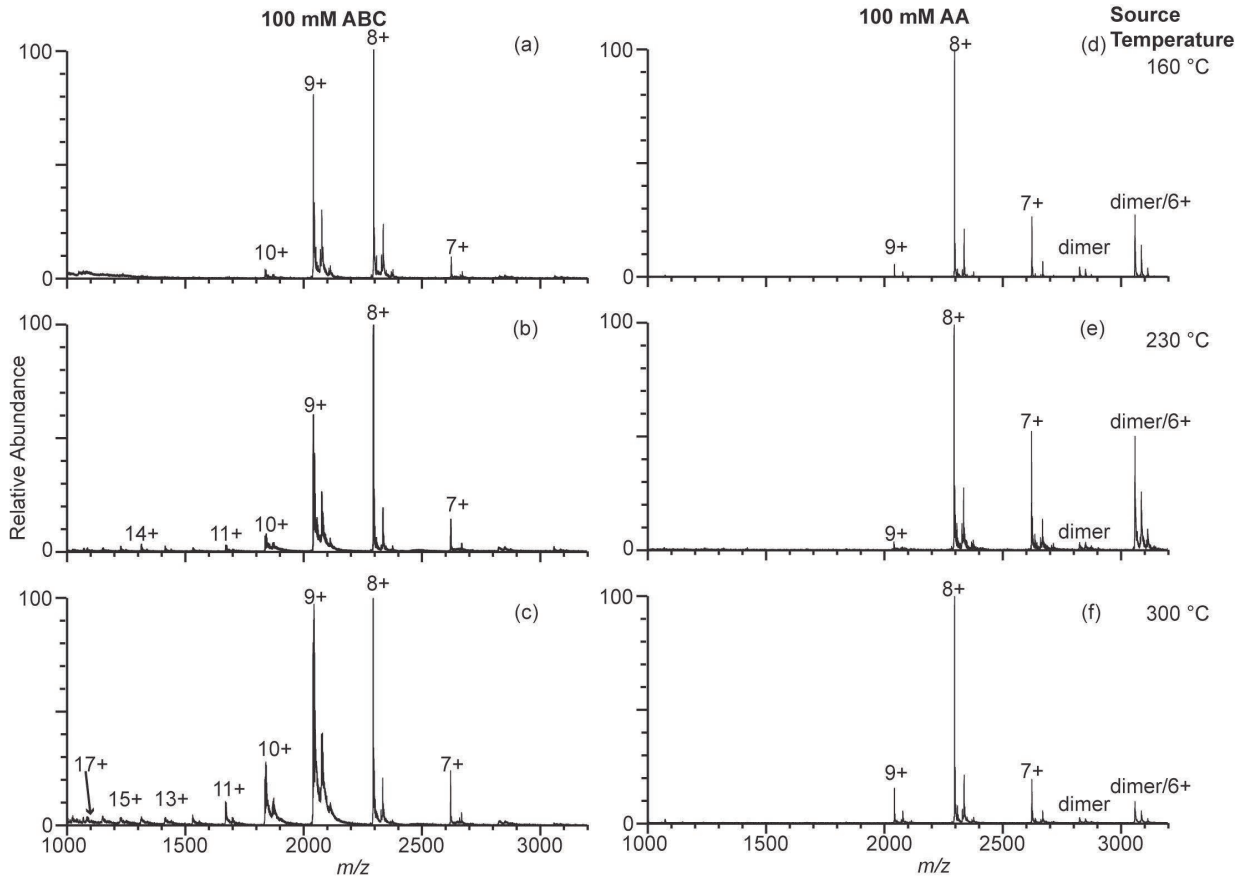


**Supplemental Figure 5.1.** Electrospray ionization mass spectra obtained from solutions consisting of 10 μM β-lactoglobulin in 100 mM ABC (a-c) and in 100 mM AA (d-f) using 1.7 μm theta tip emitters at source temperatures of 160 °C (a, d), 230 °C (b, e), and 300 °C (c, f). Peaks at slightly higher *m*/*z* corresponds to lactosyl covalently bound to β-lactoglobulin.[3]

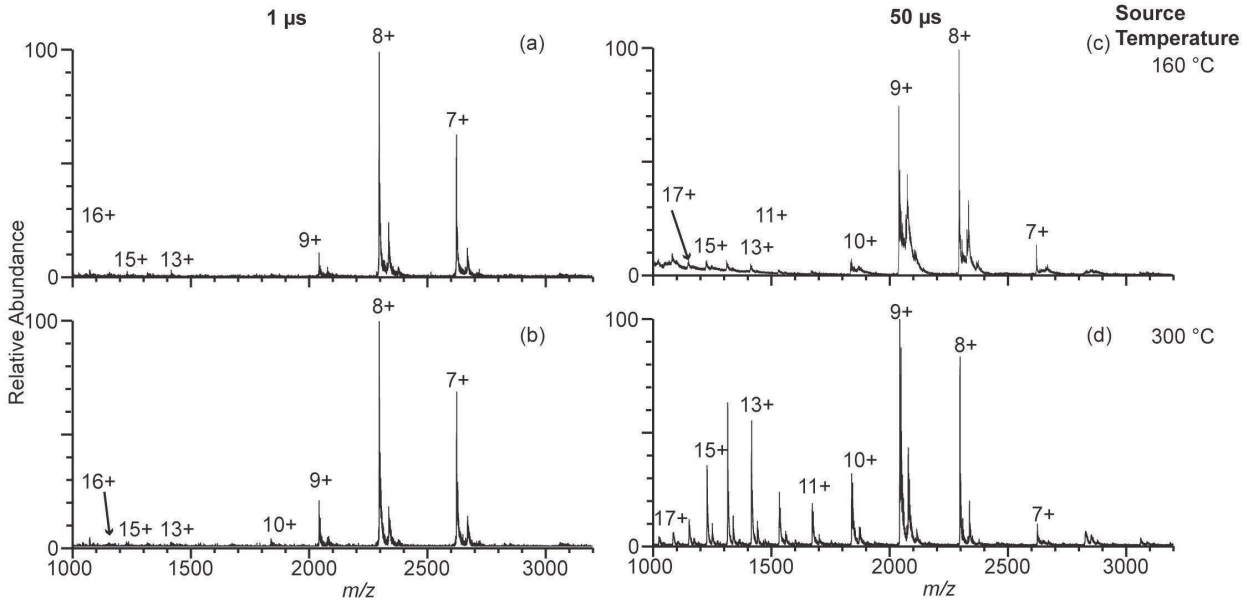


**Supplemental Figure 5.2.** Electrospray ionization mass spectra obtained from solutions consisting of 10 µM β-lactoglobulin in 100 mM ABC with 3% ammonium hydroxide using 300 nm and 4.4 µm theta tip emitters at source temperatures of 160 °C (a, c) and 300 °C (b, d). The lifetime of the droplets formed from 317 nm and 4.4 µm theta emitter is approximately 1 µs and 50 µs, respectively. Peaks at slightly higher *m*/*z* corresponds to lactosyl covalently bound to β-lactoglobulin.[3]

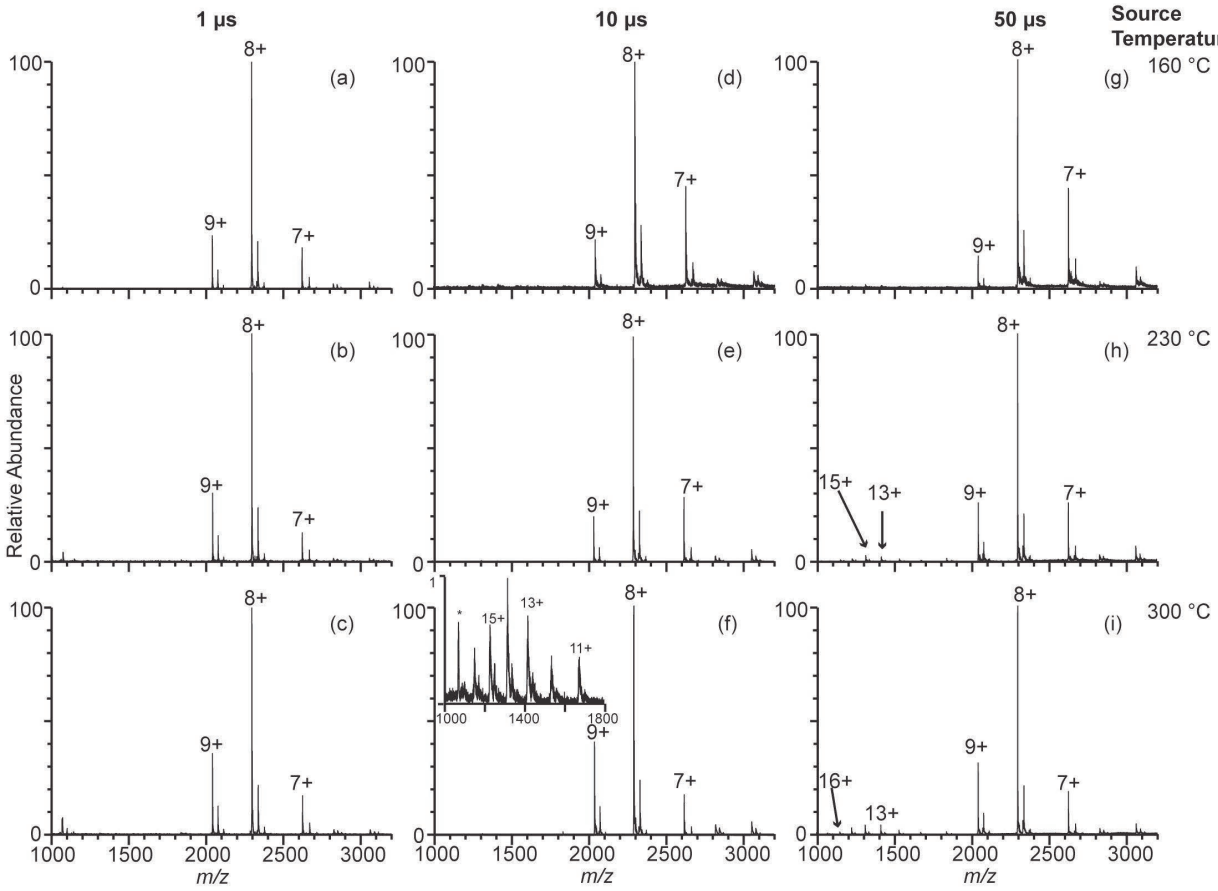


**Supplemental Figure 5.3.** Electrospray ionization mass spectra obtained from solutions consisting of 10 µM β-lactoglobulin in 10 mM AA using 300 nm (a-c), 1.7 µm (d-f), and 4.4 µm (g-i) theta tip emitters at source temperatures of 160 °C (a, d, g), 230 °C (b, e, h), and 300 °C (c, f, i). The lifetime of the droplets formed from 317 nm, 1.7 µm, and 4.4 µm theta emitter is approximately 1 µs, 10 µs and 50 µs, respectively. Peaks at slightly higher *m*/*z* corresponds to lactosyl covalently bound to β-lactoglobulin.[3]

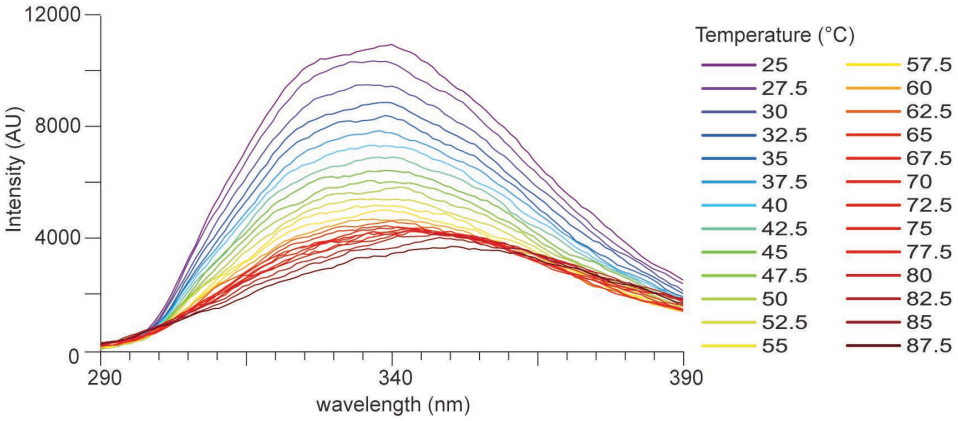


**Supplemental Figure 5.4.** Example tryptophan fluorescent emission results of β-lactoglobulin measured from 200 nm to 390 nm wavelength at temperatures between 25 °C and 87.5 °C measured in 2.5 °C increments.

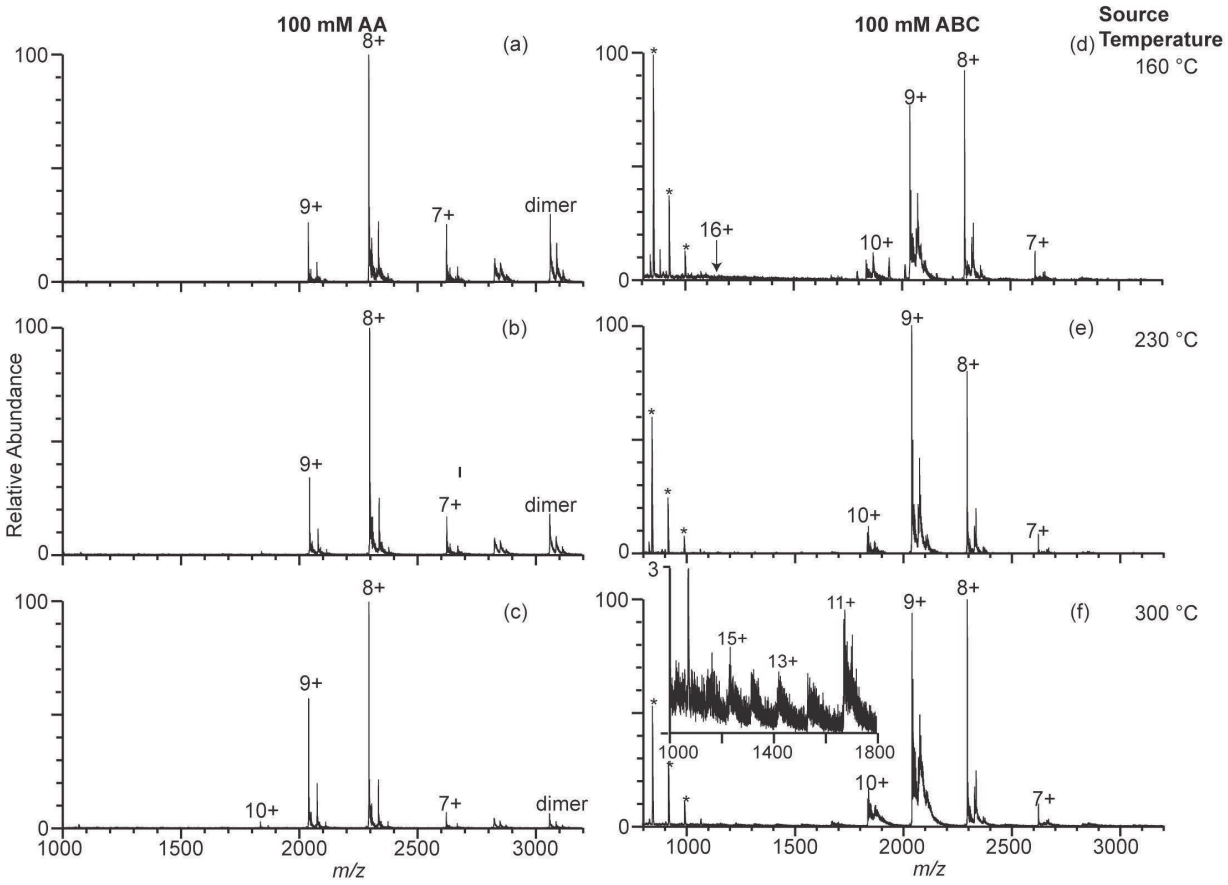


**Supplemental Figure 5.5.** Electrospray ionization mass spectra obtained with electrothermal supercharging of 10 μM β-lactoglobulin in 100 mM ABC (a-c) and 100 mM AA (d-f) at a spray voltage of 0.8 kV using 1.7 μm single barrel emitters at source temperature 160 °C (a, d), 230 °C (b, e), and 300 °C (c, f). Peaks at slightly higher *m*/*z* corresponds to lactosyl covalently bound to β-lactoglobulin.[3] * indicates polydimethylsiloxane clusters that are present as an impurity.

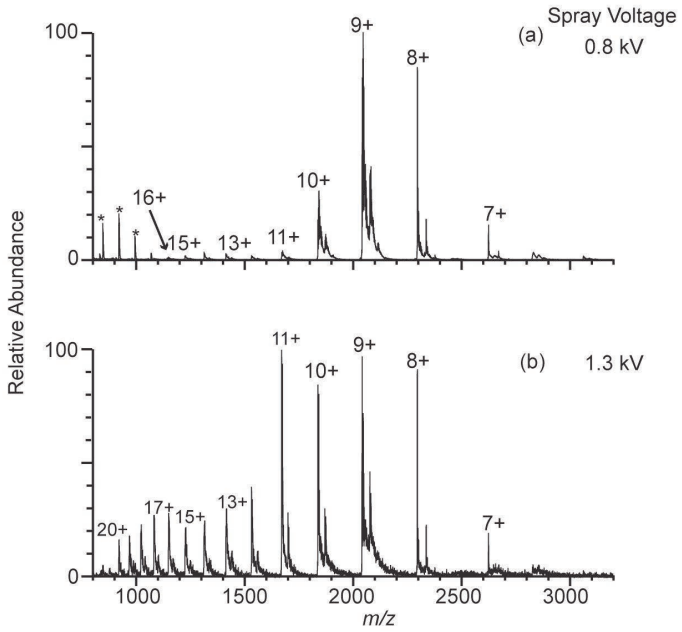


**Supplemental Figure 5.6.** Electrospray ionization mass spectra obtained from solutions consisting of 10 μM β-lactoglobulin in 100 mM ABC using 1.7 μm theta tip emitters at source temperatures of 300 °C with spray voltage of 0.8 kV (a) and 1.3 kV (b). Peaks at slightly higher *m*/*z* corresponds to lactosyl covalently bound to β-lactoglobulin.[3] * indicates polydimethylsiloxane clusters that are present as an impurity.

## 5.10 Supplemental Information References


(1) Mortensen, D. N.; Williams, E. R. Investigating Protein Folding and Unfolding in Electrospray Nanodrops Upon Rapid Mixing Using Theta-Glass Emitters. *Anal. Chem.* **2015**, *87* (2), 1281–1287.

(2) Mortensen, D. N.; Williams, E. R. Ultrafast (1 Ms) Mixing and Fast Protein Folding in Nanodrops Monitored by Mass Spectrometry. *J. Am. Chem. Soc.* **2016**, *138* (10), 3453–3460.

(3) Leonil, J.; Molle, D.; Fauquant, J.; Maubois, J. L.; Pearce, R. J.; Bouhallab, S. Characterization by Ionization Mass Spectrometry of Lactosyl β-Lactoglobulin Conjugates Formed During Heat Treatment of Milk and Whey and Identification of One Lactose-Binding Site. *J. Dairy Sci.* **1997**, *80* (10), 2270–2281.

# Chapter 6

# Native Mass Spectrometry Beyond Ammonium Acetate: Effects of Nonvolatile Salts on Protein Stability and Structure

This chapter is reproduced with permission from:

Zijie Xia, Joseph B. DeGrandchamp, Evan R. Williams

"Native mass spectrometry beyond ammonium acetate: effects of nonvolatile salts on protein stability and structure"

*Analyst*, **2019**, *144*(8): 2565–2573



## 6.1 Abstract

Native mass spectrometry is widely used to probe the structures, stabilities, and stoichiometries of proteins and biomolecular complexes in aqueous solutions, typically containing volatile ammonium acetate or ammonium bicarbonate buffer. In this study, nanoelectrospray emitters with submicron tips are used to produce significantly desalted ions of RNase A and a reduced, alkylated form of this protein, RA-RNase A, from solutions containing 175 mM ammonium acetate, as well as sodium chloride and Tris containing solutions with the same nominal ionic strength and pH. The charge-state distributions formed by nanoelectrospray ionization and tyrosine fluorescent emission data as a function of temperature from these solutions indicate that the folded form of RA-RNase A *in solution* is stabilized when ammonium acetate is replaced by increasing quantities of NaCl and Tris. Ion mobility data for the 7+ charge state of RA-RNase A indicates that the protein conformation in ammonium acetate changes with increasing concentration of NaCl which favors more compact structures. These results are consistent with observations reported 130 years ago by Hofmeister who found that ion identity can affect the stabilities and the structures of proteins in solution. This study indicates the importance of buffer choice when interpreting native mass spectrometry data.

## 6.2 Introduction

Native mass spectrometry (MS) is widely used to transfer intact biological molecules and macromolecular complexes from buffered aqueous solutions in which the analytes are thought to have native or native-like structures into the gas phase for analysis by mass spectrometry.[1–3] Since the detection of noncovalent protein-ligand interactions using electrospray ionization (ESI) MS

was first reported in the early 1990's,[4] there have been many demonstrations that elements of solution-phase biomolecule structures can be kinetically trapped and maintained in the gas phase without solvent.[5,6] Thus, information about structures and stabilities of biological molecules *in solution* can be probed using many different powerful gas-phase techniques. The stoichiometries of protein or other biomolecule complexes can be readily determined from mass measurements, making native mass spectrometry well suited for investigating kinetics and thermodynamics of macromolecular complex assemblies as well as providing information about intermediates in disease-related protein aggregates, such as αβ aggregates.[2,7] In combination with collisional activation and ion mobility spectrometry, information about the number and stabilities of different domains within proteins has been obtained.[8–10] Native MS has been extended to membrane proteins through the use of solubilizing detergents, which can be released from the proteins by collisional activation in the gas phase.[11]

Volatile buffers, such as ammonium acetate and ammonium bicarbonate, are predominantly used in native MS to provide the necessary ionic strength and pH for proteins and protein complexes to fold and assemble.[2] In contrast, the intracellular and the extracellular environments surrounding proteins and complexes consist of tens to hundreds of millimolar of nonvolatile salt ions, such as sodium, potassium, phosphate, and chloride ions.[12] Many different buffers are commonly used to mimic physiological conditions in order to maintain the structures and functions of proteins and protein complexes. Common biochemical buffers for protein preparations, such as Tris buffer and phosphate buffered saline, contain on average 100 mM to 200 mM of nonvolatile salts. However, high concentrations of nonvolatile salts are a bain to native MS because they adversely affect accurate mass measurements and signal. Nonvolatile salts adduct onto protein ions causing the mass spectral peaks to broaden, resulting in loss of resolution, mass measuring accuracy, and sensitivity. Salt adduction decreases sensitivity by spreading the protein ion signal over multiple different masses, and salt clusters can increase baseline noise and cause ion suppression of the analytes of interest.[13,14] Concentrations of nonvolatile salts greater than 100 mM can lead to broad, unresolved peaks in a mass spectrum from which no mass information is typically obtained with common biochemical buffers.[15,16]

Methods in native MS to desalt protein ions from the solutions with nonvolatile salts by adding a low concentration of desalting agents into solution[14,17–19] or in the gas phase have been developed.[20] Although these methods are effective at producing gaseous ions exhibiting significantly reduced levels of salt adduction for solutions with lower than 25 mM nonvolatile salts, this is far short of physiological conditions and the concentration of nonvolatile salts in common biochemical buffers. As a result, aqueous protein solutions are typically buffer exchanged from nonvolatile buffers to volatile buffers before native MS by using methods such as dialysis,[21] diafiltration[22] or ion chromatography.[2] This process, however, changes the solution environment of the biological molecules and complexes. For protein and protein complexes that require a specific nonvolatile salt for proper folding and function, buffer exchange into ammonium acetate can result in loss of structural information. For example, NtrC4 (activator protein) from *Aquifex aeolicus* needs millimolar concentrations of some nonvolatile salts to form a hexamer that dominates in physiological conditions. In ammonium acetate solution without these salts, the heptamer of NtrC4 is instead the dominant species.[23] Thus, complete removal of nonvolatile salts in native MS can lead to changes in the stabilities of different protein complexes.[23,24]

More generally, it has been known for over 130 years that protein stability, solubility, and conformations depend not only on the ionic strength and pH of a solution but also on the identity of the constituent ions. This observation has led to what is known as the Hofmeister ion series in

which both anions and cations are ordered based on their propensity to either stabilize or destabilize proteins in solution.[25,26] For example, guanidinium in the form of a chloride or thiosulfate salt is widely used to destabilize the native form of proteins and can lead to the denatured form being more stable at high salt concentrations.[27] Ammonium sulfate is often used to stabilize or "salt-out" the native form of proteins in order to form crystals suitable for crystallography.[28] The origin of the effect of ions on protein stability has been attributed to direct ion-protein interactions[26,27] and to ion-water interactions that can affect the hydrogen-bonding network of water molecules that surround the protein ions.[29,30] The latter effect is significant for higher charged anions in aqueous solutions, which affect hydrogen bonding networks of water molecules located remotely from the ion.[30] Effects of low concentrations of high valency ions in methanol containing aqueous solution were shown to affect the gaseous conformations of misfolded concanavalin A ions and by inference, the solution-phase structure and therefore stability of the protein complex.[24]

We have recently introduced a new method that is sufficiently effective at desalting protein and protein complex ions during the ESI process that resolved charge-state distributions can be obtained directly from solutions containing high concentrations of nonvolatile salts.[15,16,31,32] Hence, analyte masses can be measured from traditional biochemical buffers without protein denaturation during the ESI process. This method uses submicron electrospray emitters to produce sufficiently small nanodrops that most of the nonvolatile salts are separated from analyte molecules during droplet formation.[16] Here, this method is used to investigate the effects of ammonium acetate, sodium chloride, and Tris buffers on protein stability and structure at solution concentrations that are typically used in studies of protein chemistry that employ other biochemical methods. Results from protein charge-state distribution and ion mobility arrival time measurements of reduced, alkylated RNase A indicate that both the conformation and the stability of the folded forms of this protein depend on the identity of the ions present in solution. Temperature-dependent fluorescence measurements show that the thermal stability of this protein is different in ammonium acetate versus Tris buffers, consistent with the mass spectral results. These results demonstrate that there can be differences in the conformation and stability of a protein in ammonium acetate versus a more commonly used biochemical buffer solution. Thus, the choice of the solution environment can be important for interpreting native MS data.

## 6.3 Experimental Method

### 6.3.1 Mass Spectrometry

Mass spectrometry experiments are performed using a Waters SYNAPT G2Si mass spectrometer (Milford, MA). Electrospray emitters with an inner diameter of 0.66 ± 0.02 μm are pulled from borosilicate capillaries (1.0 mm o.d./0.78 mm i.d., Sutter Instruments, Novato, CA) using a Flaming/Brown micropipette puller (Model P-87, Sutter Instruments, Novato, CA). The emitter diameter is measured with a scanning electron microscope (Hitachi TM-1000 SEM, Schaumburg, IL). Protein ions are formed from aqueous buffered solutions by applying 0.8 kV to 1.3 kV on a 0.127 mm diameter platinum wire that is inserted into the emitters and is in contact with the solution. The emitter tip is positioned ~5 mm away from the instrument entrance with a Z-spray configuration. Traveling wave ion mobility spectrometry (TWIMS) arrival time data are acquired using a wave velocity of 900 m/s, and a wave height of 40 V. Helium and ion mobility

(nitrogen) gas flow rates are 180 mL/min and 90 mL/min, respectively. These TWIMS parameters were selected to minimize ion heating during TWIMS.[33] Ubiquitin, β-lactoglobulin, lysozyme, α-lactalbumin, ribonuclease A, ovalbumin and avidin ions, formed from 200 mM ammonium acetate (AA), are used to calibrate the arrival time data to obtain collisional cross sections using the procedure described previously by Ruotolo and et al. (Supplemental Figure 6.1).[34] The uncertainties reported on the collisional cross sections are based on the precision of three measurements on the same sample but do not reflect the accuracy of the measurements.

### 6.3.2 Protein Modification and Sample Preparation

Reduced and alkylated bovine pancreatic ribonuclease A is prepared as previously described[35] by dissolving lyophilized powder of ribonuclease A in 200 mM ammonium acetate (pH 8.8) solutions containing 6 M guanidine hydrochloride, 15 mM dithiothreitol, and 80 mM iodoacetamide. The reaction is incubated in the dark for approximately two hours. The reaction solution is buffer exchanged into 175 mM AA with a Biospin column (Bio-Rad, Hercules, CA). The final concentration of reduced/alkylated RNase A stock solution is ~200 μM. Lyophilized protein powders of ubiquitin, β-lactoglobulin, bovine pancreatic ribonuclease A (RNase A), cytochrome *c*, ovalbumin, avidin, ammonium acetate, Tris hydrochloride, NaCl, guanidine hydrochloride, dithiothreitol, and iodoacetamide are from Sigma (St. Louis, MO). All buffer solutions containing various concentrations of ammonium acetate, sodium chloride, and Tris are pH adjusted with ammonium hydroxide and acetic acid to pH 6.8 ± 0.3. 10 μM protein samples are prepared by diluting protein stock solution with pH adjusted buffers.

### 6.3.3 Tyrosine Fluorescence

Tyrosine fluorescence emission spectra of reduced, alkylated RNase A in 175 mM AA, 25 mM AA with150 mM NaCl, and 25 mM Tris with 150 mM NaCl are obtained with a FluoroMax-3 spectrometer (Horiba Scientific, Kyoto, Japan). The samples are excited at 280 nm, and the emission spectra are scanned from 290 nm to 400 nm. The slits widths for both excitation and emission are 3 nm. Each sample is heated from 25 °C to 77.5 °C (± 0.2 °C tolerance) in 2.5 °C increments. The solutions are equilibrated for five minutes at each temperature before emission spectra are measured. Three emission spectra are obtained, background subtracted, and averaged for each sample at each temperature.

Tyrosine emission intensity of reduced, alkylated RNase A and a short peptide (AAAYGGF) in 175 mM AA, 25 mM AA with150 mM NaCl, and 25 mM Tris with 150 mM NaCl are obtained with a multi-mode microplate reader (Synergy H4 hybrid reader, BioTek, Winooski, VT) in 384-well polystyrene solid black low volume flat bottom microplates (Corning, New York, NY). The plate reader is operated at the top reading mode. Each protein/peptide sample is measured five times, averaged and background subtracted in emission acquisition mode with 280 nm ±10 nm excitation and 302 ±10 nm emission at 25 °C ± 0.2 °C.

## 6.4 Results and Discussion

### 6.4.1 Solution Ion Effects on RA-RNase A Stability and Structure

Effects of different salts on the ESI mass spectra of reduced, alkylated bovine pancreatic ribonuclease A (RA-RNase A) were investigated from solutions with the same nominal ionic strength (175 mM) and pH (6.8) but containing different concentrations of AA, NaCl and Tris buffer. RA-RNase A has at least two distinct conformations or families of unresolved conformers that coexist in solution corresponding to folded and unfolded forms, making this an ideal system to investigate effects of ion identity on conformational energetics.[32,35] A representative mass spectrum from 175 mM AA is shown in Figure 6.1a. The charge-state distribution of RA-RNase A is bimodal with a distribution of high charge states between 10+ and 14+, indicating a largely unfolded structure, and a distribution of lower charge states between 6+ and 9+, consistent with a molten globular or more compact structure. Results from circular dichroism (CD),[36] hydrogen-deuterium exchange,[37] and X-ray scattering[38] indicate that the RA-RNase A has a structure that is close to either a random coil or a molten globule depending on solution composition, pH, and temperature. For example, CD results indicate that about 66% of the structure of RA-RNase A is random coil in 50 mM phosphate buffer (pH 6).[36] The mass spectrometry results from 175 mM AA also indicate substantial random coil structure, but native mass spectrometry has the advantage that it is able to reveal two coexisting structures in solution that are not identified by CD. There is also signal for intact (not reduced) RNase A, which appears at just the lower charge states 6+ to 8+. There are no high charge states of RNase A, indicating that this protein is essentially fully folded. The four internal disulfide bonds of RNase A constrain the protein, so it cannot adopt as a fully unfolded form as RA-RNase A. The lower charge-state distribution of RA-RNase A is similar to the charge states of RNase A, indicating that the conformation of RA-RNase A at lower charge states is largely compact or similarly folded as RNase A. The abundance of the folded form of RA-RNase relative to the unfolded form is estimated to be ~58% ± 3% based on the abundances of ions that make up the two respective charge-state distributions.

Results obtained from solutions in which 10 mM of AA is replaced by 10 mM of NaCl are shown in Figure 6.1b. The ion signal in the lower charge states is significantly broadened owing to sodium ion adduction, but the high charge state ions are notably less adducted, consistent with earlier reports of more sodium ions adducting to low charge states of a protein.[39,40] Although the peaks in the lower charge-state distribution are significantly broadened, the integrated abundances of charge states in the high and low charge-state distributions indicate that there is a similar fraction of the unfolded form of the protein (~55% ± 2%) as there is for the solution with no NaCl (~58% ± 3%; Figure 6.1a).

For solutions in which 50 mM of AA is replaced by the same concentration of NaCl, the mass spectra show significantly broadened peaks in both distributions corresponding to more heavily adducted folded and unfolded conformers (Figure 6.1c). Moreover, the abundance of the lower charge-state distribution is significantly enhanced over that of the high charge-state distribution despite the more adducted, broader peaks in the former. Shifts in the average charge of both distributions are also apparent with the higher charge-state distribution shifting slightly to lower charge and the lower charge-state distribution shifting slightly to higher charge. Based on the integrated abundances of the ions in these two distributions, the relative abundance of the unfolded form of RA-RNase A is ~37% ± 10%.

The mass spectra from solutions consisting of 25 mM AA and 150 mM NaCl (Figure. 6.1d) are notably different from those obtained from solutions with significantly less NaCl. There is predominantly one charge-state distribution, and the center of this distribution is shifted to even higher charge than that of the folded population with 50 mM NaCl (Figure 6.1c). The population of unfolded conformers is significantly reduced compared to that of solutions with lower NaCl concentrations. The relative abundances of the high charge states (10+ to 14+) indicate that only ~16% ± 3% of the RA-RNase A population is unfolded. The decreasing abundance of the high charge-state distribution relative to the lower charge-state distribution with increasing NaCl concentration indicates that the folded form of RA-RNase A is stabilized with increasing NaCl despite the nearly identical ionic strength and pH of these solutions. The shift in the center of the charge-state distribution to higher charges for the folded form of RA-RNase A in 150 mM NaCl and 25 mM AA compared to that in 175 mM AA alone suggests that the conformation of the protein may differ in these two solutions. It should be noted that sodium adduction to the ions does not appear to be responsible for the increased charging of the folded form because sodium adduction to the unfolded form results in lower charge states. Thus, the changes in charge-state distributions likely reflect a change in solution conformation.

Replacing 25 mM AA with 25 mM Tris in solutions containing 150 mM NaCl results in a predominant charge-state distribution at lower charges (6+ to 9+). Higher charge states (10+ to 14+) are formed to some extent, but their abundance is difficult to quantitate because of the high baseline chemical noise as a result of unresolved salt clusters. After baseline subtraction, the abundance of these higher charges states relative to the low charge states is only ~3% ± 4%. These results indicate that RA-RNase A adopts a predominantly folded conformation in solutions of 25 mM Tris and 150 mM NaCl.

The concentration of sodium chloride in the Tris buffer and that in 25 mM AA with 150 mM NaCl is the same and the extent of adduction to the folded forms of these ions is similar (Figure 6.1d and e, respectively), yet the charge-state distributions differ. These results provide further evidence that the difference in charge-state distributions observed for these two solutions reflects differences in conformations of the folded form of the protein.

Solution compositions may also affect other factors, such as droplet temperature and ionization efficiency, resulting different mass spectra results. In the previous study, ~300 nm theta emitters produce initial droplets that are fully desolvated before the droplets enter the instrument due to the short lifetime (~ 1 μs). Similarly, droplets from a 500 nm single barrel emitter are expected to have such a short droplet lifetime that they are desolvated before entering the instrument. Because the droplets formed from different solutions should charge to the same extend with similar surface tensions, no significant impact from droplet temperature is expected. Ionization efficiency is not considered in this study. However, the relative change in the charge-state distributions from one solution to another should be independent of the ionization efficiency.

The quality of the mass spectra from solutions consisting of more than 50 mM NaCl (Figure 6.1c-e) appears poor compared to those obtained from solutions with significantly less NaCl. The background is high owing to the chemical noise of various salt clusters that are typically below $m/z$ ~4000, which can interfere with small protein ions in this same $m/z$ range. Moreover, preliminary results indicate that the extent of adduction onto protein ions formed with a single emitter tip size is roughly related to protein surface areas. Thus, the desalting effects of small emitters are generally more prominent for larger protein complexes owing to their lower surface area-to-mass ratios and the formation of ions above $m/z$ 3000 which reduces effects of chemical noise from salt clusters. Despite the broad mass spectral peaks, the conclusions about the effects

of high concentrations of nonvolatile salts on the relative stability of the unfolded and folded forms of this protein, which are determined from the relative abundances of the corresponding charge-distributions, can still be deduced from these data.

### 6.4.2 Effects of Different Ions on RA-RNase A Thermal Stability in Solution.

In order to investigate the effects of different ions on the solution-phase thermal stability of RA-RNase A, tyrosine fluorescence emission spectra were obtained for this protein in three solutions consisting of 1) 175 mM AA, 2) 25 mM AA and 150 mM NaCl, and 3) 25 mM Tris and 150 mM NaCl at temperatures between 25 °C and 77.5 °C. The emission peak of RA-RNase A is broad, centered around 302 nm, and the intensity at 302 nm generally decreases with increasing temperature (Figure 6.2). The gradual decrease in fluorescence emission intensity with increasing temperature is attributed to competitive non-radiative deactivation pathways at higher temperatures.[41,42] The emission intensity of tyrosine fluorescence is also influenced by the environment that surrounds the six tyrosine residues (Tyr-25, Tyr-73, Tyr-76, Tyr-92, Tyr-97, Tyr-115) in the protein, including both solvent accessibility as well as proximity to other residues. Three tyrosine residues in RNase A, Tyr-25, Tyr-73, and Tyr-97, are buried inside the protein interior whereas the other three are partially exposed to the solvent based on the structure obtained through NMR and X-ray crystallography.[43,44] Thus, these measurements monitor local changes around tyrosine residues rather than more global measures of protein conformational change. As a result, a sigmoidal melting curve often characteristic of protein melting data obtained from other methods, such as CD, does not always occur with tyrosine fluorescence emission. CD was not used in these experiments because of interference from ammonium acetate at high concentration.

The temperature dependent emission data from the three solutions show differences in both fluorescent emission intensity and temperature dependence. The emission intensity of RA-RNase in 175 mM AA is consistently lower than that of the two solutions containing 150 mM NaCl. This difference in intensity can be attributed to either differences in solution composition and/or differences in protein conformation.[43] In order to determine how different ions in solution might affect the emission intensity of tyrosine, the emission intensity of a short tyrosine-containing peptide (AAAYGGFL) was measured from the three solutions at 25 °C. This peptide was chosen because tyrosine has neighboring residues and is not expected to have a particularly stable folded form. The tyrosine is also remote from the C- and N- terminus to avoid any effects of charge on tyrosine fluorescence. The emission intensity of tyrosine at 302 nm in both solutions containing AA is similar, but the emission in 25 mM Tris and 150 mM NaCl is slightly higher (Supplemental Table 6.1). This indicates that AA interacts with the tyrosine side chain and results in fluorescent quenching. Acetate is a proton acceptor that has been reported previously to quench tyrosine fluorescence.[43,45].

The emission intensity of tyrosine in RA-RNase A in 25 mM AA and 150 mM NaCl is consistently higher than that in 175 mM AA, whereas the emission intensity from AAAYGGFL is essentially the same in these two solutions (Figure 6.2 and Supplemental Table 6.1). This result suggests that the differences in fluorescence intensity of RA-RNase A are not due to quenching by different ions in solution but rather due to conformational differences throughout this temperature range. Moreover, the trend of emission intensity with increasing temperature is different at temperatures above 65 °C with these three solutions (Figure 6.2). In solutions containing 175 mM AA or 25 mM AA and 150 mM NaCl, the intensity increases slightly between 65 °C and 75 °C and decreases rapidly at higher temperatures. In contrast, the signal for the solution with 25 mM

Tris and 150 mM NaCl increases between 67.5 °C and 72.5 °C before decreasing at higher temperatures. The signal rise is higher and is shifted by ~2.5 °C compared to that for the other two solutions.

An increase in the tyrosine emission intensity also occurs for RNase A in this temperature range. This phenomenon was attributed to an increase in distance between disulfide bonds and two tyrosine residues that occurs upon unfolding at ~62 °C in 10 mM phosphate buffer (pH 7), which decreases the extent of fluorescence quenching by the disulfide bonds.[43] The similar trend in fluorescence emission with temperature for both native RNase A and RA-RNase A indicates that the alkylated cysteine residues may also quench emission and that the folded structure of RA-RNase A has similar contacts as RNase A in these regions. This result and the similar charge-state distributions suggest that many other regions of the folded form of RA-RNase A may be similar to that of RNase A as well. Both the higher emission intensity at elevated temperatures and the shift in fluorescence intensity between 67.5 and 72.5 °C observed from the Tris/NaCl solution indicates that RA-RNase A is more stable in this solution. The emission data also suggest that the conformation in this solution may be closer to that of native RNase A than the other two solutions, which is consistent with the mass spectral results.

### 6.4.3 Ion Mobility and Ion Effects on Solution Structure.

Both the mass spectral data and the tyrosine emission temperature melt data indicate that the folded form of RA-RNase A is more stable (relative to the unfolded or random coil form) in a solution consisting of 25 mM Tris and 150 mM NaCl than it in a 175 mM AA solution. Also, the shift in the charge states corresponding to the folded form of RA-RNase A with increasing NaCl and with Tris suggests that the actual conformation of the folded form of the protein is affected by these different ions, which is consistent with the fluorescence data as well. To investigate the structures of the folded form of the protein in solutions with various concentrations of AA and NaCl, ion mobility data was acquired for the 6+ and 7+ ions under conditions identified in Figure 6.1. Because ion conformation can depend on charge state, the same charge states produced from the different solutions are compared.[46] Gas-phase protein ion conformations can also depend on the number and the identity of salt adducts. Adducted ions are typically more compact [46,47] and are also more stable in the gas phase.[48,49] For cations, these effects become more apparent with increasing number of adducts and higher valency salts.[46,49] For this reason, a relatively narrow mass window was chosen to isolate the precursors that are either fully protonated or have up to two sodium adducts in this study. This level of of sodium adduction is expected to have minimal effect on protein structure.[46]

Arrival time data from traveling wave ion mobility spectrometry (TWIMS) measurements for the 7+ charge state of RA-RNase A formed from 175 mM AA is shown in Figure 6.3a. There is an abundant peak (~90 %) at 13.7 ± 0.1 ms and a much less abundant peak (~10 %) at 11.3 ± 0.2 ms. These data indicate that the 7+ ion has at least two gas-phase conformations (or families of conformers) that can be distinguished by ion mobility. By calibrating these arrival time data (Supplemental Figure 6.1), an average collisional cross section of 1562 ± 7 $Å^2$ and 1392 ± 15 $Å^2$ are obtained for the major and minor conformers, respectively. There are also two peaks in the arrival time distributions of 7+ intact RNase A corresponding to two conformers with cross sections of 1496 ± 5 $Å^2$ (~ 92%) and 1365 ± 7 $Å^2$ (~ 8%). The minor conformers for both RA-RNase A and RNase A have cross sections that are similar to the value reported from radio-frequency confining drift tube ion mobility measurements of RNase A (1340 $Å^2$; 200 mM AA; pH

7),[50] but the minor conformer of RA-RNase A is slightly larger than that of RNase A. The major conformers of both proteins have a much larger cross section, but the cross section of RA-RNase A is again larger than that of RNase A, consistent with a slightly more unfolded form of the reduced species in this solution. TWIMS measurements under identical solution conditions to those reported previously result in the same cross sections as those measured in 175 mM AA indicating that the ions may be heated somewhat in these TWIMS measurements. By comparison, the cross section of the 6+ ion is 1313 ± 3 $Å^2$ for RA-RNase A and 1282 ± 3 $Å^2$ for RNase A, which is consistent with the reported value 1290 $Å^2$ for RNase A (Supplemental Figure 6.2 and Supplemental Figure 6.3).[50] The collisional cross section for the 6+ charge state of RA-RNase is slightly larger and may be attributable to its higher mass and hence volume. Conformations of gaseous protein ions can be influenced by instrument conditions. A similar heating effect has been reported for other proteins with charge states close to the transition observed between folded and unfolded forms using TWIMS.[33,51] It is interesting that the more compact structure or structures of RA-RNase A have collisional cross sections that are similar to that of native RNase A, indicating that the more compact structures of RA-RNase A may closely resemble the native form of the protein.

The ion mobility arrival time data for RA-RNase A 7+ in solutions with 10 mM NaCl and 50 mM NaCl are shown in Figure 6.3b and 6.3c, respectively. Both similarly compact and a less compact structure are observed from these NaCl containing solutions, but the relative abundance of the more compact structure is significantly increased when NaCl is present. The collisional cross section of the more compact conformation (arrival time ~11 ms) is also slightly smaller from the solutions containing NaCl than it is from 175 mM AA. The more compact conformation has a collisional cross section of 1353 ± 8 $Å^2$ from the solutions with 10 mM NaCl or 50 mM NaCl compared to 1397 ± 21 $Å^2$ from 175 mM AA. The results in Figure 6.3 indicate that the population of more compact protein structures increases with increasing NaCl in the aqueous solution. Because the same charge state ions with a similar number of sodium adducts are compared, these results indicate that the solution-phase conformations of the folded form of RA-RNase A are different in solutions containing higher concentrations of NaCl from those containing just AA. Ion mobility data for the RA-RNase A 6+ charge state shows a single peak for the protein corresponding to a collisional cross section of 1302 ± 3 $Å^2$ from each of these solutions, which is consistent with the reported value for RNase A 6+ ion. (Supplemental Figure 6.3).[50]

A key challenge in interpreting ion mobility data for solutions containing NaCl concentrations above 50 mM is interference from large salt clusters, including multiply charged clusters, which increase significantly in abundance and complexity with salt concentration. The arrival times of some of these salt clusters in the selected *m*/*z* window can overlap with those of the protein conformers. Below 50 mM, these interferences are relatively minor and the arrival times do not overlap significantly with those of the protein conformers. For example, the normalized abundances in the arrival times of salt clusters generated from solutions without protein are also shown in Figure 6.3. The ion identity, abundances, and arrival times change with increasing NaCl concentration. When the concentration of NaCl is 50 mM or lower, the most abundant peak in the arrival time distribution of the salt solutions without protein does not appear to a significant extent in the distributions with the proteins. Moreover, these peaks appear at different arrive times indicating that these salt clusters do not interfere significantly with the ion mobility data for the protein ions.

At 150 mM NaCl with either 25 mM AA or 25 mM Tris, salt clusters overlap with protein signal to a large extent both in *m*/*z* and ion mobility arrival times. For the 7+ charge state, there is

no significant overlap between salt clusters and protein in the region between ~11 and 13 ms for the 25 mM AA and 150 mM NaCl solution and between ~12 and 14 ms for the 25 mM Tris and 150 mM NaCl solution (Supplemental Figure 6.4). In these regions, there is an abundant signal for the 7+ ion. There is little apparent protein signal above 13.5 ms. These results indicate that a more compact form of the protein is favored in these solutions compared to 175 mM AA, but little additional information about the nature of these structures can be obtained from these experiments.

It is interesting that the ion mobility data for the 7+ ion indicates that there is compaction in structure with increasing NaCl concentration, yet the distribution of lower charge states shifts to slightly higher charge. This phenomenon may be due to the incomplete folding of higher charge state population that is formed at low or no NaCl resulting in the slightly higher charge states in the lower charge-state distribution. The formation of intermediates along the folding and unfolding pathways have been observed for many different proteins.[52,53] It should also be noted that a reduction of the collisional cross section can be accompanied by an increase in charge as a result of a change in molecular shape which favors more charge separation.[54]

## 6.5 Conclusion

Native mass spectrometry of soluble proteins is nearly exclusively performed from volatile aqueous buffered solutions consisting of either ammonium acetate or ammonium bicarbonate. These conditions are not typically used to investigate the structures and the functions of proteins or macromolecular complexes using other methods. A key question is how the identity of different ions that make up the necessary ionic strength of a solution may affect the interpretation of native MS data obtained from different solutions. For RA-RNase A, mass spectral charge-state distributions and tyrosine fluorescence data as a function of temperature indicate that the folded form of the protein is stabilized by replacing ammonium acetate with NaCl and Tris for solutions with the same nominal ionic strength and pH. Moreover, the charge-state distributions and ion mobility data for the 7+ ion indicate that the conformation of the folded protein differs in these solutions where AA is replaced with NaCl. Thus, both the structure and the stability of this protein is different in solutions containing high levels of NaCl compared to those in just AA.

In cases where the folded form of a protein is much more stable, effects of different ions on the stabilities and structures of proteins and protein complexes are likely to be much less apparent. Thus, in numerous cases documented in the literature, native mass spectrometry using ammonium acetate or ammonium bicarbonate leads to conclusions about structure and stability comparable to those obtained by other methods from solutions that more accurately mimic either the intracellular or the extracellular environment. However, when there are multiple conformers of a protein or multiple stoichiometries for protein complexes in solution, differences in the stabilities are much lower, and the identity of the constituent ions in solution will likely make a difference in the forms and structures of the proteins formed from these solutions in native mass spectrometry.[23,24] Very recent studies using submicron emitter tips with mass spectrometry indicate that the stoichiometries and the stabilities of large protein complexes and protein-ligand complexes can also be affected by high concentrations of nonvolatile salts.[55, 56] Mass spectrometry has the advantage that multiple conformers or forms of a complex can be readily identified based on charge-state distributions, masses, and ion mobility data. Native mass

spectrometry can now be performed from a range of traditional biochemical buffers, including phosphate and Tris with >150 mM of $Na^+$ or $K^+$ using nanoelectrospray emitters with submicron tips. The use of such tips should be beneficial for native mass spectrometry of proteins and macromolecular complexes where multiple forms are present to better compare to other methods that use traditional biochemical buffers.

## 6.6 Acknowledgments

This material is based upon work supported by the National Science Foundation Division of Chemistry under grant number CHE-1609866. The authors are grateful for financial support from CALSOLV and also thank Dr. Anna Susa and Dr. Ethan McSpadden for helpful discussions.

## 6.7 Reference

(1) Loo, J. A. Electrospray Ionization Mass Spectrometry: A Technology for Studying Noncovalent Macromolecular Complexes. *Int. J. Mass Spectrom.* **2000**, *200* (1–3), 175–186.
(2) Hernández, H.; Robinson, C. V. Determining the Stoichiometry and Interactions of Macromolecular Assemblies from Mass Spectrometry. *Nat. Protoc.* **2007**, *2* (3), 715–726.
(3) Leney, A. C.; Heck, A. J. R. Native Mass Spectrometry: What Is in the Name? *J. Am. Soc. Mass Spectrom.* **2017**, *28* (1), 5–13.
(4) Ganem, B.; Li, Y. T.; Henion, J. D. Detection of Noncovalent Receptor-Ligand Complexes by Mass Spectrometry. *J. Am. Chem. Soc.* **1991**, *113* (16), 6294–6296.
(5) Gross, D. S.; Zhao, Y.; Williams, E. R. Dissociation of Heme-Globin Complexes by Blackbody Infrared Radiative Dissociation: Molecular Specificity in the Gas Phase? *J. Am. Soc. Mass Spectrom.* **1997**, *8* (5), 519–524.
(6) El-Baba, T. J.; Woodall, D. W.; Raab, S. A.; Fuller, D. R.; Laganowsky, A.; Russell, D. H.; Clemmer, D. E. Melting Proteins: Evidence for Multiple Stable Structures upon Thermal Denaturation of Native Ubiquitin from Ion Mobility Spectrometry-Mass Spectrometry Measurements. *J. Am. Chem. Soc.* **2017**, *139* (18), 6306–6309.
(7) Esparza, T. J.; Wildburger, N. C.; Jiang, H.; Gangolli, M.; Cairns, N. J.; Bateman, R. J.; Brody, D. L. Soluble Amyloid-Beta Aggregates from Human Alzheimer's Disease Brains. *Sci. Rep.* **2016**, *6* (1), 38187.
(8) Benesch, J. L. P.; Aquilina, J. A.; Ruotolo, B. T.; Sobott, F.; Robinson, C. V. Tandem Mass Spectrometry Reveals the Quaternary Organization of Macromolecular Assemblies. *Chem. Biol.* **2006**, *13* (6), 597–605.
(9) Zhou, M.; Dagan, S.; Wysocki, V. H. Protein Subunits Released by Surface Collisions of Noncovalent Complexes: Nativelike Compact Structures Revealed by Ion Mobility Mass Spectrometry. *Angew. Chemie Int. Ed.* **2012**, *51* (18), 4336–4339.
(10) Zhong, Y.; Han, L.; Ruotolo, B. T. Collisional and Coulombic Unfolding of Gas-Phase Proteins: High Correlation to Their Domain Structures in Solution. *Angew. Chemie Int. Ed.* **2014**, *53* (35), 9209–9212.
(11) Laganowsky, A.; Reading, E.; Hopper, J. T. S.; Robinson, C. V. Mass Spectrometry of Intact Membrane Protein Complexes. *Nat. Protoc.* **2014**, *8* (4), 639–651.

(12) Diem, K.; Lentner, C. *Blood – Inorganic Substances*; CIBA-GEIGY Ltd.: Basle, Switzerland, 1970.
(13) Pan, P.; McLuckey, S. A. The Effect of Small Cations on the Positive Electrospray Responses of Proteins at Low PH. *Anal. Chem.* **2003**, *75* (20), 5468–5474.
(14) Iavarone, A. T.; Udekwu, O. A.; Wiliams, E. R. Buffer Loading for Counteracting Metal Salt-Induced Signal Suppression in Electrospray Ionization. *Anal. Chem.* **2004**, *76* (14), 3944–3950.
(15) Susa, A. C.; Xia, Z.; Williams, E. R. Native Mass Spectrometry from Common Buffers with Salts That Mimic the Extracellular Environment. *Angew. Chemie Int. Ed.* **2017**, 1–5.
(16) Susa, A. C.; Xia, Z.; Williams, E. R. Small Emitter Tips for Native Mass Spectrometry of Proteins and Protein Complexes from Nonvolatile Buffers That Mimic the Intracellular Environment. *Anal. Chem.* **2017**, *89* (5), 3116–3122.
(17) Flick, T. G.; Cassou, C. a.; Chang, T. M.; Williams, E. R. Solution Additives That Desalt Protein Ions in Native Mass Spectrometry. *Anal. Chem.* **2012**, *84* (17), 7511–7517.
(18) Clarke, D. J.; Campopiano, D. J. Desalting Large Protein Complexes during Native Electrospray Mass Spectrometry by Addition of Amino Acids to the Working Solution. *Analyst* **2015**, *140* (8), 2679–2686.
(19) Cassou, C. A.; Williams, E. R. Desalting Protein Ions in Native Mass Spectrometry Using Supercharging Reagents. *Analyst* **2014**, *139* (19), 4810–4819.
(20) Demuth, J. C.; McLuckey, S. A. Electrospray Droplet Exposure to Organic Vapors: Metal Ion Removal from Proteins and Protein Complexes. *Anal. Chem.* **2015**, *87* (2), 1210–1218.
(21) Xiang, F.; Lin, Y.; Wen, J.; Matson, D. W.; Smith, R. D. An Integrated Microfabricated Device for Dual Microdialysis and On-Line ESI-Ion Trap Mass Spectrometry for Analysis of Complex Biological Samples. *Anal. Chem.* **1999**, *71* (8), 1485–1490.
(22) Prodanov, M.; Garrido, I.; Vacas, V.; Lebrón-Aguilar, R.; Dueñas, M.; Gómez-Cordovés, C.; Bartolomé, B. Ultrafiltration as Alternative Purification Procedure for the Characterization of Low and High Molecular-Mass Phenolics from Almond Skins. *Anal. Chim. Acta* **2008**, *609* (2), 241–251.
(23) Batchelor, J. D.; Sterling, H. J.; Hong, E.; Williams, E. R.; Wemmer, D. E. Receiver Domains Control the Active-State Stoichiometry of Aquifex Aeolicus Σ54 Activator NtrC4, as Revealed by Electrospray Ionization Mass Spectrometry. *J. Mol. Biol.* **2009**, *393* (3), 634–643.
(24) Han, L.; Ruotolo, B. T. Hofmeister Salts Recover a Misfolded Multiprotein Complex for Subsequent Structural Measurements in the Gas Phase. *Angew. Chemie Int. Ed.* **2013**, *52* (32), 8329–8332.
(25) Hofmeister, F. Zur Lehre von Der Wirkung Der Salze - Zweite Mittheilung. *Arch. Exp. Pathol. und Pharmakologie* **1888**, *24* (4–5), 247–260.
(26) Tadeo, X.; López-Méndez, B.; Castaño, D.; Trigueros, T.; Millet, O. Protein Stabilization and the Hofmeister Effect: The Role of Hydrophobic Solvation. *Biophys. J.* **2009**, *97* (9), 2595–2603.
(27) Monera, O. D.; Kay, C. M.; Hodges, R. S. Protein Denaturation with Guanidine Hydrochloride or Urea Provides a Different Estimate of Stability Depending on the Contributions of Electrostatic Interactions. *Protein Sci.* **1994**, *3* (11), 1984–1991.

(28) Wingfield, P. Protein Precipitation Using Ammonium Sulfate. In *Current Protocols in Protein Science*; John Wiley & Sons, Inc.: Hoboken, NJ, USA, 1998; Vol. Appendix 3, p A.3F.1-A.3F.8.
(29) Hribar, B.; Southall, N. T.; Vlachy, V.; Dill, K. A. How Ions Affect the Structure of Water. *J. Am. Chem. Soc.* **2002**, *124* (41), 12302–12311.
(30) DiTucci, M. J.; Williams, E. R. Nanometer Patterning of Water by Tetraanionic Ferrocyanide Stabilized in Aqueous Nanodrops. *Chem. Sci.* **2017**, *8* (2), 1391–1399.
(31) Susa, A. C.; Lippens, J. L.; Xia, Z.; Loo, J. A.; Campuzano, I. D. G.; Williams, E. R. Submicrometer Emitter ESI Tips for Native Mass Spectrometry of Membrane Proteins in Ionic and Nonionic Detergents. *J. Am. Soc. Mass Spectrom.* **2018**, *29* (1), 203–206.
(32) Xia, Z.; Williams, E. R. Protein-Glass Surface Interactions and Ion Desalting in Electrospray Ionization with Submicron Emitters. *J. Am. Soc. Mass Spectrom.* **2018**, *29* (1), 194–202.
(33) Merenbloom, S. I.; Flick, T. G.; Williams, E. R. How Hot Are Your Ions in TWAVE Ion Mobility Spectrometry? *J. Am. Soc. Mass Spectrom.* **2012**, *23* (3), 553–562.
(34) Ruotolo, B. T.; Benesch, J. L. P.; Sandercock, A. M.; Hyung, S.-J.; Robinson, C. V. Ion Mobility-Mass Spectrometry Analysis of Large Protein Complexes. *Nat. Protoc.* **2008**, *3* (7), 1139–1152.
(35) Sterling, H. J.; Cassou, C. A.; Trnka, M. J.; Burlingame, A. L.; Krantz, B. A.; Williams, E. R. The Role of Conformational Flexibility on Protein Supercharging in Native Electrospray Ionization. *Phys. Chem. Chem. Phys.* **2011**, *13* (41), 18288–18296.
(36) Takahashi, S.; Kontani, T.; Yoneda, M.; Ooi, T. A Circular Dichroic Spectral Study on Disulfide-Reduced Pancreatic Ribonuclease A and Its Renaturation to the Active Enzyme. *J. Biochem.* **1977**, *82* (4), 1127–1133.
(37) Woodward, C. K.; Rosenberg, A. Oxidized RNase as a Protein Model Having No Contribution to the Hydrogen Exchange Rate from Conformational Restrictions. *Proc. Natl. Acad. Sci. U. S. A.* **1970**, *66* (4), 1067–1074.
(38) Jacob, J.; Dothager, R. S.; Thiyagarajan, P.; Sosnick, T. R. Fully Reduced Ribonuclease A Does Not Expand at High Denaturant Concentration or Temperature. *J. Mol. Biol.* **2007**, *367* (3), 609–615.
(39) Yue, X.; Vahidi, S.; Konermann, L. Insights into the Mechanism of Protein Electrospray Ionization from Salt Adduction Measurements. *J. Am. Soc. Mass Spectrom.* **2014**, *25* (8), 1322–1331.
(40) Flick, T. G.; Merenbloom, S. I.; Williams, E. R. Anion Effects on Sodium Ion and Acid Molecule Adduction to Protein Ions in Electrospray Ionization Mass Spectrometry. *J. Am. Soc. Mass Spectrom.* **2011**, *22* (11), 1968–1977.
(41) Allison, S. W.; Gillies, G. T. Remote Thermometry with Thermographic Phosphors: Instrumentation and Applications. *Rev. Sci. Instrum.* **1997**, *68* (7), 2615–2650.
(42) Gally, J. A.; Edelman, G. M. The Effect of Temperature on the Fluorescence of Some Aromatic Amino Acids and Proteins. *Biochim. Biophys. Acta* **1962**, *60* (3), 499–509.
(43) Noronha, M.; Lima, J. C.; Paci, E.; Santos, H.; Maçanita, A. L. Tracking Local Conformational Changes of Ribonuclease A Using Picosecond Time-Resolved Fluorescence of the Six Tyrosine Residues. *Biophys. J.* **2007**, *92* (12), 4401–4414.
(44) Santoro, J.; Gonzales, C.; Bruix, M.; Neira, J. L.; Nieto, J. L.; Herranz, J.; Rico, M. High-Resolution Three-Dimensional Structure of Ribonuclease A in Solution by Nuclear Magnetic Resonance Spectroscopy. *J. Mol. Biol.* 1993, pp 722–734.

(45) Willis, K. J.; Szabo, A. G. Fluorescence Decay Kinetics of Tyrosinate and Tyrosine Hydrogen-Bonded Complexes. *J. Phys. Chem.* **1991**, *95* (4), 1585–1589.
(46) Flick, T. G.; Merenbloom, S. I.; Williams, E. R. Effects of Metal Ion Adduction on the Gas-Phase Conformations of Protein Ions. *J. Am. Soc. Mass Spectrom.* **2013**, *24* (11), 1654–1662.
(47) Merenbloom, S. I.; Flick, T. G.; Daly, M. P.; Williams, E. R. Effects of Select Anions from the Hofmeister Series on the Gas-Phase Conformations of Protein Ions Measured with Traveling-Wave Ion Mobility Spectrometry/Mass Spectrometry. *J. Am. Soc. Mass Spectrom.* **2011**, *22* (11), 1978–1990.
(48) Han, L.; Hyung, S. J.; Mayers, J. J. S.; Ruotolo, B. T. Bound Anions Differentially Stabilize Multiprotein Complexes in the Absence of Bulk Solvent. *J. Am. Chem. Soc.* **2011**, *133* (29), 11358–11367.
(49) Han, L.; Hyung, S.-J.; Ruotolo, B. T. Bound Cations Significantly Stabilize the Structure of Multiprotein Complexes in the Gas Phase. *Angew. Chemie Int. Ed.* **2012**, *51* (23), 5692–5695.
(50) Allen, S. J.; Giles, K.; Gilbert, T.; Bush, M. F. Ion Mobility Mass Spectrometry of Peptide, Protein, and Protein Complex Ions Using a Radio-Frequency Confining Drift Cell. *Analyst* **2016**, *141* (3), 884–891.
(51) Morsa, D.; Gabelica, V.; De Pauw, E. Fragmentation and Isomerization Due to Field Heating in Traveling Wave Ion Mobility Spectrometry. *J. Am. Soc. Mass Spectrom.* **2014**, *25* (8), 1384–1393.
(52) Baldwin, R. L.; Frieden, C.; Rose, G. D. Dry Molten Globule Intermediates and the Mechanism of Protein Unfolding. *Proteins Struct. Funct. Bioinforma.* **2010**, *78* (13), 2725–2737.
(53) Clemmer, D. E.; Russell, D. H.; Williams, E. R. Characterizing the Conformationome: Toward a Structural Understanding of the Proteome. *Acc. Chem. Res.* **2017**, *50* (3), 556–560.
(54) Sterling, H. J.; Kintzer, A. F.; Feld, G. K.; Cassou, C. A.; Krantz, B. A.; Williams, E. R. Supercharging Protein Complexes from Aqueous Solution Disrupts Their Native Conformations. *J. Am. Soc. Mass Spectrom.* **2012**, *23* (2), 191–200.
(55) Native Mass Spectrometry of Membrane Proteins in Physiological Salts Preserve Binding of Endogenous Lipids, M. T. Agasid, I, Liko, J, Gault, C. V. Robinson, Citation # 293014, Jun 4th, *Proceedings of the 66th ASMS Conference on Mass Spectrometry and Allied Topic*, San Diego, CA,Jun 3rd to Jun 7th, 2018.
(56) Is Native Mass Spectrometry Really Native? Comparisons of Protein Structures in Ammonium Acetate and in Common Biochemical Buffers, Z. Xia, J. B. DeGrandchamp, E. R. Williams, Citation # 295392, Jun 4th, *Proceedings of the 66th ASMS Conference on Mass Spectrometry and Allied Topic*, San Diego, CA,Jun 3rd to Jun 7th, 2018.

## 6.8 Figures

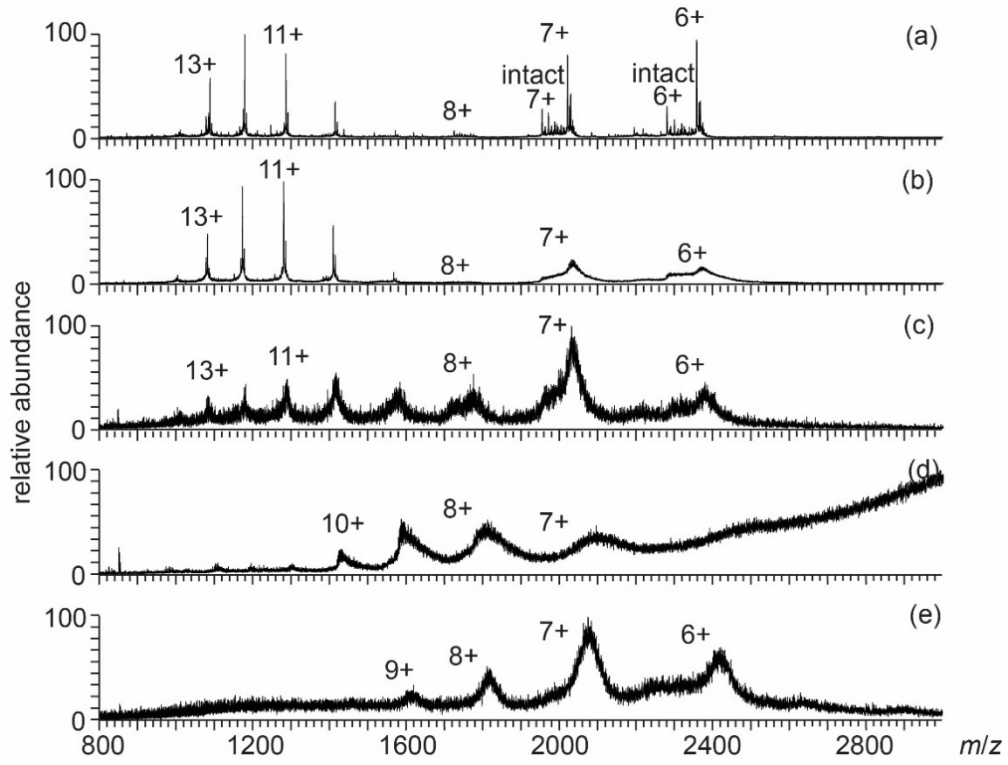


**Figure 6.2.** Electrospray ionization mass spectra of reduced RNase A in (a) 175 mM AA, (b) 165 mM AA and 10 mM NaCl, (c) 125 mM AA and 50 mM NaCl, (d) 25 mM AA and 150 mM NaCl, and (e) 25 mM Tris and 150 mM NaCl at pH 6.8. A small abundance of intact RNase A appears at lower charge state (6+ and 7+).

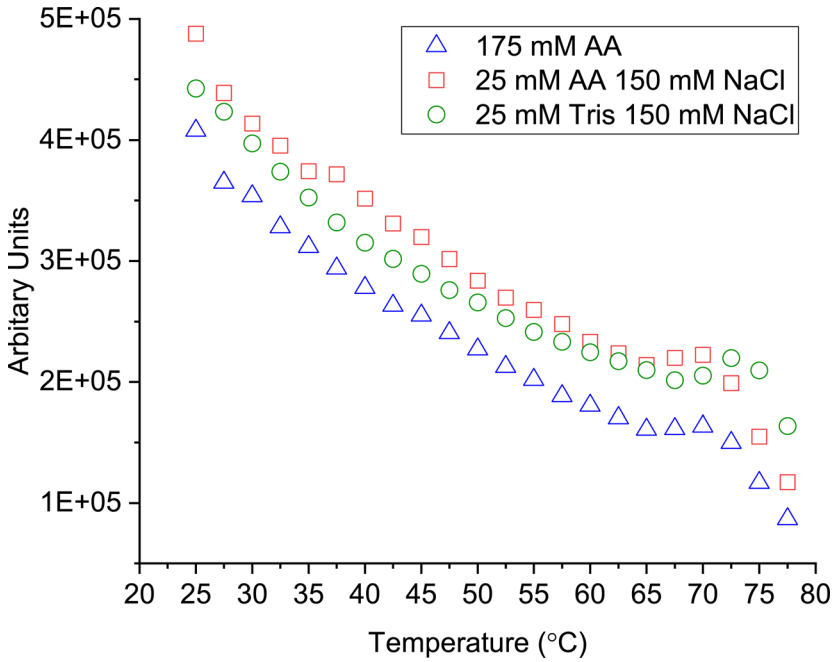


**Figure 6.3.** Tyrosine emission intensity at 302 nm as a function of temperature for RA-RNase A in 175 mM AA (black square), in 25 mM AA 150 mM NaCl (red circle), and in 25 mM Tris 150 mM NaCl (green triangle) solutions. The sample is excited at 280 nm.

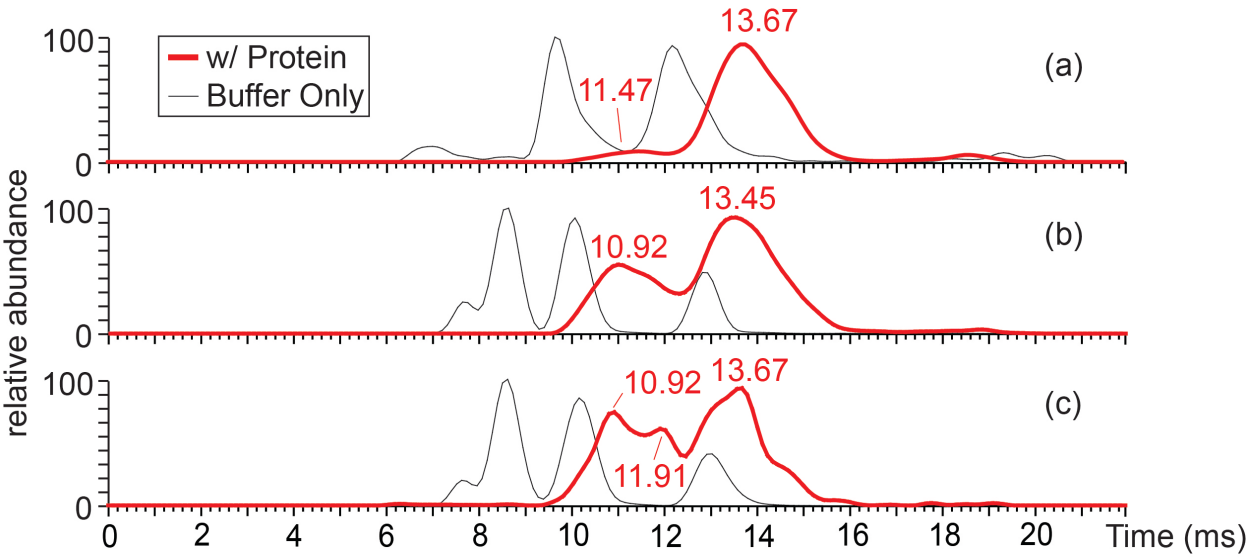


**Figure 6.4**. Ion mobility arrival time data for RA-RNase A 7+ (*m*/*z* 2020.5 – 2028.5) in (a) 175 mM AA, (b) in 165 mM AA 10 mM NaCl, and (c) in 125 mM Tris 50 mM NaCl solutions. Data for the 7+ ion of RA-RNase A (red) are overlaid with data from corresponding solutions without the protein (black) showing the arrival time data for unresolved salt clusters.

## 6.9 Supplemental Information

**Supplemental Table 6.1.** Tyrosine emission intensity (in arbitrary units) at 302 nm for AAAYGGFL and RA-RNase A at 25 °C in 175 mM AA, 25 mM AA with 150 mM NaCl, and 25 mM Tris with 150 mM NaCl.

| | AAAYGGFL | | RA-RNase A | |
|---|---|---|---|---|
| Solution | **Average** | **Standard Deviation** | **Average** | **Standard Deviation** |
| 175 mM AA | **1589.82** | **110.04** | **6079.50** | **454.39** |
| 25 mM AA<br>150 mM NaCl | **1635.00** | **247.28** | **6892.07** | **488.72** |
| 25 mM Tris<br>150 mM NaCl | **1790.65** | **82.76** | **6919.80** | **229.32** |

**Collisional Cross Section Measurements**

The lowest charge state for each protein or protein complex with a previously reported collisional cross section is used in the calibration curve. The corrected drift times ($t_D''$) are plotted as a function of cross section measured with helium gas in a static or radio-frequency confining drift tube (Figure S-1).[1,2] A previous study showed that similar instrument conditions to ones used in this study minimize ion heating but ion heating still occurs.[3] This can shift the transition between folded and unfolded conformations to lower charge state. This effect can be minimized or eliminated by selecting low charge states and larger proteins or protein complexes that are less affected by ion heating.

The average and highest deviation of these calibrant data from the linear-fitted line is 1.7% and 3.8%, respectively. The collisional cross sections reported in this paper is the average of three measurements from three different submicron electrospray ionization emitters. The precision of three measurements for the same sample ranges from 0.2% to 1%, which is reported as an uncertainty of the measurements in the paper.

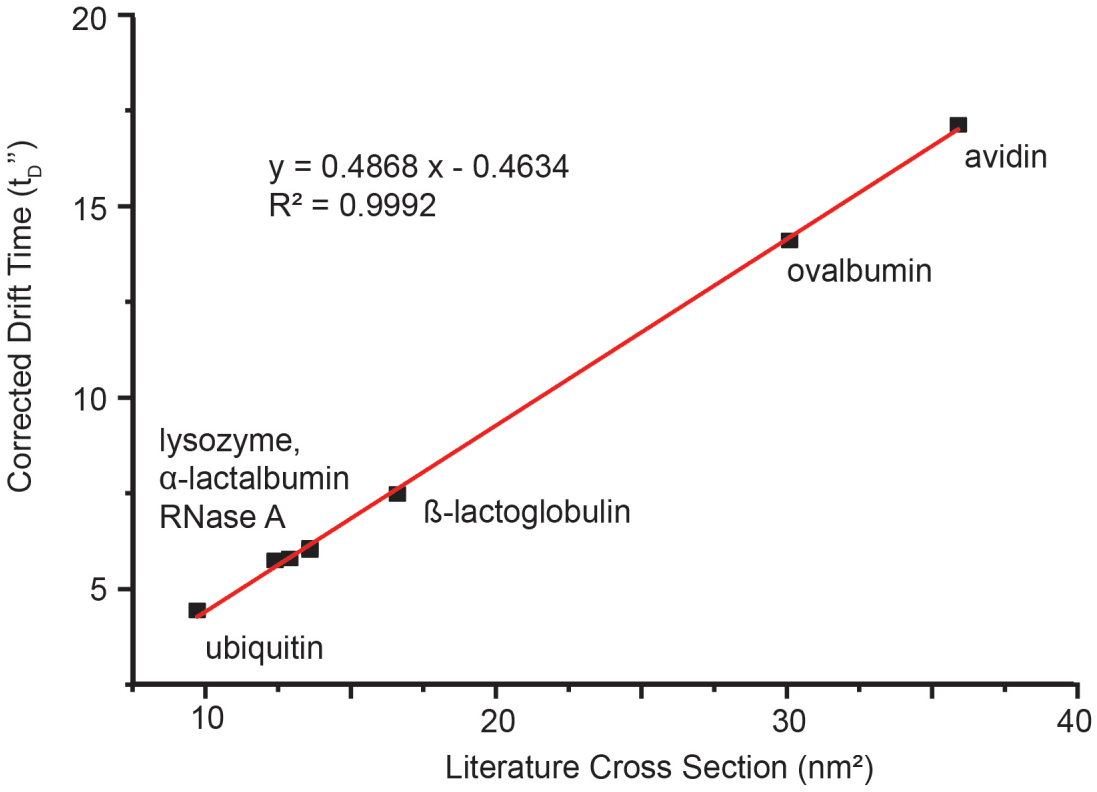


**Supplemental Figure 6.1.** Calibration curve for converting drift time measured on SYNAPT G2Si to collision cross section.

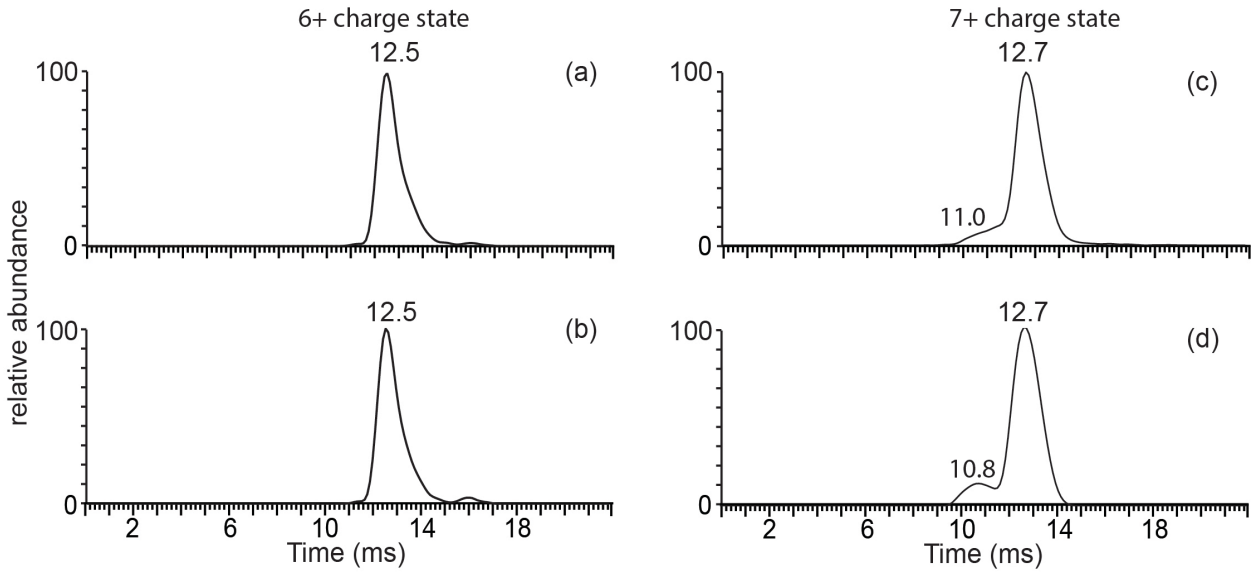


**Supplemental Figure 6.2.** TWIMS arrival time data for intact RNase A 6+ charge state in (a) conditions identified in Figure 1a. (175 mM AA) and (b) in 200 mM AA, and 7+ charge state in (c) conditions identified in Figure 1a. (175 mM AA) and (d) in 200 mM AA.

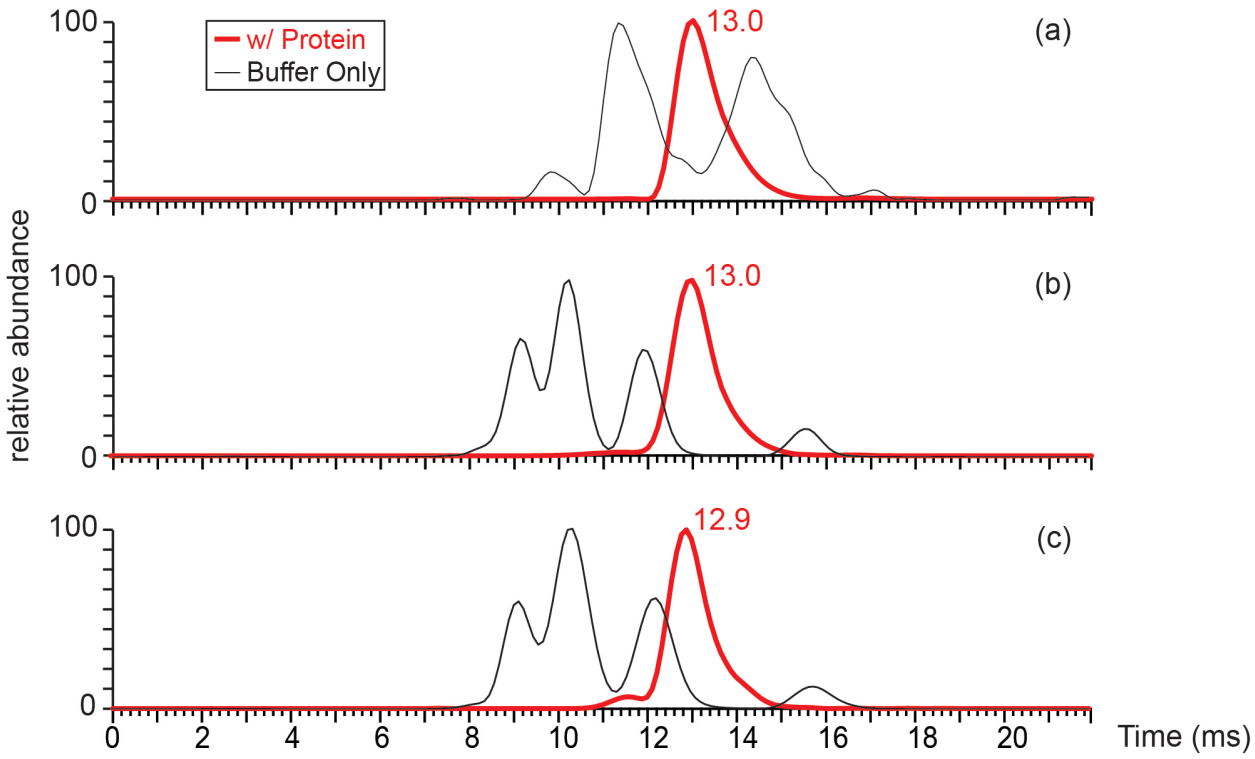


**Supplemental Figure 6.3.** TWIMS arrival time data for reduced RNase A 6+ charge state (*m/z* 2357 – 2366.5) in (a) 175 mM AA, (b) in 165 mM AA 10 mM NaCl, and (c) in 125 mM Tris 50 mM NaCl solutions. Data for the 6+ ion of RA-RNase A (red) are overlaid with data from corresponding solutions without the protein (black) showing the arrival time data for unresolved salt clusters.

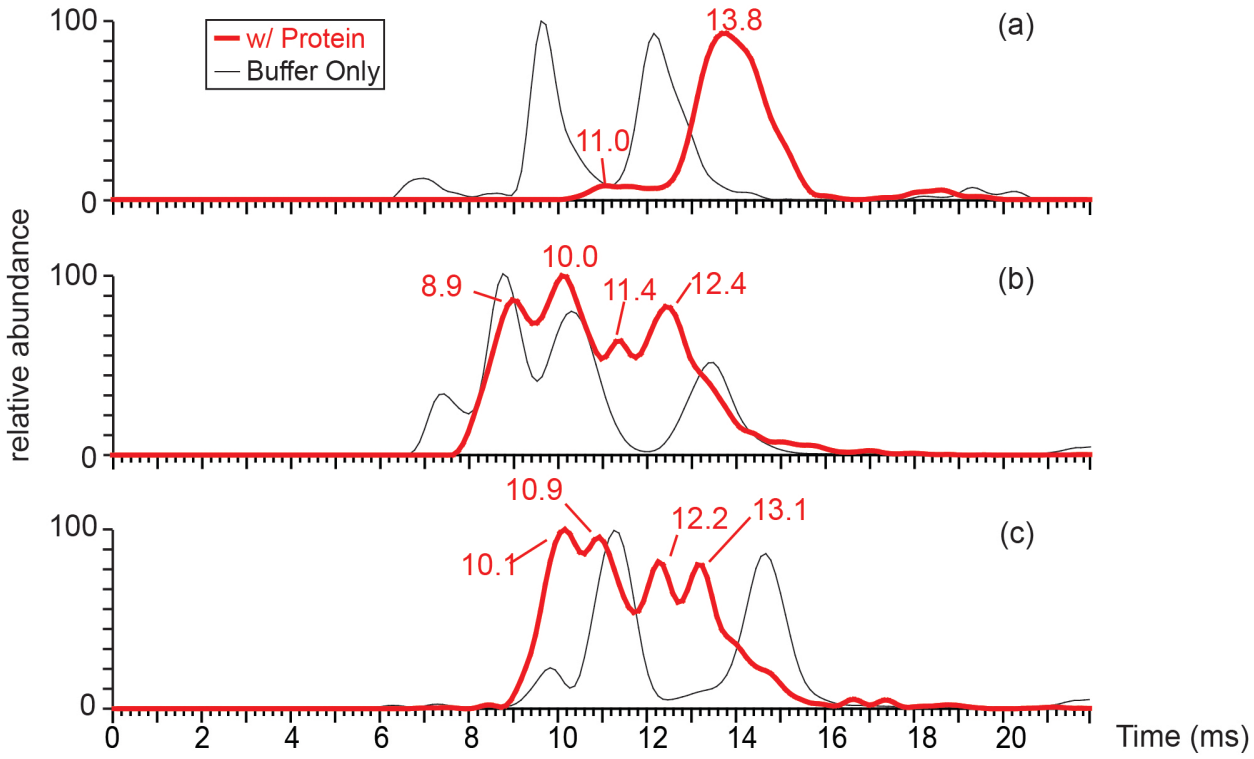


**Supplemental Figure 6.4.** Ion mobility spectra of reduced RNase A 7+ charge state (*m*/*z* 2020.5 – 2028.5) in (a) 175 mM AA, (b) in 25 mM AA 150 mM NaCl, and (c) in 25 mM Tris 150 mM NaCl solutions. Data for the 7+ ion of RA-RNase A (red) are overlaid with data from corresponding solutions without the protein (black) showing the arrival time data for unresolved salt clusters.

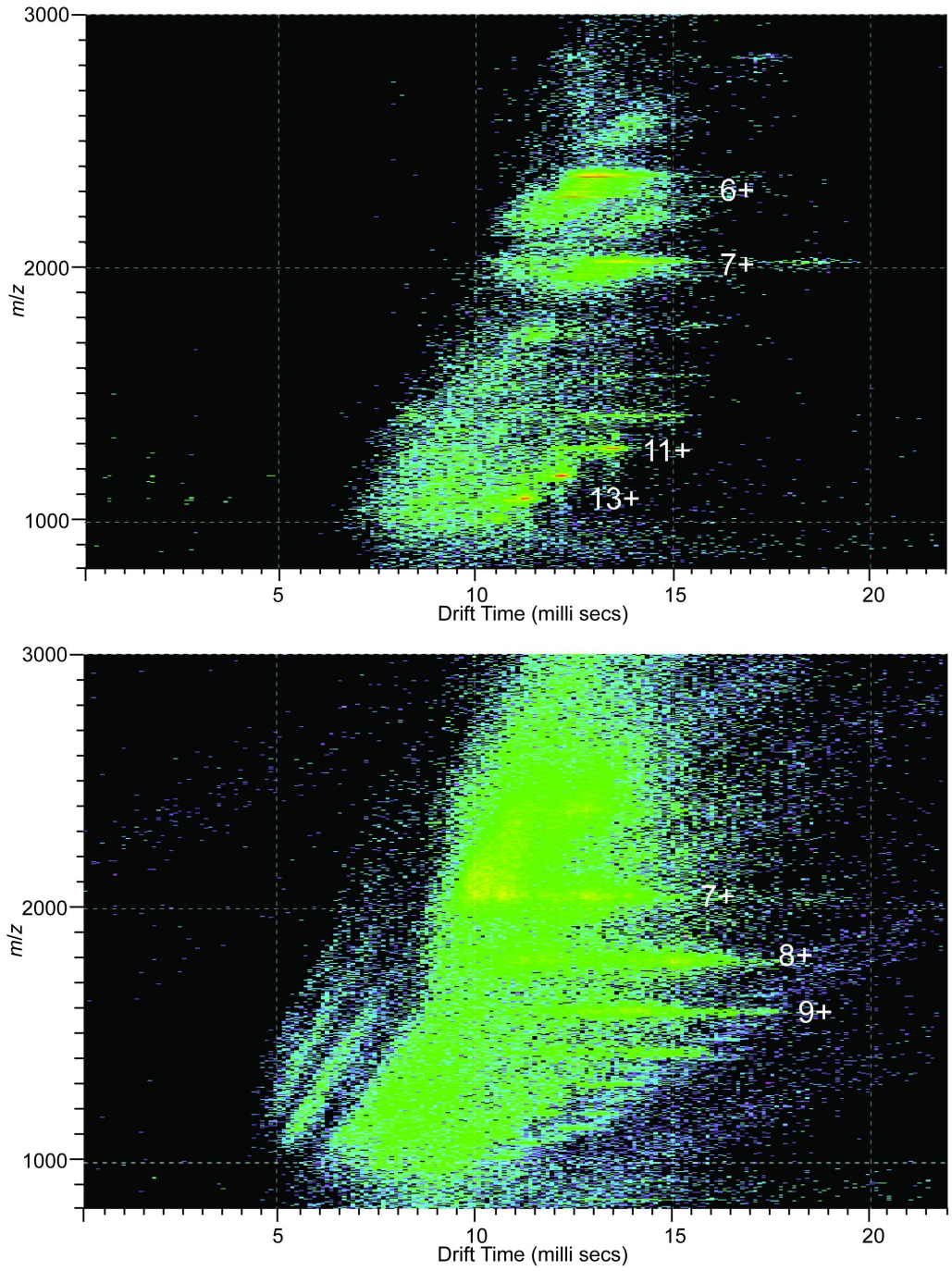


**Supplemental Figure 6.5.** Mobiligrams of reduced RNase A in 175 mM AA (top) and in 25 mM Tris 150 mM NaCl (bottom). Isolated spots for protein are observed in the top mobiligram. Protein signals and salt signals are overlapped in the bottom mobiligram, which complicates the interpretation of the data.

## 6.10 Supplemental Information References


(1) Allen, S. J.; Giles, K.; Gilbert, T.; Bush, M. F. Ion Mobility Mass Spectrometry of Peptide, Protein, and Protein Complex Ions Using a Radio-Frequency Confining Drift Cell. *Analyst* **2016**, *141* (3), 884–891.

(2) Bush, M. F.; Hall, Z.; Giles, K.; Hoyes, J.; Robinson, C. V.; Ruotolo, B. T. Collision Cross Sections of Proteins and Their Complexes: A Calibration Framework and Database for Gas-Phase Structural Biology. *Anal. Chem.* **2010**, *82* (22), 9557–9565.

(3) Merenbloom, S. I.; Flick, T. G.; Williams, E. R. How Hot Are Your Ions in TWAVE Ion Mobility Spectrometry? *J. Am. Soc. Mass Spectrom.* **2012**, *23* (3), 553–562.

# Chapter 7

# Is Native Mass Spectrometry Really Native? Effects of Nonvolatile Salts on Protein Stoichiometry, Structure and Stability

## 7.1 Abstract

Effects of ammonium acetate, commonly used in native mass spectrometry, on the dimer-tetramer equilibrium and structures of concanavalin A were investgated and compared with the effects of nonvolatile salts/buffers that are commonly used with more conventional biochemical structural methods. Submicron electrospray emitters were used to form ions from ammonium acetate solutions containing up to 150 mM NaCl or KCl and from both Tris and 1xPBS buffers. Replacement of ammonium acetate with equal concentrations of NaCl or KCl leads to a shift in the equilibrium between the dimeric and tetrameric forms to favor the dimeric and even the monomeric forms of this protein. A reduction in the charge states of both oligomers is also observed, consistent with a change in structures of these complexes in solutions with higher concentrations of nonvolatile salts. The resulting mass spectra with 150 mM NaCl or KCl are similar to those from Tris and 1xPBS buffers with the same ionic strength and pH. Ion mobility results indicate that the conformations of the dimer are substantially different in ammonium acetate compared to those in solutions containing 150 mM nonvolatile salts. Results for an intrinsically disordered protein, C-terminal sidearm of rat neurofilament heavy subunit, show that this protein aggregates in ammonium acetate at low pH but is stable in Tris buffers at the same pH. These results show the advantages of using submicron emitters to form ions for native mass spectrometry analysis from solutions where the protein and protein complex structures are directly related to the forms of proteins investigated using many other structural methods in which conventional biochemical buffers are employed

## 7.2 Introduction

Osmolytes play an important role in many biochemical processes ranging from maintaining cell shape to regulating cell signaling pathways and functions.[1,2] Osmolytes affect protein solubility, structure, and folding, and influence interactions important for complexation between macromolecules.[3–6] In some cases, specific salt ions are essential to regulate protein function, activity, interaction with ligands and cofactors, and oligomerization.[7–9] The importance of salts to protein solubility and stability was first reported over 130 years ago by Franz Hofmeister, who ordered ions based on their ability to "salt in" or "salt out" proteins.[4] This ordering of ions by their propensity to affect protein solubility and stability is referred to as the Hofmeister series. The origin of Hofmeister series is still hotly debated, but two primary mechanisms along with

experimental support have been reported: direct protein-salt interactions[10–12] and salt ion effects on the hydrogen-bonding network of water molecules which affect the solution environment of the protein.[13–15]

Native mass spectrometry is now widely used to provide information about protein conformations and the stoichiometries of macromolecular complexes in solution.[16] Volatile buffers, including ammonium bicarbonate (ABC) and more typically ammonium acetate (AA), are used in order to provide a solution environment with sufficient ionic strength and to avoid adverse effects associated with the use of nonvolatile salts, such as NaCl or KCl. Nonvolatile salts can adduct onto protein ions, thereby reducing mass measuring accuracy and sensitivity.[17,18] Nonvolatile salts can lead to a complete loss of mass information when present at concentrations above a few 10s of mM.[19,20] Tris or phosphate buffered saline (PBS) solutions typically contain ~150 mM of NaCl or KCl and are often used to mimic intracellular or extracellular environments. Diafiltration,[21] chromatography,[22] and dialysis[23] are typically used to replace nonvolatile salts with AA or ABC in solution. Until very recently, native MS from solutions containing such high concentrations of nonvolatile salts resulted in mass spectra with no interpretable protein signal.[19,20,24]

Electrophoretic desalting during electrospray ionization can desalt analyte ions from traditional biochemical buffers, but this method leads to acidification of the solution and concomitant denaturing of proteins.[25] Submicron electrospray ionization emitters can produce protein and protein complex ions directly from traditional biochemical buffers with resolved low charge states that suggest that these ions have folded, compact forms.[19,20,26] Largely desalted biological ions, including ions of water-soluble and membrane proteins, protein complexes, RNA, and DNA, with both positive and negative charges, can be obtained from solutions containing high concentrations of nonvolatile salts using submicron emitters.[19,20,26–28] Nguyen et al. used this method recently to significantly reduce sodium ion adduction enabling the measurement of protein-ligand binding constants from solutions containing a high concentration of nonvolatile salts that would otherwise obscure the binding of the small ligand molecules.[29]

When comparing results from native mass spectrometry using ammonium acetate solutions to results obtained from other structural methods where more conventional biochemical buffers are used, an important question to ask is what effects do these different ions have on protein structure and stoichiometries of macromolecular complexes? Ammonium is near both sodium and potassium in the Hofmeister series, and acetate and bicarbonate are near chloride, so non-specific ion effects are expected to be relatively minor. However, there can be significant differences in protein stability in AA versus ABC, which leads to more effective electrothermal supercharging with the latter.[30,31] With electrothermal supercharging, higher electrospray voltages leads to droplet heating outside of the mass spectrometer and concomitant thermal denaturation of proteins inside of the electrospray droplets. Even more compelling evidence that protein structures in ammonium acetate can differ from solutions containing high concentrations of NaCl and Tris buffers was reported recently for a small protein, reduced and alkylated ribonuclease A.[32] This protein can adopt both an unfolded and a folded form under many solution conditions. The folded form was stabilized with increasing substitution of NaCl for AA,and the structure of the folded form of this protein differed with these two salts. These results indicate that the buffer choice can be important when interpreting native mass spectrometry data.[32] In this study, submicron emitters are used to investigate the effect of different aqueous solutions containing AA, NaCl, KCl, Tris or phosphate on the stoichiometries and structures of a protein complex, concanavalin A, as well as their effect on the stability of an intrinsically disordered protein (IDP). These results provide compelling

evidence that the choice of buffers can affect the interpretation of native MS results for large proteins and macromolecular complexes.

## 7.3 Experimental Method

### 7.3.1 Mass Spectrometry

Electrospray ionization mass spectra are acquired using a Water SYNAPT G2-Si mass spectrometer (Milford, MA). Borosilicate capillaries (1.0 mm o.d./0.78 mm i.d., Sutter Instruments, Novato, CA) are pulled into electrospray emitters using a Flaming/Brown micropipette puller (Model P-87, Sutter Instruments, Novato, CA). The inner diameter of electrospray emitters measured using an electron scanning microscope (Hitachi TM-1000 SEM, Schaumburg, IL) is 0.66 ± 0.02 μm. A 0.127 mm diameter platinum wire is inserted into the emitters and is in contact with the solution in order to establish electrical contact. The emitter tip is positioned ~5 mm away from the instrument entrance. Electrospray ionization is initiated by applying 0.8 – 1.3 kV to the platinum wire. The populations of concanavalin A monomer, dimer, and tetramer are estimated from the abundances of ions in the corresponding charge-state distributions. The free energy for dissociation of concanavalin A tetramer to two dimers at equilibrium is determined with equation 1 (see Supplemental Information):

$$\Delta \quad = -RTln\, K_{eq} = -RTln\frac{4[T_0]A_D^2}{(4A_T + 2A_D + A_M)A_T} \qquad \text{(Eq. 1)}$$

where $K_{eq}$ is the equilibrium constant, $R$ is the ideal gas constant, $T$ is the temperature (298 K), $A$ is the ion abundance of the corresponding oligomers in a mass spectrum, and $[T_0]$ is the concentration of concanavalin A if the protein is entirely in its tetrameric form. The protein ion abundance was not corrected for possible differences in ionization efficiency or ion transmission/detection efficiency. Therefore, the free energies determined from these data are approximate values.

Traveling wave ion mobility spectrometry (TWIMS) arrival time data are acquired with a wave velocity of 650 m/s and a wave height of 40 V. Helium and ion mobility (nitrogen) gas flow are 180 mL/min and 90 mL/min, respectively. The ion mobility arrival time data for each charge state from different solutions are fitted with a minimal number of Gaussian peaks with fixed centers and width (FWHM = 0.5 ms at full abundance) using OriginPro (Northampton, MA). The peak width was chosen based on the minimum experimental peak width obtained for conconavolin dimer 13+. This width is wider than the 0.3 ms at full abundance width of $(NaCl)_{13}Na^+$ (Supplemental Figure 7.1) for which a cubic structure is favored.[33] This difference may indicate that there may be even more ion structures than modeled here. The number of the Gaussian peaks and the center of the Gaussian peaks are chosen as the minimum necessary to to achieve ≥0.9 $R^2$ fit for ion mobility data of each charge state from different solutions. The free energy for the equilibrium between two structures of concanavalin A in solution is determined with equation 2:

$$\Delta \quad = -RTln\frac{A_1}{A_2} \qquad \text{(Eq. 2)}$$

in which $R$ is the ideal gas constant, $T$ is the temperature (298 K), $A$ is the area under the corresponding Gaussian peak. Bovine serum albumin, avidin tetramer, and yeast alcohol

dehydrogenase in 200 mM ammonium acetate (AA) are used to calibrate the arrival time data to obtain the collisional cross sections using the procedure described by Ruotolo *et al.* (Supplemental Figure 7.2).[34]

Concanavalin A (Jack Bean), bovine serum albumin, avidin, alcohol dehydrogenase, AA, NaCl, KCl, Tris, potassium phosphate, sodium phosphate, acetic acid, and ammonium hydroxide are obtained from Sigma (St Louis, MO). All proteins are directly used without further purification. All solutions containing AA, NaCl, KCl, Tris, and phosphate buffered saline (PBS) are pH adjusted with ammonium hydroxide or acetic acid to pH 6.8 ± 0.3. 1x PBS solution contains 137 mM NaCl, 2.7 mM KCl, 10 mM $Na_2HPO_4$ and 1.8 mM $KH_2PO4$. AA with NaCl solutions and Tris with NaCl solution have a nominal ionic strength of 175 mM; AA with KCl solutions and 1x PBS buffer have a nominal ionic strength of 163 mM except the solutions described above. 10 μM (calculated with the molecular weight of tetramer) concanavalin A samples are prepared by diluting the stock protein solution with pH adjusted solutions.

The intrinsically disordered protein, a recombinant C-terminal sidearm domain of the rat neurofilament heavy subunit (rNFH-SA) containing residues 426–1066, was expressed and purified as described in a previous study.[35] A 40 mM Tris stock solution of the protein is then prepared by buffer exchange. 20 mM AA and 20 mM Tris are adjusted to pH 5, 6.6, and 9. rNFH-SA samples for MS are prepared by diluting the stock solution with pH adjusted AA and Tris solutions.

### 7.3.2 Fluorescence

The fluorescence emission spectra of concanavalin A are obtained in 163 mM AA, 13 mM AA with 150 mM NaCl, 13 mM AA with 150 mM KCl, 13 mM Tris with 150 mM NaCl, and 1x PBS buffer with a multi-mode microplate reader (Synergy H4 hybrid reader, BioTek, Winooski, VT) in 384-well polystyrene solid black low volume flat bottom microplates (Corning, New York, NY). The plate reader is operated at the top reading and emission acquisition mode. The samples are excited at 280 nm, and the emission spectra are scanned from 300 nm to 390 nm at 25 °C ± 0.2°C. Both excitation and emission windows are 9 nm. Each sample is measured five times, averaged, and background subtracted. The fluorescent intensity is normalized for comparisons between solutions.

## 7.4 Results and Discussion

### 7.4.1 Ion Effects on Dimer-Tetramer Equilibrium of Concanavalin A in Solution

Concanavalin A is a lectin extracted from Jack Bean that forms an equilibrium distribution of dimer and tetramer in solution, making it ideal for investigating how the solution environment consisting of different ions affects the structures and the stoichiometries of these complexes. Many factors, such as temperature, ionic strength, pH, and ligands, can affect the dimer-tetramer equilibrium.[7,36,37] For example, concanavalin A is predominantly a dimer at pH < 5.5, but is primarily a tetramer at pH > 7.[36] To determine whether ammonium acetate, a volatile osmolyte commonly used in native mass spectrometry, affects the structures and stoichiometries of these complexes compared to nonvolatile salts, such as NaCl or KCl and traditional biological buffers

(Tris and 1x PBS buffers), solutions containing various concentrations of these ions were prepared so that the final ionic strength (163 or 175 mM) and the pH (6.8) are constant. A native mass spectrum of concanavalin A in 163 mM AA is shown in Figure 7.1a. Both the dimeric (charge states 13+ to 16+) and tetrameric (charge states 19+ to 23+) complexes are produced. Some monomer (charge states 9+ and 10+) is observed as well at low abundance. Based on ion abundances (peak areas), the tetrameric form of the complex is about 48% ± 3% of the ion population. This abundance does not take into account any differences in ionization, detection, or transmission efficiencies for these different ions but is useful for comparisons of the populations of oligomeric forms between different solutions. Replacing 10 mM AA with 10 mM KCl has no apparent effect on the mass spectra where the tetrameric form remains ~48% ± 4% abundance (Figure 7.1b). With 50 mM KCl (and 113 mM AA), the spectra are different both in the relative abundances of the different forms of the complex as well as shifts in the charge-state distribution to lower charge. The population of the tetrameric form is reduced to 37% ± 6% and the monomeric form increases in abundance (Figure 7.1c). The tetrameric form of concanavalin A is only 29% ± 6% of total protein ion abundance from a solution consisting of 13 mM AA and 150 mM KCl (Figure 7.1d) and the protein monomer abundance is increased from ~3% in the solutions containing 50 mM KCl to 11%± 2% in solultions with 150 mM KCl. These results indicate that the higher order complexes are destabilized by the replacement of AA with KCl in solution.

Both Tris and PBS are conventional buffers in biochemistry that are used to study the structures and functions of proteins. The mass spectra obtained from these two buffers show that the relative abundances of the tetramer, dimer, and monomer of concanavalin A are similar from these two solutions. The relative abundance of tetramer to the total protein ion abundance is 31% ± 4% and 28% ± 6% from the Tris buffer and 1x PBS buffer, respectively (Figure 7.1e and 7.1f). This is similar to the tetramer abundance obtained from the 13 mM AA and 150 mM KCL solution (29% ± 6%).

Mass spectra of concanavalin A in 163 mM and 175 mM AA are similar (Figure 7.1a and Supplemental Figure 7.2a) with the tetramer corresponding to 48% ± 3% and 58% ± 1% of total protein ion signal in these respective solutions. The small difference in tetramer abundance is likely due to unintentional variations in experimental conditions because these two sets of data were obtained three months apart. Mass spectra of concanavalin A from 163 mM and 175 mM AA obtained back-to-back on the same day are more consistent with each other (Supplemental Figure 7.3).

Potassium is one of the most essential nutrient elements for plants[38] and concanavalin A is a plant protein.[39] To determine if there are differences between potassium and sodium in solution, mass spectra of concanavalin A were obtained from solutions containing a different concentration of AA and NaCl with a nominal ionic strength of 175 mM and pH 6.8 (Supplemental Figure 7.3). The mass spectra of concanavalin A from the solution containing 10 mM NaCl, 50 mM NaCl, and 150 mM NaCl with AA in solution are the same as those from the solutions containing the same concentrations of KCl (Supplemental Figure 7.3). This result indicates that a potassium-rich or sodium-rich solution environment makes little difference for concanavalin A.

These mass spectral results from ten solutions containing AA, Tris, PBS, NaCl, and KCl indicate that low concentrations (25 mM or 13 mM) of AA, Tris and phosphate do not contribute significantly to the different tetramer-dimer equilibrium of concanavalin A, but high concentrations (>50 mM) of NaCl and KCl have a measurable effect on the stoichiometry equilibrium compared to that with ammonium acetate (Figure 1 and Supplemental Figure 7.3). An approximate value of the free energy for this dimer-tetramer equilibrium from each solution can

be obtained from equation 1 using the abundance of concanavalin A tetramer and dimer ions obtained from the mass spectra (Table 7.1). The estimated free energy for the dissociation of concanavalin A tetramer into dimer in 163 mM AA is -2.4 kcal/mol. Replacing AA with 150 mM nonvolatile salts results in a change of free energy on the tetramer-dimer equilibrium to -2.8 kcal/mol, a ~0.4 kcal/mol change in free energy for reaction. This is slightly lower than the ~0.8 kcal/mol change in free energy resulting from a temperature increase from 15 °C to 25 °C in a phosphate buffer at neutral pH.[36]

### 7.4.2 Effects of Osmolyte Identity on Charge-State Distributions of Concanavalin A

The average charge state of concanavalin A dimer and tetramer depends on salt identity and concentration. In AA only solutions, the charge-state distribution of the dimer is centered around 14+ and 15+, and the charge-state distribution of the tetramer is centered between 21+ and 20+ (Figure 7.1a and Supplemental Figure 7.3a). Replacing 10 mM AA with 10 mM NaCl or KCl does not noticeably change that e charge-state distributions for concanavalin A oligomers (Figure 7.1b and Supplemental Figure 7.3b). However, the charge states of both forms of concanavalin A decrease when 50 mM of AA is replaced by 50 mM KCl (Figure 7.1c). The charges states of both species are also lower for solutions containing 125 mM AA and 50 mM NaCl (Supplemental Figure 7.3c).

A further reduction in charge of both the dimer and tetramer occurs when the nonvolatile salt concentration is increased to 150 mM (Figure 7.1d-f and Supplemental Figure 7.3d). The charge-state distributions of concanavalin A tetramer from these solutions is centered at 19+, which is two charge states lower than that in just AA solutions. The dimer charge-state distributions are centered around 13+. Interestingly, the PBS and Tris buffers do not result in different charge-state distributions comparing to the solutions consisting of AA and 150 mM NaCl or KCl. This result indicates that high concentrations of NaCl or KCl have a dominant effect on the resulting charging by electrospray ionization, whereas Tris, AA, and phosphate, which are present at six to ten times lower concentration than Na or K ions, have limited effect.

A reduction in the charge for concanavalin A dimer and tetramer ions from solutions containing high concentrations of nonvolatile salts may indicate different solution-phase structures resulting from different solution compositions. Previous studies have shown that even small shifts in the charge state can reflect changes in the structures of proteins and protein complexes.[32,40] It is also possible that charge reduction is a result of nonvolatile salts carrying away charges during the droplet evaporation process leading to fewer charges available to the protein ions.

To investigate the origin of the charge shifts further, the charging of polypropylenimine dotriacontaamine dendrimer-32 (DAB-32) as a function of nonvolatile ion concentration was investigated. DAB-32 is a roughly spherical molecule that has limited ability to undergo significant structural changes.[41,42] Mass spectra of DAB-32 obtained from 175 mM AA show similar abundances of the 4+ and 3+ charge states (Supplemental Figure 7.5). Replacement of 150 mM AA with NaCl, results in just the 4+ detectable indicating that there is a small shift to higher charge (detection of the 3+ is partially obscured by abundant salt clusters) (Supplemental Figure 7.6). These results indicate that the shift to lower charge for concanavalin A dimer and tetramer at high levels of NaCl must be due to a conformational change and not a result of nonvolatile salts carrying away charge.

### 7.4.3 Ion Mobility Results of Concanavalin A from Various Solutions

The charge-state distributions in the mass spectra of concanavalin A indicate that the conformations of the dimers and tetramers depend on the identity of the salts in solutions. In order to gain additional insights into how the solution-phase conformations of concanavalin A depend on the types of ions in solution, the conformations of the gaseous ions formed from these solutions were investigated using ion mobility spectrometry. Because the structures of gas-phase ions can depend on charge state, ions that have the same charge state are compared from different solutions.[43] Salt adducts on ions can also alter their structure, typically by compacting and stabilizing the gaseous ions.[43–46] This effect is more apparent for high-valency cations and a large number of cation adducts.[43,45] Therefore, the ion mobility results for the same $m/z$ range is compared from the different solutions to curtail the effect of a different number of cation adducts on the conformations of the gas-phase protein ions.

Ion mobility arrival time data for concanavalin A dimer 13+ from solutions containing different concentrations of AA, KCl, Tris buffer, and 1x PBS buffer are shown in Figure 7.2. A single dominant peak is observed from each of these solutions with a general trend of increasing arrival time with an increasing concentration of nonvolatile salt. With 163 mM ammonium acetate, the main peak is at ~12.6 ms, but there is some signal at slightly shorter arrival times (Figure 7.2a). The peak obtained with 25 mM Tris/150 mM NaCl (centered at ~13 ms) is narrower than that obtained from the other solutions (Figure 7.2e). This suggests that there are almost certainly multiple different unresolved conformers present in the other solutions that contribute to the width of the ion mobility arrival time distributions. These arrival time distributions were fitted with Gaussian peaks with fixed centroids and widths that were selected based on the narrowest peak shape observe in Figure 7.2e. A minimum of four peaks centered at arrival times of 11.36 ms, 12.44 ms, 12.8 ms, and 13.13 ms, are required in order to adequately fit ($R^2 \geq 0.9$) the arrival time data from all of these solutions. The arrival time data is calibrated with the method described by Ruotolo et al.[34] The four ion mobility arrival times correspond to ions with collisional cross sections (CCS) of 32.6 $nm^2$, 34.5 $nm^2$, 35.1 $nm^2$, and 35.7 $nm^2$. The collisional cross sections measured in this study are comparable with previously reported value of ~35 $nm^2$.[47]

The 32.6 $nm^2$ conformer is most abundant for 163 mM AA (~8%) but steadily decreases to ~1% in 13 mM AA and 150 mM KCl (and also in 1x PBS). The 34.5 $nm^2$ conformer is the most abundant form in 163 mM AA (~40%), but it too decreases to zero with increasing KCl and in 1x PBS. The 35.1 $nm^2$ conformer is nearly equally abundant, but its abundance does not depend strongly on salt identity. The largest 35.7 $nm^2$ conformer has a relatively low abundance (~11%) in 163 mM AA, but it increases to 70% abundance in 13 mM AA and 150 mM KCl (similarly with 1x PBS). The trend in the relative abundances of each protein conformation as a function of the concentration of nonvolatile salts is shown in Figure 7.3. The two most compact forms decrease in abundance with increasing substitution of KCl for AA and the largest conformer increases in abundance. A similar trend is observed from solutions containing various concentrations of AA and NaCl (Supplemental Figure 7.7 and Supplemental Figure 7.8). It is interesting that the collisional cross section of concanavalin A dimer increases with increasing concentration of nonvolatile salts whereas the average charge state produced by electrospray ionization decreases. The latter is often interpreted as a result in the compaction of a structure whereas the collisional cross sections indicate a less compact structure. However, the actual shape of the molecule can affect these measured values differently. For example, the octomeric form of the protein transporter anthrax lethal toxin undergoes a prechannel-to-channel transition (a conformational

change) around pH 7.1 that can be monitored by circular dichroism, electron microscopy, a shift in charge-state distribution, and a change in collisional cross section.[40,48] Formation of the channel form of the complex at lower pH results in an *increase* in the charge-state distribution but a concomitant *decrease* in the collisional cross section.[40]

An approximate ΔG value for the energy difference between conformers in these different solutions can be obtained from the corresponding ion abundances in the ion mobility spectrometry (IMS) data. These values for formation of the most abundant compact structures (34.5 $nm^2$) structure from the most abundant least compact (CCS 35.7 $nm^2$) structure from the ten solutions (Table 7.2) clearly show increasing stability of the more open structure with increasing nonvolatile salt concentration. This value for expanding structure from the most abundant compact structure steadily increases with increasing NaCl concentration from -1.0 ± 0.2 kcal/mol in 163 mM AA to +2.1 ± 0.6 kcal/mol in 13 mM AA and 150 mM KCl, a value similar to that in 1x PBS (+2.8 ± 0.8 kcal/mol) (Table 7.3). This change in ΔG values is larger than that for the change in dimer-tetramer equilibrium indicating that the salts have a larger effect on the dimer structure than the stoichiometry equilibrium between dimeric and tetrameric forms of concanavalin A.

The ion mobility results for the dimer 14+ show similar trends (Supplemental Figure 7.9 to Supplemental Figure 7.12). These data can be fit by three Gaussian peaks centered at arrival times of 10.3 ms, 11.4 ms, and 11.75 ms corresponding to collisional cross sections of 33.0 $nm^2$, 35.1 $nm^2$, and 35.7 $nm^2$. The abundance of the 33.0 $nm^2$ conformer is low in solutions with little NaCl. The cross sections of the two most abundant conformations (CCS 35.1 $nm^2$ and 35.7 $nm^2$) are the same as those for the 13+, but here the 34.5 $nm^2$ conformer for dimer 13+ is not present for the dimer 14+ charge state in any of the solutions.

In contrast to the results for the dimer, ion mobility results do not provide clear evidence for any effects of ion identity on the gas-phase structures for the tetramer (Supplemental Figure 7.13 to Supplemental Figure 7.18). There are no significant differences in ion mobility arrival times for concanavalin A tetramer 20+ and 21+ from any of the solutions. The ion mobility spectra for these two charge states were fit with two Gaussian peaks). These data indicate that the cross sections for these two conformers are between 55.3 and 56.2 $nm^2$ for the two charge states, consistent with a previously reported value of 55.5 $nm^2$ for these ions formed from 200 mM AA.[49] The shifts in charge states of the tetramer to lower charge from solutions containing high concentration (150 mM) of nonvolatile salts is indicative of different solution-phase tetramer structures, although it appears that any changes in structure are not revealed by these ion mobility measurements alone.

### 7.4.4 Fluorescence of Concanavalin A in Solution

In order to further investigate how nonvolatile ions in solution affect the stability and structure of concanavalin A, results from fluorescent emission spectroscopy were obtained. Thermal destabilization of this protein complex at higher temperatures results in aggregation of concanavalin A in solution, consistent with prior results that show aggregates of concanavalin A form above 45 °C in 100 mM sodium citrate solution (pH = 6).[50] Therefore, a common chemical denaturant, guanidine hydrochloride, was used to destabilize the protein complex in solution and to study energetic differences from different solution compositions. Fluorescent emission spectra in five solutions consisting of (1) 163 mM AA, (2) 13 mM AA and 150 mM NaCl, (3) 13 mM AA and 150 mM KCl, (4) 13 mM Tris and 150 mM NaCl, and (5) 1x PBS containing between 0 to 4 M guanidine chloride were obtained. Concanavalin A monomer has four tryptophan residues and seven tyrosine residues that fluoresce, which leads to a broad emission spectrum due to the mixed

contributions of emission at ~302 nm (tyrosine) and ~336 nm (tryptophan).[51] Emission of concanavalin A has a maximum at 302 nm when there is no guanidine in solution (Supplemental Figure 7.19). With increasing guanidine hydrochloride concentration, the maximum of the fluorescent emission shifts to longer wavelengths (Supplemental Figure 7.19). Figure 4 summarizes fluorescent emission intensity at 302 nm of concanavalin A from five solutions as a function of guanidine concentration. The trends in the fluorescent emission intensity as a function of guanidine chloride concentration from these five solutions are similar. A sigmoidal fit of the data from 0.5 M to 2.6 M guanidine hydrochloride in each solution was done to examine the extent of the difference (Supplemental Table 7.1). The 163 mM AA solution and the 1x PBS buffer have a midpoint that is ~ 0.1 M guanidine lower than that of the other three solutions. Interpreting these data is complicated by the fact that it is not clear whether any changes observed come about from the dissociation of the tetramer or from conformational differences. This is a general problem for many other commonly used biological techniques, such as circular dichroism, which was not used in this study because of the interference from ammonium acetate at high concentration.

### 7.4.5 Stabilities of An Intrinsically Disordered Protein in Different Solutions

Concanavalin A has a well-defined family of structures in solution. The mass spectral and IMS data indicate that different osmolytes can affect the relative stabilities of these structures consistent with what might be expected from Hofmeister effects. To determine whether different osmolytes may also affect the structures and solubilities of proteins that do not have well-defined structure, these effects for a recombinant C-terminal sidearm of rat neurofilament heavy subunit (rNFH-SA), an intrinsically disordered protein (IDP), were investigated. In contrast to folded protein complexes, IDPs do not have well-defined three-dimensional structures in solution.[52,53] The rNFH-SA sequence has a large and nearly equal number of positive (Lys and Arg) and negative-charged (Asp and Glu) amino acid residues and has an extended and disordered conformation in solution.[35,54]

Electrospray of rNFH-SA from 20 mM AA pH = 9 or pH = 6.6 solution (Figure 7.5a and 7.5b, respectively) results in a broad range of charge states between $m/z$ 1000 and ~2600 that is superimposed on a broad band of unresolved signal. Such high charge states are similar to those observed for largely denatured proteins in solution consistent with a structure in which rNFH-SA is largely unfolded. At pH = 5, individual charge states are no longer resolved, but a broad band between at $m/z$ 1200 and 2800 is observed (Figure 7.5c). In comparison, mass spectra with well-resolved charge states are obtained from 20 mM Tris at all three pHs (Figure 7.5d-f). With 20 mM Tris at pH = 5, the higher mass broad band observed around $m/z$ 2300 with 20 mM AA is absent and individual charge states are clearly observed. The origin of the unresolved broad band with AA at pH = 5.5 is likely due to protein aggregation in solution. Because this is a largely disordered protein, aggregates of this protein are also likely to be highly unstructured and still appear at relative low $m/z$. The heterogeneity resulting from protein aggregations would lead to loss of useful mass information as observed here. These results show that the stability of this protein in AA and Tris buffer at the same ionic strength and pH differs. AA is an effective buffer around pH 5 and pH 9 but not at neutral pH. Tris, on the other hand, is a poor buffer at a pH lower than 6. Thus, these results do not appear to be an effect of electrospray ionization on solution pH but rather the structure and aggregation propensity of rNFH-SA is impacted by buffer ion identity.

## 7.5 Conclusion

The use of submicron electrospray emitters in native mass spectrometry makes it possible to measure the masses of proteins and protein complexes from almost any buffer, including common biochemical buffers containing high concentrations of nonvolatile salts. The relative abundances of concanavalin A dimer and tetramer ions formed from solutions at the same pH and ionic strength depend on the concentration of NaCl or KCl indicating that the equilibrium between these two forms of the protein depends on the identity of different ions in solution. The charge-state distributions are also different from these solutions, suggesting that the conformations of the protein complexes themselves also depend on the identity of the ions in solution. Ion mobility spectrometry provides additional support for different solution-phase conformations of the dimeric form of the protein from different solutions.

The free energy difference between the dimer and tetramer form of the complex is about 0.5 kcal/mol between 165 mM ammonium acetate and Tris buffer at the same ionic strength and pH. The dimer-tetramer equilibrium from1xPBS buffers and 165 mM ammonium acetate show a similar energy difference. The effect of ion identity on the energy differences between different dimeric forms of the protein are larger, up to 2 kcal/mol for ammonium acetate vs. Tris at the same ionic strength and pH. The dominant form of the dimer in ammonium acetate with a gas phase collisional cross section of 34.5 $nm^2$ (41%) is reduced to <1% in Tris or 1xPBS buffers and a minor conformer with a collisional cross section of 35.7 $nm^2$ in ammonium acetate becomes the dominant form of the complex in Tris and 1xPBS buffers (70% and 63%, respectively). These results suggest that the dimer-tetramer equilibrium may be affected by these structural differences in the different solutions.

The energetic difference in the stoichiometric equilibrium of concanavalin A in ammonium acetate vs. Tris or 1xPBS buffer is relatively small. This suggests that comparisons of measurements of complex stoichiometry from native mass spectrometry experiments to those of other structural methods that use conventional biochemical buffers may be minimally affected by the use of these different salts. The energetic differences between different dimeric forms of the complex are larger and differences in structure are more significant in ammonium acetate vs. Tris or 1xPBS. This observation is consistent with recent results for reduced ribonuclease A, which also has different structures in ammonium acetate vs. Tris.[32] Results for the IDP rat neurofilament heavy subunit shows that this protein aggregates in ammonium acetate at low pH but is stable and remains soluble in Tris at the same pH. Thus, different ions can affect the stabilities of different forms of the proteins and protein complexes irrespective of whether they have well-ordered, stable structures, such as concanavalin A, or are more disordered as is the case for rNFH-SA. These results indicate that caution should be used in comparing protein structural information using native mass spectrometry and volatile buffers to other structural methods that use typical biochemical buffers unless methods, such as the use of submicron emitters, are used for mass spectrometry to produce ions of proteins and protein complexes from the same biochemical buffers.

## 7.6 Acknowledgments

This material is based upon work supported by the National Science Foundation Division of Chemistry under grant number CHE-1609866. The authors also thank CALSOLV for funding.

## 7.7 References


(1) Wehner, F.; Olsen, H.; Tinel, H.; Kinne-Saffran, E.; Kinne, R. K. Cell Volume Regulation: Osmolytes, Osmolyte Transport, and Signal Transduction. *Rev Physiol Biochem Pharmacol.* **2003**, *148*, 1–80.

(2) Burg, M. B.; Ferraris, J. D. Intracellular Organic Osmolytes: Function and Regulation. *J. Biol. Chem.* **2008**, *283* (12), 7309–7313.

(3) Auton, M.; Rösgen, J.; Sinev, M.; Holthauzen, L. M. F.; Bolen, D. W. Osmolyte Effects on Protein Stability and Solubility: A Balancing Act between Backbone and Side-Chains. *Biophys. Chem.* **2011**, *159* (1), 90–99.

(4) Hofmeister, F. Zur Lehre von Der Wirkung Der Salze - Zweite Mittheilung. *Arch. Exp. Pathol. und Pharmakologie* **1888**, *24* (4–5), 247–260.

(5) Kumar, R. Role of Naturally Occurring Osmolytes in Protein Folding and Stability. *Arch. Biochem. Biophys.* **2009**, *491* (1–2), 1–6.

(6) Han, L.; Ruotolo, B. T. Hofmeister Salts Recover a Misfolded Multiprotein Complex for Subsequent Structural Measurements in the Gas Phase. *Angew. Chemie Int. Ed.* **2013**, *52* (32), 8329–8332.

(7) Brewer, C. F.; Brown, R. D.; Koenig, S. H. Stoichiometry of Manganese and Calcium Ion Binding to Concanavalin A. *Biochemistry* **1983**, *22* (15), 3691–3702.

(8) Batchelor, J. D.; Sterling, H. J.; Hong, E.; Williams, E. R.; Wemmer, D. E. Receiver Domains Control the Active-State Stoichiometry of Aquifex Aeolicus Σ54 Activator NtrC4, as Revealed by Electrospray Ionization Mass Spectrometry. *J. Mol. Biol.* **2009**, *393* (3), 634–643.

(9) Loh, S. N. The Missing Zinc: P53 Misfolding and Cancer. *Metallomics* **2010**, *2* (7), 442–449.

(10) Tadeo, X.; López-Méndez, B.; Castaño, D.; Trigueros, T.; Millet, O. Protein Stabilization and the Hofmeister Effect: The Role of Hydrophobic Solvation. *Biophys. J.* **2009**, *97* (9), 2595–2603.

(11) Monera, O. D.; Kay, C. M.; Hodges, R. S. Protein Denaturation with Guanidine Hydrochloride or Urea Provides a Different Estimate of Stability Depending on the Contributions of Electrostatic Interactions. *Protein Sci.* **1994**, *3* (11), 1984–1991.

(12) Heiles, S.; Cooper, R. J.; DiTucci, M. J.; Williams, E. R. Hydration of Guanidinium Depends on Its Local Environment. *Chem. Sci.* **2015**, *6* (6), 3420–3429.

(13) Hribar, B.; Southall, N. T.; Vlachy, V.; Dill, K. A. How Ions Affect the Structure of Water. *J. Am. Chem. Soc.* **2002**, *124* (41), 12302–12311.

(14) Chen, X.; Yang, T.; Kataoka, S.; Cremer, P. S. Specific Ion Effects on Interfacial Water Structure near Macromolecules. *J. Am. Chem. Soc.* **2007**, *129* (40), 12272–12279.

(15) DiTucci, M. J.; Williams, E. R. Nanometer Patterning of Water by Tetraanionic Ferrocyanide Stabilized in Aqueous Nanodrops. *Chem. Sci.* **2017**, *8* (2), 1391–1399.

(16) Leney, A. C.; Heck, A. J. R. Native Mass Spectrometry: What Is in the Name? *J. Am. Soc. Mass Spectrom.* **2017**, *28* (1), 5–13.

(17) Pan, P.; McLuckey, S. A. The Effect of Small Cations on the Positive Electrospray Responses of Proteins at Low PH. *Anal. Chem.* **2003**, *75* (20), 5468–5474.

(18) Iavarone, A. T.; Udekwu, O. A.; Wiliams, E. R. Buffer Loading for Counteracting Metal Salt-Induced Signal Suppression in Electrospray Ionization. *Anal. Chem.* **2004**, *76* (14), 3944–3950.
(19) Susa, A. C.; Xia, Z.; Williams, E. R. Native Mass Spectrometry from Common Buffers with Salts That Mimic the Extracellular Environment. *Angew. Chemie Int. Ed.* **2017**, 1–5.
(20) Susa, A. C.; Xia, Z.; Williams, E. R. Small Emitter Tips for Native Mass Spectrometry of Proteins and Protein Complexes from Nonvolatile Buffers That Mimic the Intracellular Environment. *Anal. Chem.* **2017**, *89* (5), 3116–3122.
(21) DeMarco, M. L.; Burnham, C. A. D. Diafiltration MALDI-TOF Mass Spectrometry Method for Culture-Independent Detection and Identification of Pathogens Directly from Urine Specimens. *Am. J. Clin. Pathol.* **2014**, *141* (2), 204–212.
(22) Hernández, H.; Robinson, C. V. Determining the Stoichiometry and Interactions of Macromolecular Assemblies from Mass Spectrometry. *Nat. Protoc.* **2007**, *2* (3), 715–726.
(23) Xiang, F.; Lin, Y.; Wen, J.; Matson, D. W.; Smith, R. D. An Integrated Microfabricated Device for Dual Microdialysis and On-Line ESI-Ion Trap Mass Spectrometry for Analysis of Complex Biological Samples. *Anal. Chem.* **1999**, *71* (8), 1485–1490.
(24) Susa, A. C.; Lippens, J. L.; Xia, Z.; Loo, J. A.; Campuzano, I. D. G.; Williams, E. R. Submicrometer Emitter ESI Tips for Native Mass Spectrometry of Membrane Proteins in Ionic and Nonionic Detergents. *J. Am. Soc. Mass Spectrom.* **2018**, *29* (1), 203–206.
(25) Zhang, Z.; Pulliam, C. J.; Flick, T.; Cooks, R. G. Electrophoretic Desalting to Improve Performance in Electrospray Ionization Mass Spectrometry. *Anal. Chem.* **2018**, *90* (6), 3856–3862.
(26) Susa, A. C.; Lippens, J. L.; Xia, Z.; Loo, J. A.; Campuzano, I. D. G.; Williams, E. R. Submicrometer Emitter ESI Tips for Native Mass Spectrometry of Membrane Proteins in Ionic and Nonionic Detergents. *J. Am. Soc. Mass Spectrom.* **2018**, *29* (1), 203–206.
(27) Kenderdine, T.; Xia, Z.; Williams, E. R.; Fabris, D. Submicrometer Nanospray Emitters Provide New Insights into the Mechanism of Cation Adduction to Anionic Oligonucleotides. *Anal. Chem.* **2018**, *90*, 13541–13548.
(28) Xia, Z.; Williams, E. R. Protein-Glass Surface Interactions and Ion Desalting in Electrospray Ionization with Submicron Emitters. *J. Am. Soc. Mass Spectrom.* **2018**, *29* (1), 194–202.
(29) Nguyen, G. T. H.; Tran, T. N.; Podgorski, M. N.; Bell, S. G.; Supuran, C. T.; Donald, W. A. Nanoscale Ion Emitters in Native Mass Spectrometry for Measuring Ligand-Protein Binding Affinities. *ACS Cent. Sci.* **2019**, *5* (2), 308–318.
(30) Sterling, H. J.; Cassou, C. A.; Susa, A. C.; Williams, E. R. Electrothermal Supercharging of Proteins in Native Electrospray Ionization. *Anal. Chem.* **2012**, *84* (8), 3795–3801.
(31) Cassou, C. A.; Williams, E. R. Anions in Electrothermal Supercharging of Proteins with Electrospray Ionization Follow a Reverse Hofmeister Series. *Anal. Chem.* **2014**, *86* (3), 1640–1647.
(32) Xia, Z.; DeGrandchamp, J. B.; Williams, E. R. Native Mass Spectrometry beyond Ammonium Acetate: Effects of Nonvolatile Salts on Protein Stability and Structure. *Analyst* **2019**, *144* (8), 2565–2573.
(33) Häkkinen, H.; Barnett, R. N.; Landman, U. Metallization of the Na 14 Cl 13 Cluster. *Europhys. Lett.* **1994**, *28* (4), 263–269.

(34) Ruotolo, B. T.; Benesch, J. L. P.; Sandercock, A. M.; Hyung, S.-J.; Robinson, C. V. Ion Mobility-Mass Spectrometry Analysis of Large Protein Complexes. *Nat. Protoc.* **2008**, *3* (7), 1139–1152.
(35) Lei, R.; Lee, J. P.; Francis, M. B.; Kumar, S. Structural Regulation of a Neurofilament-Inspired Intrinsically Disordered Protein Brush by Multisite Phosphorylation. *Biochemistry* **2018**, *57* (27), 4019–4028.
(36) Senear, D. F.; Teller, D. C. Thermodynamics of Concanavalin A Dimer-Tetramer Self-Association: Sedimentation Equilibrium Studies. *Biochemistry* **1981**, *20* (11), 3076–3083.
(37) Huet, C.; Lonchampt, M.; Huet, M.; Bernadac, A. Temperature Effects on the Concanavalin A Molecule and on Concanavalin A Binding. *Biochim. Biophys. Acta - Protein Struct.* **1974**, *365* (1), 28–39.
(38) Wang, M.; Zheng, Q.; Shen, Q.; Guo, S. The Critical Role of Potassium in Plant Stress Response. *Int. J. Mol. Sci.* **2013**, *14* (4), 7370–7390.
(39) Bhattacharyya, L.; Brewer, C. F. Isoelectric Focusing Studies of Concanavalin A and the Lentil Lectin. *J. Chromatogr. A* **1990**, *502* (C), 131–142.
(40) Sterling, H. J.; Kintzer, A. F.; Feld, G. K.; Cassou, C. A.; Krantz, B. A.; Williams, E. R. Supercharging Protein Complexes from Aqueous Solution Disrupts Their Native Conformations. *J. Am. Soc. Mass Spectrom.* **2012**, *23* (2), 191–200.
(41) Fernandez de la Mora, J. Electrospray Ionization of Large Multiply Charged Species Proceeds via Dole's Charged Residue Mechanism. *Anal. Chim. Acta* **2000**, *406* (1), 93–104.
(42) Iavarone, A. T.; Williams, E. R. Mechanism of Charging and Supercharging Molecules in Electrospray Ionization. *J. Am. Chem. Soc.* **2003**, *125* (8), 2319–2327.
(43) Flick, T. G.; Merenbloom, S. I.; Williams, E. R. Effects of Metal Ion Adduction on the Gas-Phase Conformations of Protein Ions. *J. Am. Soc. Mass Spectrom.* **2013**, *24* (11), 1654–1662.
(44) Han, L.; Hyung, S. J.; Mayers, J. J. S.; Ruotolo, B. T. Bound Anions Differentially Stabilize Multiprotein Complexes in the Absence of Bulk Solvent. *J. Am. Chem. Soc.* **2011**, *133* (29), 11358–11367.
(45) Han, L.; Hyung, S.-J.; Ruotolo, B. T. Bound Cations Significantly Stabilize the Structure of Multiprotein Complexes in the Gas Phase. *Angew. Chemie Int. Ed.* **2012**, *51* (23), 5692–5695.
(46) Merenbloom, S. I.; Flick, T. G.; Daly, M. P.; Williams, E. R. Effects of Select Anions from the Hofmeister Series on the Gas-Phase Conformations of Protein Ions Measured with Traveling-Wave Ion Mobility Spectrometry/Mass Spectrometry. *J. Am. Soc. Mass Spectrom.* **2011**, *22* (11), 1978–1990.
(47) Ujma, J.; Giles, K.; Morris, M.; Barran, P. E. New High Resolution Ion Mobility Mass Spectrometer Capable of Measurements of Collision Cross Sections from 150 to 520 K. *Anal. Chem.* **2016**, *88* (19), 9469–9478.
(48) Kintzer, A. F.; Sterling, H. J.; Tang, I. I.; Abdul-Gader, A.; Miles, A. J.; Wallace, B. A.; Williams, E. R.; Krantz, B. a. Role of the Protective Antigen Octamer in the Molecular Mechanism of Anthrax Lethal Toxin Stabilization in Plasma. *J. Mol. Biol.* **2010**, *399* (5), 741–758.
(49) Bush, M. F.; Hall, Z.; Giles, K.; Hoyes, J.; Robinson, C. V.; Ruotolo, B. T. Collision Cross Sections of Proteins and Their Complexes: A Calibration Framework and Database for Gas-Phase Structural Biology. *Anal. Chem.* **2010**, *82* (22), 9557–9565.

(50) Kudou, M.; Shiraki, K.; Takagi, M. Characterization of Heat-Induced Aggregates of Concanavalin A Using Fluorescent Probes. *Sci. Technol. Adv. Mater.* **2004**, *5* (3), 339–341.
(51) Reeke, G. N.; Becker, J. W.; Cunningham, B. A.; Wang, J. L.; Yahara, I.; Edelman, G. M. Structure and Function of Concanavalin A. *Adv. Exp. Med. Biol.* **1975**, *55*, 13–33.
(52) Dyson, H. J.; Wright, P. E. Intrinsically Unstructured Proteins and Their Functions. *Nat. Rev. Mol. Cell Biol.* **2005**, *6* (3), 197–208.
(53) Oldfield, C. J.; Dunker, A. K. Intrinsically Disordered Proteins and Intrinsically Disordered Protein Regions. *Annu. Rev. Biochem.* **2014**, *83* (1), 553–584.
(54) Srinivasan, N.; Bhagawati, M.; Ananthanarayanan, B.; Kumar, S. Stimuli-Sensitive Intrinsically Disordered Protein Brushes. *Nat. Commun.* **2014**, *5*, 1–8.

## 7.8 Tables and Figures

**Table 7.1.** The free energy for dissociation of tetramer to dimer at equilibrium calculated based on the abundance of concanavalin A dimer and tetramer in mass spectra from 10 different solutions with the same nominal ionic strengths (163 mM or 175 mM) and pH 6.8

| Solution Composition | $\Delta G$ (kcal/mol) | Solution Composition | $\Delta G$ (kcal/mol) |
|---|---|---|---|
| **163 mM AA** | -2.37 ± 0.10 | **175 mM AA** | -2.68 ± 0.02 |
| **153 mM AA 10 mM KCl** | -2.35 ± 0.14 | **165 mM AA 10 mM NaCl** | -2.61 ± 0.21 |
| **113 mM AA 50 mM KCl** | -2.13 ± 0.14 | **125 mM AA 50 mM NaCl** | -2.58 ± 0.14 |
| **13 mM AA 150 mM KCl** | -1.73 ± 0.21 | **25 mM AA 150 mM NaCl** | -2.09 ± 0.21 |
| **1x PBS** | -1.65 ± 0.21 | **25 mM Tris 150 mM NaCl** | -1.85 ± 0.19 |

**Table 7.2**. The percentage abundance of concanavalin A dimer conformers with CCS 32.6 $nm^2$, 34.5 $nm^2$, 35.1 $nm^2$, and 35.7 $nm^2$ from 5 different solutions with the same nominal ionic strengths (163 mM) and pH 6.8. The abundance of a conformer is determined by the area under the Gaussian peak.

| Solution Condition | 32.6 $nm^2$ conformers | 34.5 $nm^2$ conformers | 35.1 $nm^2$ conformers | 35.7 $nm^2$ conformers |
|---|---|---|---|---|
| **163 mM AA** | 8.2% ± 5.5% | 41% ± 10% | 39% ± 13% | 11% ± 8% |
| **153 mM AA 10 mM KCl** | 5.4% ± 3.2% | 34% ± 26% | 36% ± 15% | 24% ± 13% |
| **113 mM AA 50 mM KCl** | 3.4% ± 1.5% | 18% ± 5% | 48% ± 6% | 30% ± 1% |
| **13 mM AA 150 mM KCl** | 1.0% ± 0.4% | 0 (not observed) | 28% ± 8% | 70% ± 8% |
| **1x PBS** | 1.0% ± 0.3% | 0.8% ± 1.1% | 35% ± 14% | 63% ± 14% |

**Table 7.3.** The free energy for the most abundant least compact structure going to the most abundant compact structure calculated based on the abundance of concanavalin A dimer 13+ charge state conformations with collisional cross section of 34.5 $nm^2$ and 35.7 $nm^2$ in ion mobility spectra from 10 different solutions with the same nominal ionic strengths (163 mM or 175 mM) and pH 6.8

| Solution Composition | $\Delta G$ (kcal/mol) | Solution Composition | $\Delta G$ (kcal/mol) |
|---|---|---|---|
| **163 mM AA** | -0.38 ± 0.55 | **175 mM AA** | -0.95 ± 0.16 |
| **153 mM AA 10 mM KCl** | -0.62 ± 0.63 | **165 mM AA 10 mM NaCl** | -0.50 ± 0.46 |
| **113 mM AA 50 mM KCl** | 0.31 ± 0.18 | **125 mM AA 50 mM NaCl** | -0.13 ± 0.45 |
| **13 mM AA 150 mM KCl** | N/A* | **25 mM AA 150 mM NaCl** | 2.09 ± 0.61 |
| **1x PBS** | 2.59 ± 0.76 | **25 mM Tris 150 mM NaCl** | 2.66 ± 0.81 |

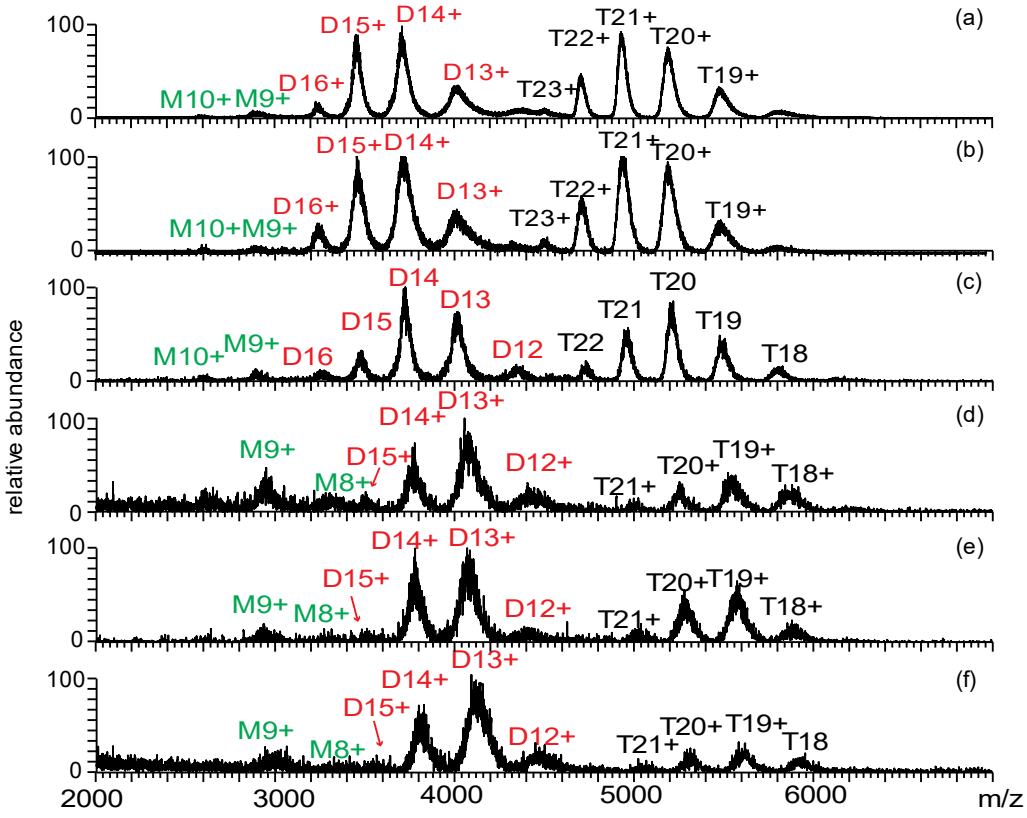


**Figure 7.1.** Electrospray ionization mass spectra of concanavalin A in (a) 163 mM AA, (b) 153 mM AA and 10 mM KCl, (c) 113 mM AA and 50 mM KCl, (d) 13 mM AA and 150 mM KCl, (e) 25 mM Tris and 150 mM NaCl, and (f) 1x PBS at pH 6.8. Concanavalin A tetramer (T), dimer (D), and monomer (M) are observed from all solutions.

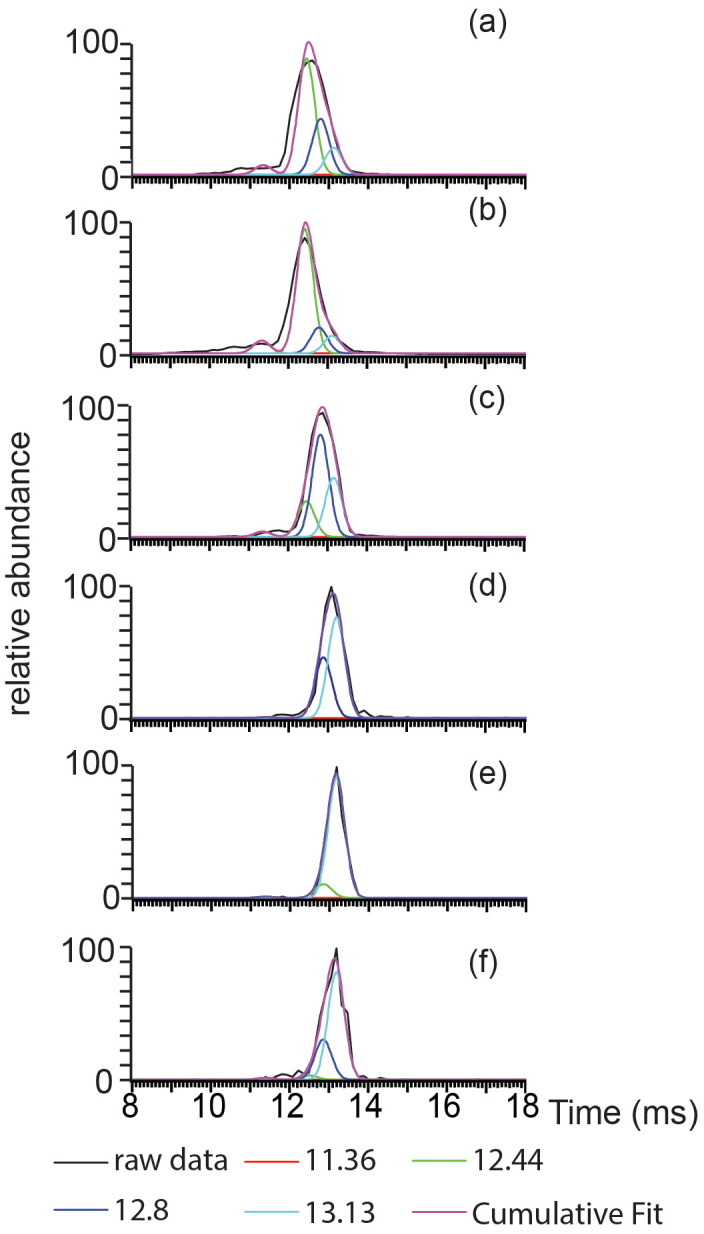


**Figure 7.2.** Ion mobility arrival time data (black) for concanavalin A dimer 13+ charge state (*m*/*z* 4000-4100, approximately 56 sodium adducts) in (a) 163 mM AA, (b) 153 mM AA and 10 mM KCl, (c) 113 mM AA and 50 mM KCl, (d) 13 mM AA and 150 mM KCl, (e) 25 mM Tris and 150 mM NaCl, and (f) 1x PBS all at pH = 6.8. The ion mobility arrival time data are fitted with four Gaussian peaks centered at 11.36 ms (red), 12.44 ms (green), 12.8 ms (dark blue), and 13.13 ms (mint). The purple trace corresponds to the cumulative fit.

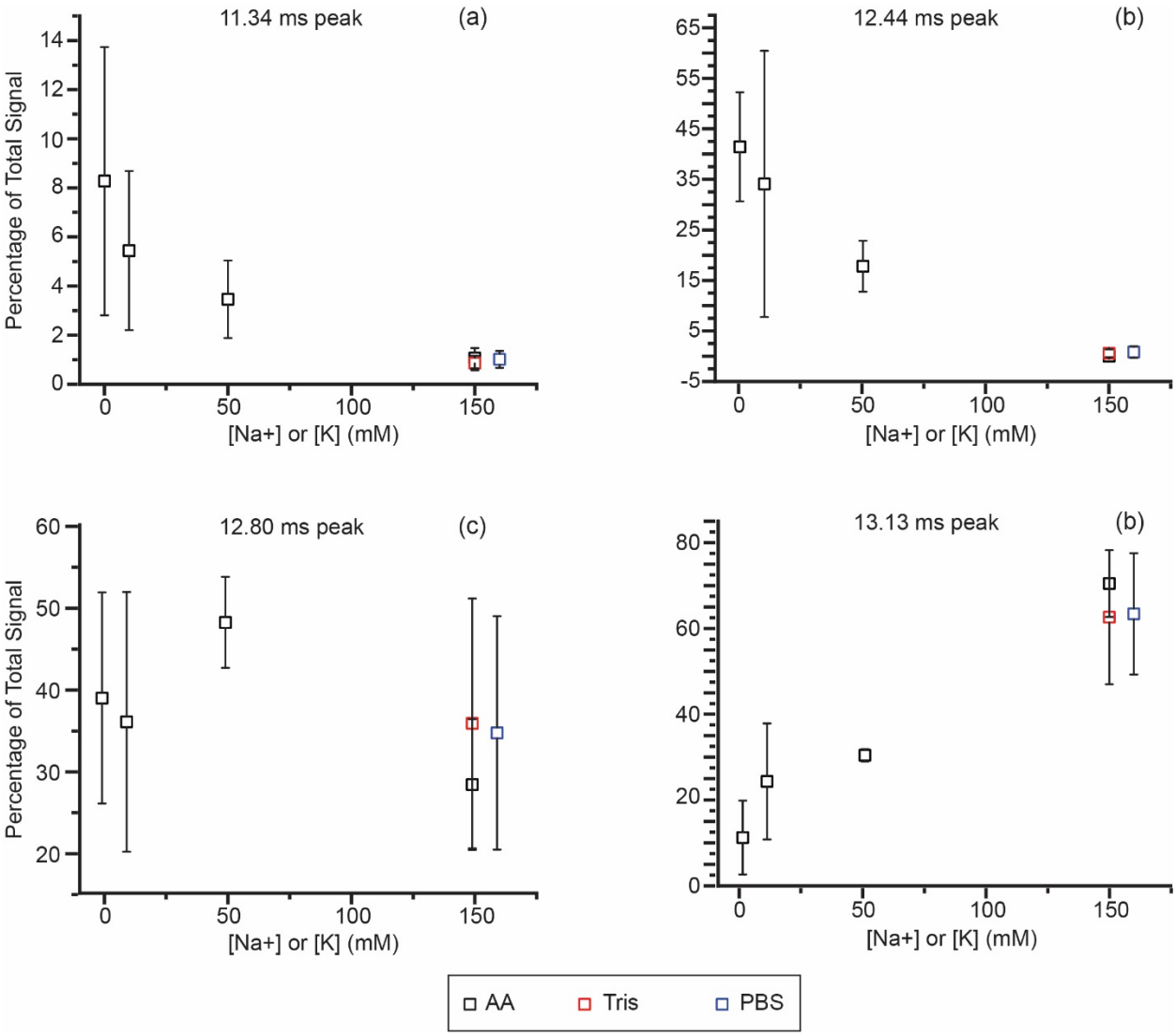


**Figure 7.3.** The relative abundance of the four fitted Gaussian peaks for concanavalin A dimer 13+ charge state (*m*/*z* 4000-4100) in six different solutions as a plot of sodium ion or potassium ion concentration in solution. The solutions containing AA and KCl (black) have the same nominal ionic strength (163 mM). The results from 25 mM Tris with 150 mM NaCl (red) and 1x PBS (blue) are plotted based on sodium ion concentration.

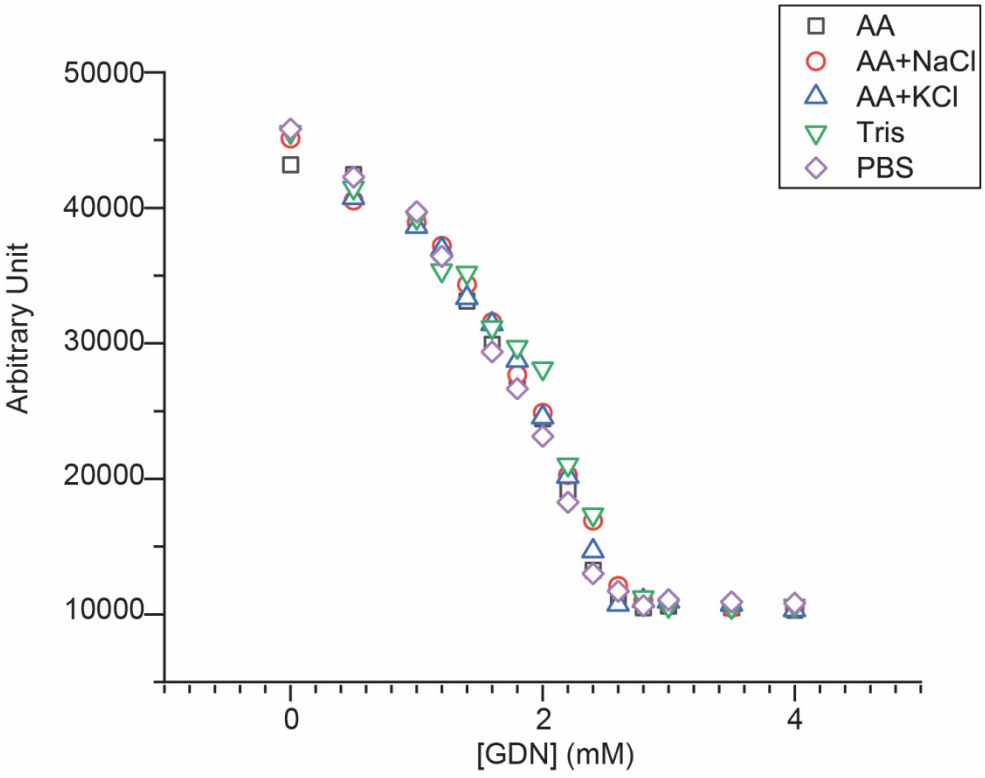


**Figure 7.4.** Fluorescent emission intensity at 302 nm as a function of guanidine concentration for concanavalin A in 163 mM AA (black square), in 13 mM AA 150 mM NaCl (red circle), in 13 mM AA 150 mM KCl (blue triangle), in 13 mM Tris 150 mM NaCl (green inverse triangle), and 1x PBS (purple diamond) solutions. The samples are excited at 280 nm.

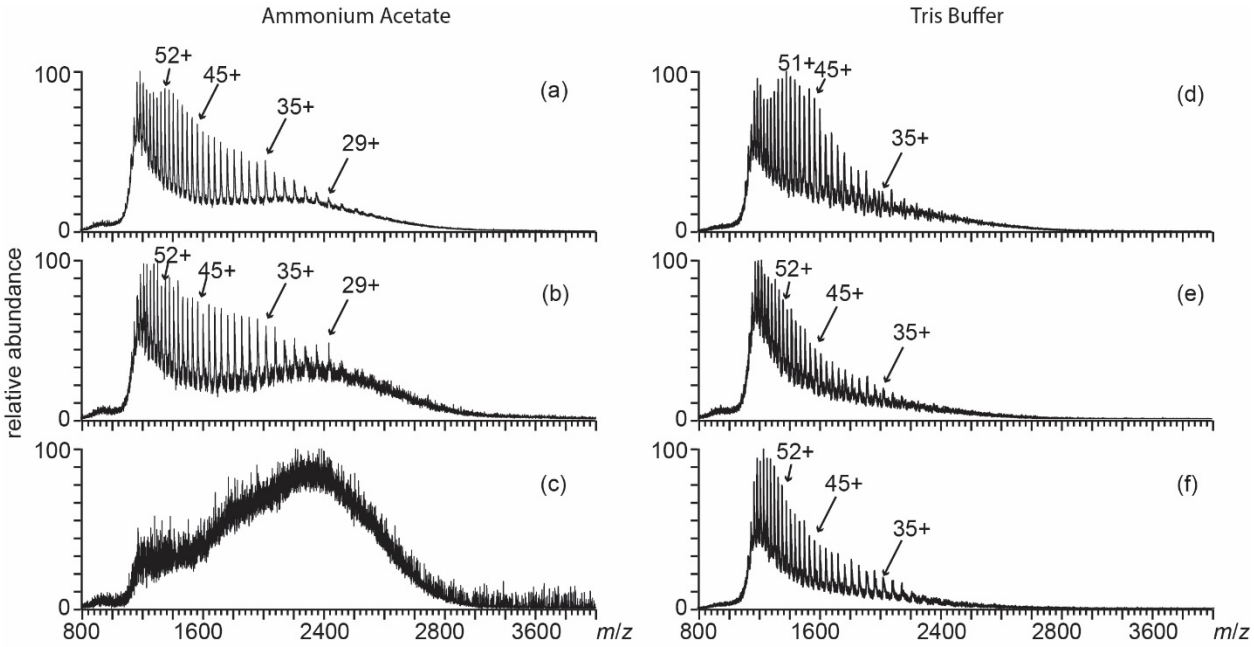


**Figure 7.5.** Electrospray ionization mass spectra of rNFH-SA in (a-c) 20 mM AA and (d-f) 20 mM Tris. Mass spectra are obtained from solutions with three different pHs, (a, d) pH 9, (b, e) pH 6.6, and (c, f) pH 5.

## 7.9 Supplemental Information

### Mathematical Deduction for Equation 1

$$\text{Chemical equation: T} \rightleftarrows \text{2D} \rightleftarrows \text{4M}$$

where T, D, and M correspond to concanavalin A tetramer, dimer, and monomer, respectively.

Gibbs free energy for the equilibrium between tetramer and dimer:

$$\Delta \quad = -RTlnK_{eq} = -RTln\frac{[D]^2}{[T]}$$

in which [D] and [T] are the corresponding to the concentrations of concanavalin A tetramer and dimer in solution in equilibrium. The initial protein concentration assuming that all concanavalin A is in the tetrameric form, $[T_0]$, is given by:

$$[T_0] = [T] + \frac{[D]}{2} + \frac{[M]}{4}$$

where [M] is the concentration of concanavalin A monomer in solution at any given time.

The solution-phase concentration of each component is estimated from the corresponding ion abundances using the following relationships:

$$[\text{T}] = cA_T$$

$$[\text{D}] = cA_D$$

$$[\text{M}] = cA_M$$

where, $A_T$, $A_D$, and $A_M$ are ion abundance of concanavalin A tetramer, dimer and monomer in the mass spectra, respectively, and $c$ is a proportional constant relating ion abundance and protein concentration.

Therefore,

$$[T_0] = c(A_T + \frac{A_D}{2} + \frac{A_M}{4})$$

$$\text{c} = \frac{4[T_0]}{4A_T + 2A_D + A_M}$$

These equations can be combined to establish the following relationship:

$$\Delta \quad = -RTln\frac{c^2A_D^2}{cA_T} = -RTln\frac{4[T_0]A_D^2}{(4A_T + 2A_D + A_M)A_T}$$

**Supplemental Table 7.1.** Summary of the fitting parameters and statistics of the sigmoidal function

$$y = \frac{a}{1 + e^{-k(x-x_c)}}$$

for five different solutions shown in Figure 4. Data from solutions containing 0.5 M to 2.6 M guanidine hydrochlode are used for the fitting.

| | a | a | xc | xc | k | k | Statistics | Statistics |
|---|---|---|---|---|---|---|---|---|
| | Value | Std Dev | Value | Std Dev | Value | Std Dev | Reduced $X^2$ | Adj. $R^2$ |
| **163 mM AA** | 44495.12 | 1496.38 | 2.03 | 0.047 | -1.91 | 0.15 | 1.1E+06 | 0.991 |
| **13 mM AA 150 mM NaCl** | 42503.70 | 663.36 | 2.15 | 0.021 | -1.95 | 0.09 | 2.6E+05 | 0.997 |
| **13 mM AA 150 mM KCl** | 41503.74 | 792.04 | 2.14 | 0.025 | -2.18 | 0.12 | 5.1E+05 | 0.995 |
| **13 mM Tris 150 mM NaCl** | 45061.11 | 2353.67 | 2.17 | 0.083 | -1.52 | 0.19 | 1.4E+06 | 0.983 |
| **1x PBS** | 45341.52 | 1420.16 | 1.98 | 0.045 | -1.84 | 0.14 | 7.7E+05 | 0.994 |

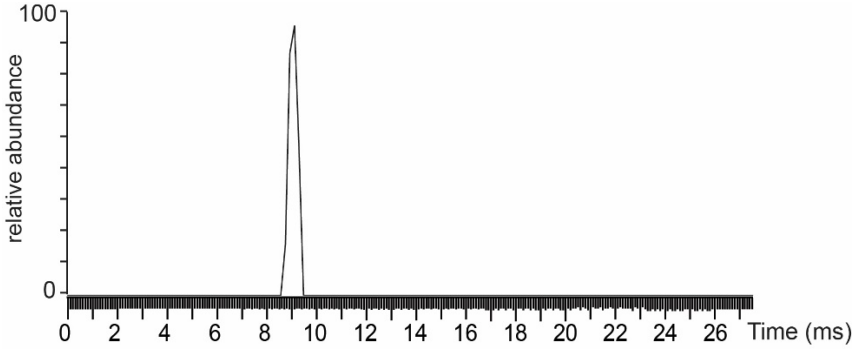


**Supplemental Figure 7.1.** Ion mobility results for $(NaCl)_{13}Na^+$ salt cluster ion. A cubic structure is favored for $(NaCl)_{13}Na^+$, so a singular conformation of the salt cluster is expected in solution.[1] The FWHM for this ion mobility peak is ~0.3 ms, which is narrower than the sharpest peak observed for concanvalin A dimer 13+ (FWHM = 0.5 ms).

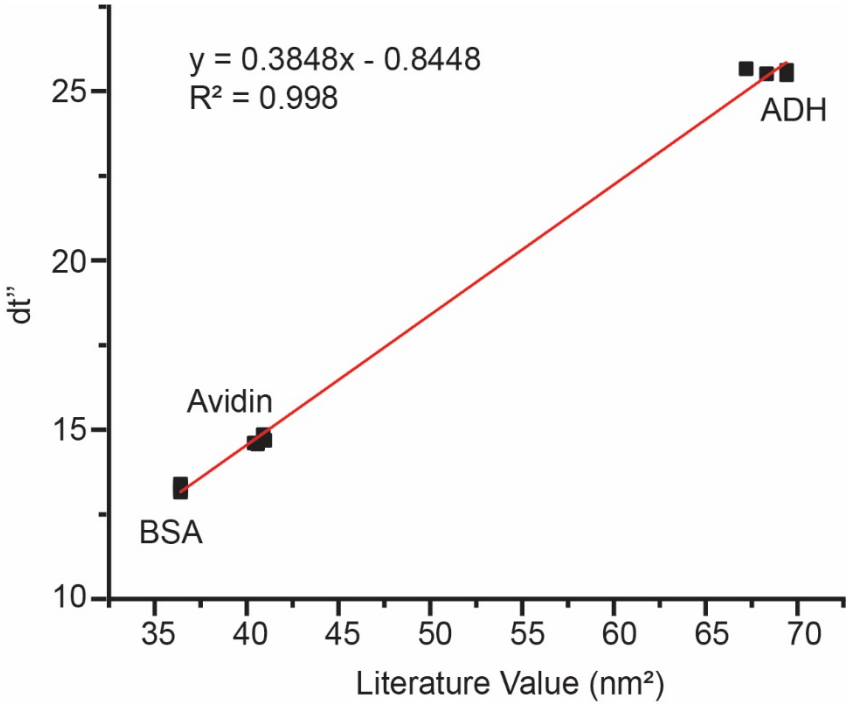


**Supplemental Figure 7.2.** Calibration curve for converting drift time measured on SYNAPT G2Si mass spectrometer to collision cross section.[2]

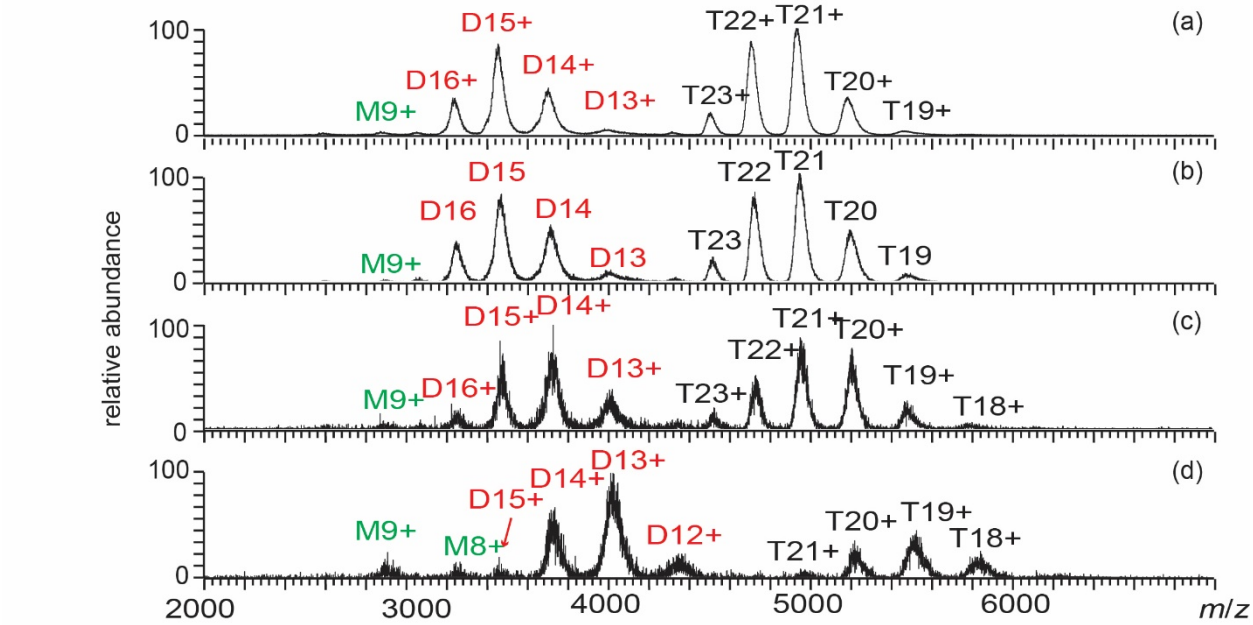


**Supplemental Figure 7.3.** Electrospray ionization mass spectra of concanavalin A in (a) 175 mM AA, (b) 165 mM AA and 10 mM NaCl, (c) 125 mM AA and 50 mM NaCl, (d) 25 mM AA and 150 mM NaCl all at pH = 6.8. Concanavalin A tetramer (T), dimer (D), and monomer (M) are observed from all solutions.

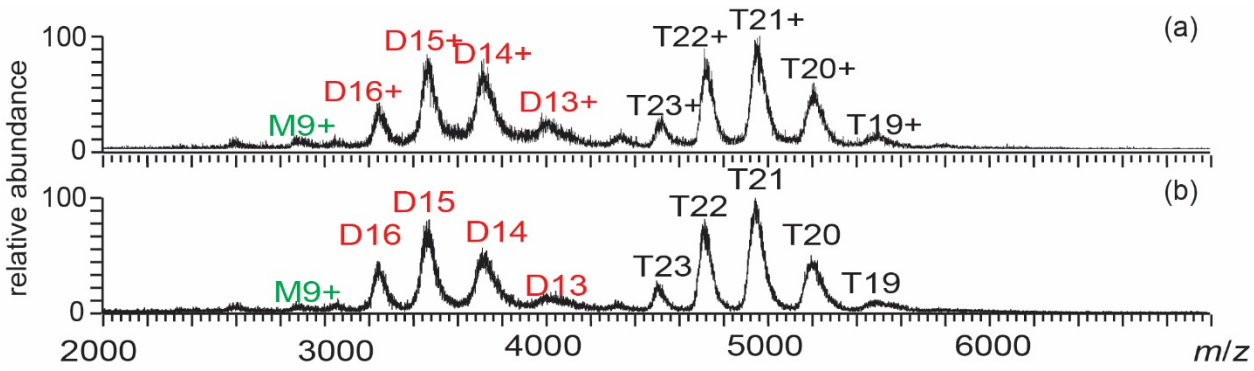


**Supplemental Figure 7.4.** Electrospray ionization mass spectra of concanavalin A in (a) 175 mM AA and (b) 163 mM AA both at pH = 6.8. The two mass spectra were obtained back to back.

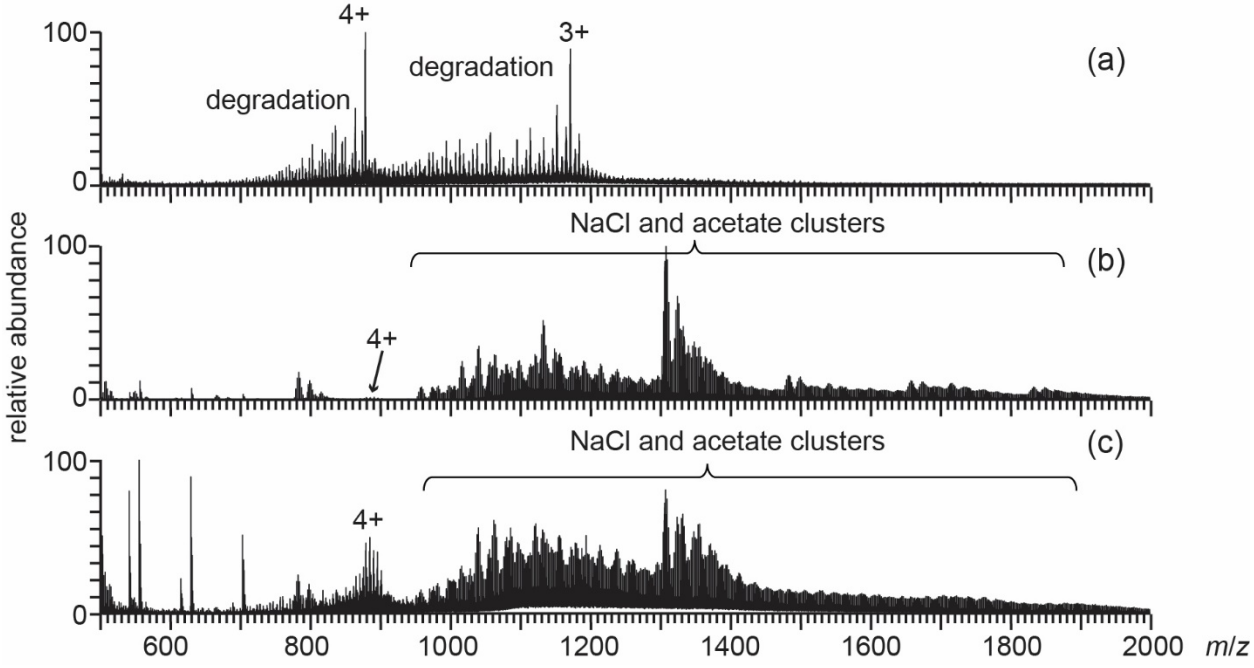


**Supplemental Figure 7.5.** Electrospray ionization mass spectra of (a) 20 μM DAB-32 in 175 mM AA, (b) 20 μM DAB-32 in 25 mM AA and 150 mM NaCl, and (c) 80 μM DAB-32 in 25 mM AA and 150 mM NaCl at pH 6.8 obtained with submicron emitters.

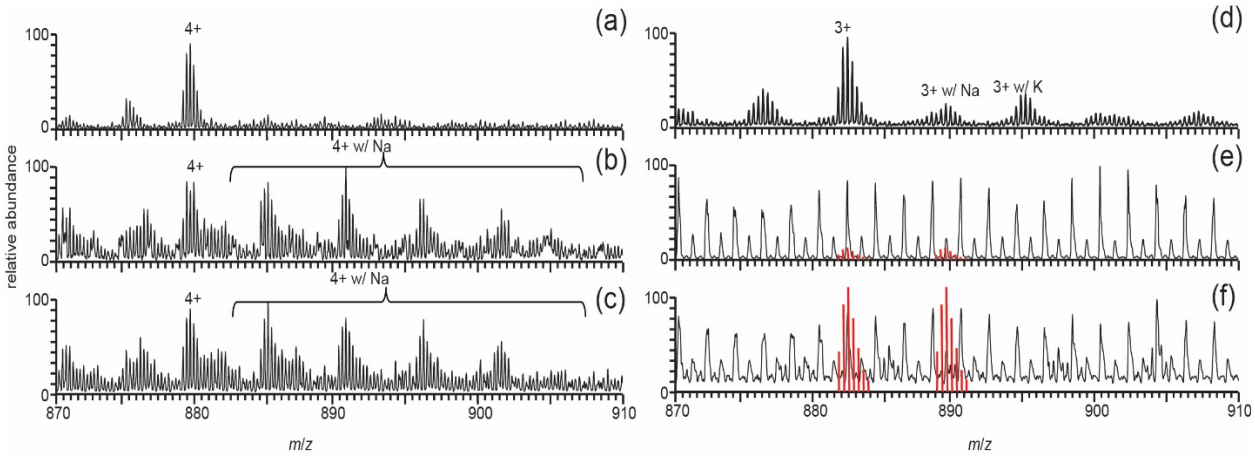


**Supplemental Figure 7.6.** Zoomed in electrospray ionization mass spectra of (a, d) 20 μM DAB-32 in 175 mM AA, (b, e) 20 μM DAB-32 in 25 mM AA and 150 mM NaCl, and (c, f) 80 μM DAB-32 in 25 mM AA and 150 mM NaCl at pH 6.8 obtained with submicron emitters. (a – c) Charge state 4+ and sodium adducted 4+ charge state are observed from all three solutions in contrast to the reduced signal abundance corresponding to charge state 3+ (d – f) from solutions containing 150 mM NaCl. Red lines correspond to expected 3+ ion signal calculated based on the ratio of ion abundance of 4+ and 3+ charge state from 175 mM AA.

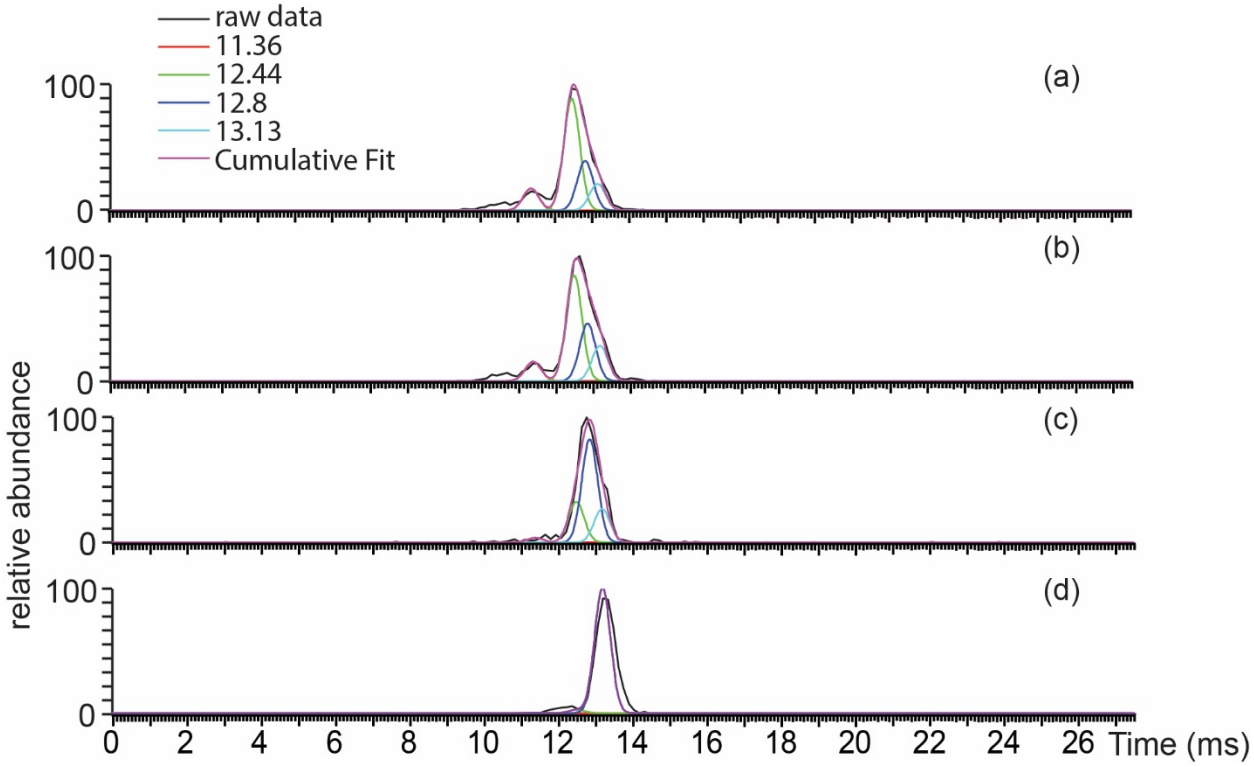


**Supplemental Figure 7.7.** Ion mobility arrival time data (black) for concanavalin A dimer 13+ charge state (*m*/*z* 4000-4100) in (a) 175 mM AA, (b) 165 mM AA and 10 mM NaCl, (c) 125 mM AA and 50 mM NaCl, (d) 25 mM AA and 150 mM NaCl all at pH = 6.8. The ion mobility arrival time data are fitted with four Gaussian peaks centered at 11.36 ms (red), 12.44 ms (green), 12.8 ms (dark blue), and 13.13 ms (mint). The purple trace corresponds to the cumulative fit.

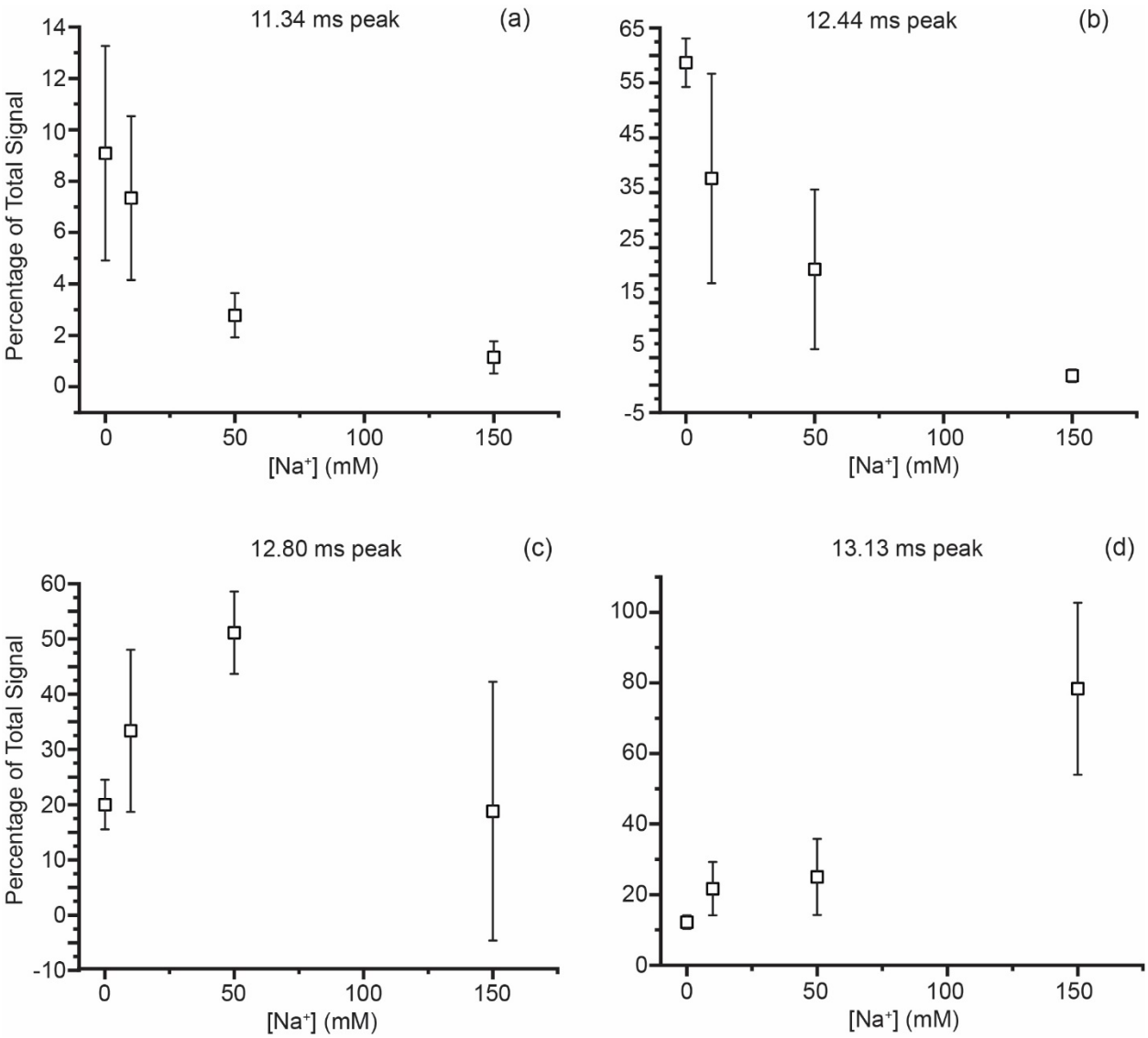


**Supplemental Figure 7.8.** The relative abundance of the four fitted Gaussian peaks centered at the arrival times of (a) 11.34 ms, (b) 12.44 ms, (c) 12.80 ms, and (d) 13.13 ms for concanavalin A dimer 13+ charge state (*m*/*z* 4000-4100) in four different solutions described in Supplemental Figure 7.7 as a function of sodium ion concentration. The solutions containing AA and NaCl have the same nominal ionic strength (175 mM).

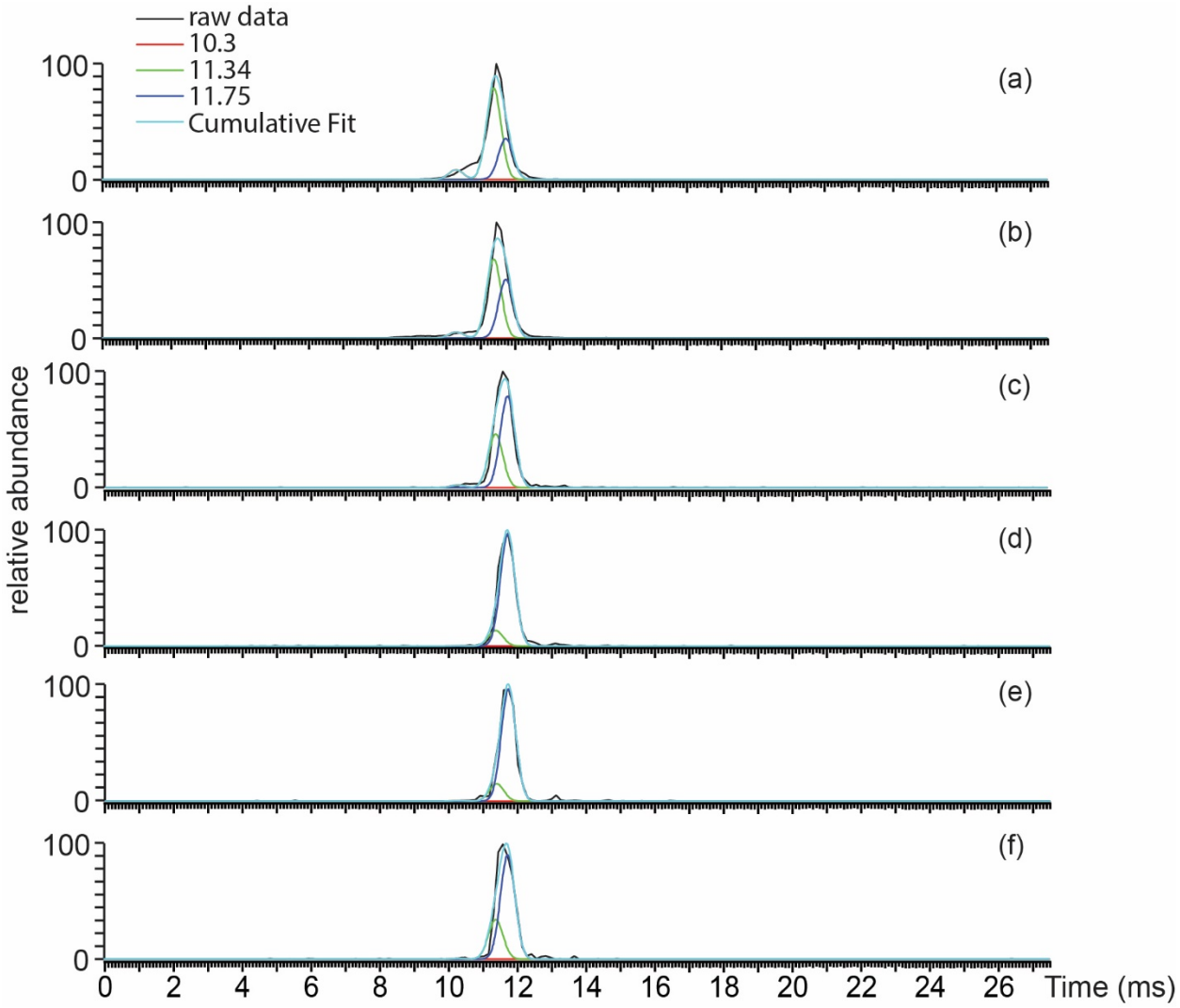


**Supplemental Figure 7.9.** Ion mobility arrival time data (black) for concanavalin A dimer 14+ charge state (*m*/*z* 3750-3850) in (a) 163 mM AA, (b) 153 mM AA and 10 mM KCl, (c) 113 mM AA and 50 mM KCl, (d) 13 mM AA and 150 mM KCl, (e) 25 mM Tris and 150 mM NaCl, and (f) 1x PBS all at pH = 6.8. The ion mobility arrival time data are fitted with three Gaussian peaks centered at 10.3 ms (red), 11.34 ms (green), 11.75 ms (dark blue). The mint trace corresponds to the cumulative fit.

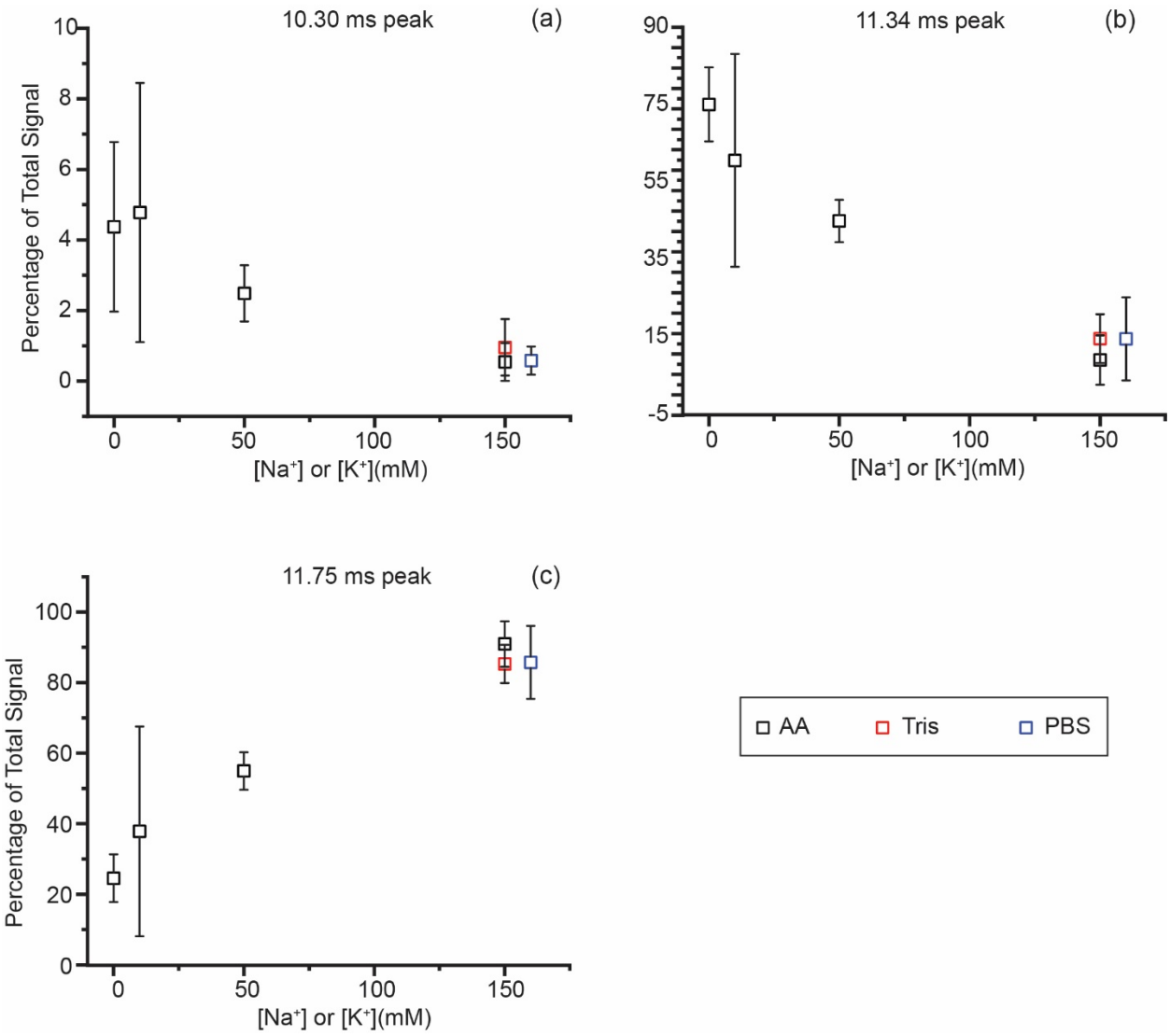


**Supplemental Figure 7.10.** The relative abundance of the three fitted Gaussian peaks centered at the arrival times of (a) 11.30 ms, (b) 11.34 ms, and (c) 11.75 ms for concanavalin A dimer 14+ charge state (*m*/*z* 3750-3850) in six different solutions described in Supplemental Figure 7.9 as a function of sodium ion or potassium ion concentration. The solutions containing AA and KCl (black) have the same nominal ionic strength (163 mM). The results from 25 mM Tris with 150 mM NaCl (red) and 1x PBS (blue) are plotted based on sodium ion concentration.

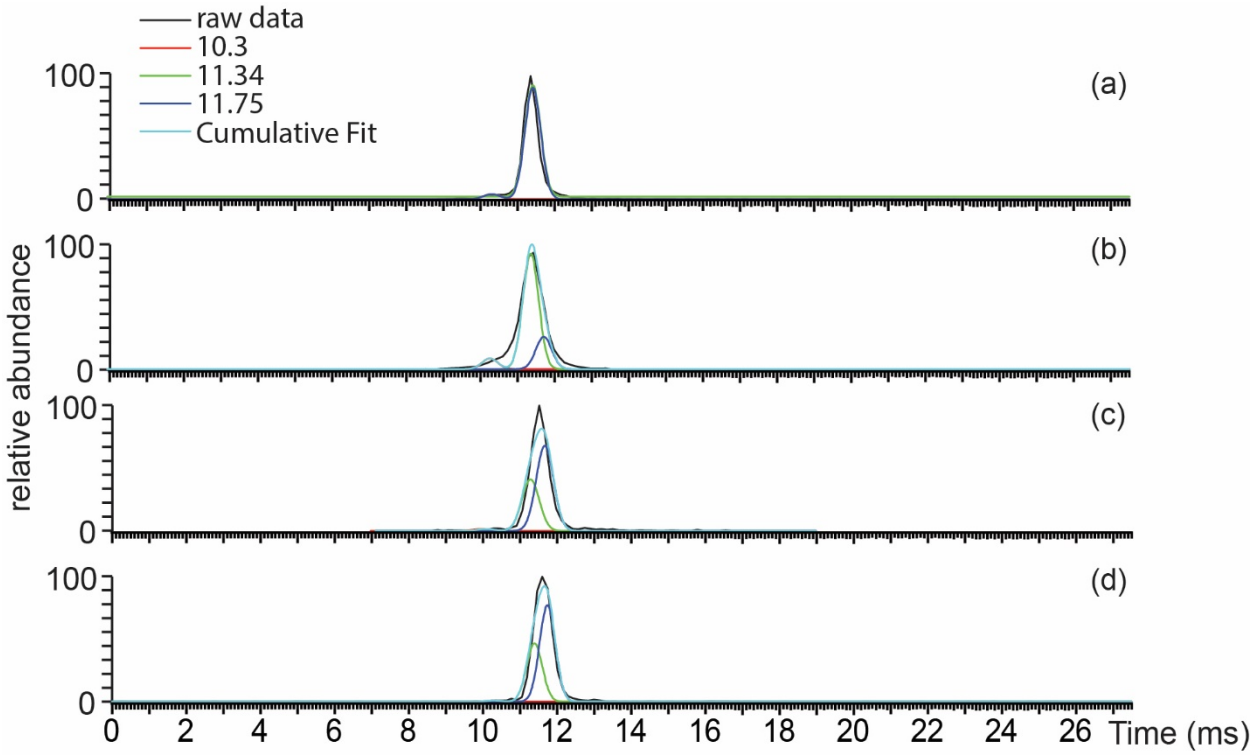


**Supplemental Figure 7.11.** Ion mobility arrival time data (black) for concanavalin A dimer 14+ charge state (*m/z* 3750-3850) in (a) 175 mM AA, (b) 165 mM AA and 10 mM NaCl, (c) 125 mM AA and 50 mM NaCl, (d) 25 mM AA and 150 mM NaCl all at pH = 6.8. The ion mobility arrival time data are fitted with three Gaussian peaks centered at 10.3 ms (red), 11.34 ms (green), 11.75 ms (dark blue). The mint trace corresponds to the cumulative fit.

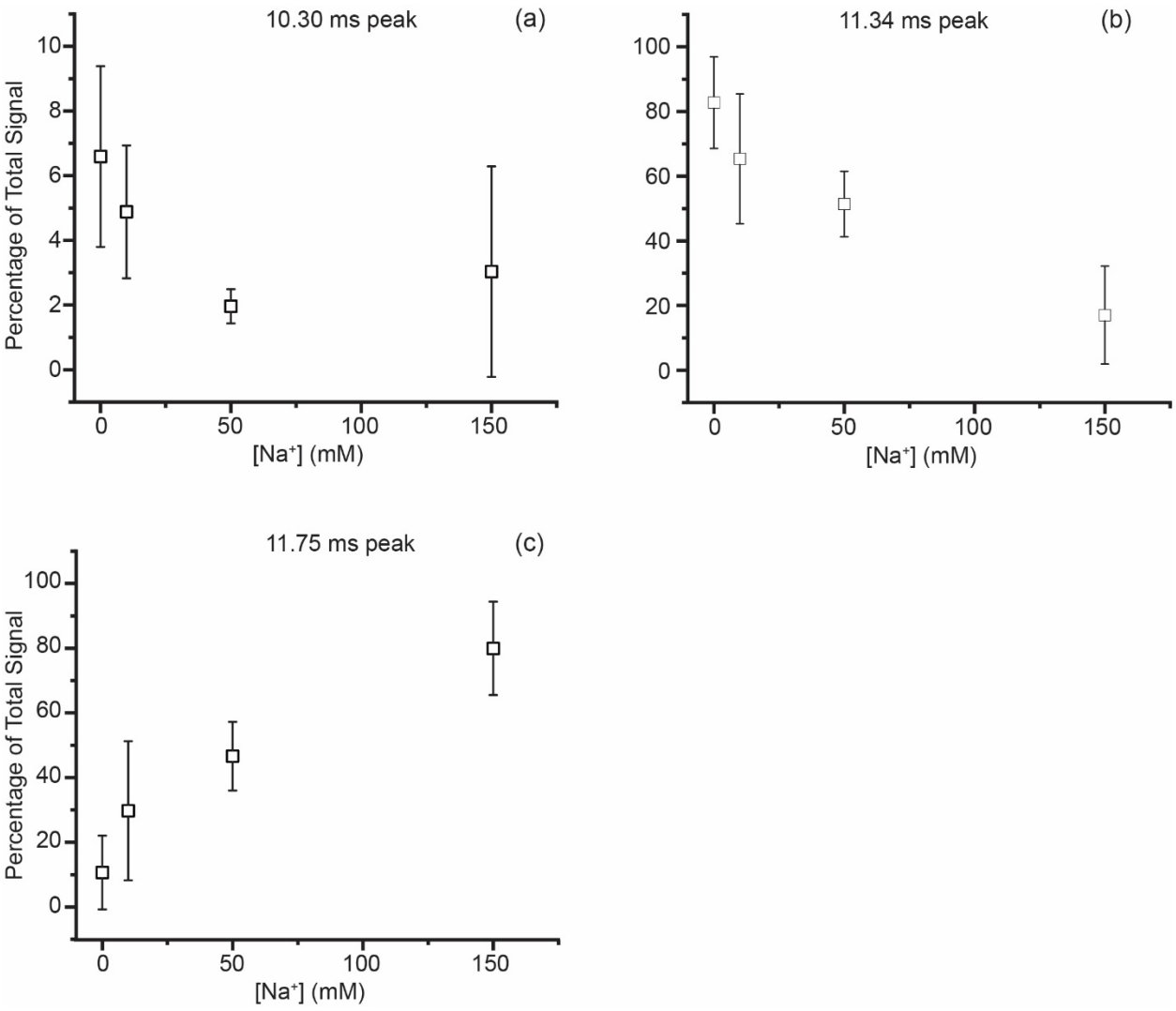


**Supplemental Figure 7.12.** The relative abundance of the three fitted Gaussian peaks centered at the arrival times of (a) 10.30 ms, (b) 11.34 ms, and (c) 11.75 ms for concanavalin A dimer 14+ charge state (*m*/*z* 3750-3850) in four different solutions described in Supplemental Figure 7.11 as a function of sodium ion concentration. The solutions containing AA and NaCl have the same nominal ionic strength (175 mM).

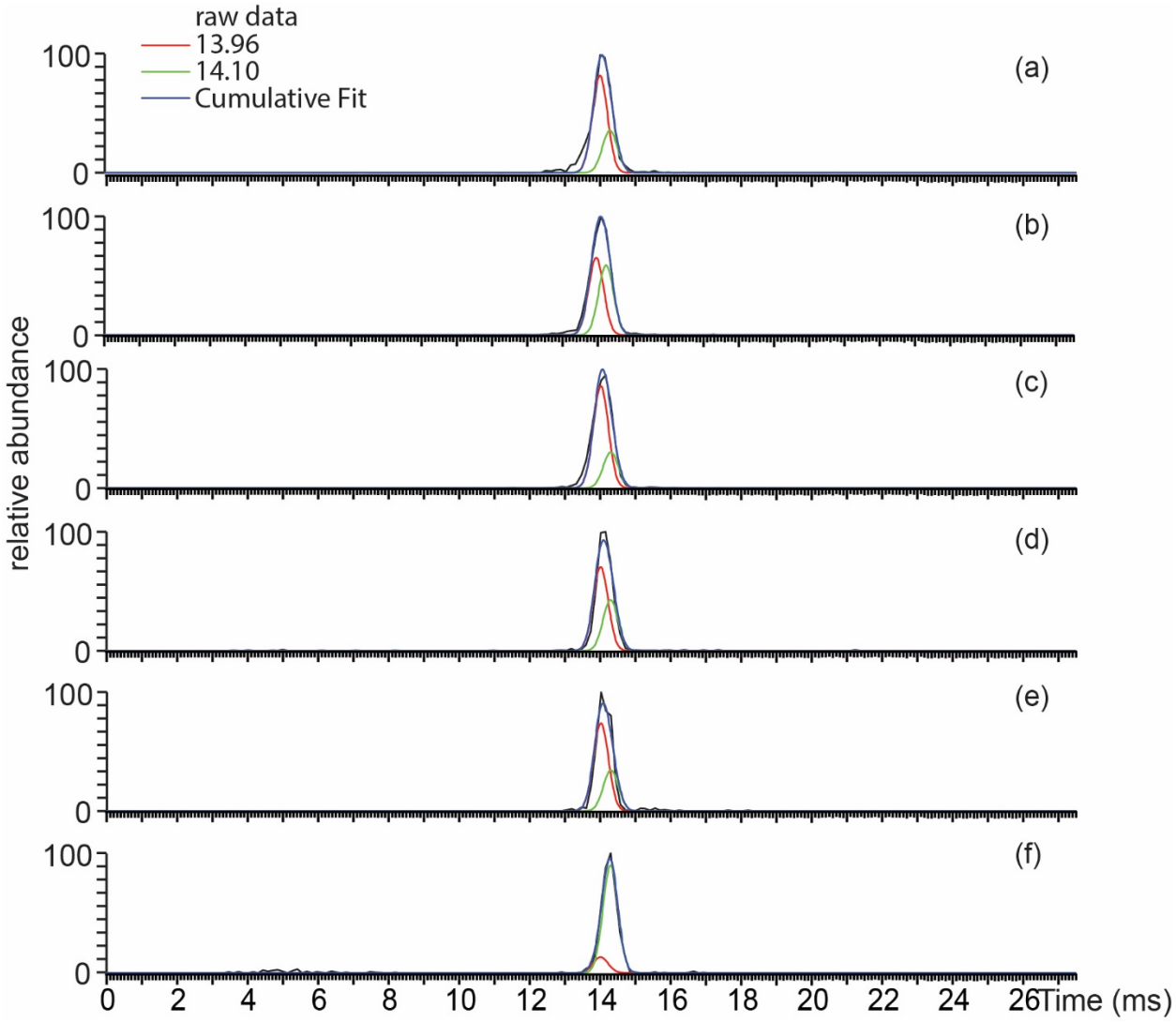


**Supplemental Figure 7.13.** Ion mobility arrival time data (black) for concanavalin A tetramer 21+ charge state (*m*/*z* 4950-5050) in (a) 163 mM AA, (b) 153 mM AA and 10 mM KCl, (c) 113 mM AA and 50 mM KCl, (d) 13 mM AA and 150 mM KCl, (e) 25 mM Tris and 150 mM NaCl, and (f) 1x PBS all at pH = 6.8. The ion mobility arrival time data are fitted with two Gaussian peaks centered at 13.96 ms (red) and 14.24 ms (green). The dark blue trace corresponds to the cumulative fit.

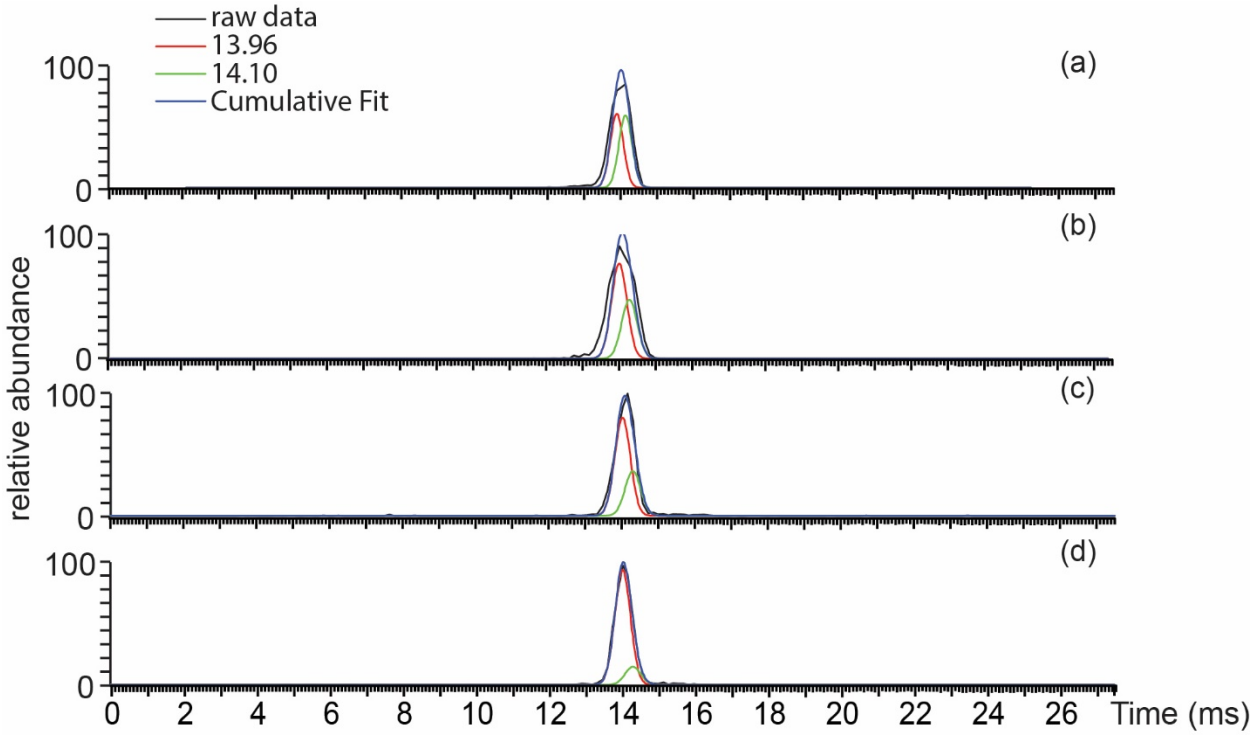


**Supplemental Figure 7.14.** Ion mobility arrival time data (black) for concanavalin A tetramer 21+ charge state (*m*/*z* 4950-5050) in (a) 175 mM AA, (b) 165 mM AA and 10 mM NaCl, (c) 125 mM AA and 50 mM NaCl, (d) 25 mM AA and 150 mM NaCl all at pH = 6.8. The ion mobility arrival time data are fitted with two Gaussian peaks centered at 13.96 ms (red) and 14.24 ms (green). The dark blue trace corresponds to the cumulative fit.

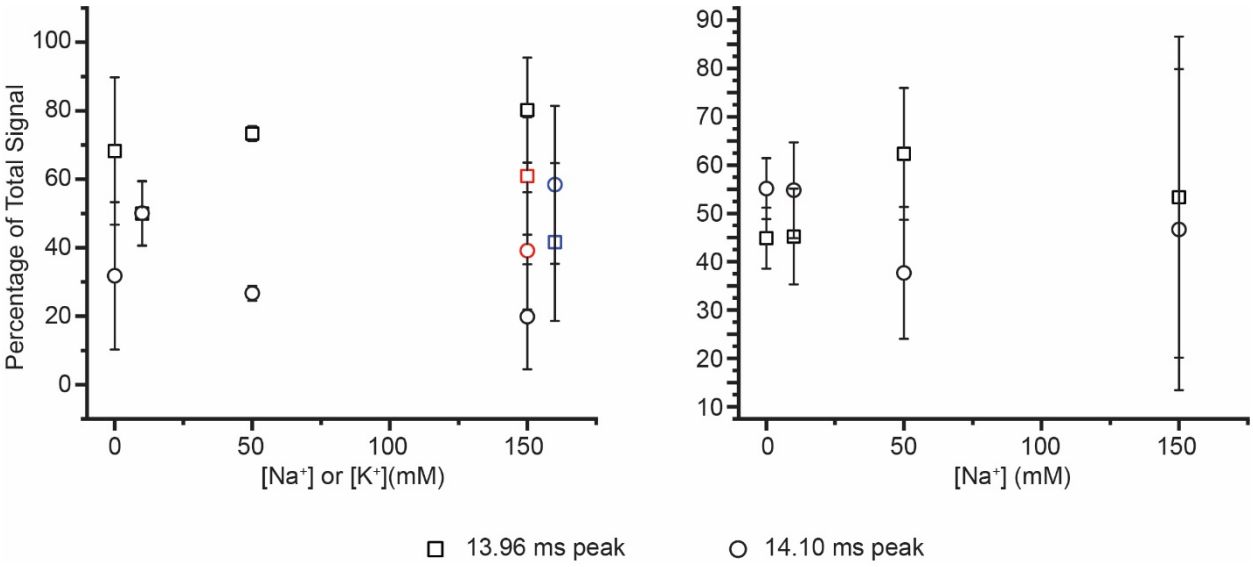


**Supplemental Figure 7.15.** (a) The relative abundance of the two fitted Gaussian peaks with the center of 13.96 ms (square) and 14.10 ms (circle) for concanavalin A tetramer 21+ charge state (*m*/*z* 4950-5050) in six different solutions described in Supplemental Figure 7.13 as a function of sodium ion or potassium ion concentration. The solutions containing AA and KCl (black) have the same nominal ionic strength (163 mM). The results from 25 mM Tris with 150 mM NaCl (red) and 1x PBS (blue) are plotted based on sodium ion concentration. (b) The relative abundance of the two fitted Gaussian peaks with the center of 13.96 ms (square) and 14.10 ms (circle) for concanavalin A for the same charge state in four different solutions described in Supplemental Figure 7.14 containing various concentrations of AA and NaCl with ionic strength of 175 mM

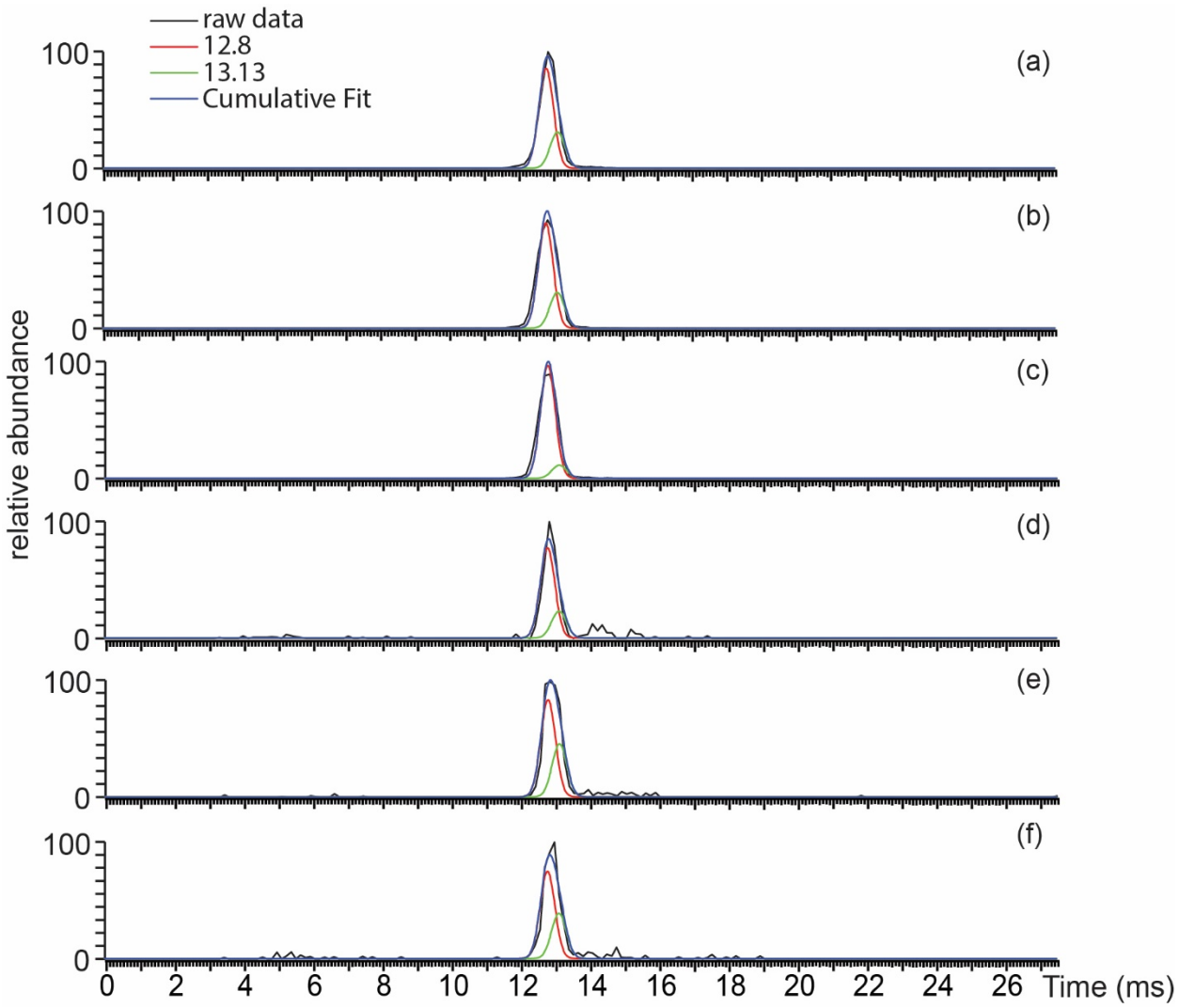


**Supplemental Figure 7.16.** Ion mobility arrival time data (black) for concanavalin A tetramer 20+ charge state (*m*/*z* 5250-5350) in (a) 163 mM AA, (b) 153 mM AA and 10 mM KCl, (c) 113 mM AA and 50 mM KCl, (d) 13 mM AA and 150 mM KCl, (e) 25 mM Tris and 150 mM NaCl, and (f) 1x PBS at pH 6.8. The ion mobility arrival time data are fitted with two Gaussian peaks centered at 12.8 ms (red) and 13.13 ms (green). The dark blue trace corresponds to the cumulative fit.

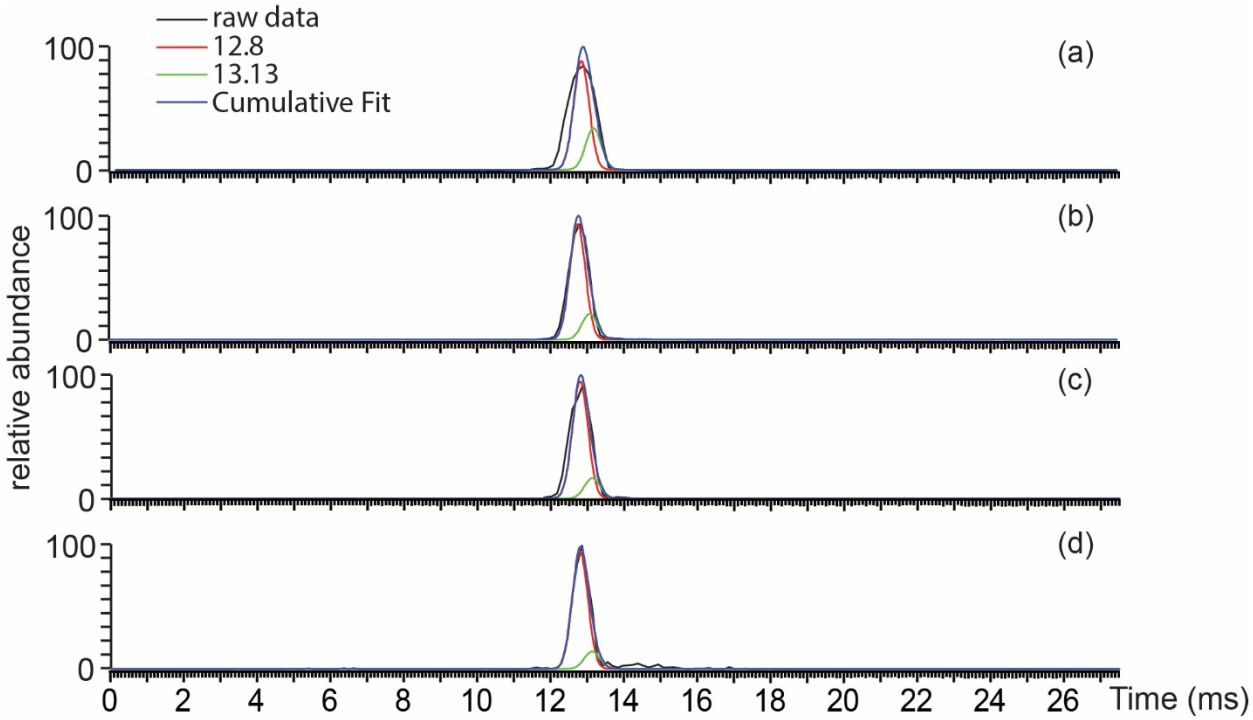


**Supplemental Figure 7.17.** Ion mobility arrival time data (black) for concanavalin A tetramer 20+ charge state (*m*/*z* 5250-5350) in (a) 175 mM AA, (b) 165 mM AA and 10 mM NaCl, (c) 125 mM AA and 50 mM NaCl, (d) 25 mM AA and 150 mM NaCl at pH 6.8. The ion mobility arrival time data are fitted with two Gaussian peaks centered at 12.8 ms (red) and 13.13 ms (green). The dark blue trace corresponds to the cumulative fit.

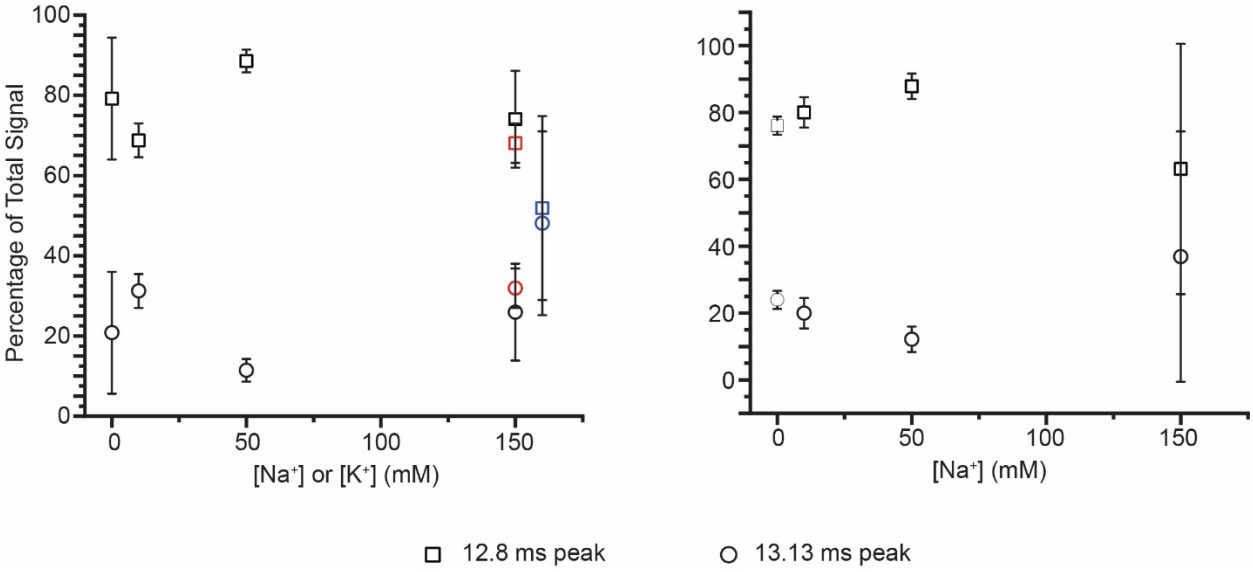


**Supplemental Figure 7.18.** (a) The relative abundance of the two fitted Gaussian peaks with the center of 12.8 ms (square) and 13.13 ms (circle) for concanavalin A tetramer 20+ charge state (*m*/*z* 5250-5350) in six different solutions described in Supplemental Figure 7.16 as a function of sodium ion or potassium ion concentration. The solutions containing AA and KCl (black) have the same nominal ionic strength (163 mM). The results from 25 mM Tris with 150 mM NaCl (red) and 1x PBS (blue) are plotted based on sodium ion concentration. (b) The relative abundance of the two fitted Gaussian peaks for concanavalin A for the same charge state in four different solutions described in Supplemental Figure 7.17 containing various concentrations of AA and NaCl with the ionic strength of 175 mM.

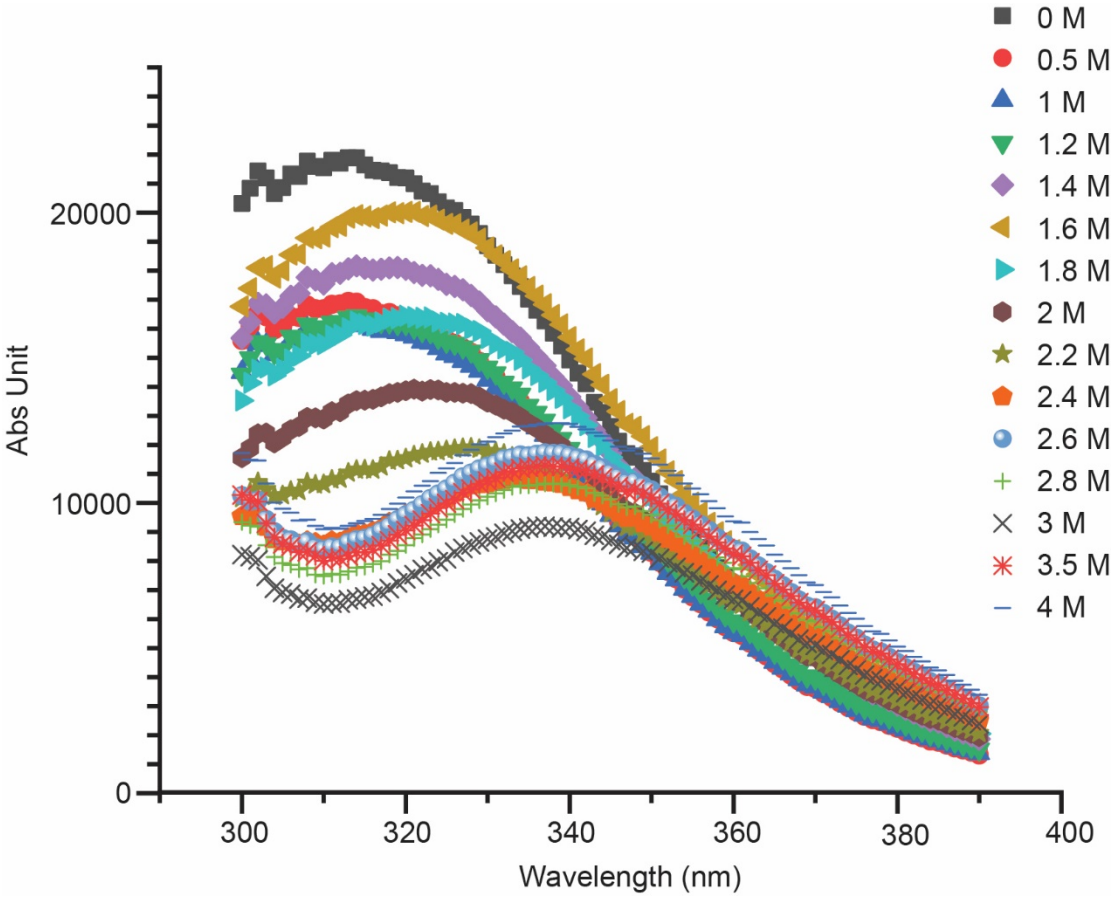


**Supplemental Figure 7.19.** An example of fluorescence emission spectra of concanavalin A in solutions containing an increasing concentration of guanidine from 0 M to 4 M. The sample is excited at 280 nm.

## 7.10 Supplemental Information References

(1) Häkkinen, H.; Barnett, R. N.; Landman, U. Metallization of the Na 14 Cl 13 Cluster. *Europhys. Lett.* **1994**, *28* (4), 263–269.

(2) Ruotolo, B. T.; Benesch, J. L. P.; Sandercock, A. M.; Hyung, S.-J.; Robinson, C. V. Ion Mobility-Mass Spectrometry Analysis of Large Protein Complexes. *Nat. Protoc.* **2008**, *3* (7), 1139–1152.

# Chapter 8

# Summary and Future Directions

The work in this dissertation focuses on the effect of nanoESI emitters used for mass spectrometry. The theta emitters provide two major benefits of (1) mixing two different solutions and (2) controllable droplet lifetimes and mixing times. The applications of theta emitters can range from studying fast reaction intermediates to the fundamentals of electrospray ionization. Submicron emitters (both single barrel and theta emitters) have a significant benefit to desalt protein and protein complexes from traditional biological solutions that contain on average more than 150 mM nonvolatile salts. The discovery of submicron emitters expands the choice of buffers for native MS from volatile salts, such as ammonium acetate and ammonium bicarbonate to all possible buffers, including traditional biological buffers that containing hundreds of millimolars of nonvolatile salts, such as Tris buffer and phosphate buffered saline. For proteins and protein complexes with multiple conformations in solution, the buffer needs to be considered for the data interpretation of MS and for direct data comparison between MS and other methods for structural biology. These emitters provide extra analytical benefits including low sample consumption rate, reduction of nonspecific protein aggregation during electrospray ionization, and producing results that are independent of instrument interface conditions. Choosing the appropriate emitters for the experimental requirements expands the applications of mass spectrometry to fast mixing experiments and solution-phase study of biological molecules in different solutions, and eases some concerns of using native mass spectrometry as a tool for structural biology because of the buffer differences.

Chapter 3, 6, and 7 are all studies that rely on submicron emitters to generated desalted protein ions from solutions containing ~150 mM nonvolatile salts for MS analysis. One issue with submicron emitters used to desalt proteins from solutions containing a high concentration of nonvolatile salts is the instability of the desalted protein ion signals. The instability could result from spray mode changes during the continuous electrospray ionization process. Different spray mode can result in different droplet sizes from a single emitter. It would be interesting to develop a method to monitor droplet sizes and spray mode changes during the ESI process. The droplet sizes can be estimated by studying salt cluster sizes, such as NaCl or CsI, formed from the submicron emitters during the period with desalted protein ions and without desalted proteins ions. It will require ion mobility mass spectrometry to separate salt ions of different charges with overlapping $m/z$ and determine the salt cluster sizes. Confirming the droplet size formed from submicron emitters can also help to better understand the underlying mechanism of desalting with submicron emitters, which can lead to an improvement of submicron emitters as a direct desalting device.

Another issue of submicron emitters observed during experiments for Chapter 3, 6 and 7 is the short duration of the ESI spray when high concentrations of salts present in the solutions. Due to the high concentration of nonvolatile salts and small emitter diameter, the submicron emitters are more susceptible to clogging due to the formation of the salt cluster and the aggregation of biological molecules near the opening of the emitters. As a result, submicron emitters are not

suitable for data acquisition periods that need to last for hours. The trade-off between emitter lifetime and the efficiency of the desalting makes this issue difficult to solve. Possible solutions include a system that integrates multiple emitters sequentially or a microchannel plate that mimics submicron emitters. It will also be interesting to see whether applying intermittent gas pressure at the end of the emitters can extend the duration of the spray. The hypothesis is, when the gas is on, the gas pressure may break the clogs but some desalting efficiency will be sacrificed. When the gas is off, the desalting effect should be observed for a period of time before the clogs build up again.

Despite some limitations of submicron emitters, the submicron emitters have significant advantages (Chapter 3 and 5) and can be used in more applications other than desalting protein ions from buffers containing high concentrations of nonvolatile salts. A potentially new application for submicron theta emitters is to coat the interior of the emitter with different functional groups. Chapter 4 has shown that there is an interaction between a positively charged protein in solution and negatively charged emitter surface of submicron theta emitters. Coating the interior surface of the submicron theta emitters with a functional group possibly converts the submicron theta emitters to reversed-phase columns or ion exchange columns. Although coating the emitters can be difficult and time-consuming, it can be a cheap replacement for current commercial liquid chromatography columns or ion exchange columns, combining all the benefits coming from a submicron emitter.

This dissertation has also provided some insight into how salts can influence the structures, stabilities, and stoichiometries of proteins and protein complexes, and even intrinsically disordered protein using submicron emitters using native MS coupled with submicron emitters in Chapter 6 and 7. It will be interesting to expand the application to temperature melts of protein and protein complexes. The common biological methods, such as fluorescence, circular dichroism, and differential scanning calorimetry, to study protein thermal stability, provide minimal structural information. Mass spectrometry can separate coexistent conformations of proteins in the gas phase combined with the advantage of low sample consumption rate. With submicron emitters, the same solution used in other biological techniques can be directly transferred for thermodynamics studies of protein and protein complexes using mass spectrometry, which can be a new area of application for biological mass spectrometry.